
**Uptake, Distribution and Speciation of Heavy
Metals within *Miscanthus* Grown in
Contaminated Soils**

INNES JOHN DEANS

Submitted in accordance with the requirements for the degree of Doctor of
Philosophy and Master of Science

UNIVERSITY OF LEEDS
SCHOOL OF CHEMICAL & PROCESS ENGINEERING

December 2022

Intellectual Property & Publication Statement

The candidate confirms that the work submitted is his own, except where work which has formed part of jointly authored publications has been included. The contribution of the candidate and the other authors to this work has been explicitly indicated below. The candidate confirms that appropriate credit has been given within the thesis where reference has been made to the work of others.

Some work in chapter 4 – “Soil Characterisation” and chapter 5 – “Bulk Uptake and Speciation” was published in Journal of Hazardous Materials:

Deans, Innes, Douglas I. Stewart, Jenny Jones, Jason Kam, and Bhoopesh Mishra. “Uptake and Speciation of Zn and Pb by *Miscanthus* Grown in Contaminated Soils.” *Journal of Hazardous Materials* (2022): 129899.

The candidate conceptualised the project, designed the experimental methodology, collected most of the experimental data, performed all experimental data analysis and drafted the article. Mr Stuart Micklethwaite performed SEM-EDX imaging. Mr Simon Lloyd performed ICP-MS analysis.

This copy has been supplied on the understanding that it is copyright material and that no quotation from the thesis may be published without proper acknowledgement. The right of Innes John Deans to be identified as Author of this work has been asserted by him in accordance with the Copyright, Designs and Patents Act 1988.

Copyright © 2022 The University of Leeds and Innes John Deans.

Acknowledgements

This PhD could not have been realised without the considerable support from my project partners and colleagues. I am very grateful for the support of Terravesta Ltd. (UK) for their provision of the *Miscanthus* plants; Bell Brothers Nursery Ltd (UK) for seed germination through and initial cultivation of *Miscanthus plants*; the staff at Spen Farm (University of Leeds) (UK) for facilitating collection of soil; and Simon Lloyd (University of Leeds) for running the ICP-MS analyses. XAFS data was collected at MRCAT (beamline 10-BM-B) of the Advanced Photon Source, Argonne National Laboratory. MRCAT operations are supported by the Department of Energy and the MRCAT member institutions. This research used resources of the Advanced Photon Source, a U.S. Department of Energy (DOE) Office of Science User Facility operated for the DOE Office of Science by Argonne National Laboratory under Contract No. DE-AC02-06CH11357. Innes Deans was funded through EPSRC CDT in Bioenergy (grant reference: EP/L014912/1) for this study.

Miscanthus seed-based hybrid cultivar used in this project were developed with support from the UK's Biotechnology and Biological Sciences Research Council (BBSRC) and Department for Environment, Food and Rural Affairs (DEFRA) through the GIANT-LINK project (LK0863) and by the Innovate UK/BBSRC 'MUST' BB/N016149/1 project. I must also thank Dick Flavell and Ceres for the uses of the *Miscanthus* cultivars, which were bred at Aberystwyth University, IBERS, under the leadership of John Clifton-Brown, the research group leader for Plant Biology for the Sustainable Bio-economy.

I also acknowledge the Institute for Ecology of Industrial Areas, Katowice, Poland, for contributions with respect to soil and plant samples from the *Miscanthus* field experiment, operated under MISCOMAR + project. This project is funded by The Polish National Centre for Research and Development, under the flag of Era-Net Cofound FACCE SURPLUS, in the frame of the Joint Programming Initiative on Agriculture, Food Security and Climate Change (FACCE-JPI), grant number FACCE SURPLUS/III/MISCOMAR+/03/2020.

I am also grateful for the practical support I received in the various labs from Lucy Leonard, Stuart Micklethwaite at Leeds Electron Microscopy and Spectroscopy Centre for the SEM-EDX work, Martin Fuller at the Astbury Biostructure Laboratory for the microtome work and Fiona Moulton at the Plant Growth Suite. Also, fellow PhD student Nick Humphries for his help on soil sampling.

I would like to express my immense gratitude to my supervisors Bhoopesh Mishra, Doug Stewart and Jenny Jones. This project would certainly not have been possible for me without you. I must say particular thanks to Bhoopesh, not just for introducing me to the wonderful world of synchrotron science, but for the constant input and support even during the worst periods of COVID lockdowns – the fact that got to the end of this PhD is to a very large extent down to you.

One of the best aspects of undertaking this project was the opportunity to meet and work with my colleagues in the Mishra group: Stella Foster, Flora Brocza, and Luke Higgins; thanks for the support with running the synchrotron experiments, and somehow keeping sharp minds and good humor even during late nights on the various beamtimes we shared together. It was a pleasure to spend time in the company of such intelligent and motivated people! I am also grateful to the 2017 cohort of the Bioenergy Centre for Doctoral Training, in particular Doug Bray and Poppy Cooney for their good company, shared values and companionship throughout the last few years.

Abstract

This project assessed uptake of Zn and Pb by a novel *Miscanthus* hybrid grown in contaminated soils. Data from a young plants grown as part of a pot-trial under controlled conditions were compared with those from biomass derived from a long-term field trial. Sequential extractions combined with analysis of X-ray Absorption Fine Structures (XAFS) were used to characterise the bioavailable Zn and Pb within the soil at the field trial site. These data were used to engineer a suite of different soil conditions for the pot-trial. The pot-trial soils encompassed bioavailable Zn and Pb comparable to that at the field-trial location and a range of incrementally increasing contamination levels. Both Zn and Pb uptake by the plant increased in proportion to their concentrations within the soil. Retention of both Zn and Pb differed between leaf and stem structures, and within mature biomass compared to juvenile plants. XAFS analysis of the biomass revealed different Zn species within stems and leaves, and differences between growth phase and the mature biomass at time of harvest. Sulfur complexes were the dominant Zn species in juvenile plant leaves, with a minority contribution from octahedral O/N complexes. Sulfur complexes were also prevalent in stems from juvenile plants, but predominant O/N speciation shifted towards more tetrahedral O/N coordination. In contrast, the biomass crop was typified by tetrahedral O/N complexes. X-ray Fluorescence (XRF) imaging identified that Zn retention in the plants displayed greater abundance within vascular bundles, in particular around phloem tissues. Despite S complexes being the predominant form of Zn sequestration, signal intensity within XRF maps demonstrated that location of peak S and Zn concentration were not spatially correlated proving a degree of mutual independence. Microprobe analysis (μ XAFS) of Zn speciation revealed that tetrahedral O/N complexes significantly increased at locations of highest Zn concentration.

Contents

Intellectual Property & Publication Statement	i
Acknowledgements	ii
Abstract	iv
List of Figures	x
List of Tables	xvi
Abbreviations	xix
1 Introduction	1
1.1 Overview	2
1.2 Aims, Scope and Objectives	4
1.3 Thesis Structure	5
1.4 References	7
2 Literature Review	14
2.1 Introduction	15
2.2 Contaminated Land	15
2.2.1 Definitions	15
2.2.2 Contamination of Agricultural Land	18
2.3 Sources of Heavy Metals in Agricultural Soil	20
2.3.1 Lithogenic Source	20
2.3.2 Atmospheric Deposition	21
2.3.3 Inorganic Wastes	22

2.3.4	Organic Wastes	25
2.3.5	Agrochemicals	26
2.3.6	Metals' Mass Balance for Agricultural Soil	26
2.4	Remediation Strategies – an Overview	27
2.4.1	Containment Strategies	27
2.4.2	Source Control Strategies	29
2.4.3	Phytoremediation	34
2.4.4	Measuring Plant Suitability for Phytoremediation	40
2.4.5	Relative Costs of Remediation	41
2.5	Heavy Metals and Plant Uptake	43
2.5.1	Heavy Metal Uptake and Sequestration	45
2.6	<i>Miscanthus</i>	50
2.6.1	Species Overview	50
2.6.2	Biomass Properties	51
2.6.3	<i>Miscanthus</i> for Phytoremediation	54
2.6.4	Biofuel Standards for Heavy Metals	58
2.7	Conclusions	59
2.8	References	61
3	Materials and Techniques	81
3.1	Introduction	82
3.2	Materials	82
3.2.1	Field Trial Soil	84
3.2.2	Field Trial Biomass	84
3.2.3	Pot Trial Growth Media	86
3.2.4	Pot Trial Plants	87
3.3	General Laboratory Techniques	88
3.3.1	X-Ray Fluorescence Spectrometry	88
3.3.2	Scanning Electron Microscopy with Energy Dispersive X-Ray Spectrometry	90
3.3.3	Sequential Extraction	92
3.3.4	Atomic Absorption Spectroscopy	92
3.4	Synchrotron Techniques	94

3.4.1	Overview	94
3.4.2	X-Ray Absorption Fine Structure	96
3.4.3	X-Ray Fluorescence Mapping	104
3.5	References	106
4	Soil Characterisation: the Fractionation, Speciation and Distribution of Zn and Pb in the Bytom Soil	108
4.1	Introduction	109
4.1.1	Zinc in the Environment	110
4.1.2	Lead in the Environment	112
4.2	Experimental Methods	115
4.2.1	Soil	115
4.2.2	Energy Dispersive X-Ray Fluorescence Analysis	115
4.2.3	Tessier Extraction	116
4.2.4	Atomic Absorption Spectroscopy	117
4.2.5	Scanning Electron Microscopy with Energy Dispersive X-Ray Analysis	117
4.2.6	XAFS Analysis	117
4.3	Results	119
4.4	Discussion	125
4.5	Conclusions	132
4.6	Appendix	134
4.7	References	136
5	Biomass Characterisation: Uptake Response, Retention Pattern and Speciation	140
5.1	Introduction	141
5.2	Methods	143
5.2.1	Field Trial Biomass	143
5.2.2	Pot Trial Growing Media	143
5.2.3	Pot Trial Growth Conditions	146
5.2.4	Harvesting and Sample Preparation	147
5.2.5	Analysis of Biomass Metal Concentration	147

5.2.6	XAFS Analysis	148
5.3	Results	149
5.3.1	Zinc and Lead Uptake by the Bytom Biomass	149
5.3.2	Zinc and Lead Uptake by Pot Trial	149
5.3.3	XAFS Results	150
5.3.4	Qualitative Analysis of EXAFS	154
5.3.5	Quantitative Modelling of EXAFS	156
5.4	Discussion	159
5.4.1	Uptake by Pot Trial Plants	159
5.4.2	Zn and Pb Distribution	159
5.4.3	Pot Trial Plants vs Mature Crop	161
5.4.4	Zn Speciation	162
5.4.5	Limitations of XAFS Techniques	167
5.5	Conclusions	170
5.6	Appendix	172
5.7	References	176

6	Spatial Analysis: Tissue Distribution and the Location of Differing Species	184
6.1	Introduction	185
6.2	Methods	187
6.2.1	Plant Growth	187
6.2.2	Sample Preparation	188
6.2.3	XRF and μ XAS	189
6.2.4	Statistical Methods	190
6.3	Results	191
6.4	Discussion	196
6.4.1	XRF Mapping of Leaves	196
6.4.2	XRF Mapping of Stem	198
6.4.3	Zinc μ XAFS	200
6.5	Conclusions	203
6.6	Appendix	205
6.7	References	211

7	Conclusions	215
7.1	Summary	216
7.2	Future Directions	220
7.3	References	223

List of Figures

2.1	Percentage of samples taken from European agricultural land which exceed threshold values for heavy metals (Toth et al., 2016a)	19
2.2	Boxplots of the HM concentrations (mg/kg) for Pb/Zn mine tailings (BVSC: Background values for soils in China; GIIEQSSC: Grade II environmental quality standard for soils in China) (Kan et al., 2021)	23
2.3	HM concentrations in soils surrounding Pb/Zn smelting operations in China (Luo et al., 2023)	24
2.4	Applicability of physical separation according to liberation degree of the HM for the particulate forms (G. et al., 2008) . . .	30
2.5	Feed particle size range for application of physical separation technique (G. et al., 2008)	31
2.6	Diagrammatic representation of three plant response categories to increasing HM concentrations in soil (Ghosh and Singh, 2005)	38
2.7	Three-step concept of HM bioavailability in soils for plants showing the relationship between ‘environmental availability’, ‘environmental bioavailability’ and ‘toxicological availability’ (Kim et al., 2015)	46
2.8	Molecular structure of phytochelatin (PC) (Clemens, 2006) . . .	47

2.9	Summary of potential cellular mechanisms for heavy metal (M) tolerance in plants with Cd as an example. 1) restriction of movement to roots by mycorrhizas 2) binding to cell wall root and exudates 3) reducing influx across the plasma membrane 4) efflux across the plasma membrane 5) chelation in the cytosol by metallothionines (MT), phytochelatins (PC) and organic acids 6) repair of the plasma membrane 7) transport and sequestration within the vacuole with PC-sulphide complexes (PC-Cd-S) 8) Transport and accumulation within the vacuole (Marschner, 1995)	48
2.10	Sequestration of Pb^{2+} by cross linking between polymers of pectins displacing the Ca^{2+} bridge (Caffall and Mohnen, 2009) .	49
2.11	TEM images of Pb accumulation in cell walls: left) examples of large crystalline Pb deposits in root cell wall of <i>Populus tremula x tremuloides</i> (Scale bar 500 nm); right) Large Pb deposits with localised callose layer deposit at the plasma membrane (white arrow) in <i>Funaria hygrometrica</i> (Scale bar 200 nm) (Krzyszowska, 2011)	50
2.12	Cross section stem of <i>M. sinensis</i> stained using Fuchsin, safranin, aniline (FSA); E, epidermis; OU, outer ring; VB, vascular bundle; P, parenchyma (Kaack et al., 2003)	53
2.13	Box plots showing variation across <i>M. sinensis</i> stem and leaf fraction: (a) cell wall content; (b) cellulose; (c) hemicellulose; and (d)) lignin (Kaack et al., 2003)	55
3.1	map of Poland showing location of Bytom (TUBS, 2011)	83
3.2	aerial image of the Bytom site and surrounding area	83
3.3	Mature <i>Miscanthus</i> cultivated in a field (mid-summer)	85
3.4	shredded biomass from the Bytom site	85
3.5	collecting soil at Spen Farm with a core auger	86
3.6	<i>Miscanthus</i> plug prior to planting in the pot trial	88
3.7	schematic of the X-ray fluorescence process	89
3.8	example energy dispersive X-ray (EDX) fluorescence spectrum .	90

3.9	example back scattered electron (BSE) image of soil particles using scanning electron microscope (SEM)	91
3.10	schematic of AAS showing Beer-Lambert law dimensions	93
3.11	synchrotron facilities used by the project: Diamond Light Source (left) and the Advanced Photon Source	94
3.12	schematic of synchrotron internal layout	95
3.13	the absorption cross section μ/ρ for Pb, Cd, Fe and O (Newville, 2004)	97
3.14	decay of the excited state. X-ray fluorescence (left) and Auger emission (right) (Newville, 2004)	97
3.15	XAFS for FeO (Newville, 2004)	98
3.16	The energy of the X-ray K and L absorption edges as a function of atomic number Z (Newville, 2004)	99
3.17	XANES spectra of sulfur compounds with different oxidation states (Castillo-Michel et al., 2016)	100
3.18	X-ray absorption and backscattering from neighbouring atoms .	101
3.19	isolation of EXAFS data: (top) $\mu(E)$ or FeO shown with smooth background function $\mu_0(E)$ and the edge-step $\Delta\mu_0$; (middle) isolated EXAFS (k) for FeO; (bottom) k -weighted EXAFS for $k^2\chi(k)$ (Newville, 2004)	103
3.20	schematic of XRF mapping beamline 13-ID-E at APS, Chicago (USA)	104
4.1	SEM-EDX images of Bytom soil showing $K\alpha_1$ transition fluorescence ($M\alpha_1$ for Pb). All scale bar = 100 μm	121
4.2	XAFS for Bytom soil and Zn standards: (Left) XANES; (Right) Real part of the Fourier Transform	123
4.3	EXAFS fitting for Bytom soil. Left) weighted Real part of the Fourier Transform for first and second shell O, C and S paths; Right) Real part of the Fourier Transform for Bytom soil and final Fit result	124

4.4	Idealised phyllosilicate structure (top left) and proposed Zn substitution into related mineral structures. After Manceau et al. (2000)	131
4.5	Xk for Bytom soil and Zn standard	135
5.1	Pot trial a) single <i>Miscanthus</i> 'plug' at the start of the trial; b) pots of <i>Miscanthus</i> growing under controlled conditions, including artificial lighting	146
5.2	Bulk Zn and Pb concentrations in stem and leaf materials across soil conditions adopted in the pot trial	151
5.3	Zn XANES spectra for: (a) Zn standard compounds (Mishra et al., 2020); (b) biomass samples. Absorption edge energies are shown for Zn-cysteine (9661.4 eV) and Zn-malate (9664.4 eV).	152
5.4	Fourier Transforms of EXAFS: (a) magnitude $ \chi(R) $ for Zn standards; (b) magnitude $ \chi(R) $ for <i>Miscanthus</i> samples; (c) Real part $\text{Re} \chi(R) $ for Zn standards; (d) Real part $\text{Re} \chi(R) $ for <i>Miscanthus</i> samples	153
5.5	Results of LCF of the relative weight for Zn species in <i>Miscanthus</i> from the Bytom Field Trial and the Growth Trial plant sections	154
5.6	Fourier Transform (FT) analyses of biomass samples. Dashed lines are measured experimental data. Solid lines are fit simulations. Fit range (1.2 – 2.7 Å) is highlighted. (a) FT magnitude and fit results; (b) expanded real part of the FT and fit results.	156
5.7	Exponential curve fits for Zn uptake in (a) stem and (b) leaf structures of growth trial plants. Soil Zn concentration are reported as sum of the bioavailable fractions (chloride and carbonate). Single outlier point (980 mg/kg) in the stem data is masked during the fitting process	160

5.8	Exponential curve fits for Pb uptake in (a) stem and (b) leaf structures of growth trial plants. Soil Pb concentration are reported as sum of the bioavailable fractions (chloride and carbonate).	160
5.9	Coordination numbers derived from EXAFS fitting of samples .	165
5.10	XANES spectra for biomass samples and weighted LCFs. Dashed lines are measured experimental data for the samples. Solid lines are weighted Zn standards and fit simulations: (a) measured spectra for all biomass samples; (b) Bytom Crop LCF; (c) 1x(Zn+Pb) Stem LCF; (d) 1x(Zn+Pb) Leaf LCF; (e) 5x(Zn+Pb) Stem LCF; (f) 5x(Zn+Pb) Leaf LCF.	173
5.11	X(k) for biomass EXAFS	174
5.12	Five sequential XANES for the 1x(Zn+Pb) Stem sample demonstrating low levels of beam damage through consistency of results	175
6.1	XRF maps of leaf in plan view: A) Large scale map showing K (green), Zn (blue) and S (red) with area of detailed maps highlighted; B) small scale map showing Zn; C) small scale map showing S. All scale bars = 100 μm	191
6.2	Leaf in plan view and associated data. A) small scale XRF map showing Zn (blue) and S (red) and spot locations for μXAFS acquisition (scale bar = 100 μm); B) correlation plot of signal intensity (sum of MCA counts) for Zn and S in each pixel of the detailed map; C) XANES spectra for spot locations and Zn standards, and; D) EXAFS data and LCF results (red line) against for highlighted spot locations and Zn standards.	192

6.3	Leaf in cross section and associated data: A) XRF map for Zn showing spot locations for μ XAFS acquisition and Y-plane scans; B) XRF map for S showing spot locations for μ XAFS acquisition and Y-plane scans; C) plot of Zn and S signal intensity across Y-planes; D) XANES spectra for spot locations and Zn standards. All scale bars = 100 μ m.	193
6.4	Stem cross section and associated data. A) Large scale XRF map of stem in cross section showing Zn (blue), S (red) and Ca (green) with area of the detailed XRF map highlighted; B) correlation plot of Zn and S signal intensity for the large scale XRF map; C) detailed XRF map of Zn (blue) and S (red) with locations of μ XAFS spots displayed; D) spectra for μ XANES locations in stem and Zn standards. All XRF scale bars = 100 μ m.	194
6.5	Small scale XRF maps of stem. A) Zn fluorescence; B) S fluorescence. All Scale bars = 50 μ m.	195
6.6	LCF results (mean and range) for Zn μ XAFS locations across the sample types grouped as high Zn fluorescence (hot) and low fluorescence (cool). Letters indicate of data with significant differences ($p < 0.05$).	201
6.7	XANES for S K-edge: experimental data (top) and S standard spectra with peak energy positions marked (bottom) .	206
6.8	Data for the twenty six μ XAFS sample points (range and mean value) and Zn-standards.	209

List of Tables

2.1	Finnish statutory threshold and guideline values denoting metals' contamination in soils (mg/kg) (MEF, 2007)	16
2.2	US screening values ("SQiRTs") for inorganics in soil (mg/kg) (NOAA, 2008)	17
2.3	Limits on total HM concentrations in sludge amended soils (mg/kg _(dm)) (DEFRA, 1989)	19
2.4	Guidelines for maximum limits of HM in agricultural soils and vegetables as recommended by World Health Organization (mg/kg _(dm)) (WHO, 1996)	20
2.5	Annual mean atmospheric deposition fluxes of HM to soil (mg/m ² /year)	22
2.6	Inorganic materials for HM immobilisation (Guo et al., 2006)	28
2.7	Organic materials for HM immobilisation (Guo et al., 2006)	29
2.8	Mechanisms of phytoremediation (Alkorta et al., 2004)	35
2.9	Classification of some example HM metallophyte plants	39
2.10	Costs of different remediation options	41
2.11	Typical chemical composition of <i>Miscanthus</i> as collated from the Phyllis2 database for biomass and waste (mg/kg _(dm)) (ECN, 2018)	51
2.12	Uptake of HM by <i>Miscanthus</i> versus total and bioavailable soil concentration (mg/kg)	57
2.13	Specifications for threshold HM concentrations from "Solid Biofuels — Fuel Specifications and Classes — Part 6: Graded Non-Woody Briquettes" (17225, 2014) (mg/kg _(dm))	58
3.1	Soil characterisation for Bytom (Rusinowski et al., 2019)	84

3.2	major elemental analysis of soil from the Bytom field trial and the Spen Farm soil used for the pot trial (NRM, 2017) . . .	86
4.1	Percentage contributions of Tessier extractions of Zn mean(range) in contaminated soils from southwest Poland which display low/medium/high levels of contamination (Chlopecka et al., 1996)	112
4.2	Emission factors for total particulates from Pb smelting prior to emissions abatement (Vandegrift et al., 1971)	113
4.3	Percentage contributions of Tessier extractions of Pb mean(range) in contaminated soils from southwest Poland which display low/medium/high levels of contamination (Chlopecka et al., 1996)	115
4.4	Major elements of Bytom soil as determined by XRF	119
4.5	Results of Tessier extractions for Pb and Zn in Bytom soil . . .	120
4.6	SEM-EDX spot samples' elemental composition (n = 14, wt%) .	122
4.7	EXAFS fitting parameters for Zn standards and Bytom soil . .	124
4.8	Comparison of XRF results for the sample soil with mean values for Bytom site data (Rusinowski et al., 2019a) and mean values for spot samples (n=14) for the sample soil using SEM-EDX	126
5.1	Major elemental analysis of soil from the Bytom field trial and the Spen Farm soil used for the pot trial	144
5.2	Results of Tessier extractions for Pb and Zn in the Spen Farm soil	144
5.3	Concentrations of metal added to Spen Farm soil in the pot trials ($\text{mg}_{(\text{metal})}/\text{kg}_{(\text{dm})}$)	145
5.4	Comparison of HM concentration in Bytom soil and biomass compared with uncontaminated <i>Miscanthus</i> and example threshold values for defining contaminated soils. All values in $\text{mg}_{(\text{metal})}/\text{kg}_{(\text{dm})}$	150
5.5	EXAFS fitting parameters for biomass samples	157
5.6	Published EXAFS fitting parameters for Zn compounds samples	158

6.1	Results of LCF on μ XAFS sample points	196
6.2	Mann-Whitney U test results comparing Zn-histidine (O/N) weighting in LCFs for hot and cool spots in each sample type .	210

Abbreviations

AAS	Atomic Absorption Spectroscopy
APS	Advanced Photon Source
Ara	Arabinose
BAF	Bio-Accumulation Factor
BCF	Bio-Concentration Factor
CEL	Cellulose
DLS	Diamond Light Source
EDTA	Ethylene Diamine Tetra-Acetic acid
EXAFS	Extended X-Ray Absorption Fine Structure
GAC	Granular Activated Carbon
Glu	Glucose
HEM	Hemicellulose
HHV	Higher Heating Value
HM	Heavy Metal(oid)
LVB	Large Vascular Bundle
MT	Metallothionein
PC	Phytochelatin
pCA	p-Courmaric Acid
PRB	Permeable Reactive Barrier
rFT	Real part of a Fourier Transform
SEM-EDX	Scanning Electron Microscopy – Energy Dispersive X-Ray
SVB	Small Vascular Bundle
TF	Translocation Factor
TFA	Trans-Ferulic Acid
TRM	Transformed Red Mud
XAFS	X-Ray Absorption Fine Structures
XAS	X-Ray Absorption Spectroscopy
XRF	X-Ray Fluorescence
Xyl	Xylose
ZVI	Zero Valent Iron

Chapter 1

Introduction

1.1 Overview

Miscanthus is a genus of perennial grasses which possess high crop yields and the ability to grow on marginal soils due to their low nutrient requirement (Cadoux et al., 2012; Evans et al., 2015; Qin et al., 2011; Van der Weijde et al., 2017). The resilience of *Miscanthus* is such that some species can produce viable crops on land contaminated with Heavy Metals (HM). However, such studies also demonstrate that *Miscanthus* plants can uptake and retain HM to varying degrees depending on the nature and extent of the contamination within the soil (Al Souki et al., 2021; Angelova and Zapryanova, 2021; Barbosa et al., 2015; Deng et al., 2004; Korzeniowska and Stanislawska-Glubiak, 2015; Krzyzak et al., 2017; Li et al., 2014; Nsanganwimana et al., 2021; Pidlisnyuk et al., 2019; Wanat et al., 2013).

Some species of *Miscanthus* such as *Miscanthus x giganteus* (Greef et al., 2001) have been identified as holding significant potential as biomass feedstocks for the subsequent production of bioenergy (Clifton-Brown et al., 2017; Jones and Walsh, 2007; Wagner et al., 2019). Producing bioenergy crops on contaminated lands has the potential to offer a productive use of land that may be blighted for utilisation for other purposes (e.g. food crop production) and such a strategy is beginning to be investigated (Kocoń and Jurga, 2017; Pidlisnyuk et al., 2014). However, HM content of the biomass is one of the key consideration regarding feedstock quality (ISO17225, 2014). Consequently, the ability of some *Miscanthus* species to absorb certain HM raises questions regarding the extent to which HM retention potentially negates the crop's use for bioenergy recovery and therefore undermines the initial strategy of growing such crops on contaminated lands.

Some of the research into *Miscanthus*' uptake of HM identifies, at a macro level, a degree of spatial variability as to where HM are retained within the plant's major structures, e.g. above/below ground structures, roots compared with shoots (Barbosa et al., 2015; Korzeniowska and Stanislawska-Glubiak, 2015; Wanat et al., 2013). Beyond this basic categorisation there has been no research into understanding the detail of what tissues retain HM within

Miscanthus, HM compartmentalisation at a cellular level, or the biochemistry responsible for HM sequestration within the final biomass product.

In a different field, considerable research has been invested into understanding how genotypic variations can be exploited to optimise nutrient content (e.g. Zn and Fe) of food crops, particularly for countries with nutrient deficient diets (Bowen, 1987; Srivastava et al., 2015; Zhao and McGrath, 2009). Such studies aim to identify key mechanisms and traits of different crops which are useful in developing crop varieties, by traditional breeding or genetic engineering methods, with improved nutrient content resulting from changes in the overall biomass chemistry.

It has been established that *Miscanthus* exhibits a wide range of biochemical and morphological characteristics some of which influence biomass properties (Kaack et al., 2003; Van der Weijde et al., 2017). However, the relationship between these quantifiable traits of *Miscanthus* and its retention of HM has not been researched in detail to date.

Synchrotron X-ray techniques, such as X-ray Absorption Fine Structure (XAFS) analysis, are powerful tools which are increasingly finding application in the environmental and biological sciences. These techniques can be used to investigate HM speciation in biological systems and provide insight into uptake and sequestration mechanisms within plants (Adediran et al., 2015, 2016; Adele et al., 2018; Cui et al., 2020; Lombi and Susini, 2009; Vijayan et al., 2015). X-ray Absorption Near Edge Structures (XANES) can identify different species of a HM, with high reproducibility between environmental samples, by comparing the position of the absorption edge and variations in the post-edge features with standard compounds (Castorina et al., 2019). HM speciation can also be identified through Extended X-ray Absorption Fine Structure (EXAFS) analysis whereby the dominant biochemical ligands responsible for HM sequestration can be distinguished (Mishra et al., 2020; Thomas et al., 2019). Micro X-ray Fluorescence (μ XRF) microscopy is another powerful application of synchrotron technology which has been used successfully in the study of HM retention and location within plant tissues (Blamey et al., 2018; Moore et al.,

2014; Tian et al., 2017).

1.2 Aims, Scope and Objectives

The aim of this project is to develop a more detailed understanding of the uptake and retention of HM by *Miscanthus* than is currently available within published literature. Central to the project is the study of a particular *Miscanthus* hybrid that has been successfully established for a number of years as part of a field trial at a contaminated site in Poland. The same hybrid is adopted in this project for pot trials where juvenile plants propagated from seeds are grown under controlled conditions. The pot trials utilise engineered soil conditions which mimic the conditions at the field trial site, and provide a matrix of differing contamination levels which allow the plant's response to be observed under differing and calibrated conditions.

The scope of this work focusses on the above ground, aerial biomass of the plants as this is the harvested crop used within bioenergy conversion. Consequently, only HM which translocate above the soil and root level are considered. Focus is placed on Zn and Pb as these were identified during an early screening exercise (chapter 5) as being present at elevated levels within the aerial biomass as a result of soil contamination. Consequently, Zn and Pb are particularly relevant as they have the potential to impact biomass quality, and hence the viability of the crop for use in bioenergy conversion.

Through studying the uptake and retention of Zn and Pb in *Miscanthus*' aerial structures, both within mature biomass at time of harvest and within juvenile plant during the growth phase, this project aims to identify the governing structural and biochemical characteristics of *Miscanthus* which influence its retention of these HM.

The following objectives have been identified to assist in achieving the project's aim:

1. To characterise the HM in the soil at the field trial location in sufficient detail to facilitate the development of a growth media with comparable contamination levels for bioavailable HM species;
2. To develop a series of pot trials using engineered growth media which allow Zn and Pb uptake by *Miscanthus* to be studied under controlled conditions, including soil conditions which mimic the field trial site;
3. To establish how bulk Zn and Pb concentration within *Miscanthus* biomass changes with varying degrees of soil contamination;
4. To identify the speciation of Zn within the aerial biomass in order to provide insight into the complexation environment employed by *Miscanthus*' biochemistry to sequester Zn. This to be quantified at different locations across the plant's structures and across multiple scales (general vs local);
5. To identify the spatial distribution of Zn and Pb with the aerial biomass at multiple scales (macro vs micro) and thereby identify which anatomical features (tissues and cells) are responsible for the storage of Zn and Pb within the biomass.

1.3 Thesis Structure

This thesis begins with an overview of HM contaminated land, identifying the historic and ongoing sources of the contamination. Remedial approaches to HM contamination are reviewed with an emphasis on the principles of phytoremediation as it applies to the establishment of plants on contaminated sites. Specific information is provided regarding *Miscanthus* as a bioenergy crop and existing studies into its growth on HM contaminated soils. The next chapter sets out the materials and techniques which underpin this project.

Three results chapters form the basis of the primary research from this project, each of which describes the multiple techniques used to achieve the project's objectives. Each chapter provides a precise description of the methods used.

The first results chapter characterises the HM contamination within the soil from the field trial site. The next results chapter contains macro-scale analyses of bulk Zn and Pb uptake across the pot trial plants and compares them to the mature biomass crop from the field trial. Bulk XAFS analyses are applied to identify high-level patterns of Zn speciation across the samples. The final results chapter uses detailed XRF imaging and μ XAFS to provide precision analysis of Zn and Pb retention in specific plant tissues.

The thesis is concluded with a summary chapter detailing the project's findings. This summary chapter concludes by considering the implications of the project's findings and provides suggestions for future studies.

1.4 References

- Adediran, G. A., Ngwenya, B. T., Mosselmans, J. F., Heal, K. V., and Harvie, B. A. (2015). Mechanisms behind bacteria induced plant growth promotion and zn accumulation in brassica juncea. *J Hazard Mater*, 283:490–9. Adediran, Gbotemi A Ngwenya, Bryne T Mosselmans, J Frederick W Heal, Kate V Harvie, Barbra A eng Research Support, Non-U.S. Gov't Netherlands J Hazard Mater. 2015;283:490-9. doi: 10.1016/j.jhazmat.2014.09.064. Epub 2014 Oct 8.
- Adediran, G. A., Ngwenya, B. T., Mosselmans, J. F., Heal, K. V., and Harvie, B. A. (2016). Mixed planting with a leguminous plant outperforms bacteria in promoting growth of a metal remediating plant through histidine synthesis. *Int J Phytoremediation*, 18(7):720–9. Adediran, Gbotemi A Ngwenya, Bryne T Mosselmans, J Frederick W Heal, Kate V Harvie, Barbra A eng Research Support, Non-U.S. Gov't Int J Phytoremediation. 2016;18(7):720-9. doi: 10.1080/15226514.2015.1131235.
- Adele, N. C., Ngwenya, B. T., Heal, K. V., and Mosselmans, J. F. W. (2018). Soil bacteria override speciation effects on zinc phytotoxicity in zinc-contaminated soils. *Environmental Science and Technology*, 52(6):3412–3421. Ga3hu Times Cited:0 Cited References Count:74.
- Al Souki, K. S., Burdová, H., Mamirova, A., Kuráň, P., Kříženecká, S., Oravová, L., Tolaszová, J., Nebeská, D., Popelka, J., Ust'ak, S., Honzík, R., and Trögl, J. (2021). Evaluation of the miscanthus × giganteus short term impacts on enhancing the quality of agricultural soils affected by single and/or multiple contaminants. *Environmental Technology and Innovation*, 24:101890.
- Angelova, V. and Zapryanova, V. (2021). Miscanthus x giganteus as a biofuel crop for phytoremediation of heavy metal contaminated soils. *Sci. Papers. Ser. E Land Reclam. Earth Obs. Surv. Environ. Eng*, 10:192–203.
- Barbosa, B., Boléo, S., Sidella, S., Costa, J., Duarte, M. P., Mendes, B., Cosentino, S. L., and Fernando, A. L. (2015). Phytoremediation of heavy

metal-contaminated soils using the perennial energy crops miscanthus spp. and arundo donax l. *Bioenergy Research*, 8(4):1500–1511. Cited By :28
Export Date: 1 August 2018.

Blamey, F. P. C., McKenna, B. A., Li, C., Cheng, M. M., Tang, C. X., Jiang, H. B., Howard, D. L., Paterson, D. J., Kappen, P., Wang, P., Menzies, N. W., and Kopittke, P. M. (2018). Manganese distribution and speciation help to explain the effects of silicate and phosphate on manganese toxicity in four crop species. *New Phytologist*, 217(3):1146–1160. Fv4kh Times Cited:5
Cited References Count:62.

Bowen, J. E. (1987). Physiology of genotypic differences in zinc and copper uptake in rice and tomato. *Plant and soil*, 99(1):115–125.

Cadoux, S., Riche, A. B., Yates, N. E., and Mchet, J. M. (2012). Nutrient requirements of miscanthus x giganteus: Conclusions from a review of published studies. *Biomass and Bioenergy*, 38:14–22. Sp. Iss. SI 910ad Times Cited:97
Cited References Count:44.

Castorina, E., Ingall, E. D., Morton, P. L., Tavakoli, D. A., and Lai, B. (2019). Zinc k-edge xanes spectroscopy of mineral and organic standards. *Journal of Synchrotron Radiation*, 26:1302–1309. 4 Sp. Iss. SI Ih4if Times Cited:0
Cited References Count:39.

Clifton-Brown, J., Hastings, A., Mos, M., Mccalmont, J. P., Ashman, C., Awty-Carroll, D., Cerazy, J., Chiang, Y. C., Cosentino, S., Cracroft-Eley, W., Scurlock, J., Donnison, I. S., Glover, C., Golazb, I., Greef, J. M., Gwyn, J., Harding, G., Hayes, C., Helios, W., Hsu, T. W., Huang, L. S., Jezowski, S., Kim, D. S., Kiesel, A., Kotecki, A., Krzyzak, J., Lewandowski, I., Lim, S. H., Liu, J. X., Loosely, M., Meyer, H., Murphy-Bokern, D., Nelson, W., Pogrzeba, M., Robinson, G., Robson, P., Rogers, C., Scalici, G., Schuele, H., Shafiei, R., Shevchuk, O., Schwarz, K. U., Squance, M., Swaller, T., Thornton, J., Truckses, T., Botnari, V., Vizir, I., Wagner, M., Warren, R., Webster, R., Yamada, T., Youell, S., Xi, Q. G., Zong, J. Q., and Flavell, R. (2017). Progress in upscaling miscanthus biomass production for the euro-

- pean bio-economy with seed-based hybrids. *Global Change Biology Bioenergy*, 9(1):6–17. Sp. Iss. SI Ef3ia Times Cited:40 Cited References Count:51.
- Cui, J. L., Zhao, Y. P., Chan, T. S., Zhang, L. L., Tsang, D. C. W., and Li, X. D. (2020). Spatial distribution and molecular speciation of copper in indigenous plants from contaminated mine sites: Implication for phytostabilization. *J Hazard Mater*, 381:121208. Cui, Jin-Li Zhao, Yan-Ping Chan, Ting-Shan Zhang, Li-Li Tsang, Daniel C W Li, Xiang-Dong eng Research Support, Non-U.S. Gov't Netherlands J Hazard Mater. 2020 Jan 5;381:121208. doi: 10.1016/j.jhazmat.2019.121208. Epub 2019 Sep 11.
- Deng, H., Ye, Z. H., and Wong, M. H. (2004). Accumulation of lead, zinc, copper and cadmium by 12 wetland plant species thriving in metal-contaminated sites in china. *Environmental Pollution*, 132(1):29–40. 847hz Times Cited:350 Cited References Count:31.
- Evans, S. G., Ramage, B. S., DiRocco, T. L., and Potts, M. D. (2015). Greenhouse gas mitigation on marginal land: a quantitative review of the relative benefits of forest recovery versus biofuel production. *Environ Sci Technol*, 49(4):2503–11. Evans, Samuel G Ramage, Benjamin S DiRocco, Tara L Potts, Matthew D eng Research Support, Non-U.S. Gov't Review Environ Sci Technol. 2015 Feb 17;49(4):2503-11. doi: 10.1021/es502374f. Epub 2015 Jan 29.
- Greef, J. M., Deuter, M., Hodgkinson, T. R., and Renvoize, S. A. (2001). *Miscanthus x giganteus*. *Kew Bulletin*, 56(3): 759.
- ISO17225 (2014). 17225-7: 2014. *Solid Biofuels. Solid biofuels. Fuel specifications and classes. Part, 7:1–14*.
- Jones, M. B. and Walsh, M. (2007). *Miscanthus for energy and fibre*. Earthscan, London. GBA152336 (Uk)009720682 edited by Michael B. Jones and Mary Walsh. ill., maps ; 25 cm. First published by James and James (Science Publishers) in 2001, reprinted by Earthscan in 2007. Includes bibliographical references and index.

- Kaack, K., Schwarz, K. U., and Brander, P. E. (2003). Variation in morphology, anatomy and chemistry of stems of miscanthus genotypes differing in mechanical properties. *Industrial Crops and Products*, 17(2):131–142. 651cc Times Cited:35 Cited References Count:37.
- Kocoń, A. and Jurga, B. (2017). The evaluation of growth and phytoextraction potential of miscanthus x giganteus and sida hermaphrodita on soil contaminated simultaneously with cd, cu, ni, pb, and zn. *Environmental Science and Pollution Research*, 24(5):4990–5000. Cited By :4 Export Date: 1 August 2018.
- Korzeniowska, J. and Stanislawska-Glubiak, E. (2015). Phytoremediation potential of miscanthus × giganteus and spartina pectinata in soil contaminated with heavy metals. *Environmental Science and Pollution Research*, 22(15):11648–11657. Cited By :14 Export Date: 1 August 2018.
- Krzyzak, J., Pogrzeba, M., Rusinowski, S., Clifton-Brown, J., McCalmont, J. P., Kiesel, A., Mangold, A., and Mos, M. (2017). Heavy metal uptake by novel miscanthus seed-based hybrids cultivated in heavy metal contaminated soil. *Civil and Environmental Engineering Reports*, 26(3):121–132. Fp4zu Times Cited:2 Cited References Count:22.
- Li, C., Xiao, B., Wang, Q. H., Yao, S. H., and Wu, J. Y. (2014). Phytoremediation of zn- and cr-contaminated soil using two promising energy grasses. *Water, Air, and Soil Pollution*, 225(7). Cited By :12 Export Date: 1 August 2018.
- Lombi, E. and Susini, J. (2009). Synchrotron-based techniques for plant and soil science: opportunities, challenges and future perspectives. *Plant and Soil*, 320(1):1–35.
- Mishra, B., McDonald, L., Roy, M., Lanzirrotti, A., and Myneni, S. (2020). Uptake and speciation of zinc in edible plants grown in smelter contaminated soils. *PLoS ONE*, 15(4):.
- Moore, K. L., Chen, Y., van de Meene, A. M., Hughes, L., Liu, W., Geraki, T., Mosselmans, F., McGrath, S. P., Grovenor, C., and Zhao, F. J.

- (2014). Combined nanosims and synchrotron x-ray fluorescence reveal distinct cellular and subcellular distribution patterns of trace elements in rice tissues. *New Phytol*, 201(1):104–15. Moore, Katie L Chen, Yi van de Meene, Allison M L Hughes, Louise Liu, Wenju Geraki, Tina Mosselmans, Fred McGrath, Steve P Grovenor, Chris Zhao, Fang-Jie eng BB/H006303/1/Biotechnology and Biological Sciences Research Council/United Kingdom Research Support, Non-U.S. Gov't England 2013/10/11 06:00 New Phytol. 2014 Jan;201(1):104-15. doi: 10.1111/nph.12497. Epub 2013 Sep 24.
- Nsanganwimana, F., Al Souki, K. S., Waterlot, C., Douay, F., Pelfrène, A., Ridošková, A., Louvel, B., and Pourrut, B. (2021). Potentials of miscanthus x giganteus for phytostabilization of trace element-contaminated soils: Ex situ experiment. *Ecotoxicology and Environmental Safety*, 214:112125.
- Pidlisnyuk, V., Erickson, L., Stefanovska, T., Popelka, J., Hettiarachchi, G., Davis, L., and Trögl, J. (2019). Potential phytomanagement of military polluted sites and biomass production using biofuel crop miscanthus x giganteus. *Environmental Pollution*, 249:330–337. Export Date: 08 May 2022; Cited By: 19.
- Pidlisnyuk, V., Stefanovska, T., Lewis, E. E., Erickson, L. E., and Davis, L. C. (2014). Miscanthus as a productive biofuel crop for phytoremediation. *Critical Reviews in Plant Sciences*, 33(1):1–19. doi: 10.1080/07352689.2014.847616.
- Qin, Z., Zhuang, Q., Zhu, X., Cai, X., and Zhang, X. (2011). Carbon consequences and agricultural implications of growing biofuel crops on marginal agricultural lands in china. *Environ Sci Technol*, 45(24):10765–72. Qin, Zhangcai Zhuang, Qianlai Zhu, Xudong Cai, Ximing Zhang, Xiao eng Research Support, U.S. Gov't, Non-P.H.S. Environ Sci Technol. 2011 Dec 15;45(24):10765-72. doi: 10.1021/es2024934. Epub 2011 Nov 28.
- Srivastava, P. C., Rawat, D., Pachauri, S. P., and Shrivastava, M. (2015).

- Strategies for enhancing zinc efficiency in crop plants. pages 87–101. Springer.
- Thomas, S. A., Mishra, B., and Myneni, S. C. B. (2019). High energy resolution-x-ray absorption near edge structure spectroscopy reveals zn ligation in whole cell bacteria. *Journal of Physical Chemistry Letters*, 10(10):2585–2592. Hy8hz Times Cited:0 Cited References Count:55.
- Tian, S. K., Xie, R. H., Wang, H. X., Hu, Y., Hou, D. D., Liao, X. C., Brown, P. H., Yang, H. X., Lin, X. Y., Labavitch, J. M., and Lu, L. L. (2017). Uptake, sequestration and tolerance of cadmium at cellular levels in the hyperaccumulator plant species *sedum alfredii*. *Journal of Experimental Botany*, 68(9):2387–2398. Ew1sh Times Cited:9 Cited References Count:43.
- Van der Weijde, T., Kiesel, A., Iqbal, Y., Muylle, H., Dolstra, O., Visser, R. G. F., Lewandowski, I., and Trindade, L. M. (2017). Evaluation of miscanthus sinensis biomass quality as feedstock for conversion into different bioenergy products. *Global Change Biology Bioenergy*, 9(1):176–190. Sp. Iss. SI Ef3ia Times Cited:19 Cited References Count:52.
- Vijayan, P., Willick, I. R., Lahlali, R., Karunakaran, C., and Tanino, K. K. (2015). Synchrotron radiation sheds fresh light on plant research: The use of powerful techniques to probe structure and composition of plants. *Plant and Cell Physiology*, 56(7):1252–1263. Cp1py Times Cited:16 Cited References Count:84.
- Wagner, M., Mangold, A., Lask, J., Petig, E., Kiesel, A., and Lewandowski, I. (2019). Economic and environmental performance of miscanthus cultivated on marginal land for biogas production. *Global Change Biology Bioenergy*, 11(1):34–49. Sp. Iss. SI Hk9cx Times Cited:4 Cited References Count:82.
- Wanat, N., Austruy, A., Joussein, E., Soubrand, M., Hitmi, A., Gauthier-Moussard, C., Lenain, J. F., Vernay, P., Munch, J. C., and Pichon, M. (2013). Potentials of miscanthus x giganteus grown on highly contaminated technosols. *Journal of Geochemical Exploration*, 126:78–84. 300yk Times Cited:29 Cited References Count:35.

Zhao, F.-J. and McGrath, S. P. (2009). Biofortification and phytoremediation.
Current Opinion in Plant Biology, 12(3):373–380.

Chapter 2

Literature Review

2.1 Introduction

This chapter provides the context and rationale for researching *Miscanthus* cultivation on heavy metal contaminated land. In particular, the extent to which heavy metal contamination is an issue impacting agricultural land is examined. Phytoremediation is placed in the context of alternative management strategies. A review of research establishes both the opportunities and challenges to growing *Miscanthus* as a viable bioenergy crop in soils blighted by contamination. There then follows an overview of mechanisms by which plants uptake and sequester heavy metals within their tissues – this forms the basis for the mechanistic study presented in the results chapters which follow.

2.2 Contaminated Land

2.2.1 Definitions

Heavy metals and metalloids (HM) include those metals with a relatively high atomic number. HM can represent a toxicological threat to health or the environment if present at high level. As a group HM are commonly considered to include: Cr, Pb, Hg, Ni, As, Cu, Zn, and Cd (Oladoye et al., 2022).

There is no internationally consistent definition as to what level of contamination constitutes a site being ‘contaminated land’, whether as a result of HM contamination or other forms of contamination. The UK, for example, does not specify quantitative standards (thresholds) to define contamination. Rather, under UK law contaminated land is identified through Part IIA of the Environmental Protection Act 1990, which states that contaminated land is:

“...in such a condition, by reason of substances in, on or under the land that – (a) significant harm is being caused or there is a significant possibility of such harm being caused; or (b) significant pollution of controlled waters is being caused, or there is a significant possibility of such pollution being caused”

(DEFRA, 1990).

This approach establishes a reliance upon risk assessment within the UK system, and effectively mandates the appraisal of ‘source, pathway, receptor’ (S-P-R) relationships to assess the possibility of harm arising, now or in the future. Whilst there are non-statutory Soil Guideline Values (SGV) for a range of contaminants which are suggested to assist within a risk assessment process, these form only part of the assessment framework and the final definition of contaminated land in the UK is ultimately site-specific (EA, 2009).

Internationally, other countries may adopt a different approaches. Many of these are more prescriptive and operate through codifying specific limits for individual contaminants. An example of such an approach can be seen within the framework adopted by Finland which sets three limit values for HM, as follows:

- a ‘*Threshold Value*’ applies to all sites and is used to indicate if further assessment is required;
- a ‘*Higher Guideline Value*’ is applicable to industrial or transport areas; and
- a ‘*Lower Guideline Value*’ is applicable to all other land uses, such as domestic settings.

Details of these statutory values are shown in table 2.1 which give a useful ‘order of magnitude’ reference of what is considered as representing unacceptable risks for different land use options under the Finnish system.

Table 2.1: Finnish statutory threshold and guideline values denoting metals’ contamination in soils (mg/kg) (MEF, 2007)

Element	Threshold Value	Lower Guide-line Value	Higher Guide-line Value
Sb	2	10	50
As	5	50	100
Hg	0.5	2	5
Cd	1	10	20
Co	20	100	250
Cr	100	200	300
Cu	100	150	200
Pb	60	200	750
Ni	50	100	150
Zn	200	250	400
V	100	150	250

A similar approach of codifying threshold values is observed in the United States (US). The National Oceanic and Atmospheric Administration (NOAA) propose a set of guideline values within Screening Quick Reference Tables (SQiRTs) for various environmental media including soils. These tables are intended for preliminary screening purposes only, but provide another basis for identifying potential for establishing if the presence of HM constitutes contaminated land (table 2.2).

Overall, it is estimated that there are 2.5 million potentially contaminated sites in the European Union (EU)(van Liedekerke et al., 2014). Others have estimated that the total land area is 1.2 M km² within the EU with contamination exceeding the relevant threshold for one or more HM, this equates to 28.3% of the land area (Toth et al., 2016b). An estimate has been developed which puts the annual remediation cost for all of this land at around €17.3 billion per year which demonstrates the extent of the liability which contaminated land represents today (CEC, 2006).

Table 2.2: US screening values (“SQiRTs”) for inorganics in soil (mg/kg) (NOAA, 2008)

Element	Background Range	Target Standard	Intervention Standard
Sb	0 – 8.8	3	15
As	0 - 97	0.9	55
Hg	0 – 4.6	0.3	10
Cd	-	0.8	12
Co	70	2.4	180
Cr	-	0.38	220
Cu	0 – 700	3.4	96
Pb	0 – 700	55	530
Ni	0 – 700	260	100
Zn	0 – 0.29%	16	350
V	0 – 500	42	250

2.2.2 Contamination of Agricultural Land

Research estimates that if the Finnish Lower Guideline Value (see above) is applied to agricultural land in Europe that some 137,000 km² is affected by metal contamination, and 2.56% of that land is sufficiently contaminated that it would warrant remediation even if it were to be used for transport or industrial purposes (Toth et al., 2016a).

Similar research conducted in China concluded that c.10% of this nation’s farm land was polluted, with Cd, Hg Cu and Ni being responsible for the bulk of these impacts (Zhang et al., 2015).

The varying systems of defining ‘contaminated land’ discussed above have relevance in a large part to establishing legal liability for pollution and identifying acute pollution risks. However, parallel regulatory systems are adopted in the UK and EU in order to protect the quality of agricultural land. Here the objective is not to regulate acute pollution risks from the land itself, but rather to ensure food security and the safety of the food supply chain. Subsequently, the tolerated thresholds for HM may be much lower. Under the agricultural soil

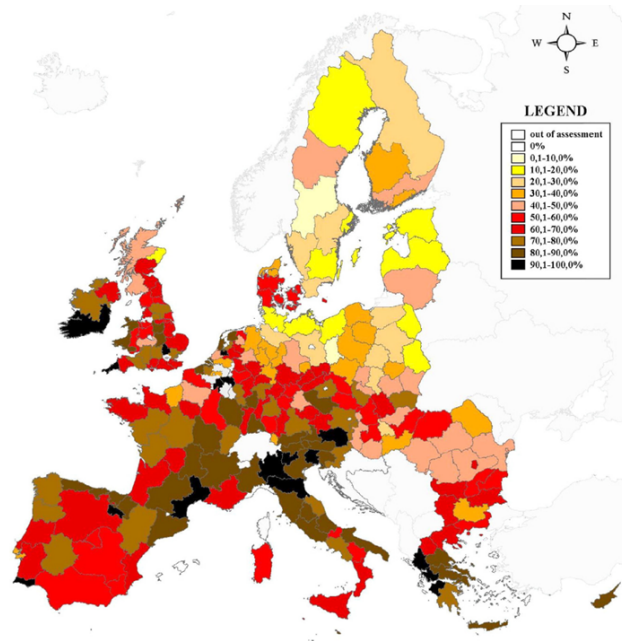


Figure 2.1: Percentage of samples taken from European agricultural land which exceed threshold values for heavy metals (Toth et al., 2016a)

frameworks HM are scaled against soil pH in recognition of metals' increasing mobility and bioavailability under more acidic soil conditions (table 2.3).

Table 2.3: Limits on total HM concentrations in sludge amended soils (mg/kg_(dm)) (DEFRA, 1989)

Metal	pH			
	5.0-5.5	5.5-6.0	6.0-7.0	>7.0
Zn	200	250	300	450
Cu	80	100	1357	200
Ni	50	60	75	110
Cd	3	3	3	3
Pb	300	300	300	300
Hg	1	1	1	1

These regulatory standards aim to provide protection to agricultural soils in-

cluding pasture/grazing land. However, more precise consideration may be given to arable land used for food crop production (table 2.4).

Table 2.4: Guidelines for maximum limits of HM in agricultural soils and vegetables as recommended by World Health Organization (mg/kg_(dm)) (WHO, 1996)

Metal	Agricultural Soil	Vegetables
Ni	0.05	1.0
Cr	0.1	1.3
Pb	0.1	0.1-0.3
Cd	0.003	0.02
Hg	-	0.1

Whilst the WHO figures are not regulations, it can be seen that the suggested thresholds for HM in soil are significantly lower, e.g. for Pb the WHO suggest 0.1 mg/kg versus 300 mg/kg. Furthermore, implicit within the WHO values is a recognition that concentrations within vegetables may be higher than that observed within the soil, i.e. HM may accumulate within plant tissue.

2.3 Sources of Heavy Metals in Agricultural Soil

Clearly HM contamination of agricultural soil has taken place and may be of concern. Whether HM contamination is now a legacy issue or an actual ongoing concern depends on whether there remains a source of continuing soil pollution.

2.3.1 Lithogenic Source

HM occur naturally in many soils as a result of weathering processes acting on the parent rock materials. HM rarely exist in the environment in elemental

state, but rather in the form of complexes with silicates, hydroxides, sulphides, oxides, phosphates and as part of larger organic molecules (Oladoye et al., 2022). Soil weathering through pedogenic processes can also account for HM release into soil however in most environments this would only be expected to result in trace quantities (typically less than 1000 mg/kg) (Kabata-Pendias and Pendias, 2001).

Soil contamination in the Yangtze Delta (China) has been extensively studied in recent years. Zhao et al studied seven HM (Cu, Zn, Pb, Cr, Ni, Cd, and Hg) and concluded that parent rock material explains >27% of spatial variance in the soil concentrations only for Cu & Zn and Cr & Ni (with each pair of elements exhibiting geochemical affinities). Overall, however, lithogenic sources (considered separate from mining related sources) would not be expected to result in widespread concerns for soil quality except under unusual circumstance (Zhao et al., 2010).

2.3.2 Atmospheric Deposition

On long-range scales (national or regional) atmospheric deposition has been identified as perhaps the largest overall flux of HM entering soil (Gray et al., 2003; Pereira et al., 2007). HM contamination can also be heavily influenced at a local level by short-range atmospheric deposition. For example, large fossil fuel combustion plant, metal smelting operations (point sources), roads with high traffic (linear sources) particularly in urbanised environments and proximity to mining operations (area sources) can all result in readily measurable impacts on soil HM concentration (Alloway, 2013).

Atmospheric deposition is regarded as being particularly relevant to some specific HM. For example, studies in China concluded that atmospheric deposition represented the most important input into agricultural soil for Zn and Pb, responsible for 72% and 84% of respective inputs (Hou et al., 2014). Air deposition of Cd is estimated to be 35% of inputs to Chinese soil with the annual flux estimated as being 4 g/ha/year (Luo et al., 2009). Whilst in the EU

the Cd atmospheric deposition rate is considered to be significantly lower, it remains significant at an estimated 0.35 g/ha/year (Six and Smolders, 2014).

Due to the role air deposition has been shown to play in the accumulation of HM in soils over the long-term, a number of studies have tried to estimate total flux attributable to air deposition in western countries (table 2.5).

Table 2.5: Annual mean atmospheric deposition fluxes of HM to soil (mg/m²/year)

Location	Annual Deposit						
	As	Cd	Cr	Cu	Ni	Pb	Zn
England & Wales ¹	0.31	0.19	0.75	5.70	1.60	5.40	22.10
Paris, France ²	-	0.24	-	6.00	0.62	4.20	30.00
Los Angeles, USA ³	-	-	1.68	7.67	1.89	6.90	43.80
References							
¹ (Nicholson et al., 2003); ² (Connan et al., 2013); ³ (Lim et al., 2006)							

HM in the atmosphere are mostly in particulate form or absorbed onto the surface of aerosols. Consequently, particulate deposition is considered to be the dominant mechanism for the flux of HM to the soil from the atmosphere. Atmospheric Hg is the notable exception to this generalisation as 95% is in the vapour phase (Feng et al., 2019). Subsequent deposition may occur via wet and/or dry deposition mechanisms, and interactions between these two mechanisms. A detailed exposition of the mechanistic processes by which air deposition occurs is beyond the scope of this review as it depends on a wide range of specific issues including: particle size, surface, and particle characteristics as well as atmospheric parameters including wind speed, humidity, air stability/turbulence, and temperature (Pacyna, 2008).

2.3.3 Inorganic Wastes

HM contamination can arise from poorly controlled disposal of inorganic wastes, including both solid wastes and effluents from industrial sources. Very large

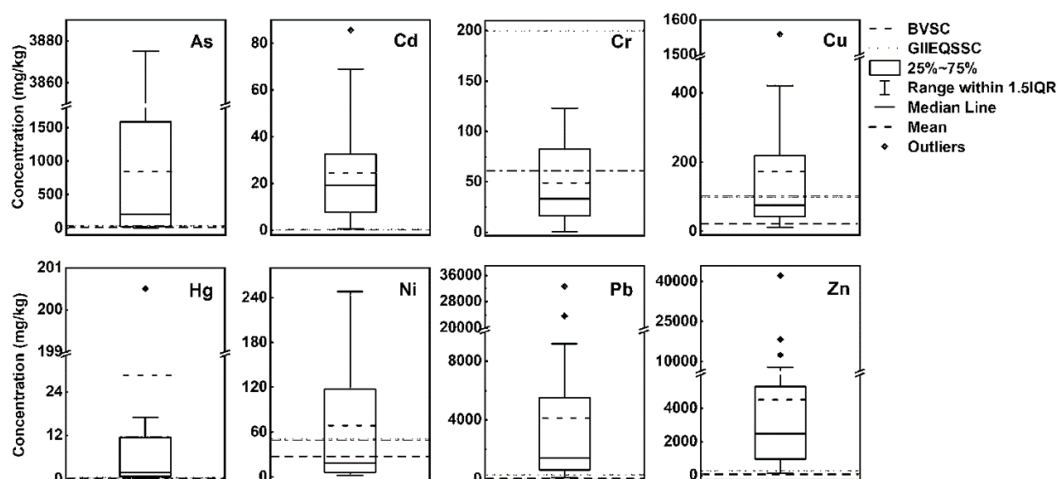


Figure 2.2: Boxplots of the HM concentrations (mg/kg) for Pb/Zn mine tailings (BVSC: Background values for soils in China; GIEQSSC: Grade II environmental quality standard for soils in China) (Kan et al., 2021)

producers of inorganic wastes include the mining sector and smelting industries. HM pollution arising from mine tailings or smelting slag tend to diffuse off-site into surrounding soils in a radial or funnel shape, governed by processes of surface water runoff, leaching and erosion (Luo et al., 2018; Wang et al., 2017).

Kan et al. (2021) characterised the range of different HM associated with Pb and Zn mine tailings (figure 2.2). The tailings were found to contain very high levels not only of Zn and Pb but also Cu, As and Cd. Furthermore, Cu and Ni were also present at elevated levels within the tailing but to a lesser extent. In contrast, Cr was observed only at low levels within the tailings, comparable to the expected background levels observed in soils across China. Zhuang et al. (2009) studied HM soil concentrations around the large polymetallic mine and established that surrounding agricultural land was heavily contaminated with Cu (703 mg/kg), Zn (1100 mg/kg), Pb (386 mg/kg) and Cd (5.5 mg/kg). Indicating that these HM have the potential to move offsite and contaminate the surrounding soils where they are present within mine tailings.

Significant quantities of contaminated slags are produced as a result of smelting

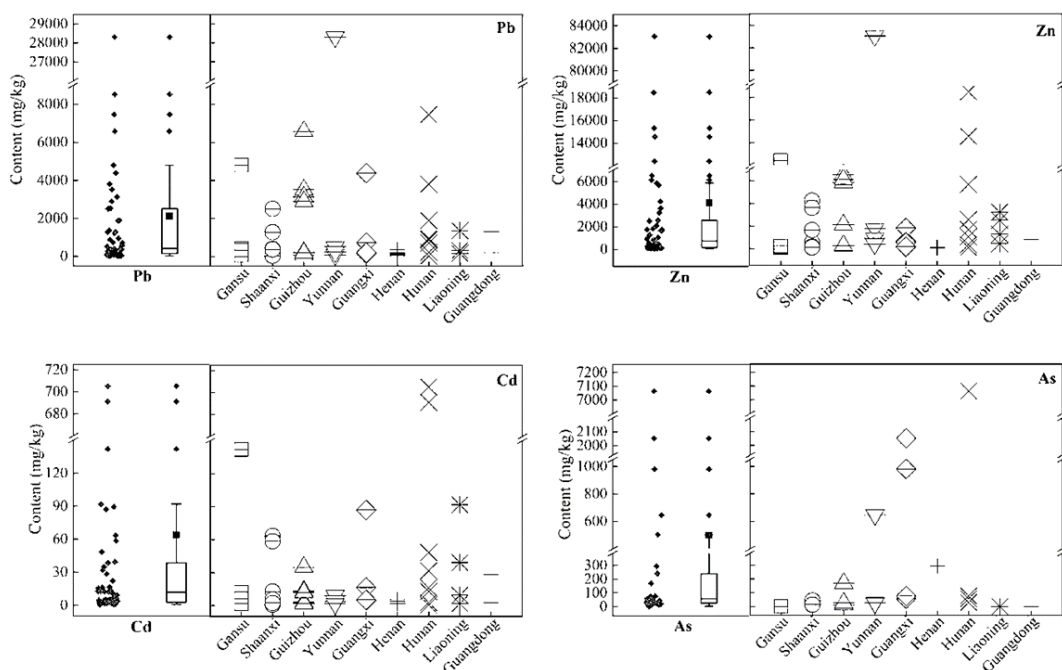


Figure 2.3: HM concentrations in soils surrounding Pb/Zn smelting operations in China (Luo et al., 2023)

operations. It has been estimated that for every 1 tonne of Pb and Zn extracted approximately 0.71-0.96 tonnes of slag are produced (Zhang et al., 2020). In contrast to volatile HM such as Pb, Zn, As which concentrate in flue gas/fly ash (and be associated with air deposition), refractory HM such as Cr are often found in more elevated concentration in the slag material (Křibek et al., 2010). Consequently the chemical profile of smelter slags may be different to that associated with both stack emission and mine tailings pollution sources. Yang et al. researched smelting slags and established consequential increases in HM contamination in local agricultural soils (Yang et al., 2010).

Even after pollution control systems are put in place (which historically may be viewed as comparatively recent), smelting plant may remain sources of significant HM pollution. For example, pre-treatment of the raw ores using hydrometallurgy produce large quantities of wastewater, or where wet flue gas scrubbing technology is employed this results in effluents rich metals (Duan

et al., 2021). Over long timeframes discharge of these wastewaters into the local environment can lead to soil pollution as a result of pore-water advection/convection and diffusion of dissolved species. Due to the chronic persistence in the environment such this leads to HM accumulating in soils around the points of discharge over extended periods of time (Khalil et al., 2013).

2.3.4 Organic Wastes

A unique concern for agricultural land quality is related to the common practice of spreading sewage sludge as a soil fertiliser. It is estimated that 30% of sewage sludge produced in Europe is disposed to agricultural land (Silveira et al., 2003). Whilst this does represent a beneficial use of valuable nutrients, and therefore confers a fertilizer and economic benefit, the discharge of trade and industrial effluents to many urban sewerage networks results in HM being present within the sludge. In this way, the application of sludges can contribute to accumulation of As, Pb, Cu, Cr, Hg, Ni, Se, Mo, Zn, Ti and Sb in agricultural soils (Basta et al., 2005).

A further source of heavy metal contamination of agricultural lands are animal manures. Manures can be rich in As, Co, Cu, Mn and Zn which can accumulate in soil if regularly applied over an extended timeframe, with pig and poultry manures being particularly high in HM (Chaney and Oliver, 1996; Sharma et al., 2017; Sumner, 2000). Collectively sludges and manures are often grouped together under the term ‘biosolids’.

In arid countries the direct irrigation of wastewaters onto arable land may be practiced and can pose similar issue. In parts of Africa and Asia it has been estimated that up to 50% agricultural food production relies on land upon which are irrigated with treated wastewaters (Bjuhr, 2007). Whilst the HM content of treated wastewater is generally low, increasing industrialisation and its continued application to land will lead to accumulation of HM over time. Hou et al. examined input fluxes of HM into the agricultural lands around the Yangtze River and concluded that in this area irrigation was the main source

of As, Cd, Cu and Hg, contributing 60-71% of total inputs of these HM (Hou et al., 2014).

2.3.5 Agrochemicals

Western intensive farming methods are heavily reliant on the use of fertilisers to provide N, P and K for optimised crop production. These fertilisers contain trace amounts of heavy metals, such as Cd, Cr, Hg, Ni, Pb, and Zn (Jones and Jarvis, 1981; Toth et al., 2016a).

In the past several pesticide and fungicidal sprays have both been identified as contributing to historic contamination of heavy metals in agricultural soil. Examples include the use of Cu as sulphate and oxychloride as fungicides, and As and Pb within some pesticides (Jones and Jarvis, 1981; Vhahangwele and Mugeru, 2015).

2.3.6 Metals' Mass Balance for Agricultural Soil

A simple mass balance has been proposed for HM which seeks to classify the sources and sinks of HM in an agricultural context (adapted from (Lombi and Gerzabek, 1998)):

$$M_{total} = (M_p + M_a + M_{ag} + M_{ow} + M_{ip}) - (M_{cr} + M_l) \quad (2.1)$$

where M is the HM within the soil; P is the parent material; a is atmospheric deposition; ag are the agrochemical sources; ow are the organic waste sources; ip are other inorganic pollutants; cr is crop removal; and l is losses by leaching and volatilization.

An overview of the different inputs of HM to the system has been provided in the sections above. The outputs (M_{cr} and M_l) are relevant in the context of phytoremediation strategies discussed in the sections below.

2.4 Remediation Strategies – an Overview

The United States Environmental Protection Agency (USEPA) identify two broad classifications of remediation strategy. Strategies are either ‘containment’ or ‘source control’ interventions (USEPA, 2004). Containment interventions involve engineered constructions designed to prevent the migration of contaminants. Source control is designed to treat or remove contaminants from the soil.

2.4.1 Containment Strategies

Containment strategies can either be implemented *ex situ* or *in situ*. *Ex situ* containment may involve excavation of highly contaminated soil for storage in an engineered containment cell e.g. landfill. Wuana and Okieimen (2011) lists the perceived advantages of *ex situ* strategies as including speed and broad applicability. However, such strategies are highly invasive and require the permanent control of stored wastes. Consequently, *ex situ* strategies are typically only considered in situations representing large ecological or health risks.

In situ containment strategies require the construction of engineered caps, impermeable barriers or liners to prevent the migration of metals offsite. In this way, whilst the source of hazard is not removed, by managing (breaking) the pathway through which contaminants may reach receptors the risk is mitigated to an acceptable level. There are several types of impermeable barriers including soil–bentonite barriers, slurry trench walls, and soil mix technologies (Al-Tabbaa et al., 2012; Yeo et al., 2005). These limit the migration of heavy metals by redirecting or controlling groundwater by establishing barriers with low hydraulic conductivity of between 10^{-7} - 10^{-9} m/s (Du et al., 2021; Jefferis, 2012).

In situ Vitrification is a high-tech containment strategy. Rather than relying on constructed barriers vitrification relies on passing electric current through

the soil to create high temperatures which melt the soil in situ. The current is then removed and the soil is subsequently allowed to cool which encapsulates HM within a resultant glass-like material. The technique can be applied for reclamation of even heavily contaminated soils if sufficient conductance is achievable through the soil matrix. This typically requires the alkali content (Na₂O and K₂O) to be below 1.4 wt% (Buelt and Thompson, 1992). Disadvantages of vitrification include the heat generated by the process introducing the potential to release volatile metal species (e.g. Hg). This means vitrification is rarely applied outside applications with gross contamination of specific non-volatile metals or some radionuclide contaminated soils (USEPA, 1992).

Stabilization is a strategy closely related to containment. Rather than seek to engineer a physical barrier to prevent HM moving offsite, stabilisation encompasses a range of in situ techniques which seek to dramatically reduce the mobility of HM by changing soil properties and/or complexing the HM to minimise leaching or other means of HM moving offsite. A range of amendments may employed to effect HM stabilisation including inorganic binders such as clays, pozzolanic materials including furnace slags and fly ash, iron or manganese oxides, or zeolites which bind with HM making less mobile (Wuana and Okieimen, 2011).

Table 2.6: Inorganic materials for HM immobilisation (Guo et al., 2006)

Material	HM immobilised
Lime	Cd, Cu, Ni, Pb, Zn
Phosphate salt	Pb, Zn, Cu, Cd
Hydroxyapatite	Zn, Pb, Cu, Cd
Fly ash	Cd, Pb, Cu, Zn, Cr
Slag	Cd, Pb, Zn, Cr
Ca-montmorillonite	Zn, Pb
Portland cement	Cr, Cu, Zn, Pb
Bentonite	Pb
Lime	Cd, Cu, Ni, Pb, Zn

Alternatively, stabilisation may be achieved using a selection of organic ma-

terials. Several organic wastes have been proven to hold potential including charcoal, composts or manures (Farrell et al., 2010; Fawzy, 2008).

Table 2.7: Organic materials for HM immobilisation (Guo et al., 2006)

Material	HM immobilised
Bark saw dust	Cd, Pb, Hg, Cu
Xylogen	Zn, Pb, Hg
Chitosan	Cd, Cr, Hg
Bagasse	Pb
Poultry manure	Cu, Pb, Zn, Cd
Cattle manure	Cd
Rice hulls	Cd, Cr, Pb
Sewage sludge	Cd
Leaves	Cr, Cd
Straw	Cd, Cr, Pb

Many of these stabilising amendments are wastes and represent a potentially lower cost solution when compared with the heavily engineered containment strategies mentioned previously. This potentially makes them an economically attractive option on the basis of material cost. Furthermore, in situ stabilisation requires comparatively low labour and energy input if treating shallow soil contamination using conventional excavation equipment (Jasperse and Ryan, 1992).

A simple examination of the types of organic and inorganic amendments employed during stabilisation (tables 2.6 and 2.7) does reveal however that several of the amendments themselves are potential source of HM contamination, as previously mentioned (e.g. poultry manure, sewage sludge, fly ash and slags).

2.4.2 Source Control Strategies

Whilst containment strategies seek to prevent contaminants moving offsite, source control strategies seek to minimise or detoxify the contamination source itself.

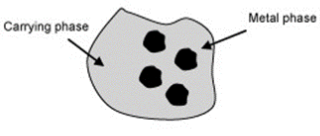
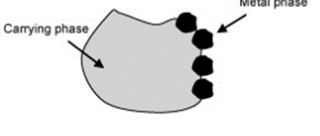
<p>(a)</p> 	<p>Metal phase included in volume</p> <ul style="list-style-type: none"> • Liberation degree is very low • Density depends primarily to minerals of carrying phase • Surface properties are constant but depend to carrying phase • Physical separation is very difficult or impossible • Crushing is required
<p>(b)</p> 	<p>Metal phase associated</p> <ul style="list-style-type: none"> • Liberation degree is medium • Density depends to minerals of metal phase and carrying phase • Surface properties are not constant • Physical separation can be applicable (gravity concentration)
<p>(c)</p> 	<p>Metal phase weakly bounded on surface</p> <ul style="list-style-type: none"> • Liberation degree is medium • Physical separation can be applicable if metal phase particles are liberated by e.g., attrition scrubbing
<p>(d)</p> 	<p>Metal phase liberated or free</p> <ul style="list-style-type: none"> • Liberation degree is very high • Density depends only to minerals of metal phase • Surface properties are constant • Physical separation is applicable (e.g., gravity concentration, froth flotation)

Figure 2.4: Applicability of physical separation according to liberation degree of the HM for the particulate forms (G. et al., 2008)

Soil washing is a group of ex situ processes comprised of physical separation techniques or chemical leaching, or a combination of both, applied to excavated soil. The strategy is to remove or minimise the quantity of contamination. Physical separation uses processing equipment such as mechanical screens, hydrodynamic separators, froth flotation, attrition scrubbing and gravity concentration to achieve a reduction in the volume of soil which represents a hazard (G. et al., 2008). These are standard processing technologies which are widely used in the mineral industry. However, their applicability is specific to the extent and nature of HM liberation relative to the surrounding soil matrix and HM particle size (figures 2.4 and 2.5).

Due the prerequisite for HM to be strongly differentiated from the bulk of the soil, physical separation is primarily applicable to solid waste contaminated sites (e.g. mine tailings, and slags) and are rarely applicable to “natural”

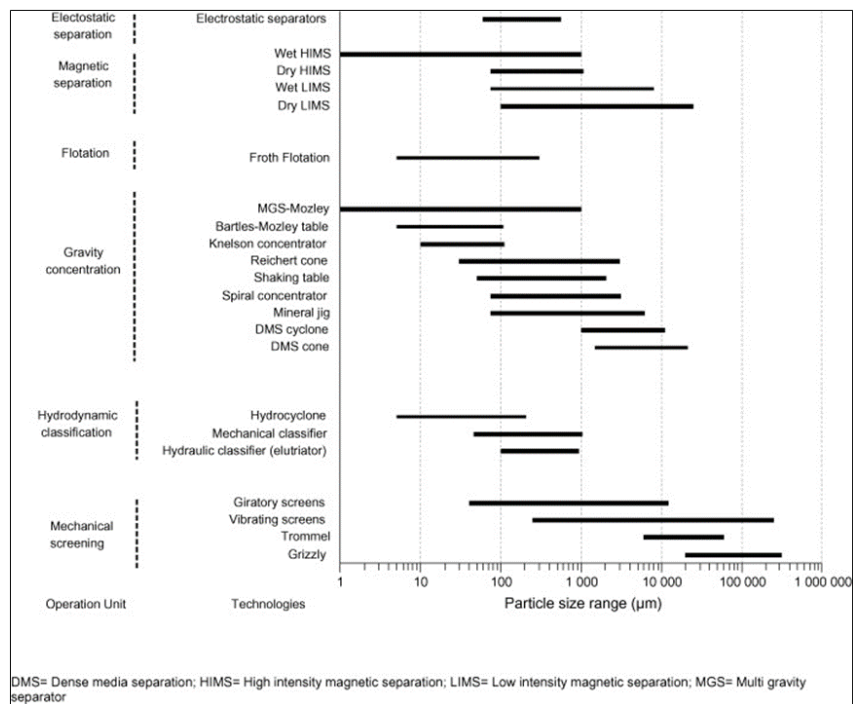


Figure 2.5: Feed particle size range for application of physical separation technique (G. et al., 2008)

soils, such as agricultural soil, impacted by diffuse pollution sources. This is due to HM being typically present in sorbed form within natural soils rather than discrete particles (G. et al., 2008).

Chemical separation strategies also borrow their techniques from the mineral processing industry. Hydro-metallurgy is a technique used recovery of metals from ores or residual materials and the same principles can be applied to soil remediation. Hydro-metallurgy uses aqueous solvents to dissolve and leach out metals to achieve separation. A range of different acids, salts, chelating agents or surfactants may be employed as the solvent (G. et al., 2008). Acids such as hydrochloric acid (HCl) and chelating agents such as ethylene diamine tetra-acetic acid (EDTA) in solution are examples of solvents which have found successful application in removing HM from soils.

The efficacy of chemical separation techniques is strongly influenced by the chemical species of HM in the soils. The sequential extraction of HM from soil is commonly used to determine by their bonding to specific substrates within the soil, and determine whether chemical extraction may be applicable (Dahlin et al., 2002; Venditti et al., 2000). The fractionation of HM in soils is usually assessed using a sequential extraction process, such as the five-stage procedure commonly referred to as “Tessier Extractions”, whereby the following fractions are isolated: (1) exchangeable; (2) carbonates; (3) Fe/Mn oxides; (4) bound to organic matter; and (5) recalcitrant/residual (Isaure et al., 2006; Kumpiene et al., 2017). Generally, the first three extracted fractions (exchangeable, carbonate, and bound to Fe/Mn oxides) are considered potentially suitable for chemical extraction remediation strategies (Peters, 1999), although this may vary according to complex interactions of soil particle size, composition and geochemistry.

Chemical processes have the advantage over physical separation processes in that they can be used to effectively remove HM bound by sorption throughout the soil matrix. Using chemical extraction techniques the metals may even be subsequently recovered. However, there are some significant potential disadvantages, including cost associated with chemical input and waste/sludge

disposal, and chemicals in the residual soil being potentially inappropriate for revegetation (G. et al., 2008). Therefore, chemical extraction may only be justifiable in cases where an acute threat of pollution or harm is apparent.

Permeable Reactive Barriers (PRB) implement an in situ source control strategy, and therefore avoid much of the material handling and disposal costs associated with employing ex situ techniques. PRB seek to intercept the groundwater plume emerging from the source area and ensure it passes through a treatment media, flowing passively via the hydraulic gradient. PRB have been employed for contaminants arising from a variety of sources including agricultural systems, industries and mines. PRB are viewed as a more sustainable intervention for groundwater treatment than ‘pump and treat’ strategies, which were energy intensive over long periods and frequently do not achieve clean up goals (Obiri-Nyarko et al., 2014).

When applied to HM contamination, PRB may achieve treatment of groundwater by adsorption, reduction, surface complexation or precipitation processes within the treatment media. Treatment media employed by PRB for HM contaminated groundwater include zero valent iron (ZVI), granular activated carbon (GAC), zeolites, Transformed Red Mud (TRM) and lime (Blowes et al., 2000; Cappai et al., 2012; Lapointe et al., 2006; Perić et al., 2004; Wilkin and McNeil, 2003).

ZVI iron is the most commonly adopted media accounting for around 60% of PRB installations (ITRC, 2005). It is applicable to HM species where reduction and/or precipitation would result in desirable treatment or removal from groundwater with frequent application used to reduce Cr(VI) to Cr(III), and precipitate As(V) and As(III). Other metal cations potentially treatable by reduction with ZVI include U, Cu and Hg (Blowes et al., 2000; McRae, 1999).

All PRB have a finite treatment capacity, limited by the mass of the treatment media and the flux of total dissolved constituents within the groundwater. The reactive material within the PRB may have its treatment capacity reduced by dissolved species other than the target contaminants and barrier porosity may

be physically compromised by clogging and fouling reducing its permeability. This leads to reduced service life and subsequent increased costs in the long term.

2.4.3 Phytoremediation

Phytoremediation is a comparatively recent concept in the field of land remediation. The concept of phytoremediation was suggested by Chaney in the early 1980s in relation to the uptake of organic wastes by plants grown in contaminated soils (Chaney, 1983). In the following decades the concept was expanded through research to include applications for managing inorganic contaminants such as HM (Chaudhry, 1998; Clemens, 2001; Salt et al., 1995).

Greipsson provides a useful concise definition of phytoremediation as “the use of plants and associated soil microbes to reduce the concentrations or toxic effects of contaminants in the environments” (Greipsson, 2011).

It has been suggested that the benefits of phytoremediation for the management of metals in contaminated soils are threefold (Vangronsveld et al., 2009):

1. the establishment of plants can achieve ‘*phytostabilization*’ of contaminants – a form of risk containment whereby the migration of contaminants offsite is reduced by effecting a change in chemical form to less mobile species, or through their physical entrapment within the soil;
2. ‘*phytoextraction*’ can be achieved whereby metals are removed from the soil by uptake into the plants and may then be disposed or even recovered; and
3. sustainable land management where soil quality gradually improves for subsequent cultivation of crops with higher market value. Others have built upon this concept by suggestion that fast-growing and high-biomass producing plants could be adopted to achieve a multi-purpose remediation strategy combined with bioenergy crop production.

Phytoremediation can occur via several possible mechanisms depending on the contaminant in question, the plants used, and the specific site conditions. Alkorta et al. (2004) identify six different categories of phytoremediation to differentiate these mechanisms (table 2.8). Of the mechanisms by which phytoremediation may operate, some are only achievable in regards to treating organic pollutants (phytovolatilization, phytodegradation, rhizodegradation) and perhaps a very limited number of inorganics (Hg, Se) which may exist in the gas phase under environmental conditions (Padmavathiamma and Li, 2007). These mechanisms are therefore of no relevance to the remediation of most HM. Phytofiltration is relevant only to the treatment groundwater, although it may also be adopted within an engineered wastewater treatment process - referred to as a ‘constructed wetland’ (Shelef et al., 2013).

Table 2.8: Mechanisms of phytoremediation (Alkorta et al., 2004)

Term	Definition
Phytoextraction	Accumulation of pollutants in harvestable aerial biomass i.e. shoots
Phytofiltration	Sequestration of pollutants from water by plants
Phytostabilisation	Limiting the mobility and bioavailability of pollutants in soil by roots
Phytovolatilization	Conversion of pollutants to volatile form and their subsequent release to the atmosphere
Phytodegradation	Degradation of organic xenobiotics by plant enzymes within plant tissues
Rhizodegradation	Degradation of organic xenobiotics in the rhizosphere by microorganisms

Phytostabilisation

Phytostabilisation is one of the mechanisms by which HM contaminated sites can achieve remediation goals. Plants can immobilize HM in the soil by precipitation, complexation or valence reduction (Ghosh and Singh, 2005; Wuana and Okieimen, 2011). These processes are facilitated within the soil by biochemi-

cals produced by plants known as exudates. Exudates are enzymes excreted by roots into the immediately surrounding soil matrix which are critical to nutrient mobilisation (Badri D., 2009). These same exudates can also be responsible for the conversion of HM to relatively less toxic species with lower solubility. Phytostabilisation may also be regarded as having been achieved where HM are sequestered within the root tissue or adsorption onto root cell wall, but do not translocate beyond the below ground plant tissues (Ginn et al., 2008).

The application of selected plants for Cr contaminated soil is an example of a potential phytostabilisation strategy. Chromium contamination can exist in soil as Cr(III) and Cr(VI) forms. Chromium (VI) species such as chromate are highly toxic, relatively soluble and more mobile than Cr(III). However, chromium (VI) is not thermodynamically stable in soils except in alkaline, oxidizing environments, and is readily reduced to Cr(III) (Cary et al., 1977). Chromium is precipitated at higher pH values as Cr(III)-hydroxide and in this form exhibits significantly lower bioavailability, and consequent the risk of harm is greatly reduced. Furthermore in a study 36 plant species no inhibition of plant growth and accumulation in aerial biomass (phytoextraction) of Cr was recorded in the presence of Cr(III) contaminated soils (Shahandeh and Hossner, 2000). It is believed that the active mechanisms ensure that that Cr(VI) species are reduced to Cr(III) and retained either within the rhizosphere in a tightly bound or insoluble form, or in a soluble organic complex by roots where they are retained below ground level (Barlett, 1988).

Phytostabilisation processes do not result in HM translocating throughout the plant, hence HM do not accumulate in the above ground biomass. Consequently, whilst phytostabilisation may be a valid element of HM remediation strategy, it is not directly relevant to the research conducted for this thesis, which focusses HM in the aerial (i.e. harvested) biomass.

Phytoextraction

The defining aspect of the phytoextraction process is a combination of plant uptake of a contaminant from the soil and its subsequent translocation into the above ground biomass. Translocation is a critical aspect of phytoextraction as harvesting roots is not generally feasible, and therefore HM being present in the above ground stems and/or leaves is essential for its removal from a site via harvesting biomass.

The phytoextraction of HM has been studied since the 1980's including As, Cd, Cr, Cu, Ni, Pb and Zn. Their interactions with a wide range of plants have been studied including native plant species (e.g. grasses, ferns and sedges), food crops (e.g. grains, squashes, beets and brassicas) as well as tree species (e.g. poplar and willow) (Rafati et al., 2011; Sekara et al., 2005; Tangahu et al., 2011; Yoon et al., 2006a; Zacchini et al., 2009).

Plants may adopt different responses to the presence of excess HM contaminating soils. Raskin et al. (1994) classified these responses as either '*excluders*', '*indicators*', or '*accumulators*' depending upon the extent to which HM accumulate in the plant's aerial tissues, as represented by figure 2.6. Excluder species resist HM entering and accumulating within their aerial tissues to any significant extent. In effect, this may constitute phytostabilisation as previously discussed. Indicator species actively accumulate HM in aerial tissues in a manner which reflects soil concentrations, whereas accumulators concentrate HM in their aerial tissues sometimes to levels far exceeding that of the soil.

At the top end of the phytoextraction spectrum are species referred to a '*hyperaccumulators*' which display active uptake resulting in very high levels of HM in the aerial tissues. Hyperaccumulators have been defined as plants which contain either: $>0.01\%$ of Cd or other rare metal; $>0.1\%$ ($1000 \text{ mg/g}_{(\text{dm})}$) of Cu, Cd, Cr, Pb, Ni Co; or $>1\%$ ($10,000 \text{ mg/g}_{(\text{dm})}$) Zn or Mn (Baker and Brooks, 1989). Around 400 species of plant have been identified as hyperaccumulators of metals with the highest number of species (87) associated with the Brassicaceae family (encompassing mustards, crucifers and cabbages) (Baker

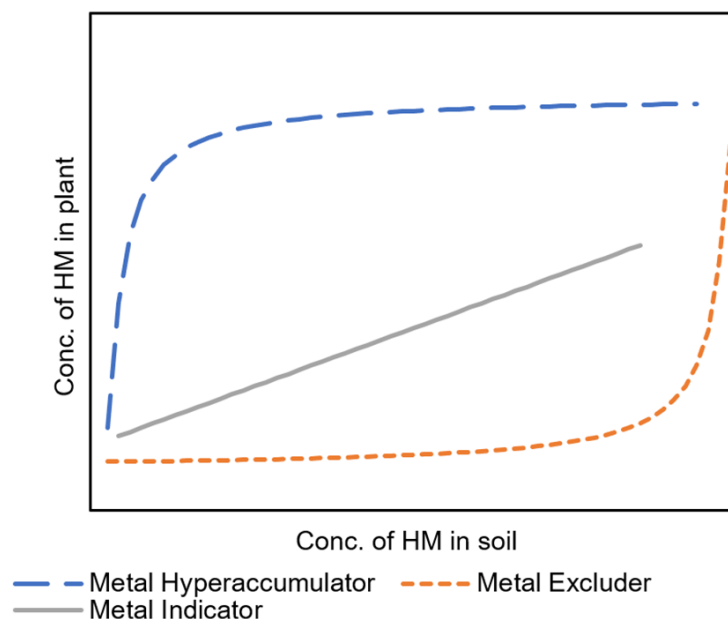


Figure 2.6: Diagrammatic representation of three plant response categories to increasing HM concentrations in soil (Ghosh and Singh, 2005)

et al., 2000).

Research interest into hyperaccumulation has led to attempts to increase phytoextraction of HM through interventions which change soil properties in an engineered manner – sometimes referred to as ‘*induced hyperaccumulation*’. To this end, soil preparation with chemicals such as acidifying agents to reduce soil pH (consequently increasing HM solubility), fertiliser, and chelating agents such as EDTA or malate have been researched to augment the phytoextraction process (Kamnev and Van der Lelie, 2000; Lasat and Kochian, 1997). This can have significant impact: Huang et al observed a 120-fold increase in the uptake of Pb into the aerial shoots of corn grown in soil spiked with EDTA compared to a control group (Huang et al., 1998).

Indicator plants also accumulate HM in aerial tissues. However, with indicator plants the HM concentration within the biomass correlates to metal concentration in the soil (Baker and Walker, 1990). Indicator species may be specific

to individual HM as the same plant species may simultaneously operate as an excluder for other HM.

Table 2.9: Classification of some example HM metallophyte plants

Category	Plant Species	Accumulation	References
Hyper-accumulator	<i>Salicornia maritima</i>	Cu, Zn	(Milić et al., 2012)
	<i>Rhizophora mangle</i>	Hg, Al, As, Cd	
	<i>Laguncularia racemosa</i>	Cr, Cu, Fe, Pb, Mg, Zn	(Mejías et al., 2013)
	<i>Eichhornia crassipes</i> , <i>Ludwigia stolonifera</i> , <i>Echinochloa stagnina</i> , and <i>Phragmites australis</i>	Cd, Ni, Pb	(Eid et al., 2020)
Excluder	<i>Bruguiera gymnorhiza</i>	Cu, Cd	(Wang et al., 2013)
	<i>Atriplex halimus</i>	Ni, Cu, Pb, Zn	Kachout et al. (2012)
Indicator	<i>Phragmites australis</i>	Cd, Cr, Cu, Hg, Mn, Ni, Pb, Zn	(Bonanno and Lo Giudice, 2010)
	<i>Phragmites australis</i> , <i>Typha capensis</i> and <i>Spartina maritima</i>	Cu, Pb, Zn	(Phillips et al., 2015)
	<i>Eichhornia crassipes</i> , <i>Ludwigia stolonifera</i> , <i>Echinochloa stagnina</i> and <i>Phragmites australis</i>	Cd, Ni, Pb	(Eid et al., 2020)

2.4.4 Measuring Plant Suitability for Phytoremediation

The distribution of HM accumulations is not typically uniform throughout all plant tissues. Bonanno et al. investigated the uptake of HM by the common reed (*Phragmites australis*) and demonstrated that different plant organ displayed different trends in HM accumulation, with each showing a positive linear relationship to metal concentration in the growing media. The trend of HM relative concentrations was found to be root > rhizome > leaf > stem. The overall trend of metal concentration was found to be Mn > Zn > Pb > Cu although the organs followed different decreasing trends (Bonanno and Lo Giudice, 2010).

Attempts to quantify the distribution of different HM across plant tissues has led to the development of number of indices which aid classification of plant behaviour:

The Bio-Concentration Factor (BCF) is the ratio of HM concentration in the root of the plant compared to that found within the soil and is calculated as follows (Gupta and Sinha, 2007; Yoon et al., 2006b):

$$BCF = (\text{metal concentration in the plant root}) / (\text{metal concentration in the soil})$$

The plant's ability to translocate HM from the root to the aerial shoots can be quantified using the Translocation Factor (TF), which is defined as the ratio of HM concentration in plant shoots (above ground) versus that in the roots (Deng et al., 2004; Yoon et al., 2006b):

$$TF = (\text{metal concentration in plant shoot}) / (\text{metal concentration in the plant root})$$

Using these first two indices together: plants with a high Bio-Concentration Factor (BCF>1) and simultaneously a low Translocation Factor (TF<1) for the same HM are suitable for phytostabilisation as this is indicative of that HM being extracted from the soil, but strongly retained in the root structures.

Perhaps of most relevance to harvesting of biomass for fuel is a third index which is the Bio-Accumulation Factor (BAF). The BAF is the ratio of HM concentration in the plant shoots (above ground) compared with the HM concentration in the soil. The BAF is useful as if the plants are cropped and removed from site it allows calculations to estimate the removal of contaminants from the site (when combine with biomass yield), and estimates of time taken to achieve a remediation goal. The BAF is calculated as follows (Cui et al., 2007; Li et al., 2007):

$$BAF = (\text{metal concentration in plant shoot}) / (\text{metal concentration in soil})$$

The plants characterized by $BAF > 1$ are accumulators whereas excluders have a $BAF \ll 1$. Furthermore, plants with a high Bio-Accumulation Factor ($BAF \gg 1$) and high biomass yield lend themselves to adoption for phytoextraction, as this indicates a significant overall mass removal of HM from the soil into harvestable biomass.

2.4.5 Relative Costs of Remediation

Accurate data regarding the cost of different remediation strategies is difficult to obtain. Much of this difficulty may be attributed to the unique site conditions preventing balanced comparisons between sites, and opaque reporting of what is included and what is not included in the project costs. Nonetheless, there is some effort within literature to express the relative costs of different remediation options (table 2.10).

Table 2.10: Costs of different remediation options

Process	Rate	Notes
Vitrification	75-45 \$/ton	Long-term monitoring
Landfilling	100-500 \$/ton	Transport/excavation/monitoring
Chemical treatment	100-500 \$/ton	Recycling or contaminants
Phyto-extraction	5-40 \$/ton	Disposal of biomass
Removal, non-hazardous	50-80 £/m ³	Disposed. Excludes landfill tax, general items and backfilling
Removal, hazardous	90-200 £/m ³	Disposed. Excludes any pre-treatment, landfill tax, general items and backfilling
Bio-remediation	10-30 £/m ³	<i>Ex-situ</i> treatment
Thermal desorption	100-250 £/m ³	Minimum 10,000 m ³ set-up
Soil washing	80-150 £/m ³	Treated material
Phyto-remediation	25-100 \$/ton	<i>In-situ</i>
References: (Flathman et al., 1999; Glass, 1999; Saunders and Vernon, 2009)		

Despite the broad range of costs suggested for different treatment options, the biological techniques of phytoremediation (*in-situ*) and bioremediation (*ex-situ*) are consistently the least cost options. These options are listed as being one or two orders of magnitude less expensive than physico-chemical or disposal strategies. Biological techniques, if applicable to the site in question, therefore appear to represent a cost effective remediation strategy.

2.5 Heavy Metals and Plant Uptake

The next sections examine the mechanistic principles governing both the uptake and sequestration of HM within the plants.

Much of the original regulatory framework regarding HM contaminated land were based around total HM content of the soil. However, more recently studies have placed emphasis on the subset of HM which comprise the biologically available (*'bioavailable'*) fraction as distinct from the fraction which is irreversibly bound to the soil matrix. This approach is based upon the assertion that an organism or ecosystem is only adversely impacted the bioavailable HM species which can be absorbed by the organism, and consequently the total HM value may overestimate the risk (Brümmer, 1986; Lanno et al., 2004).

Bioavailability is an important concept, which is directly relevant to plant uptake and therefore phytoremediation. There is no universal definition of bioavailability and no single method for its measurement. Several techniques have been applied in attempts to measure bioavailability including physical (e.g. spectroscopy), chemical (e.g. CaCl_2 extraction), and biological (e.g. bioassay using earthworms) (Kim et al., 2015).

The application of different measurement techniques has led some studies to differentiate bioavailability into *'external bioavailability'* and *'internal bioavailability'*. In this frame of reference, external bioavailability relates to the quantity of HM released from the soil matrix, whereas internal bioavailability is the extent to which HM are absorbed by an organism (including plants) and then exert subsequent toxicological effects (Caussy et al., 2003). Different disciplines may therefore place more emphasis on one or the other, e.g. engineers focussed on soil remediation may emphasise external bioavailability test, whereas a biologist may correlate their results better with internal bioavailability tests.

Time scales are also important to the concept of bioavailability as the quantity of HM which can be released from a soil matrix is influenced by desorption kinetics working to maintain an equilibrium with the pore water from which there may in turn be leaching losses (e.g. phytoextraction or groundwater

flow offsite). Depending on the soil conditions and the HM in question, the transformation from non-accessible/chemically bound form into dissolved (and readily bioavailable) species within soil pore water may take hours, days or even years (Fedotov et al., 2012). Consequently the exposure duration is an influencing factor in determining how much of specific HM is assessed as being bioavailable.

In an attempt to clarify the terminology used, develop understanding across disciplines and standardise the measurement techniques employed, the ISO/TC90 working group described in three steps which span the complete process by which bioavailability occurs, as follows (ISO, 2008):

1. availability of HM in the soil (*'environmental availability'*);
2. uptake of HM by the organism (*'environmental bioavailability'*); and
3. accumulation and toxic effect of HM within the organism (*'toxicological bioavailability'*).

Within this ISO framework 'environmental availability' represents the maximum amount of HM which can be desorbed from the soil matrix under the relevant conditions within a given exposure time. The potential quantity of environmentally available HM will depend upon dynamic interaction between a range of parameters including total metal content, pH, redox conditions, and contents of organic matter, clay minerals, and oxides within the soil. Measurement can be achieved using chemical extraction techniques including neutral salt solutions such as 0.01 M CaCl₂ for relatively mobile HM (e.g. Cd, Ni, Zn) or mild acids such as 0.43 M HNO₃ for low mobile metals (e.g. Cu, Cr, Pb) (Kim et al., 2015). The ISO standard stresses that 'environmental availability' should not be considered as a fixed fraction but as a continuum, as total quantity depends on exposure time.

Environmental bioavailability represents the HM species dissolved in the soil pore water which can be taken up by organisms, i.e. plants in the case of

phytoremediation. Uptake can either be passive (diffusion), or active and enhanced by enzymatic processes e.g. root exudates. Typical HM species in pore water of non-contaminated soils include -Cl, -OH, -CO₃, -SO₄ and bound to Dissolved Organic Carbon (DOC) (Kim et al., 2015). Because environmentally bioavailable HM are in solution, measurement can be achieved directly using spectroscopy (e.g. Atomic Absorption Spectroscopy (AAS)) after pore water extraction, although pre-filtration is recommended to remove colloid-bonded HM as these materials may be relatively recalcitrant and resistant to plant uptake.

Toxicological bioavailability represents accumulation of HM within and subsequent toxic effect upon target organisms. It is the equivalent to ‘internal bioavailability’ previously mentioned and may be determined by bioassays, including plants and earth worms.

A key emphasis of the ISO framework is the recognition that bioavailability is a continuum which spans a dynamic, multi-stage and time-dependant process (figure 2.7).

2.5.1 Heavy Metal Uptake and Sequestration

Plant interaction with soil HM begins outside the plant itself. Plants secrete enzymes known as exudates into the rhizosphere which increase the bioavailability of HM and allow them to mobilise towards and subsequently into the plant tissues. An example of this would be the release of phytosiderophores (PS), a group of organic moieties including mugenic and avinic acids, which solubilise Fe(III) compounds and allow plants to increase uptake via Fe(II) in soils with iron deficiency (Kinnersley, 1993).

The uptake of HM into the plant at the root level is mediated by proteins acting as secondary transporters, including H⁺ coupled carrier proteins inside the root cells’ plasma membrane creating a negative potential, which drive uptake of cations including HM into the cells (Clemens et al., 2002).

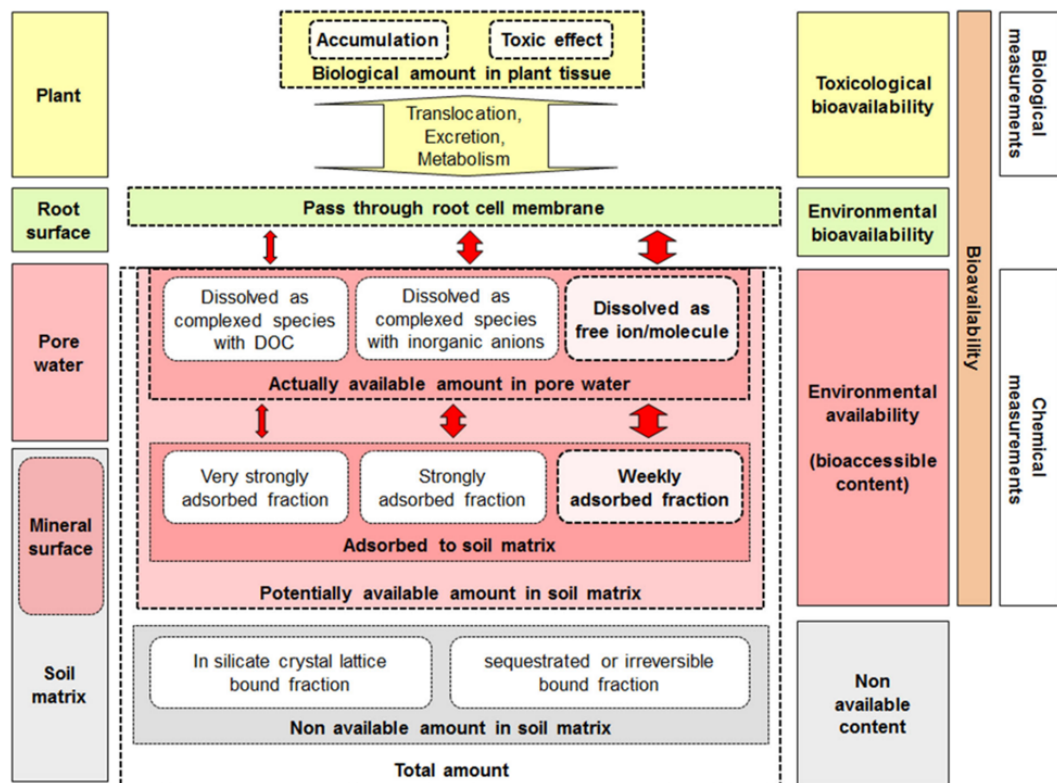


Figure 2.7: Three-step concept of HM bioavailability in soils for plants showing the relationship between ‘environmental availability’, ‘environmental bioavailability’ and ‘toxicological availability’ (Kim et al., 2015)

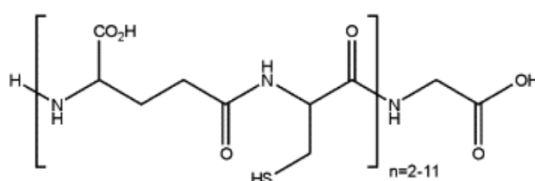


Figure 2.8: Molecular structure of phytochelatin (PC) (Clemens, 2006)

HM which cross the cell plasma membrane and enter cell cytoplasm and require biochemical responses to avoid disruption of cell function. Cellular management of HM within the cytoplasm is facilitated by complexation with high-affinity ligands. Examples of these ligands include: organic and amino acids (including citrate, malate and histidine); and two classes of cysteine-rich peptides – phytochelatin (PC) and metallothioneins (MT) (Hall, 2002).

PC act as HM chelators and consist of three amino acids – cysteine, glycine and glutamic acid – arranged in a $(\gamma\text{-GluCys})_n\text{-Gly}$ configuration. They have been identified in wide range of plants, including both monocot and dicots (Suresh and Ravishankar, 2004). The role and function of PC has perhaps been most extensively researched in relation to plant response to Cd contamination and its sequestration at a cellular level. It has been established that PC bind with Cd^{2+} ions forming low molecular weight PC-Cd complexes which pass into the cell vacuole. In the vacuole the PC-Cd complexes react with sulphides to form high molecular weight PC-Cd-S complexes (Marschner, 1995; Raskin et al., 1997). Final stabilisation within the vacuole involves the incorporation of HM in sulphide form (Rea et al., 1998; Salt and Rauser, 1995).

MT functionally resemble PC in that they both have a high cysteine content leading to them readily forming complexes with HM ions. However, MT do not show a consistent structure and exhibit high heterogeneity regarding both molecular weight, number and distribution of cysteine groups (Raskin et al., 1997). The exact role of MT in sequestering/transport of HM is not fully resolved. MT as chelators may have a role as storage pools for excess HM, or may act as transport proteins in moving HM throughout the plant (LaCoste et al., 2001).

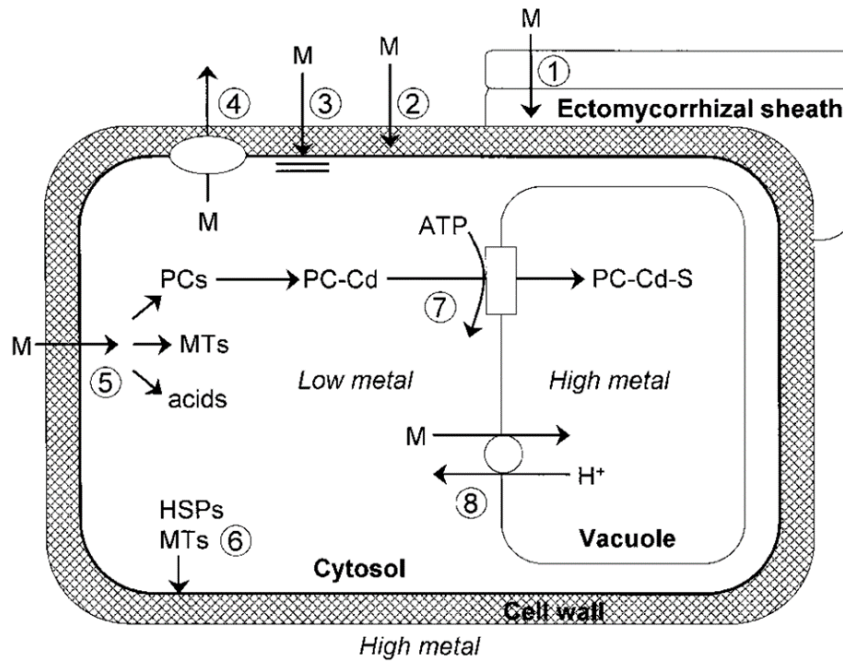


Figure 2.9: Summary of potential cellular mechanisms for heavy metal (M) tolerance in plants with Cd as an example. 1) restriction of movement to roots by mycorrhizas 2) binding to cell wall root and exudates 3) reducing influx across the plasma membrane 4) efflux across the plasma membrane 5) chelation in the cytosol by metallothionines (MT), phytochelatins (PC) and organic acids 6) repair of the plasma membrane 7) transport and sequestration within the vacuole with PC-sulphide complexes (PC-Cd-S) 8) Transport and accumulation within the vacuole (Marschner, 1995)

It is known that the cell wall can also play an important role in plant sequestration of HM at a cellular level. Cell walls are comprised of polysaccharides such as cellulose, hemicellulose, extensin, lignin and pectins, and to a lesser extent proteins, amino acids and phenolics. These compounds encompass a range of functional groups (including $-\text{COOH}$, $-\text{OH}$, and $-\text{SH}$) which can bind to cations such as HM. Within the cell wall the carboxyl group ($-\text{COOH}$) is considered the most important for HM sequestration Krzeslowska (2011).

Plants can respond to HM stress by increasing pectin production to thicken the cell walls and thereby increase their capacity to store HM (Douchiche et al., 2007; Konno et al., 2010; Paynel et al., 2009; Vollenweider et al., 2006;

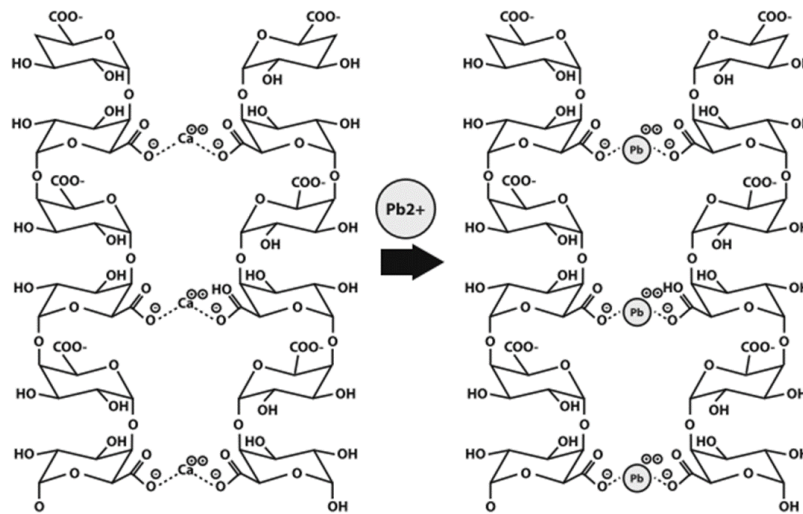


Figure 2.10: Sequestration of Pb^{2+} by cross linking between polymers of pectins displacing the Ca^{2+} bridge (Caffall and Mohnen, 2009)

Wierzbicka et al., 2007). Pectin is known to be a substrate for sequestration of divalent and trivalent cations, such as HM, and typically constitute around 30% of primary cell walls (Krzeslowska, 2011). Pectin is a heteropolysaccharide that comprises four main polysaccharide domains: homogalacturonans (HGA); rhamnogalacturonan I (RGI); rhamnogalacturonan II (RGII); and xylogalacturonans (XGA) (Gawkowska et al., 2018). Of these four domains HGA is believed to be the main pectin domain responsible for binding to divalent and trivalent cations, with HM potentially displacing the calcium bridge to form an egg-box structure (figure 2.10).

Binding studies have attempted to rank the affinities of different cations to pectin and have found different results, but could be as follows: $\text{Al}^{3+} > \text{Cu}^{2+} > \text{Pb}^{2+} > \text{Zn}^{2+} = \text{Ca}^{2+}$ (Dronnet et al., 1996); or, $\text{Cu}^{2+} = \text{Pb}^{2+} > \text{Cd}^{2+} = \text{Zn}^{2+} > \text{Ca}^{2+}$ (Ernst et al., 1992; Fritz, 2007; Kartel et al., 1999). Consistent within these authors' findings is that Cu^{2+} and Pb^{2+} are more strongly bound than Zn^{2+} , Ni^{2+} and Ca^{2+} .

Under conditions of acute HM stress plant response can result in localised cell

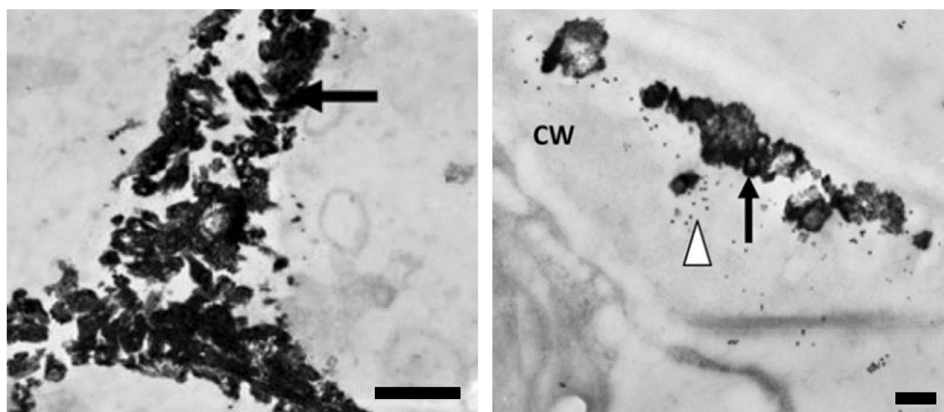


Figure 2.11: TEM images of Pb accumulation in cell walls: left) examples of large crystalline Pb deposits in root cell wall of *Populus tremula x tremuloides* (Scale bar 500 nm); right) Large Pb deposits with localised callose layer deposit at the plasma membrane (white arrow) in *Funaria hygrometrica* (Scale bar 200 nm) (Krzeslowska, 2011)

wall thickening to accommodate increased HM sequestration in the cell wall (Malone et al., 1974; Wierzbicka et al., 2007). Under these conditions large crystalline-like deposits of HM may form. Both Cd and Zn are also known to form similar crystalline deposits which are observable using a Transmission Electron Microscope (TEM) (Carrier et al., 2003; Neumann and zur Nieden, 2001).

2.6 *Miscanthus*

2.6.1 Species Overview

Miscanthus is a genus of perennial grass which contains around 20 species, several of which have been identified as holding economic value, including *M. sinensis*, *M. sacchariflorus*, *M. floridulus* and *M. x giganteus* (Deuter, 2000).

Biochemically *Miscanthus* has a C4 photosynthetic pathway as opposed to the more common C3 pathway found in most higher plant species. Adoption

of the C4 pathway endows a plant with a photosynthetic advantage in hot climates (Beale and Long, 1995). However, in contrast to other C4 species, such as sugar cane (*Saccharum officinarum*), sorghum (*Sorghum vulgare*) or maize (*Zea mays*), *Miscanthus* is able to grow in cool-temperate climates (e.g. 14 - 25°C) making it a crop with potential application across a wide geographic range (Beale et al., 1996; Naidu and Long, 2004).

One of the most productive *Miscanthus* species which is being developed as a commercial energy crop is *Miscanthus x giganteus*. *M. x giganteus* is a sterile triploid inter-specific hybrid between *M. sacchariflorus* and *M. sinensis* (Greef and Deuter, 1993; Hodkinson et al., 2015). The species is characterised by having a low nutrient/fertiliser requirements and the ability to grow on marginal soils which would be poorly suited to food crop production (Evans et al., 2015; Qin et al., 2011). Because of this, *M. x giganteus* has been identified as possessing great potential as a biomass crop: China alone is thought to possess 100 million acres of marginal and degraded land which could be suitable for cultivation of *M. x giganteus* with the potential to produce 1 billion tons of *Miscanthus* biomass fuel (Sang and Zhu, 2011).

2.6.2 Biomass Properties

The chemical composition of *Miscanthus* biomass displays seasonal variability which can be favourably manipulated to enhance combustion characteristics of the final biomass (Baxter et al., 2014; Lewandowski and Heinz, 2003). Research to date has focused on seasonal changes in the major inorganic species (N, S, Cl, K, Ca, Na, Fe, Mg). The major alkaline and earth metal concentrations are significantly lower within aerial (stem and leaf) structures when plants are senescent over winter than in other seasons and this results in changes in the fuel combustion characteristics (Baxter et al., 2012, 2014).

Table 2.11: Typical chemical composition of *Miscanthus* as collated from the Phyllis2 database for biomass and waste (mg/kg_(dm)) (ECN, 2018)

Element	Min	Max	Mean
Al	57.0	160.0	99.3
K	3,027.0	16,400.0	9 072.9
Na	27.0	640.0	307.1
Ca	990.0	2,400.0	1,440.0
Si	2,400.0	10,800.0	7,942.9
Mg	390.0	695.0	506.4
Fe	61.0	190.0	95.6
P	380.0	760.0	552.9
Cl	200.0	6,174.2	2,297.8
As	0.1	1.7	0.8
Cd	0.0	1.2	0.1
Co	0.2	1.2	0.7
Cr	0.4	16.0	3.0
Cu	1.1	5.8	2.2
Mn	7.8	82.0	19.7
Ni	0.9	2.3	1.6
Pb	0.1	10.2	2.4
V	0.2	0.4	0.3
Zn	9.1	33.0	15.5
Ba	1.4	8.0	3.1
Mo	0.5	1.7	0.9
Se	1.0	1.0	1.0
Hg	0.0	0.3	0.0

Different *Miscanthus* species possess different morphological, anatomical and chemical properties which are directly relevant to a species' crop potential (e.g. size, crop yield), biomass properties and therefore fuel characteristics. A detailed and statistically robust analysis of 16 different *Miscanthus* cultivars by Kaack et al. (2003), which included *M. sinensis* and *M. x giganteus*, demonstrated this wide variety of properties across the different species. For example, biomass ash content was found to vary between 0.4 and 3 g/100g_(dm) and lignin ranged from 9.3 to 16.3 g/100g_(dm). Despite these wide variations

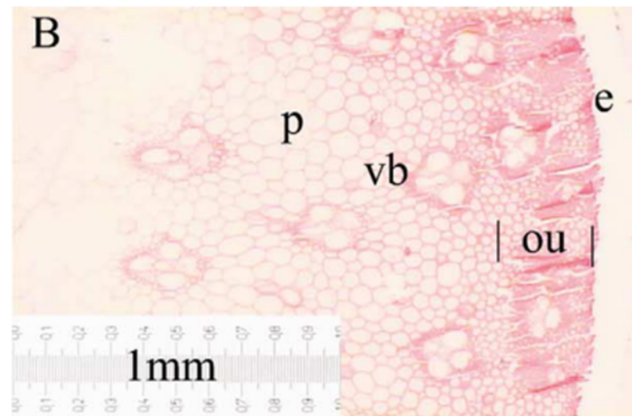


Figure 2.12: Cross section stem of *M. sinensis* stained using Fuchsin, safranine, aniline (FSA); E, epidermis; OU, outer ring; VB, vascular bundle; P, parenchyma (Kaack et al., 2003)

in composition there no significant difference was observed in the Dry Matter (DM) (Kaack et al., 2003).

Kaack et al. also identified significant anatomical differences between the different *Miscanthus* cultivars, for example:

- stem length varying between 109.2 and 249.0 cm
- area of the outer ring ranging between 4.9 and 28.5 mm²
- item area of vascular bundle /100 from 9.6 to 81.1 mm² and
- area of parenchyma from 1.1 to 30.7 mm²

The above-mentioned anatomical features within a *Miscanthus* stem cross section are identified in figure 2.12.

The evidence of Kaack et al. clearly shows the wide range of chemical and morphological characteristics that exist within different *Miscanthus* plants. It is this variation which opens the possibility of optimising biomass properties based upon informed selection of specific species/hybrids.

In a detailed study of eight different species of *M. sinensis* Van der Weijde et al. (2017) examined how different species, with different chemical compositions, affected the performance energy yields of different bioenergy conversion processes. Large differences were found between the cell wall components between different genotypes, which changed further within each species depending on the month cropping occurred, as result of senescence over the winter season.

Van der Weijde et al. (2017) cross correlated these compositional characteristics with the performance of different bioenergy conversion processes. They found that the best performing genotype provided 18% higher biogas yield using AD, whilst using enzymatic saccharification the best performer released 42% more glucose per gram. The key conclusion drawn by the authors is that “*considerable improvements in the techno-economic efficiency of bioconversion processes can be achieved by selecting more suitable feedstocks*” and that the genic diversity of *Miscanthus* allows for extensive variation to be selected.

2.6.3 *Miscanthus* for Phytoremediation

Miscanthus has been identified by the research community as a species with great potential for establishment on contaminated land due to its resistance to contaminants including HM. The extent to which *Miscanthus* phytostabilises or phytoextracts specific HM is variable within the literature and differs with location, soil conditions, time of exposure and level of growth. These aspects produce confounding factors which can make comparisons of data from different studies difficult. There are, however, some broad patterns observable within the literature.

Korzeniowska and Stanislawska-Glubiak (2015) provide data from plants grown in under controlled/engineered soil conditions (table 2.12). It was concluded that *M. x giganteus* operates as an ‘excluder’ species for Cu and Ni demonstrated by low BAF values of 0.01 (Cu) and 0.08 (Ni), and low BCF values of 0.07 (Cu) and 0.40 (Ni). Therefore *M. x giganteus* was considered unsuitable for phytoextraction or phytostabilisation of these HM. In contrast, Zn uptake

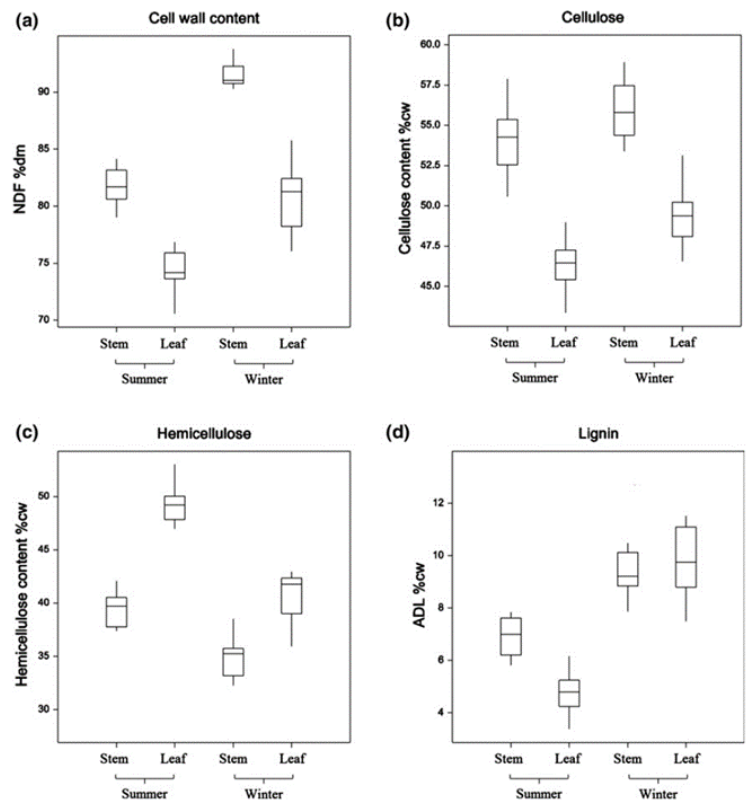


Figure 2.13: Box plots showing variation across *M. sinensis* stem and leaf fraction: (a) cell wall content; (b) cellulose; (c) hemicellulose; and (d) lignin (Kaack et al., 2003)

was found to be variable, with aerial biomass concentrations reaching up to 1086 mg/kg and BAF index reaching up to 1.68 indicating that phytoextraction was occurring. It is noteworthy that the BAF under the same conditions dropped substantially in the same plant in the second season, achieving a BAF of only 0.44.

Wanat et al. (2013) examined the uptake of As, Pb and Sb by various tissues of *M. x giganteus* under controlled growing conditions with a range of concentrations. The BCF for the HM under all conditions was >1 indicating that phytostabilisation is occurring, i.e. metals are accumulating in the roots.

The BAF indices can be calculated and indicate accumulation ($BAF > 1$) of As occurs in the stem and leaf only under low soil concentrations, whereas at higher As concentrations in the soil produce $BAF < 1$ suggesting excess is being excluded at the root level. The BAF for Pb is always < 1 , although it is inversely related to soil concentration indicating again that higher levels of soil contamination are excluded with increasing effectiveness at the root level as the contamination level become more acute.

The pattern of *Miscanthus* producing phytostabilisation, as indicated by high levels of HM accumulating at a root level table 2.12, is consistent across different HM. What is much less clear is the extent to which phytoextraction occurs, i.e. accumulation within the shoots/leaves. Certainly the data show that to a certain extent HM in the aerial biomass increases with increasing soil concentration, but this relationship is not linear. However, due to the relatively low accumulation of HM in the aerial biomass (certainly compared to hyperaccumulating species) it is a view commonly expressed in the literature that the planting of *M. x giganteus* on HM contaminated land is favourable if biofuel use rather than phytoextraction is desired (Korzeniowska and Stanislawski-Glubiak, 2015; Nsanganwimana et al., 2014; Pidlisnyuk et al., 2014; Pogrzeba et al., 2013).

Table 2.12: Uptake of HM by *Miscanthus* versus total and bioavailable soil concentration (mg/kg)

HM	Species	Soil (bio.)	Tissue	Bio- mass	Reference
Zn	<i>M. x giganteus</i>	68(7.5)	Roots	20	(Barbosa et al., 2015)
			Shoots	23	
		457(165)	Roots	78	
	<i>Miscanthus sp.</i>	912(357)	Shoots	65	
			Roots	18	
		50-1927	Roots	61-801	
Shoots	13-605				
As	<i>M. x giganteus</i>	83000(2.1)	Roots	1284	(Wanat et al., 2013)
			Stems	5	
		Leaves	17		
	1727(10)	Roots	602		
		Stem	4		
		Leaves	4		
Pb	<i>M. x giganteus</i>	15200(134)	Roots	327	(Wanat et al., 2013)
			Stem	30	
		Leaves	43		
	325(19)	Roots	38		
		Stem	1		
		Leaves	1		
Cd	<i>Miscanthus sp.</i>	20.8(1.2) (0.4)	Shoots	4	(Pogrzeba et al., 2013)
			Roots	103	
			Stem	3	
Cr	<i>M. sacchariflor</i>	125	Roots	9	(Li et al., 2014)
			Shoots	35	
		250	Roots	9	
	Shoots		35		
	500	Roots	11		
		Shoots	47		

2.6.4 Biofuel Standards for Heavy Metals

Critical to the justification of adopting *Miscanthus* as a bioenergy crop suitable for harvesting from HM contaminated lands is the viability/marketability of the subsequent biomass. A key market for *Miscanthus* biomass is combustion processes for energy recovery. It is therefore relevant to consider the quality of *Miscanthus* biomass produced relative to an applicable biofuel standard.

Energy markets other than combustion have been investigated for *Miscanthus* biomass, in particular Anaerobic Digestion (AD) (Mangold et al., 2019; Purdy et al., 2017; Wagner et al., 2019). However, there are no industry quality standards per se for material inputs to AD processes. Generally, AD are registered as waste treatment processes, so as long as inputs are not deemed ‘Hazardous Waste’ then they may be accepted. It is beyond the scope of this review to go into detail regarding waste definitions. However, even if component substances, such as an HM, are deemed ‘Toxic if Swallowed’ (hazardous statement H301) then a threshold of 5% (50,000 mg/kg) would have to be exceeded for a material to be considered hazardous (EA, 2021).

There are quality standards for biomass materials for combustion processes. These contain standards for many aspects of fuel quality including maximum permissible thresholds for HM. An applicable ISO standard which may be applied to a *Miscanthus* biomass product is ISO 17225-6 (table 2.13).

Table 2.13: Specifications for threshold HM concentrations from “Solid Bio-fuels — Fuel Specifications and Classes — Part 6: Graded Non-Woody Briquettes” (17225, 2014) (mg/kg_(dm))

Metal	Threshold
As	1
Cd	0.5
Cr	50
Cu	20
Pb	10
Hg	0.1
Ni	10
Zn	100

As can be seen from the ISO standard, the permissible threshold for HM in biomass is low (<0.1 mg/kg in the case of Hg). Typical *Miscanthus* biomass composition (table 2.11) is well below the ISO standard thresholds for HM. However, literature data for *Miscanthus* biomass (stem/leaves) grown in contaminated soils does not universally comply with the standard (table 2.12). More specifically, the literature reveals that the concentration of Zn (up to 1,086 mg/kg), Pb (up to 43 mg/kg), Cd (up to 3 mg/kg) and As (up to 17 mg/kg) have all been observed to exceed the ISO standard by previous studies. Consequently, the economic justification of adopting *Miscanthus* as part of a management strategy for HM contaminated sites may depend on achieving suitable biomass quality for subsequent sale.

2.7 Conclusions

The literature shows that HM contamination is a significant problem. The issue is not restricted to post-industrial sites and there are ongoing fluxes of HM to agricultural land. This, combined with their persistent nature in the environment, means that HM accumulation remains an ongoing problem. HM within agricultural soils may become problematic at concentrations which are much lower than would be case for other land uses due to potential uptake by plants allowing HM to enter the food chain. Many traditional engineered interventions for soil contamination are costly and highly resource intensive.

Whilst they may be suitable for a site which represent acute environmental risks they may not be justified for addressing lower levels of pollutions. Phytoremediation has been identified as a cost effective means of remediating HM contaminated land. More recently the opportunity to combine phytoremediation with the production of bioenergy crops has been identified as a potentially enhanced solution for the management of sites.

The literature indicates that *Miscanthus* is a viable species to adopt as part of a remediation strategy, acting to either stabilise or extract different HM. However, *Miscanthus* accumulates certain HM (Zn, As, Pb, Cd) in the aerial biomass to the extent that they may impact the quality of the subsequent biofuel. Understanding how this accumulation of these specific HM occurs within *Miscanthus* may therefore be important in order to manage biomass quality, and thereby ensure the viability of a combined bioenergy/phytoremediation land use strategy. The literature also shows that *Miscanthus* species demonstrate a wide range of anatomical and biochemical variation. It has been demonstrated that taking advantage of these variations in *Miscanthus* to optimise biofuel composition and performance is possible for some applications.

2.8 References

- 17225, I. (2014). Iso 17225-6 - solid biofuels - fuel specifications and classes part 6: graded non-woody pellets.
- Al-Tabbaa, A., Liska, M., Ouellet-Plamondon, C., Jegandan, S., Shrestha, R., Barker, P., McGall, R., and Critchlow, C. (2012). *Soil mix technology for integrated remediation and ground improvement: from laboratory work to field trials*, pages 522–532.
- Alkorta, I., Hernández-Allica, J., Becerril, J. M., Amezaga, I., Albizu, I., and Garbisu, C. (2004). Recent findings on the phytoremediation of soils contaminated with environmentally toxic heavy metals and metalloids such as zinc, cadmium, lead, and arsenic. *Reviews in Environmental Science and Biotechnology*, 3(1):71–90.
- Alloway, B. (2013). *Heavy Metals in Soils: Trace Metals and Metalloids in Soils and their Bioavailability*. Springer Netherlands.
- Badri D., V. J. (2009). Regulation and function of root exudates. *Plant, cell and environment*.
- Baker, A. J. M., McGrath, S. P., Reeves, R. D., Smith, J. A. C., Terry, N., and Bañuelos, G. (2000). Phytoremediation of contaminated soil and water. *Phytoremediation of contaminated soil and water*.
- Baker, A. J. M. and Walker, P. L. (1990). Ecophysiology of metal uptake by tolerant plants. *Heavy metal tolerance in plants: evolutionary aspects.*, pages 155–177.
- Barbosa, B., Boléo, S., Sidella, S., Costa, J., Duarte, M. P., Mendes, B., Cosentino, S. L., and Fernando, A. L. (2015). Phytoremediation of heavy metal-contaminated soils using the perennial energy crops miscanthus spp. and arundo donax l. *Bioenergy Research*, 8(4):1500–1511. Cited By :28
Export Date: 1 August 2018.

- Barlett, J. R. (1988). *Mobility and bioavailability of chromium in soils*, volume 20, page 267.
- Basta, N. T., Ryan, J. A., and Chaney, R. L. (2005). Trace element chemistry in residual-treated soil: Key concepts and metal bioavailability. *Journal of environmental quality*, 34(1):49–63.
- Baxter, X. C., Darvell, L. I., Jones, J. M., Barraclough, T., Yates, N. E., and Shield, I. (2012). Study of miscanthus x giganteus ash composition - variation with agronomy and assessment method. *Fuel*, 95(1):50–62. 897bm Times Cited:24 Cited References Count:38.
- Baxter, X. C., Darvell, L. I., Jones, J. M., Barraclough, T., Yates, N. E., and Shield, I. (2014). Miscanthus combustion properties and variations with miscanthus agronomy. *Fuel*, 117:851–869. A 262vv Times Cited:22 Cited References Count:25.
- Beale, C. V., Bint, D. A., and Long, S. P. (1996). Leaf photosynthesis in the c-4-grass miscanthus x giganteus, growing in the cool temperate climate of southern england. *Journal of Experimental Botany*, 47(295):267–273. Ua121 Times Cited:83 Cited References Count:30.
- Beale, C. V. and Long, S. P. (1995). Can perennial c-4 grasses attain high efficiencies of radiant energy-conversion in cool climates. *Plant Cell and Environment*, 18(6):641–650. Rd749 Times Cited:170 Cited References Count:31.
- Bjuhr, J. (2007). Trace metals in soils irrigated with waste water in a periurban area downstream hanoi city, vietnam.
- Blowes, D. W., Ptacek, C. J., Benner, S. G., McRae, C. W. T., Bennett, T. A., and Puls, R. W. (2000). Treatment of inorganic contaminants using permeable reactive barriers. *Journal of contaminant hydrology*, 45(1-2):123–137.
- Bonanno, G. and Lo Giudice, R. (2010). Heavy metal bioaccumulation by the organs of phragmites australis (common reed) and their potential use as contamination indicators. *Ecological Indicators*, 10(3):639–645.

- Brümmer, G. W. (1986). *Heavy metal species, mobility and availability in soils*, pages 169–192. Springer.
- Buelt and Thompson (1992). The in situ vitrification integrated program: Focusing on an innovative solution on environmental restoration needs. Report, Battelle Pacific Northwest Laboratory.
- Caffall, K. H. and Mohnen, D. (2009). The structure, function, and biosynthesis of plant cell wall pectic polysaccharides. *Carbohydr Res*, 344(14):1879–900. Caffall, Kerry Hosmer Mohnen, Debra eng Research Support, U.S. Gov't, Non-P.H.S. Review Netherlands 2009/07/21 09:00 Carbohydr Res. 2009 Sep 28;344(14):1879-900. doi: 10.1016/j.carres.2009.05.021. Epub 2009 Jun 2.
- Cappai, G., De Gioannis, G., Muntoni, A., Spiga, D., and Zijlstra, J. J. P. (2012). Combined use of a transformed red mud reactive barrier and electrokinetics for remediation of cr/as contaminated soil. *Chemosphere*, 86(4):400–408.
- Carrier, P., Baryla, A., and Havaux, M. (2003). Cadmium distribution and microlocalization in oilseed rape (brassica napus) after long-term growth on cadmium-contaminated soil. *Planta*, 216(6):939–50. Carrier, Patrick Baryla, Aurore Havaux, Michel eng Germany 2003/04/11 05:00 Planta. 2003 Apr;216(6):939-50. doi: 10.1007/s00425-002-0947-6. Epub 2002 Nov 26.
- Cary, E. E., Allaway, W. H., and Olson, O. E. (1977). Control of chromium concentrations in food plants. 1. absorption and translocation of chromium by plants. *Journal of Agricultural and Food Chemistry*, 25(2):300–304. doi: 10.1021/jf60210a048.
- Caussy, D., Gochfeld, M., Gurzau, E., Neagu, C., and Ruedel, H. (2003). Lessons from case studies of metals: investigating exposure, bioavailability, and risk. *Ecotoxicology and environmental safety*, 56(1):45–51.
- CEC (2006). Impact assessment of the thematic strategy on soil protection. Report.

- Chaney, R. L. (1983). Plant uptake of inorganic waste. *Land treatment of hazardous wastes*.
- Chaney, R. L. and Oliver, D. P. (1996). *Sources, potential adverse effects and remediation of agricultural soil contaminants*, pages 323–359. Springer.
- Chaudhry, T. M. (1998). Phytoremediation: focusing on accumulator plants that remediate metal contaminated soils. *Australas. J. Ecotoxicol.*, 4:3–51.
- Clemens, S. (2001). Developing tools for phytoremediation: towards a molecular understanding of plant metal tolerance and accumulation. *International journal of occupational medicine and environmental health*, 14(3):235–239.
- Clemens, S. (2006). Evolution and function of phytochelatin synthases. *Journal of Plant Physiology*, 163(3):319–332.
- Clemens, S., Palmgren, M. G., and Krämer, U. (2002). A long way ahead: understanding and engineering plant metal accumulation. *Trends in plant science*, 7(7):309–315.
- Connan, O., Maro, D., Hébert, D., Roupsard, P., Goujon, R., Letellier, B., and Le Cavelier, S. (2013). Wet and dry deposition of particles associated metals (cd, pb, zn, ni, hg) in a rural wetland site, marais vernier, france. *Atmospheric Environment*, 67:394–403.
- Cui, S., Zhou, Q. X., and Chao, L. (2007). Potential hyperaccumulation of pb, zn, cu and cd in enduring plants distributed in an old smeltery, northeast china. *Environmental Geology*, 51(6):1043–1048. 123vf Times Cited:66 Cited References Count:27.
- Dahlin, C. L., Williamson, C. A., Collins, W. K., and Dahlin, D. C. (2002). Sequential extraction versus comprehensive characterization of heavy metal species in brownfield soils. *Environmental Forensics*, 3(2):191–201.
- DEFRA (1989). Sludge (use in agriculture) regulations (si1263).
- DEFRA (1990). Environmental protection act, part iia.

- Deng, H., Ye, Z. H., and Wong, M. H. (2004). Accumulation of lead, zinc, copper and cadmium by 12 wetland plant species thriving in metal-contaminated sites in china. *Environmental Pollution*, 132(1):29–40. 847hz Times Cited:350 Cited References Count:31.
- Deuter, M. (2000). Breeding approaches to improvmenet of yield and quality in miscanthus grown in europe. *European Miscanthus Improvement (EMI) Project*, page 25.
- Douchiche, O., Rihouey, C., Schaumann, A., Driouich, A., and Morvan, C. (2007). Cadmium-induced alterations of the structural features of pectins in flax hypocotyl. *Planta*, 225(5):1301–1312. 147mg Times Cited:51 Cited References Count:48.
- Dronnet, V. M., Renard, C. M. G. C., Axelos, M. A. V., and Thibault, J. F. (1996). Heavy metals binding by pectins: selectivity, quantification and characterisation. *Pectins and Pectinases*, 14:535–540. Bj39g Times Cited:9 Cited References Count:0 Progress in Biotechnology.
- Du, Y.-J., Shen, S.-Q., Tian, K., and Yang, Y.-L. (2021). Effect of polymer amendment on hydraulic conductivity of bentonite in calcium chloride solutions. *Journal of Materials in Civil Engineering*, 33(2):04020452.
- Duan, X., Li, X., Li, Y., Qi, X., Li, G., Lu, Z., and Yang, N. (2021). Separation and stabilization of arsenic in copper smelting wastewater by zinc slag. *Journal of Cleaner Production*, 312:127797.
- EA (2009). Using soil guideline values. techreport SC050021/SGV introduction, Environment Agency.
- EA (2021). Guidance on the classification and assessment of waste.
- ECN (2018). Phyllis2, database for biomass and waste.
- Eid, E. M., Galal, T. M., Sewelam, N. A., Talha, N. I., and Abdallah, S. M. (2020). Phytoremediation of heavy metals by four aquatic macrophytes and their potential use as contamination indicators: A comparative assessment. *Environmental Science and Pollution Research*, 27(11):12138–12151.

- Ernst, W. H. O., Verkleij, J. A. C., and Schat, H. (1992). Metal tolerance in plants. *Acta botanica neerlandica*, 41(3):229–248.
- Evans, S. G., Ramage, B. S., DiRocco, T. L., and Potts, M. D. (2015). Greenhouse gas mitigation on marginal land: a quantitative review of the relative benefits of forest recovery versus biofuel production. *Environ Sci Technol*, 49(4):2503–11. Evans, Samuel G Ramage, Benjamin S DiRocco, Tara L Potts, Matthew D eng Research Support, Non-U.S. Gov't Review Environ Sci Technol. 2015 Feb 17;49(4):2503-11. doi: 10.1021/es502374f. Epub 2015 Jan 29.
- Farrell, M., Perkins, W. T., Hobbs, P. J., Griffith, G. W., and Jones, D. L. (2010). Migration of heavy metals in soil as influenced by compost amendments. *Environmental pollution*, 158(1):55–64.
- Fawzy, E. M. (2008). Soil remediation using in situ immobilisation techniques. *Chemistry and Ecology*, 24(2):147–156.
- Fedotov, P. S., Kördel, W., Miró, M., Peijnenburg, W. J. G. M., Wennrich, R., and Huang, P.-M. (2012). Extraction and fractionation methods for exposure assessment of trace metals, metalloids, and hazardous organic compounds in terrestrial environments. *Critical Reviews in Environmental Science and Technology*, 42(11):1117–1171.
- Feng, W., Guo, Z., Peng, C., Xiao, X., Shi, L., Zeng, P., Ran, H., and Xue, Q. (2019). Atmospheric bulk deposition of heavy metal(loid)s in central south china: Fluxes, influencing factors and implication for paddy soils. *Journal of Hazardous Materials*, 371:634–642.
- Flathman, P. E., Lanza, G. R., and Glass, D. J. (1999). Phytoremediation issue. *Soil and Groundwater Cleanup*, 2:4–11.
- Fritz, E. (2007). Measurement of cation exchange capacity (cec) of plant cell walls by x-ray microanalysis (edx) in the transmission electron microscope. *Microsc Microanal*, 13(4):233–44. Fritz, Eberhard eng 2007/07/20 09:00 Microsc Microanal. 2007 Aug;13(4):233-44. doi: 10.1017/S1431927607070420.

- G., D., Bergeron, M., Mercier, G., and Richer-Laffèche, M. (2008). Soil washing for metal removal: A review of physical/chemical technologies and field applications. *Journal of Hazardous Materials*, 152(1):1–31.
- Gawkowska, D., Cybulska, J., and Zdunek, A. (2018). Structure-related gelling of pectins and linking with other natural compounds: A review. *Polymers*, 10(7). Gr3wo Times Cited:5 Cited References Count:154.
- Ghosh, M. and Singh, S. (2005). A review on phytoremediation of heavy metals and utilization of its byproducts. *Applied Ecology and Environemntal Research*, 3(1):1–18.
- Ginn, B. R., Szymanowski, J. S., and Fein, J. B. (2008). Metal and proton binding onto the roots of fescue rubra. *Chemical Geology*, 253(3):130–135.
- Glass, D. (1999). U.s. and international markets for phytoremediation, 1999-2000. Report, D. Glass Associates.
- Gray, C. W., McLaren, R. G., and Roberts, A. H. C. (2003). Atmospheric accessions of heavy metals to some new zealand pastoral soils. *Science of The Total Environment*, 305(1):105–115.
- Greef, J. M. and Deuter, M. (1993). Syntaxonomy of miscanthus-x-giganteus greef-et-deu. *Angewandte Botanik*, 67(3-4):87–90. Ma815 Times Cited:181 Cited References Count:0.
- Greipsson, S. (2011). Phytoremediation. *Nature Education Knowledge*, 3(10):7.
- Guo, G., Zhou, Q., and Ma, L. Q. (2006). Availability and assessment of fixing additives for the in situ remediation of heavy metal contaminated soils: a review. *Environmental monitoring and assessment*, 116(1):513–528.
- Gupta, A. K. and Sinha, S. (2007). Phytoextraction capacity of the plants growing on tannery sludge dumping sites. *Bioresource Technology*, 98(9):1788–1794. 144ud Times Cited:95 Cited References Count:25.

- Hall, J. L. (2002). Cellular mechanisms for heavy metal detoxification and tolerance. *J Exp Bot*, 53(366):1–11. Hall, J L eng Review England 2001/12/13 10:00 J Exp Bot. 2002 Jan;53(366):1-11.
- Hodkinson, T. R., Klaas, M., Jones, M. B., Prickett, R., and Barth, S. (2015). Miscanthus: a case study for the utilization of natural genetic variation. *Plant Genetic Resources-Characterization and Utilization*, 13(3):219–237. Cw5kw Times Cited:7 Cited References Count:178.
- Hou, Q., Yang, Z., Ji, J., Yu, T., Chen, G., Li, J., Xia, X., Zhang, M., and Yuan, X. (2014). Annual net input fluxes of heavy metals of the agroecosystem in the yangtze river delta, china. *Journal of Geochemical Exploration*, 139:68–84.
- Huang, J. W., Blaylock, M. J., Kapulnik, Y., and Ensley, B. D. (1998). Phytoremediation of uranium-contaminated soils: role of organic acids in triggering uranium hyperaccumulation in plants. *Environmental science and technology*.
- Isaure, M.-P., Fayard, B., Sarret, G., Pairis, S., and Bourguignon, J. (2006). Localization and chemical forms of cadmium in plant samples by combining analytical electron microscopy and x-ray spectromicroscopy. *Spectrochimica Acta Part B: Atomic Spectroscopy*, 61(12):1242–1252.
- ISO (2008). 17402 soil quality—requirements and guidance for the selection and application of methods for the assessment of bioavailability of contaminants in soil and soil materials.
- ITRC (2005). Permeable reactive barriers: Lessons learned/new directions. (ITRC).
- Jasperse, B. H. and Ryan, C. R. (1992). Stabilization and fixation using soil mixing. pages 1273–1284. ASCE.
- Jefferis, S. (2012). *Cement-bentonite slurry systems*, pages 1–24.
- Jones, L. H. P. and Jarvis, S. C. (1981). The fate of heavy metals. *The chemistry of soil processes*, pages 593–620.

- Kaack, K., Schwarz, K. U., and Brander, P. E. (2003). Variation in morphology, anatomy and chemistry of stems of miscanthus genotypes differing in mechanical properties. *Industrial Crops and Products*, 17(2):131–142. 651cc Times Cited:35 Cited References Count:37.
- Kabata-Pendias, A. and Pendias, H. (2001). Trace metals in soils and plants, crc press. *Boca Raton, Fla, USA*.
- Kachout, S. S., Mansoura, A. B., Mechergui, R., Leclerc, J. C., Rejeb, M. N., and Ouerghi, Z. (2012). Accumulation of cu, pb, ni and zn in the halophyte plant atriplex grown on polluted soil. *Journal of the Science of Food and Agriculture*, 92(2):336–342. <https://doi.org/10.1002/jsfa.4581>.
- Kamnev, A. A. and Van der Lelie, D. (2000). Chemical and biological parameters as tools to evaluate and improve heavy metal phytoremediation. *Bioscience Reports*, 20(4):239–258.
- Kan, X., Dong, Y., Feng, L., Zhou, M., and Hou, H. (2021). Contamination and health risk assessment of heavy metals in china’s lead–zinc mine tailings: A meta–analysis. *Chemosphere*, 267:128909.
- Kartel, M. T., Kupchik, L. A., and Veisov, B. K. (1999). Evaluation of pectin binding of heavy metal ions in aqueous solutions. *Chemosphere*, 38(11):2591–2596. 178nt Times Cited:85 Cited References Count:5.
- Khalil, A., Hanich, L., Bannari, A., Zouhri, L., Pourret, O., and Hakkou, R. (2013). Assessment of soil contamination around an abandoned mine in a semi-arid environment using geochemistry and geostatistics: pre-work of geochemical process modeling with numerical models. *Journal of Geochemical Exploration*, 125:117–129.
- Kim, R.-Y., Yoon, J.-K., Kim, T.-S., Yang, J. E., Owens, G., and Kim, K.-R. (2015). Bioavailability of heavy metals in soils: definitions and practical implementation—a critical review. *Environmental Geochemistry and Health*, 37(6):1041–1061.

- Kinnersley, A. M. (1993). The role of phytochelates in plant growth and productivity. *Plant growth regulation*, 12(3):207–218.
- Konno, H., Nakashima, S., and Katoh, K. (2010). Metal-tolerant moss scopelophila cataractae accumulates copper in the cell wall pectin of the protonema. *Journal of Plant Physiology*, 167(5):358–364. 577eg Times Cited:33 Cited References Count:42.
- Korzeniowska, J. and Stanislawska-Glubiak, E. (2015). Phytoremediation potential of miscanthus × giganteus and spartina pectinata in soil contaminated with heavy metals. *Environmental Science and Pollution Research*, 22(15):11648–11657. Cited By :14 Export Date: 1 August 2018.
- Krzeslowska, M. (2011). The cell wall in plant cell response to trace metals: polysaccharide remodeling and its role in defense strategy. *Acta Physiologiae Plantarum*, 33(1):35–51. 703rb Times Cited:161 Cited References Count:134.
- Kumpiene, J., Giagnoni, L., Marschner, B., Denys, S., Mench, M., Adriaensen, K., Vangronsveld, J., Puschenreiter, M., and Renella, G. (2017). Assessment of methods for determining bioavailability of trace elements in soils: A review. *Pedosphere*, 27(3):389–406.
- Kříbek, B., Majer, V., Veselovský, F., and Nyambe, I. (2010). Discrimination of lithogenic and anthropogenic sources of metals and sulphur in soils of the central-northern part of the zambian copperbelt mining district: a topsoil vs. subsurface soil concept. *Journal of geochemical Exploration*, 104(3):69–86.
- LaCoste, C., Robinson, B., and Brooks, R. (2001). Uptake of thallium by vegetables: Its significance for human health, phytoremediation, and phytomining. *Journal of Plant Nutrition*, 24(8):1205–1215.
- Lanno, R., Wells, J., Conder, J., Bradham, K., and Basta, N. (2004). The bioavailability of chemicals in soil for earthworms. *Ecotoxicology and environmental safety*, 57(1):39–47.

- Lapointe, F., Fytas, K., and McConchie, D. (2006). Efficiency of bauxsol™ in permeable reactive barriers to treat acid rock drainage. *Mine Water and the Environment*, 25(1):37–44.
- Lasat, M. M. and Kochian, L. V. (1997). Potential for phytoextraction of 137cs from a contaminated soil. *Plant and soil*, 195(1):99–106.
- Leung, H. M., Ye, Z. H., and Wong, M. H. (2007). Survival strategies of plants associated with arbuscular mycorrhizal fungi on toxic mine tailings. *Chemosphere*, 66(5):905–915. 130wm Times Cited:57 Cited References Count:42.
- Lewandowski, I. and Heinz, A. (2003). Delayed harvest of miscanthus—influences on biomass quantity and quality and environmental impacts of energy production. *European Journal of Agronomy*, 19(1):45–63.
- Li, C., Xiao, B., Wang, Q. H., Yao, S. H., and Wu, J. Y. (2014). Phytoremediation of zn- and cr-contaminated soil using two promising energy grasses. *Water, Air, and Soil Pollution*, 225(7). Cited By :12 Export Date: 1 August 2018.
- Li, M. S., Luo, Y. P., and Su, Z. Y. (2007). Heavy metal concentrations in soils and plant accumulation in a restored manganese mineland in guangxi, south china. *Environmental Pollution*, 147(1):168–175. 153za Times Cited:158 Cited References Count:48.
- Lim, J.-H., Sabin, L. D., Schiff, K. C., and Stolzenbach, K. D. (2006). Concentration, size distribution, and dry deposition rate of particle-associated metals in the los angeles region. *Atmospheric Environment*, 40(40):7810–7823.
- Lombi, E. and Gerzabek, M. H. (1998). Determination of mobile heavy metal fraction in soil: Results of a pot experiment with sewage sludge. *Communications in Soil Science and Plant Analysis*, 29(17-18):2545–2556. doi: 10.1080/00103629809370133.

- Luo, L., Ma, Y., Zhang, S., Wei, D., and Zhu, Y.-G. (2009). An inventory of trace element inputs to agricultural soils in china. *Journal of Environmental Management*, 90(8):2524–2530.
- Luo, L., Shen, Y., Wang, X., Chu, B., Xu, T., Liu, Y., Zeng, Y., and Liu, J. (2018). Phytoavailability, bioaccumulation, and human health risks of metal(loid) elements in an agroecosystem near a lead-zinc mine. *Environmental Science and Pollution Research*, 25(24):24111–24124.
- Luo, X., Wu, C., Lin, Y., Li, W., Deng, M., Tan, J., and Xue, S. (2023). Soil heavy metal pollution from pb/zn smelting regions in china and the remediation potential of biomineralization. *Journal of Environmental Sciences*, 125:662–677.
- Malone, C., Koeppe, D. E., and Miller, R. J. (1974). Localization of lead accumulated by corn plants. *Plant Physiol*, 53(3):388–94. Malone, C Koeppe, D E Miller, R J eng 1974/03/01 00:00 Plant Physiol. 1974 Mar;53(3):388-94. doi: 10.1104/pp.53.3.388.
- Mangold, A., Lewandowski, I., Hartung, J., and Kiesel, A. (2019). Miscanthus for biogas production: Influence of harvest date and ensiling on digestibility and methane hectare yield. *Global Change Biology Bioenergy*, 11(1):50–62. Sp. Iss. SI Hk9cx Times Cited:2 Cited References Count:35.
- Marschner, H. (1995). *Mineral nutrition of higher plants*. Academic Press, London, 2nd edition.
- McRae, C. W. T. (1999). Evaluation of reactive materials for in situ treatment of arsenic (iii), arsenic (v) and selenium (vi) using permeable reactive barriers: Laboratory study.
- MEF (2007). Government decree on the assessment of soil contamination and remediation needs. Report.
- Mejías, C. L., Musa, J. C., and Otero, J. (2013). Exploratory evaluation of retranslocation and bioconcentration of heavy metals in three species of

- mangrove at las cucharillas marsh, puerto rico. *Journal of Tropical Life Science*, 3(1):14–22.
- Milić, D., Luković, J., Ninkov, J., Zeremski-Škorić, T., Zorić, L., Vasin, J., and Milić, S. (2012). Heavy metal content in halophytic plants from inland and maritime saline areas. 7(2):307–317.
- Naidu, S. L. and Long, S. P. (2004). Potential mechanisms of low-temperature tolerance of c-4 photosynthesis in miscanthus x giganteus: an in vivo analysis. *Planta*, 220(1):145–155. 868uh Times Cited:65 Cited References Count:62.
- Neumann, D. and zur Nieden, U. (2001). Silicon and heavy metal tolerance of higher plants. *Phytochemistry*, 56(7):685–92. Neumann, D zur Nieden, U eng England 2001/04/21 10:00 Phytochemistry. 2001 Apr;56(7):685-92.
- Nicholson, F. A., Smith, S. R., Alloway, B. J., Carlton-Smith, C., and Chambers, B. J. (2003). An inventory of heavy metals inputs to agricultural soils in england and wales. *Science of the total environment*, 311(1-3):205–219.
- NOAA (2008). Screening quick reference tables.
- Nsanganwimana, F., Pourrut, B., Mench, M., and Douay, F. (2014). Suitability of miscanthus species for managing inorganic and organic contaminated land and restoring ecosystem services. a review. *Journal of Environmental Management*, 143:123–134. Cited By :42 Export Date: 1 August 2018.
- Obiri-Nyarko, F., Grajales-Mesa, S. J., and Malina, G. (2014). An overview of permeable reactive barriers for in situ sustainable groundwater remediation. *Chemosphere*, 111:243–259.
- Oladoye, P. O., Olowe, O. M., and Asemoloye, M. D. (2022). Phytoremediation technology and food security impacts of heavy metal contaminated soils: A review of literature. *Chemosphere*, 288:132555.
- Pacyna, J. M. (2008). *Atmospheric Deposition*, pages 275–285. Academic Press, Oxford.

- Padmavathiamma, P. K. and Li, L. Y. (2007). Phytoremediation technology: Hyper-accumulation metals in plants. *Water Air and Soil Pollution*, 184(1-4):105–126. 203yr Times Cited:266 Cited References Count:161.
- Paynel, F., Schaumann, A., Arkoun, M., Douchiche, O., and Morvan, C. (2009). Temporal regulation of cell-wall pectin methylesterase and peroxidase isoforms in cadmium-treated flax hypocotyl. *Annals of Botany*, 104(7):1363–1372. 523na Times Cited:24 Cited References Count:71.
- Pereira, P. A. d. P., Lopes, W. A., Carvalho, L. S., da Rocha, G. O., de Carvalho Bahia, N., Loyola, J., Quiterio, S. L., Escaleira, V., Arbilla, G., and de Andrade, J. B. (2007). Atmospheric concentrations and dry deposition fluxes of particulate trace metals in salvador, bahia, brazil. *Atmospheric Environment*, 41(36):7837–7850.
- Perić, J., Trgo, M., and Medvidović, N. V. (2004). Removal of zinc, copper and lead by natural zeolite—a comparison of adsorption isotherms. *Water research*, 38(7):1893–1899.
- Peters, R. W. (1999). Chelant extraction of heavy metals from contaminated soils. *Journal of Hazardous materials*, 66(1-2):151–210.
- Phillips, D. P., Human, L. R. D., and Adams, J. B. (2015). Wetland plants as indicators of heavy metal contamination. *Marine Pollution Bulletin*, 92(1):227–232.
- Pidlisnyuk, V., Stefanovska, T., Lewis, E. E., Erickson, L. E., and Davis, L. C. (2014). Miscanthus as a productive biofuel crop for phytoremediation. *Critical Reviews in Plant Sciences*, 33(1):1–19. doi: 10.1080/07352689.2014.847616.
- Pogrzeba, M., Krzyzak, J., and Sas-Nowosielska, A. (2013). Environmental hazards related to miscanthus x giganteus cultivation on heavy metal contaminated soil. volume 1. Cited By :8 Export Date: 1 August 2018.
- Purdy, S. J., Maddison, A. L., Nunn, C. P., Winters, A., Timms-Taravella, E., Jones, C. M., Clifton-Brown, J. C., Donnison, I. S., and Gallagher,

- J. A. (2017). Could miscanthus replace maize as the preferred substrate for anaerobic digestion in the united kingdom? future breeding strategies. *Glob Change Biol Bioenergy*, 9(6):1122–1139. Purdy, Sarah J Maddison, Anne L Nunn, Christopher P Winters, Ana Timms-Taravella, Emma Jones, Charlotte M Clifton-Brown, John C Donnison, Iain S Gallagher, Joe A eng BB/G016216/1/Biotechnology and Biological Sciences Research Council/United Kingdom BBS/E/W/00003134E/Biotechnology and Biological Sciences Research Council/United Kingdom England Glob Change Biol Bioenergy. 2017 Jun;9(6):1122-1139. doi: 10.1111/gcbb.12419. Epub 2017 Jan 21.
- Qin, Z., Zhuang, Q., Zhu, X., Cai, X., and Zhang, X. (2011). Carbon consequences and agricultural implications of growing biofuel crops on marginal agricultural lands in china. *Environ Sci Technol*, 45(24):10765–72. Qin, Zhangcai Zhuang, Qianlai Zhu, Xudong Cai, Ximing Zhang, Xiao eng Research Support, U.S. Gov't, Non-P.H.S. Environ Sci Technol. 2011 Dec 15;45(24):10765-72. doi: 10.1021/es2024934. Epub 2011 Nov 28.
- Rafati, M., Khorasani, N., Moattar, F., Shirvany, A., Moraghebi, F., and Hosseinzadeh, S. (2011). Phytoremediation potential of populus alba and morus alba for cadmium, chromuim and nickel absorption from polluted soil. *International Journal of Environmental Research*, 5(4):961–970.
- Raskin, I., Kumar, P. B. A. N., Dushenkov, S., and Salt, D. E. (1994). Bioconcentration of heavy metals by plants. *Current Opinion in biotechnology*, 5(3):285–290.
- Raskin, I., Smith, R. D., and Salt, D. E. (1997). Phytoremediation of metals: using plants to remove pollutants from the environment. *Current opinion in biotechnology*, 8(2):221–226.
- Rea, P. A., Li, Z. S., Lu, Y. P., Drozdowicz, Y. M., and Martinoia, E. (1998). From vacuolar gs-x pumps to multispecific abc transporters. *Annual Review of Plant Physiology and Plant Molecular Biology*, 49:727–760. Zv082 Times Cited:224 Cited References Count:121.

- Salt, D. E., Blaylock, M., Kumar, N. P. B. A., Dushenkov, V., Ensley, B. D., Chet, I., and Raskin, I. (1995). Phytoremediation: a novel strategy for the removal of toxic metals from the environment using plants. *Bio/technology*, 13(5):468–474.
- Salt, D. E. and Rauser, W. E. (1995). Mgatp-dependent transport of phytochelatins across the tonoplast of oat roots. *Plant Physiology*, 107(4):1293–1301. Qt402 Times Cited:276 Cited References Count:22.
- Sang, T. and Zhu, W. X. (2011). China’s bioenergy potential. *Global Change Biology Bioenergy*, 3(2):79–90. 728de Times Cited:58 Cited References Count:96.
- Saunders, D. and Vernon, D. (2009). Cost model: Land remediation.
- Sekara, A., Poniedzialek, M., Ciura, J., and Jedrszczyk, E. (2005). Cadmium and lead accumulation and distribution in the organs of nine crops: implications for phytoremediation. *Polish Journal of Environmental Studies*, 14(4):509–516.
- Shahandeh, H. and Hossner, L. R. (2000). Plant screening for chromium phytoremediation. *International Journal of Phytoremediation*, 2(1):31–51. doi: 10.1080/15226510008500029.
- Sharma, B., Sarkar, A., Singh, P., and Singh, R. P. (2017). Agricultural utilization of biosolids: A review on potential effects on soil and plant grown. *Waste Management*, 64:117–132.
- Shelef, O., Gross, A., and Rachmilevitch, S. (2013). Role of plants in a constructed wetland: current and new perspectives. *Water*, 5(2):405–419.
- Silveira, M. L. A., Alleoni, L. R. F., and Guilherme, L. R. G. (2003). Biosolids and heavy metals in soils. *Scientia Agricola*, 60:793–806.
- Six, L. and Smolders, E. (2014). Future trends in soil cadmium concentration under current cadmium fluxes to european agricultural soils. *Science of the Total Environment*, 485:319–328.

- Sumner, M. E. (2000). Beneficial use of effluents, wastes, and biosolids. *Communications in soil science and plant analysis*, 31(11-14):1701–1715.
- Suresh, B. and Ravishankar, G. A. (2004). Phytoremediation - a novel and promising approach for environmental clean-up. *Critical Reviews in Biotechnology*, 24(2-3):97–124. 851xj Times Cited:151 Cited References Count:194.
- Tangahu, B. V., Sheikh Abdullah, S. R., Basri, H., Idris, M., Anuar, N., and Mukhlisin, M. (2011). A review on heavy metals (as, pb, and hg) uptake by plants through phytoremediation. *International Journal of Chemical Engineering*, 2011.
- Toth, G., Hermann, T., Da Silva, M. R., and Montanarella, L. (2016a). Heavy metals in agricultural soils of the european union with implications for food safety. *Environment International*, 88:299–309. Df4yu Times Cited:81 Cited References Count:47.
- Toth, G., Hermann, T., Szatmari, G., and Pasztor, L. (2016b). Maps of heavy metals in the soils of the european union and proposed priority areas for detailed assessment. *Science of the Total Environment*, 565:1054–1062. Dp0uv Times Cited:32 Cited References Count:33.
- USEPA (1992). Vitrification technologies for treatment of hazardous and radioactive waste handbook. technical report epa/625/r-92/002.
- USEPA (2004). Treatment technologies for site cleanup: Annual status report. Report, EPA-542-R-03.
- Van der Weijde, T., Kiesel, A., Iqbal, Y., Muylle, H., Dolstra, O., Visser, R. G. F., Lewandowski, I., and Trindade, L. M. (2017). Evaluation of miscanthus sinensis biomass quality as feedstock for conversion into different bioenergy products. *Global Change Biology Bioenergy*, 9(1):176–190. Sp. Iss. SI Ef3ia Times Cited:19 Cited References Count:52.
- van Liedekerke, M., Prokop, G., Rabl-Berger, S., Kibblewhite, M., and Louwagie, G. (2014). Progress in the management of contaminated sites in europe. Report.

- Venditti, D., Durecu, S., and Berthelin, J. (2000). A multidisciplinary approach to assess history, environmental risks, and remediation feasibility of soils contaminated by metallurgical activities. part a: Chemical and physical properties of metals and leaching ability. *Archives of environmental contamination and toxicology*, 38(4):411–420.
- Vhahangwele, M. and Mugeru, G. W. (2015). Journal of environmental chemical engineering the potential of ball-milled south african bentonite clay for attenuation of heavy metals from acidic wastewaters: Simultaneous. *Biochem. Pharmacol.*, 3:2416–2425.
- Vollenweider, P., Cosio, C., Gunthardt-Goerg, M. S., and Keller, C. (2006). Localization and effects of cadmium in leaves of a cadmium-tolerant willow (*salix viminalis* l.) part ii microlocalization and cellular effects of cadmium. *Environmental and Experimental Botany*, 58(1-3):25–40. 089ve Times Cited:96 Cited References Count:83.
- Wagner, M., Mangold, A., Lask, J., Petig, E., Kiesel, A., and Lewandowski, I. (2019). Economic and environmental performance of miscanthus cultivated on marginal land for biogas production. *Global Change Biology Bioenergy*, 11(1):34–49. Sp. Iss. SI Hk9cx Times Cited:4 Cited References Count:82.
- Wanat, N., Austruy, A., Joussein, E., Soubrand, M., Hitmi, A., Gauthier-Moussard, C., Lenain, J. F., Vernay, P., Munch, J. C., and Pichon, M. (2013). Potentials of miscanthus x giganteus grown on highly contaminated technosols. *Journal of Geochemical Exploration*, 126:78–84. 300yk Times Cited:29 Cited References Count:35.
- Wang, L., Ji, B., Hu, Y., Liu, R., and Sun, W. (2017). A review on in situ phytoremediation of mine tailings. *Chemosphere*, 184:594–600.
- Wang, P., Menzies, N. W., Lombi, E., McKenna, B. A., de Jonge, M. D., Donner, E., Blamey, F. P. C., Ryan, C. G., Paterson, D. J., Howard, D. L., James, S. A., and Kopittke, P. M. (2013). Quantitative determination of metal and metalloids spatial distribution in hydrated and fresh roots of cowpea using synchrotron-based x-ray fluorescence microscopy. *Science of the*

Total Environment, 463:131–139. 236ww Times Cited:24 Cited References Count:43.

WHO (1996). Trace elements in human nutrition and health. Report.

Wierzbicka, M. H., Przedpelska, E., Ruzik, R., Ouerdane, L., Polec-Pawlak, K., Jarosz, M., Szpunar, J., and Szakiel, A. (2007). Comparison of the toxicity and distribution of cadmium and lead in plant cells. *Protoplasma*, 231(1-2):99–111. Wierzbicka, M H Przedpelska, E Ruzik, R Ouerdane, L Polec-Pawlak, K Jarosz, M Szpunar, J Szakiel, A eng Comparative Study Austria 2007/03/21 09:00 Protoplasma. 2007;231(1-2):99-111. doi: 10.1007/s00709-006-0227-6. Epub 2007 Mar 20.

Wilkin, R. T. and McNeil, M. S. (2003). Laboratory evaluation of zero-valent iron to treat water impacted by acid mine drainage. *Chemosphere*, 53(7):715–725.

Wuana, R. A. and Okieimen, F. E. (2011). Heavy metals in contaminated soils: A review of sources, chemistry, risks and best available strategies for remediation. *ISRN Ecology*, 2011:402647.

Yang, Y., Li, S., Bi, X., Wu, P., Liu, T., Li, F., and Liu, C. (2010). Lead, zn, and cd in slags, stream sediments, and soils in an abandoned zn smelting region, southwest of china, and pb and s isotopes as source tracers. *Journal of Soils and Sediments*, 10(8):1527–1539.

Yeo, S.-S., Shackelford, C. D., and Evans, J. C. (2005). Consolidation and hydraulic conductivity of nine model soil-bentonite backfills. *Journal of Geotechnical and Geoenvironmental Engineering*, 131(10):1189–1198.

Yoon, J., Cao, X., Zhou, Q., and Ma, L. Q. (2006a). Accumulation of pb, cu, and zn in native plants growing on a contaminated florida site. *Science of the total environment*, 368(2-3):456–464.

Yoon, J., Cao, X. D., Zhou, Q. X., and Ma, L. Q. (2006b). Accumulation of pb, cu, and zn in native plants growing on a contaminated florida site.

Science of the Total Environment, 368(2-3):456–464. 080tg Times Cited:576
Cited References Count:25.

Zacchini, M., Pietrini, F., Scarascia Mugnozza, G., Iori, V., Pietrosanti, L., and Massacci, A. (2009). Metal tolerance, accumulation and translocation in poplar and willow clones treated with cadmium in hydroponics. *Water, Air, and Soil Pollution*, 197(1):23–34.

Zhang, P., Muhammad, F., Yu, L., Xia, M., Lin, H., Huang, X., Jiao, B., Shiao, Y., and Li, D. (2020). Self-cementation solidification of heavy metals in lead-zinc smelting slag through alkali-activated materials. *Construction and Building Materials*, 249:118756.

Zhang, X., Zhong, T., Liu, L., and Ouyang, X. (2015). Impact of soil heavy metal pollution on food safety in china. *PLoS One*, 10(8):e0135182.

Zhao, Y., Wang, Z., Sun, W., Huang, B., Shi, X., and Ji, J. (2010). Spatial interrelations and multi-scale sources of soil heavy metal variability in a typical urban–rural transition area in yangtze river delta region of china. *Geoderma*, 156(3):216–227.

Zhuang, P., McBride, M. B., Xia, H., Li, N., and Li, Z. (2009). Health risk from heavy metals via consumption of food crops in the vicinity of dabaoshan mine, south china. *Science of The Total Environment*, 407(5):1551–1561.

Chapter 3

Materials and Techniques

3.1 Introduction

This chapter sets out the range of materials and techniques which underpin the experimental aspects of this project. Sources and production of key materials are described in detail. An overview of the theory underpinning both the general laboratory techniques and the synchrotron X-ray techniques employed is provided. The exact details, instruments and settings used in each experiment are described more precisely in the methods sub-sections of the results chapters which follow.

3.2 Materials

There are two origins of materials used for this project:

- those associated with a field trial site, and
- those associated with a pot trial conducted at the University of Leeds.

The field trial site is located at Bytom, near Katowice in Poland (Lat/Long: 50°20'43.0"N 18°57'19.6"E) shown in figure 3.1. Samples were provided for the project under agreement with Terravesta and Energene.

There are large scale mining/excavation operations 1 km to the northeast of the site which continue to the present day, and several smaller excavations c.600 m to the south

The Bytom site has been subject to an ongoing research project (Miscomar) studying Miscanthus cultivation, managed by the Institute for Ecology of Industrial Areas (IETU), Katowice, Poland (Krzyzak et al., 2017; Rusinowski et al., 2019). This research was financed by The Polish National Centre for Research and Development (grant agreement No. FACCE SURPLUS/MISCOMAR/01/16) under the flag of Era-Net Cofund FACCE SURPLUS, in the frame of the Joint Programming Initiative on Agriculture, Food Security and Climate Change (FACCE-JPI).



Figure 3.1: map of Poland showing location of Bytom (TUBS, 2011)



Figure 3.2: aerial image of the Bytom site and surrounding area

3.2.1 Field Trial Soil

A random grab sample of surface soil was provided for the project. Geologically the area is comprised of sandstones to limestones and the region is rich in Zn and Pb ores (Bromowicz and Magiera, 2013). The soil was classified as silty-clay loam and found to be heavily contaminated with Zn, Cd and Pb, believed to have resulted from nearby Zn and Pb smelting (Krzyzak et al., 2017). Around the Bytom site total soil HM have been found to exceed the maximum threshold values described by Polish government regulations excluding this area from food production (Dz, 2016) although cereal crops have been cultivated on this site for the last 20 years (Rusinowski et al., 2019).

Table 3.1: Soil characterisation for Bytom (Rusinowski et al., 2019)

	Unit	Mean Value	Agri. Land Threshold (EC 86/278)
pH		6.5	
EC	$\mu\text{s}/\text{cm}$	75	
Total Pb	mg/kg	719.6	300
Total Cd	mg/kg	26.5	3
Total Zn	mg/kg	3,312	450

A detailed analysis of the Bytom soil contamination is generated through primary research as part of this project and data are presented in chapter 4.

3.2.2 Field Trial Biomass

A sample of *Miscanthus* biomass was obtained from the Bytom site (above). The biomass was harvested in March 2018 at the end of the winter senescence period in accordance with conventional agricultural practice.

The *Miscanthus* is a novel seed-based hybrid (GNT43) developed by Aberystwyth University (UK) during the GIANT LINK Program (LK0863). The hy-



Figure 3.3: Mature *Miscanthus* cultivated in a field (mid-summer)



Figure 3.4: shredded biomass from the Bytom site

brid's growth performance characteristics under field trial conditions has been subjected to detailed analysis by others (Rusinowski et al., 2019). Biomass from the Bytom field trial was mechanically harvested and shredded (mixed stem and leaf material) on site before delivery to University of Leeds.



Figure 3.5: collecting soil at Spen Farm with a core auger

3.2.3 Pot Trial Growth Media

Base Soil

Soil from Spen Farm, Yorkshire, UK ($53^{\circ}51'39.8''\text{N}$ $1^{\circ}20'39.7''\text{E}$) was collected as the base material for formulation of growing media within the pot trials. The field from which the soil was collected is an arable field used for commercial crop growth. Soil was collected in October 2018 using a core auger extending through approximately the top 30 cm of the soil horizon.

Core auger samples were collected from across the field and mixed to ensure that the bulked sample represented a homogeneous average of the field as a whole. The major chemical characteristics of the Spen Farm soil have been assessed and reported in table 4.4.

Table 3.2: major elemental analysis of soil from the Bytom field trial and the Spen Farm soil used for the pot trial (NRM, 2017)

Determinand	Unit	Spen Farm Soil
pH		7.6
CEC	meq/100g	18.7
Ca	mg/kg _(dm)	1780
P	mg/kg _(dm)	20
K	mg/kg _(dm)	106
Mg	mg/kg _(dm)	499
Na	mg/kg _(dm)	8
Total nitrogen	%w/w	0.16
Organic matter	%w/w	2.8

Experimental Soil Formulation

Unadjusted Spen Farm soil was used as the clean/uncontaminated ‘Control’ soil during the pot trial. For uptake experiments in order to create a soil with Zn and Pb contamination, the base soil from Spen Farm was spiked with quantities of ZnCl₂ and PbCl₂ and ZnCO₃ and PbCO₃. All chemicals were in powder/crystal form and purchased from Sigma Aldrich with a reagent grade purity of >98%. A matrix of different soil contaminations was created for the pot trial uptake experiments. Details of the specific formulations, and how they relate to the Bytom soil, are provided in the methods sub-section of chapter 4.

3.2.4 Pot Trial Plants

Plants of the same hybrid (GNT43) as used at the Bytom field trial were used for the pot trial. The plants were germinated from seeds and three month old plants were supplied by Terravesta Ltd. (UK) in small pot (‘plug’) trays. The plants were grown at Bell Brothers Nurseries Ltd., Boston (UK).



Figure 3.6: *Miscanthus* plug prior to planting in the pot trial

3.3 General Laboratory Techniques

3.3.1 X-Ray Fluorescence Spectrometry

X-Ray Fluorescence (XRF) spectrometry is a non-destructive technique used to determine the elemental composition of a sample. A sample is subjected to high-energy X-rays that can be from a conventional laboratory ('bench top') or portable X-ray source. When an atom within the sample is struck with an incident X-ray of energy greater than the electron binding energy an electron is ejected from the inner orbitals (K or L shell) of the atom. This creates an atom in an unstable state with a 'hole' in the inner electron orbital which is rapidly filled by an electron from a higher orbital. During this process, as the electron from the higher orbital 'drops' to fill the core hole, a photon is emitted and thus fluorescence is achieved (figure 3.7).

As each element possesses a unique atomic structure its electron orbitals possess a characteristic energy unique to that element. The emitted fluorescent photon possesses an energy equal to the difference in energy of the initial and

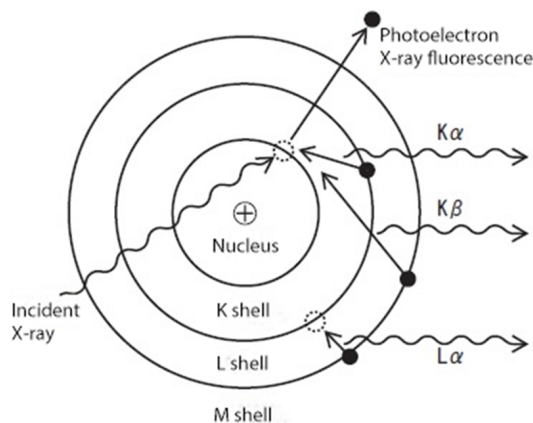


Figure 3.7: schematic of the X-ray fluorescence process

final orbital. Consequently, the energies of the fluorescence photons emitted are characteristic and unique ‘fingerprint’ related to only one specific element.

The fluorescent radiation can be analysed by sorting the energies of the photons using energy dispersive (EDX) spectrometry. This allows each characteristic energy to be identified as a separate peak, the height/intensity of which is related to the concentration of the element in the sample (figure 3.8). Each element may be identified by several peaks at different energy positions associated with different electron transitions (K_{α} , K_{β} , L_{α}).

The soils from both Bytom and Spen Farm were analysed using an Olympus X-5000 (50 kV/10 W) Energy Dispersive X-Ray Fluorescence (EDXRF) portable analyser in both trace and major element modes. A sample of each soil was first air dried at 40°C overnight. Agglomerations of soil particles were then broken up by rolling with 50 mL PET centrifuge tube to produce a fine grained, homogenised sample before mounting in the sample holders.

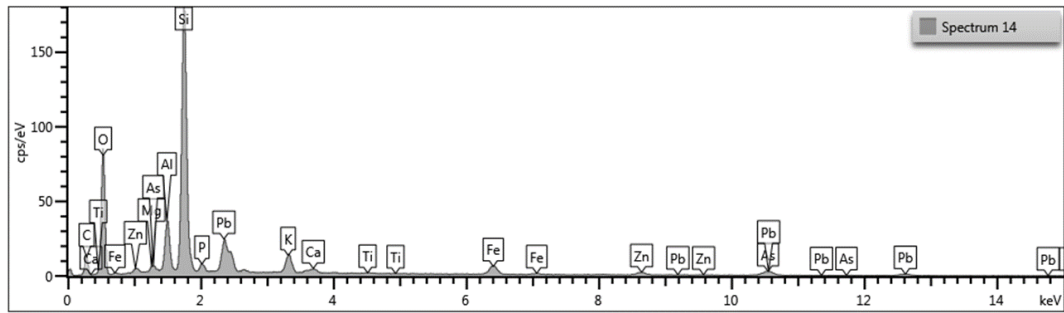


Figure 3.8: example energy dispersive X-ray (EDX) fluorescence spectrum

3.3.2 Scanning Electron Microscopy with Energy Dispersive X-Ray Spectrometry

Scanning Electron Microscopy (SEM) uses a beam of electrons to produce high resolution images. Different electron/sample interactions occur during this process including Back Scattered Electrons (BSE), Auger electron emission, Secondary Electron (SE) emission and characteristic X-ray fluorescence. The beam is focussed using condenser lenses enabling an SEM image of down to 1 nm to be obtained using Raster scanning.

SEM is typically conducted under high vacuum conditions, and therefore the samples which contain water should be dehydrated first to avoid equipment issues associated with water evaporation, although ‘environmental’ SEM instruments are also available. Due to the ionising nature of the electron beam materials may collect a charge which can cause further experimental complications. To avoid this, all samples are electrically grounded and non-conductive samples may be given a conducting surface by sputter coating with powders such as carbon or gold.

The SEM used in this project typical of most SEM and is equipped for BSE and SE imaging. BSE are reflected as a result of elastic scattering, and are therefore of comparatively high energy, equal to that of the incident X-ray beam. The BSE signal intensity is correlated to the atomic number (Z) of the elements in the sample. Therefore the BSE image contains some information

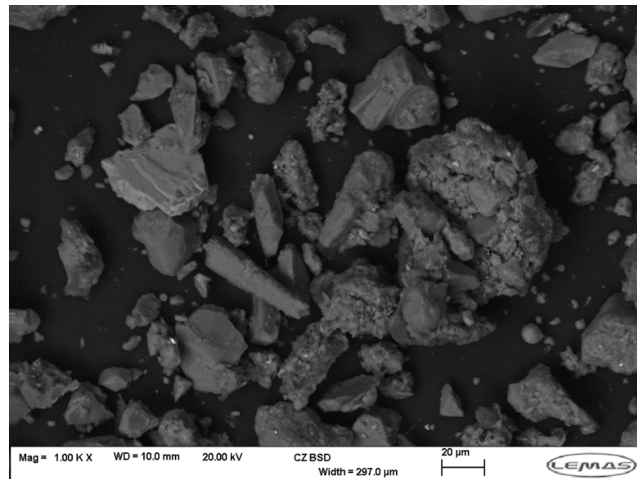


Figure 3.9: example back scattered electron (BSE) image of soil particles using scanning electron microscope (SEM)

about the distribution of elements across the sample, with the presence of heavier elements being identified as brighter within the SEM image.

In contrast, SE emission occurs as a result of emission of the valence electrons producing ionisation of the atom. SE possess much lower energy (c.50 eV) compared to BSE, meaning they are far less penetrating and therefore constrains their emission from the sample to near-surface regions within the sample. This reduces the effective interaction volume of the X-rays, improves resolution and provides more detailed images of surface topography.

Characteristic X-rays in SEM are produced by the same fluorescence process described under XRF analysis (above). Within SEM these signals enable element identification for both distribution through mapping Regions of Interest (ROI) within the fluorescence signal. In addition, elemental abundance within specific locations can be measured where EDX spectra are scanned at specific points on the sample.

3.3.3 Sequential Extraction

Sequential extraction is an analytical procedure whereby trace metals within soils or sediments are partitioned into different fractions by dissolution within consecutive solvents of increasing aggressiveness. The classical procedure was developed by Tessier et al. (1979) who defined a five-stage process whereby metals are classified into five fractions :

- exchangeable;
- bound to carbonates;
- bound to Fe-Mn oxides;
- bound to organic matter; and
- residual.

It is important to recognise that whilst each extraction is named with a species expected to be contained within it, in practice the metal in each extraction are operationally defined rather than positively identified as the particular species adopted by the naming convention.

For this project, an optimised form of Tessier extraction procedure was adopted based upon the method developed by Rauret et al. (1989). Quantification of residual species was calculated by comparison to total metals measured by XRF minus the sum of the metals in the first four extractions.

3.3.4 Atomic Absorption Spectroscopy

Atomic Absorption Spectroscopy (AAS) is an analytical technique which uses the absorption of light by free atoms in a gaseous state to determine the concentration of an element in a solution. AAS is analyte-specific in that it can quantify one single element, although the instrument may utilise multiple light

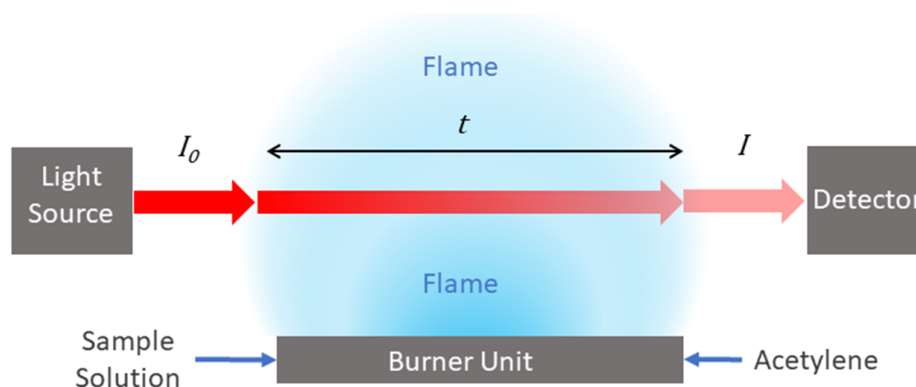


Figure 3.10: schematic of AAS showing Beer-Lambert law dimensions

sources to measure two or three elements simultaneously. In order to achieve atomisation of the sample several techniques can be employed including e.g. flame dispersion or cold vapour atomisation. This project utilised flame dispersion and this will be the focus of the section that follows.

In flame AAS a sample (aqueous) solution is injected at controlled rate through a nebuliser, which creates an aerosol spray, which is mixed with flame gases (typically acetylene and oxygen) in a spray chamber. A burner head sits on top of the spray chamber and the analyte solution is vapourised within the flame. The burner head is elongated laterally (c.5-10 cm) and the instrument is arranged to pass monochromatic light along the path of the flame before its intensity is measured at a detector at the far end.

The principle of measurement revolves around the absorption of light associated with excitation and emission of a valence electron. By selecting monochromatic light of a specific wavelength, absorption is characteristic to and allows identification of a specific element. The extent to which light is absorbed is governed by the concentration of the target element and the path length across which the light/sample interaction occurs. The quantification of this interaction is described by Beer-Lambert Law where the intensity of light at any point (I) from the source (I_0) is governed by the pathlength (t) and the absorption coefficient (μ) which is related to concentration of the analyte within



Figure 3.11: synchrotron facilities used by the project: Diamond Light Source (left) and the Advanced Photon Source

the sample.

$$I = I_0 e^{-\mu t} \quad (3.1)$$

3.4 Synchrotron Techniques

This project relies on the extensive use of synchrotron techniques to establish both the chemistry and spatial arrangement of metals within biomass and soil samples. Experiments were conducted at several beamlines at the Diamond Light Source (DLS), Oxford (UK) and the Advanced Photon Source (APS), Chicago (USA). Each beamline utilises a different X-ray technique and the principles and operation of these are discussed below.

3.4.1 Overview

Synchrotron techniques are based upon the production of intense X-ray radiation generated by acceleration of electrons to relativistic speeds. An electron source produces bunches of electrons that are fed into a Linear Accelerator (LINAC) which accelerates them to an energy of around 200 MeV. The elec-

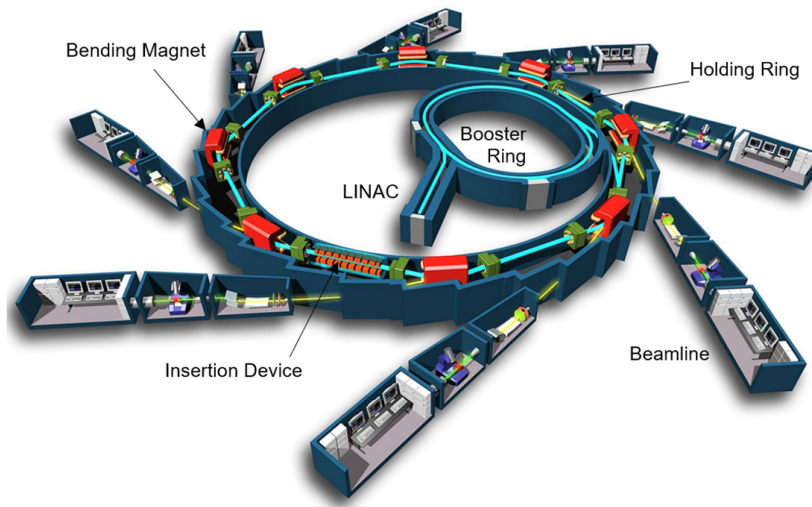


Figure 3.12: schematic of synchrotron internal layout

trons then enter a booster ring where they are further accelerated (up to around 6 GeV in third generation facilities) prior to being transferred to a large holding ring.

The holding ring is an ultra-high vacuum tube (typically 10^{-10} mbar), which may be several hundred metres in diameter, around which a series of different magnets are located. Dipole bending magnets are used to bend the beam and define the circular trajectory of the electrons whilst other types of magnet (quadrupole, sextupole, octupole) are used to bend and focus the beam. The holding ring also has a series of Radio Frequency (RF) cavities which give the beam back the energy lost in synchrotron radiation.

The second feature of bending the beam around the holding ring is that because the electrons are charged particles and are experiencing acceleration they emit electromagnetic radiation including an intense beam of broad spectrum X-rays. The Holding Ring may also possess a series of insertion devices (wigglers and undulators) which are different arrays of magnets which produce X-rays with increased brilliance and narrower energy range.

X-rays emitted by the bending magnets and insertion devices are channelled

into beamlines where the X-rays are tuned and focussed according to the needs of a specific experiment. A broad range of different beamline set ups is possible, with large synchrotron facilities having dozens of different beamlines. The principles of techniques used in this project are examined below.

3.4.2 X-Ray Absorption Fine Structure

X-Ray Absorption Fine Structure (XAFS) encompasses a range of techniques which analyse how X-rays are absorbed by an atom at energies around and above the binding energy of core level electrons.

As a general rule, the probability of absorption of X-ray photons by an atom decreases as the energy of the X-ray increases. This generalised ‘background’ can be seen in X-ray spectra where a slow trend of diminishing absorption occurs with increasing X-ray energy levels (figure 3.13). However, this general trend is abruptly reversed when the energy of the incident X-rays equals or exceeds the binding energy of core level (1s or 2p) electrons. At these energies the X-ray is destroyed (absorbed) and the core electron is ejected from the atom as a photoelectron. This gives rise to a sharp rise in the absorption of X-rays by the atom/sample known as an ‘edge’.

When quantifying X-ray absorption the primary measure is the absorption coefficient μ which provides the probability of X-rays being absorbed according to Beer-Lambert Law (Equation 3.1). Following absorption of an X-ray photon the atom is left in an excited state with a core hole in its electron shell. This is an unstable condition and the atom decays out of this excited state by one of two means: fluorescence whereby a higher energy core-level electron drops to fill the core hole emitting energy as a fluorescence X-ray; or a higher level electron drops and a second (Auger) electron is emitted (figure 3.14). Typically at higher energy levels above 2 keV (‘hard X-rays’) the fluorescence process dominates, whereas at lower energy regimes the Auger process is more likely.

The occurrence of two events (absorption and fluorescence) as a result of the X-ray interaction means that the absorption coefficient $\mu(E)$ of a sample can

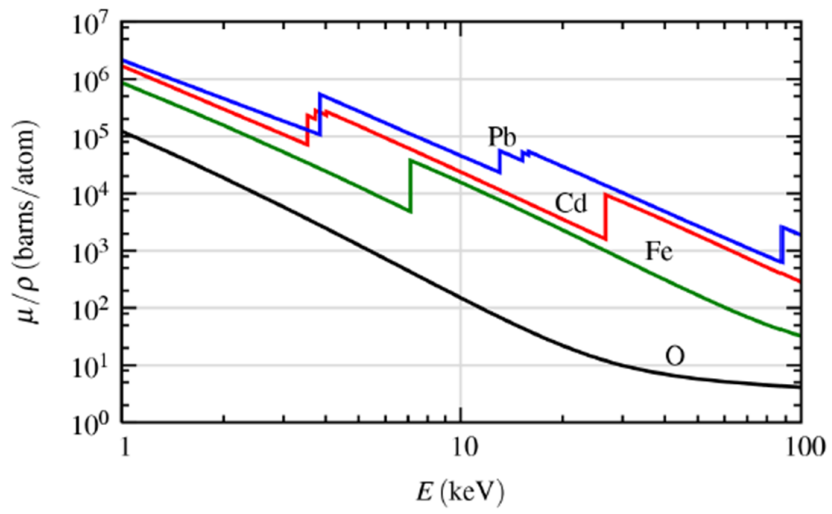


Figure 3.13: the absorption cross section μ/ρ for Pb, Cd, Fe and O (Newville, 2004)

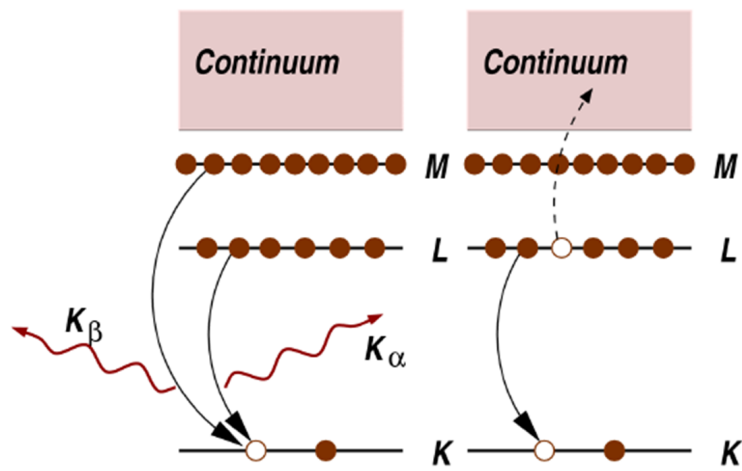


Figure 3.14: decay of the excited state. X-ray fluorescence (left) and Auger emission (right) (Newville, 2004)

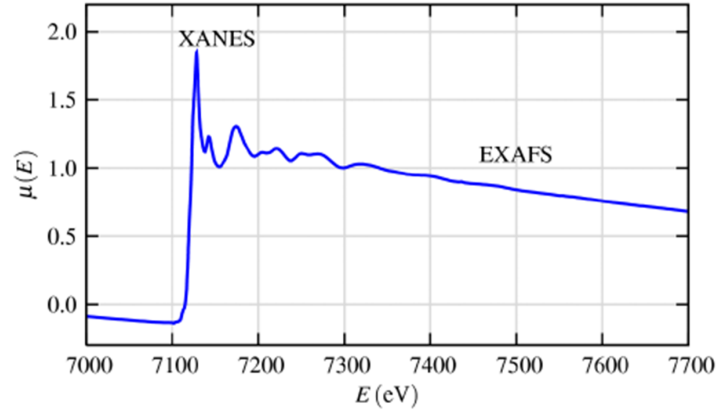


Figure 3.15: XAFS for FeO (Newville, 2004)

be quantified either via measurement of intensity of X-rays in transmission (equation 3.2) or intensity of X-ray fluorescence (equation 3.3):

$$\mu(E) = \log(I_0/I_t) \quad (3.2)$$

$$\mu(E) \propto I_f/I_0 \quad (3.3)$$

where I_0 is the incident X-ray intensity, I_t is the intensity after the sample and I_f is the fluorescence intensity.

An XAFS spectra is typically classified into two regions: X-Ray Absorption Near Edge Spectroscopy (XANES), typically within 30 eV of the absorption edge, although there is no precise definition; and Extended X-Ray Absorption Fine Structure (EXAFS) which spans the higher energy regimes.

XANES

XANES analysis is centred around the energy regime immediately surrounding the absorption edge. The position of the absorption edge energy varies with atomic number approximately as Z^2 , and both K and L electron shells can

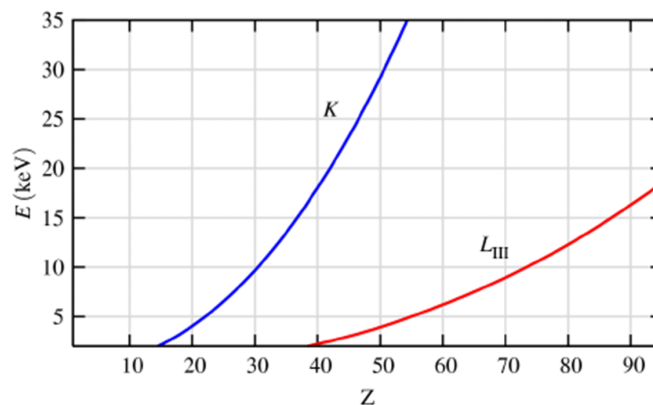


Figure 3.16: The energy of the X-ray K and L absorption edges as a function of atomic number Z (Newville, 2004)

be used. Every atom has unique electron binding energies, which are well documented, and therefore each element has a unique absorption edge energy. This allows XAFS experiments to probe specific elements by tuning the X-ray energy to an appropriate absorption edge.

The XANES region of an XAFS spectra is also strongly sensitive to the oxidation state and coordination environment (e.g. tetrahedral or octahedral) of the absorbing atom. The loss/gain of a valence electron changes the charge density of an atom which results in altered electron binding energy and a shift of the absorption edge position. An increase in oxidation state (loss of electrons) typically results in an increase in binding energy of the remaining electrons. This property can be used to fingerprint elements which display multiple oxidation states, such as sulfur (figure 3.17).

By utilising spectra obtained for known standard compounds the XANES data for a sample can be interpreted using fitting techniques such as Linear Combination Fitting (LCF) or Principal Component Analysis (PCA). Established software packages such as Larch or Athena enable fitting to be performed with recognised methodologies (Newville, 2013; Ravel and Newville, 2005).

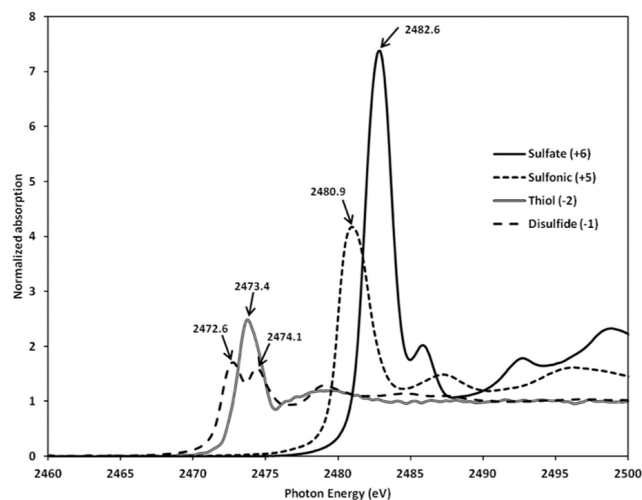


Figure 3.17: XANES spectra of sulfur compounds with different oxidation states (Castillo-Michel et al., 2016)

EXAFS

The study of EXAFS is concerned with the oscillations observed in an XAFS spectra in the energy regime >30 eV above the absorption edge. The theory behind EXAFS revolves around the interactions of the ejected photoelectron with the neighbouring coordinating atoms.

The ejected photoelectron can be regarded as a spherical wave which is reflected by neighbouring atoms (figure 3.18). The back scattered electron may interfere constructively or destructively when it returns to the original atom. If constructive interference occurs then the original atom possesses more electron density (neutral atom plus a photon) and is in a similar state to before the absorption event occurred, compared to if destructive interference occurs. In this situation, the probability of another absorption event occurring is increased and this is measurable as an increase in the absorption coefficient of the sample $\mu(E)$.

Constructive interference occurs when the round trip distance of the back scattering event is equal to a whole number of photoelectron wavelengths,

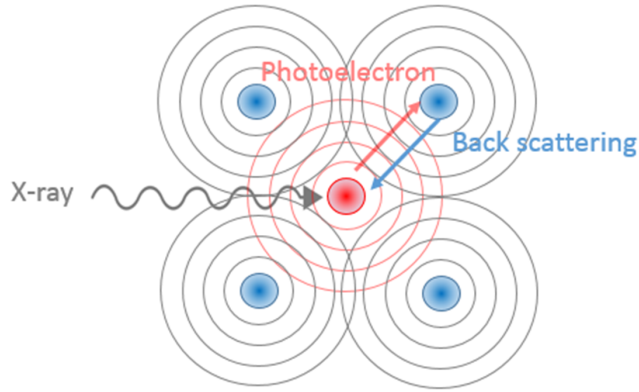


Figure 3.18: X-ray absorption and backscattering from neighbouring atoms

described as:

$$2D = n\lambda \quad (3.4)$$

where D is the distance between the absorbing atom and the scattering atom, λ is the photoelectron wavelength and n is an integer.

The emitted photoelectron possesses the energy from the incident X-ray in excess of the electron binding energy. Consequently, as the energy of the incident X-ray changes so too does the wavelength (energy) of the emitted photoelectron. Thus satisfying the precondition for constructive interference occurs periodically as the incident X-ray energy changes, resulting in a modulation of the absorption coefficient with changing X-ray energies.

The quantitative analysis of EXAFS requires isolating the oscillations by removal of a smoothed background function. The EXAFS function is $\chi(E)$, derived as:

$$\chi(E) = \frac{\mu(E) - \mu_0(E)}{\Delta\mu_0(E)} \quad (3.5)$$

where $\chi(E)$ is the absorption coefficient, $\mu_0(E)$ is a smooth background func-

tion representing the absorption of an isolated atom (i.e. in the absence of any backscattering effect), and $\Delta\mu_0$ is the measured jump in the absorption at the threshold energy E_0 (figure 3.19 top).

It is standard practice to convert X-ray energy to wave number k in units of \AA^{-1} as follows:

$$k = \sqrt{\frac{2m(E - E_0)}{h^2}} \quad (3.6)$$

where k is the wave number, E_0 is the absorption edge energy, m is the mass of an electron and h is Planck's constant.

The expression of $\chi(k)$ is the foundation of EXAFS analysis (Figure 4.19 middle). However, as the oscillations rapidly diminish with increasing values of k , the $\chi(k)$ is raised by a power to k^2 or k^3 (figure 3.19 bottom).

The different frequencies apparent in the isolated EXAFS oscillations correspond to backscattering effects from different atoms within the coordination shell of the absorbing atom. These interrelationships can be described by the EXAFS equation:

$$\chi(k) = \sum_j \frac{N_j f_j(k) e^{-2k^2\sigma_j^2}}{kR_j^2} \sin[2kR_j + \delta_j(k)] \quad (3.7)$$

where for each scattering path j , $f(k)$ is the scattering amplitude and $\delta(k)$ is the phase shift (n.b. both these properties are influenced by the atomic number Z of the coordinating atoms), N is the number of coordinating atoms, R is the bond distance, and σ^2 is a disorder factor for distance.

The EXAFS equation allows estimation for N , R , and σ^2 from the measurable $f(k)$ and $\sigma(k)$ data and thereby enables the coordination environment of the absorbing atom to be modelled. Software such as Artemis allows for these parameters to be modelled via a recognised methodology (Ravel and Newville, 2005).

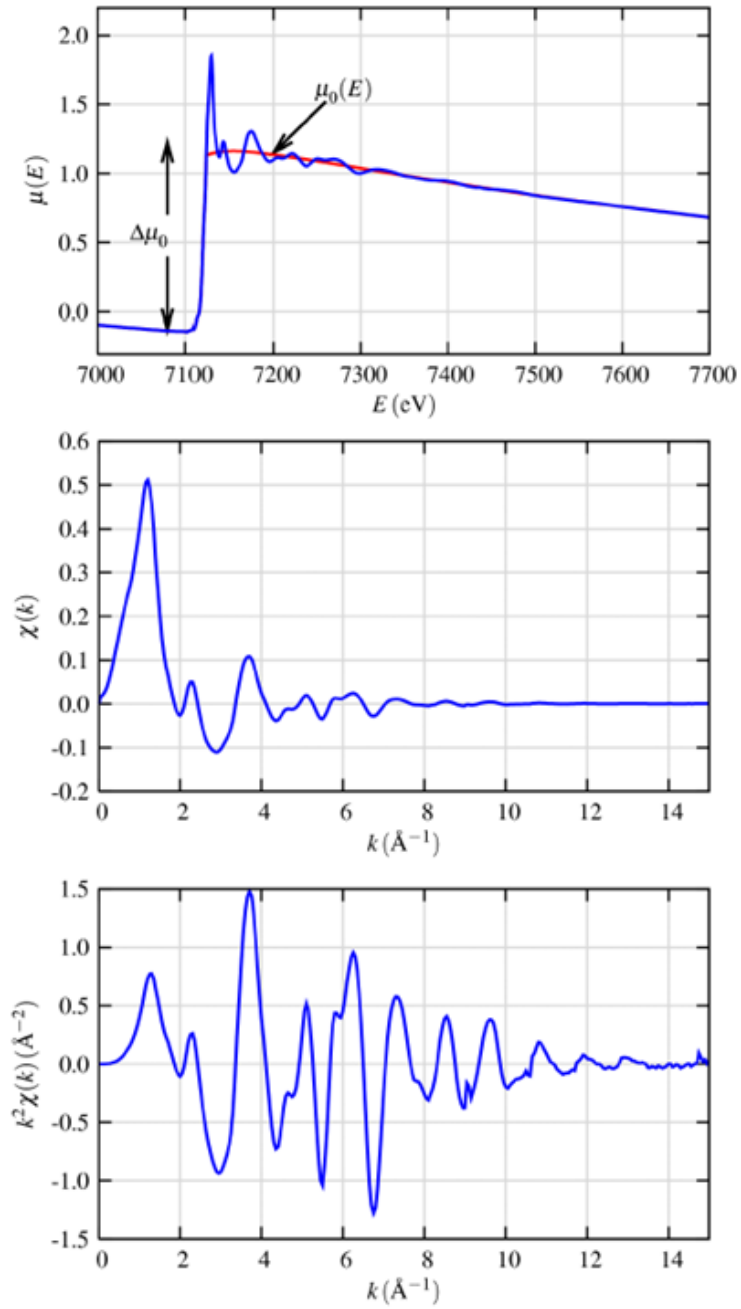


Figure 3.19: isolation of EXAFS data: (top) $\mu(E)$ for FeO shown with smooth background function $\mu_0(E)$ and the edge-step $\Delta\mu_0$; (middle) isolated EXAFS $\chi(k)$ for FeO; (bottom) k^2 -weighted EXAFS for $k^2\chi(k)$ (Newville, 2004)

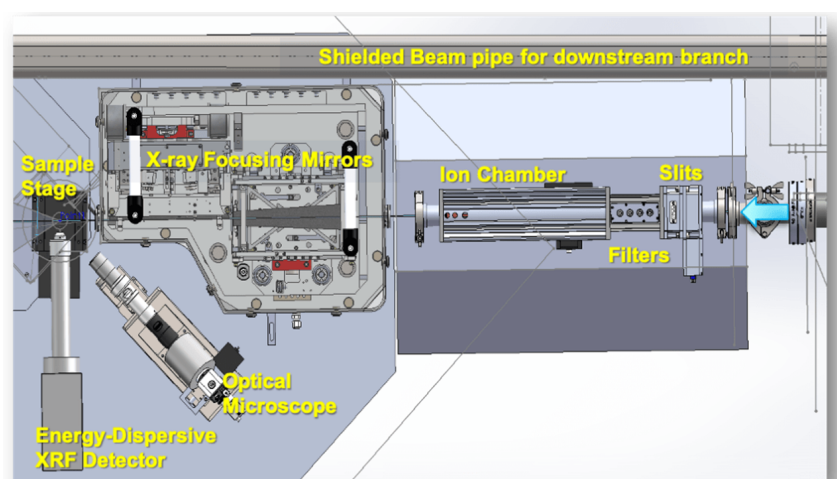


Figure 3.20: schematic of XRF mapping beamline 13-ID-E at APS, Chicago (USA)

3.4.3 X-Ray Fluorescence Mapping

X-Ray Fluorescence mapping (XRF) is an imaging technique which allows mapping and concentration of elements across a sample to be identified in a 2-dimensional image. Unlike SEM-EDX, which relies on an electron beam, XRF can be conducted at room temperature and pressure and on moist or wet samples which allows in-vivo analysis of biological samples to be performed. XRF can be conducted using lab-scale X-ray sources, but the use of synchrotron light sources offers a number of advantages, including faster data acquisition and higher resolution of elements down to ppm concentrations.

Synchrotron XRF techniques are typically built around insertion device (e.g. undulator) beamlines producing a micro-focussed X-ray beam. Mirrors are used to focus the X-ray beam with a typical spatial resolution down to c.5-2 μm in size. Map acquisition is achieved via a continuous scanning approach to produce a raster image. The beam intensity achieved at synchrotrons improves the XRF signal such that dwell times of 5-10 ms per pixel can be utilised and large elemental maps can be recorded in practical experimental time frames.

The distribution of multiple elements can be mapped simultaneously as fluores-

cence will occur concurrently for all edges (K and L) below the selected beam energy. However, overlaps in the fluorescence spectra can confound analysis depending on the composition of the sample. The incorporation of monochromators along with a focussed microprobe allows acquisition of μ XANES and μ EXAFS spectroscopic data to be gathered at spot locations in addition to the imaging data. In this way changes in speciation across the sample can be measured.

3.5 References

- Bromowicz, J. and Magiera, J. (2013). Building stones used in early mediaeval edifices of krakow and geology of the area. *Geology, Geophysics, Environment*, 39(2):95.
- Dz, U. (2016). Decision of the polish ministry of environment on the assessment of soil contamination.
- Krzyzak, J., Pogrzeba, M., Rusinowski, S., Clifton-Brown, J., McCalmont, J. P., Kiesel, A., Mangold, A., and Mos, M. (2017). Heavy metal uptake by novel miscanthus seed-based hybrids cultivated in heavy metal contaminated soil. *Civil and Environmental Engineering Reports*, 26(3):121–132. Fp4zu Times Cited:2 Cited References Count:22.
- Newville, M. (2004). Fundamentals of xafs.
- Newville, M. (2013). Larch: an analysis package for xafs and related spectroscopies. volume 430, page 012007. IOP Publishing.
- NRM (2017). Analytical report. Report EC4500900882.
- Rauret, G., Rubio, R., and Lopez Sanchez, J. F. (1989). Optimization of tessier procedure for metal solid speciation in river sediments. *International Journal of Environmental Analytical Chemistry*, 36(2):69–83. Ab800 Times Cited:96 Cited References Count:11.
- Ravel, B. and Newville, M. (2005). Athena, artemis, hephaestus: data analysis for x-ray absorption spectroscopy using ifeffit. *Journal of Synchrotron Radiation*, 12:537–541. 4 935rl Times Cited:7259 Cited References Count:23.
- Rusinowski, S., Krzyzak, J., Clifton-Brown, J., Jensen, E., Mos, M., Webster, R., Sitko, K., and Pogrzeba, M. (2019). New miscanthus hybrids cultivated at a polish metal-contaminated site demonstrate high stomatal regulation and reduced shoot pb and cd concentrations. *Environmental Pollution*, 252:1377–1387. B Iu2jf Times Cited:1 Cited References Count:67.

Tessier, A., Campbell, P. G. C., and Bisson, M. (1979). Sequential extraction procedure for the speciation of particulate trace-metals. *Analytical Chemistry*, 51(7):844–851. Gw661 Times Cited:6277 Cited References Count:48.

TUBS (2011). Location map of poland.

Chapter 4

Soil Characterisation: the Fractionation, Speciation and Distribution of Zn and Pb in the Bytom Soil

Abstract

The Zn and Pb contamination of a soil sample from Bytom (Poland) was characterised in detail using a series of techniques. XRF identified high levels of total Zn (4,006 mg/kg) and total Pb (1,859 mg/kg). SEM-EDX imaging demonstrated that the contamination is evenly and homogeneously distributed across the soil matrix. Surface sensitive techniques (especially EDX) returned much higher values for both Zn and Pb compared to bulk techniques, such as chemical extractions, indicating that the majority of these metals was sorbed onto the surface of the soil particles.

Tessier extractions identified only a minority of Zn and Pb as being within the most mobile (bioavailable) fractions: Zn exchangeable (5%) and carbonate (23%); and Pb exchangeable (3%) and carbonate (24%). The organic fraction of Zn was low (11%) compared to the Pb organic fraction (35%).

Detailed analysis using EXAFS fitting indicated Zn was present in octahedral coordination with O in the first shell: coordination number $5.2(\pm 0.7)$, radial distance $2.04(\pm 0.01)\text{\AA}$, which is consistent with carbonate species. The more recalcitrant forms of Zn were mostly identified within the Fe/Mn oxide (29%) and residual (32%) Tessier extractions. EXAFS did not identify high Z elements (Fe/Mn/Zn) in coordination with Zn. It is considered that the octahedral O coordination result may also be indicative of Zn substitution into phyllosilicates within the soil matrix, resulting in the generally low observed Zn mobility/availability.

4.1 Introduction

The aim of this study is to characterise the Heavy Metal (HM) contamination present in the soil of the Bytom site. In particular, the distribution and speciation of the bioavailable HM, as this fraction is accessible for uptake by *Miscanthus*. The information generated served as the basis by which the grow-

ing media of the pot trial was specified, in order to develop a growth media with HM contamination broadly comparable with the Bytom site. Focus is placed on Zn and Pb contamination as these metals were identified during screening analyses at the inception of this project as being present at elevated concentrations within the *Miscanthus* from Bytom. Consequently, Zn and Pb are of particular relevance to biomass quality.

The use of bulk XRF analysis was used to establish overall contamination of a sample of Bytom soil prior to adopting more detailed characterisation of Zn and Pb. Thus, the representativeness of the sample can be compared to what has been published regarding the Bytom site. The fractionation of Zn and Pb compounds is established using Tessier chemical extractions, thereby establishing the extent to which these metal are bioavailable. SEM-EDX mapping establishes the spatial distribution of metals throughout the soil matrix. Finally, the Zn in the soil is analysed using XAFS techniques to develop precise information on Zn chemical speciation. This allows the chemistry of Zn to be compared with the operationally defined categories established through the Tessier extraction technique.

The combination of techniques provides a thorough characterisation of the soil. This facilitates subsequent development of this project's overall methodology. In addition, it also enables the likely mechanisms of contamination to be hypothesised. This assists in placing the project's findings within a broader context.

4.1.1 Zinc in the Environment

On a global basis, an estimated 1,193,000 – 3,294,000 tonnes of Zn are released from anthropogenic sources to the environment every year (Nriagu and Pacyna, 1988). The primary anthropogenic sources are mining, disposal of smelter slags and wastes, mine tailings, bottom ash and fly ash from coal fired power stations, the use of some fertilizers (including sewage sludges), and wood preservatives that contain Zn (ATSDR, 1992).

Zn concentrations in the air are generally low. The exception to this is air pollution associated with specific industrial sources such as smelters or mining operations. Estimated atmospheric Zn dispersion to the atmosphere as a result of dust from mining operations has been estimated as 100 g/tonne of Zn mined, attributable to handling raw and concentrated Zn bearing ore and wind erosion acting upon tailing piles (Lloyd and Showak, 1984).

In the atmosphere Zn exists primarily in an oxidized form and bound to ultra-fine particulates (Nriagu and Davidson, 1980). Such particulates are removed from the air by dry and/or wet deposition and may contaminate the local environment. Consequently, Zn in soils and plants surrounding industrial sources is often observed to be at elevated levels. Wind blown Zn particulates with low densities (e.g. aerosols) can travel long distances from emission sources when suspended in the atmosphere (Pacyna et al., 1989).

Once deposited on the ground, Zn sorbs strongly onto soil particulates and exists almost exclusively in the +2 oxidation state (Lindsay, 1979). The properties of the soil such as cation exchange capacity (CEC), pH, redox potential and the presence of other chemical species, may impact Zn speciation. Studies have shown that when $\text{pH} < 7$ there is an inverse relationship between Zn in solution and pH due to negative charges on particulate surfaces increasing at a lower pH and thereby providing more sites for Zn adsorption onto solid phases to occur. In a similar way, Zn solubility and mobility increases with lower CEC soils (Lloyd and Showak, 1984). Counter to these observations, the presence of high levels of organic matter within a soil may result in Zn mobility increasing at $\text{pH} > 7$ as Zn complexes may become more mobile due to the increased presence of organic chelating agents (Saeed and Fox, 1977).

Notwithstanding the potential mechanisms which may result in Zn mobilisation, outside of exceptional conditions, the majority of Zn in contaminated soils will be found in relatively recalcitrant form. In a study of soils contaminated with Zn from industrial and agricultural sources in the USA the majority of Zn (55.8 - 97.6%) was found to be in recalcitrant form, whereas a much lower proportion (0.73 - 25%) was in more mobile exchangeable or carbonate forms

Table 4.1: Percentage contributions of Tessier extractions of Zn mean(range) in contaminated soils from southwest Poland which display low/medium/high levels of contamination (Chlopecka et al., 1996)

Extraction	Low	Medium	High
Exchangeable	5.0 (4-7)	12.0 (0.1-27)	2.9 (0.1-19)
Carbonate	6.8 (3-12)	9.5 (4-20)	12.7 (4-25)
Fe/Mn Oxide	26.2 (23-29)	34.8 (26-45)	32.6 (23-41)
Organic	14.8 (10-18)	15.3 (11-21)	12.4 (8-20)
Residual	47.2 (40-53)	28.4 (9-41)	39.2 (18-65)

Notes:

Contamination levels were classified as: Low) equivalent to background level; Moderate) background to maximum tolerable level; High) in excess of tolerable level. Levels are expressed within the Polish threshold for agricultural soil (Dz, 2016).

(Ma and Rao, 1997). Highly comparable results were found in a study of soils in southwest Poland contaminated with Zn up to 10,000 mg/kg; Chlopecka et al. (1996) used Tessier sequential extractions and found that the greatest proportion of Zn was in the highly recalcitrant residual fraction and Fe/Mn oxide fraction, whereas comparatively small proportions of Zn were found in organic, carbonate or exchangeable forms (table 4.1). Chlopecka concludes that there was little consistent/statistically significant shift in Zn fractionation with increasing contamination level.

4.1.2 Lead in the Environment

Mining, smelting and refining operations may give rise to releases of Pb into the environment. Pb ores are frequently found in combination with other recoverable metals such as Cu, Zn, Ag and Cd and this may result in the simultaneous release of these metals. Pb emissions to the environment are primarily of either aqueous effluent streams, or emission of fume and dust into the air. Pb discharged into surface waters is rapidly incorporated into suspended and bottom sediments, and ultimately marine sediments become

Table 4.2: Emission factors for total particulates from Pb smelting prior to emissions abatement (Vandegrift et al., 1971)

Production Method	kg/tonne
Ore crushing	1 of ore
Sintering	260 of lead
Blast furnace	125 of lead
Dross reverberatory furnace	10 of lead
Material handling	2.5 of lead

its repository (Harrison and Laxen, 1981). Perhaps of greater concern is the emission of Pb into the atmosphere due to potential health risks possible via this media.

Data for the USA show that atmospheric emissions of Pb peaked in the 1970s and declined after the use of Pb as an anti-knocking additive in transport fuel was phased out (EPA, 1986a). On a local scale the Pb smelting industry is an important source of Pb in the air. Vandegrift et al. (1971) estimated the total particulate emissions from Pb smelting processes, prior to emission abatement, and the data illustrate the potential for Pb particulate pollution to occur (table 4.2). However, modern day pollution abatement techniques are highly efficient and contemporary process emissions from smelting operations are more likely in the range of 0.1 – 100 mg/kg (Lee Jr and Von Lehmden, 1973).

Pb particles dispersed within the atmosphere are removed by dry and/or wet deposition processes to become sources of soil pollution. Dry deposition is significant for all particles $>10\ \mu\text{m}$ and is very rapid for the large particles $>50\ \mu\text{m}$ which, historically, may be associated with crude ore processing (Harrison, 1986). Wet deposition is more prevalent for smaller particles and accounts for up to 86% deposition of particulates in a range from $0.5 - 20\ \mu\text{m}$ (Tai et al., 2017). It has been shown that the median particle size for Pb emissions from modern smelting operations is $1.5\ \mu\text{m}$, with 86% of the particles being less than $10\ \mu\text{m}$ (Corrin and Natusch, 1977). Therefore, wet deposition is most relevant to Pb deposition around contemporary smelting operations. Ultimately, the

surrounding soils will become the repository for Pb, although it may be remobilised into the atmosphere in the form of wind blown dust. This latter process is considered to be an important pollution pathway around smelting facilities (EPA, 1982).

Pb is relatively immobile in soil as it sorbs strongly to soil components. It can partition between the soil water (although its solubility is low), secondary Fe and Mn oxides, carbonates, organic matter, sulfides, or the surfaces of clay, humus, or silicate particles (ATSDR, 2020). Soil pH is considered the most important factor governing Pb solubility and consequently its bioavailability. At low pH carbonates and hydroxides fractions become increasingly prevalent and Pb will more readily partition into solution. Solubility may also be enhanced in soils under anoxic conditions or in the presence of high levels of chloride (EPA, 2013). In soil with high organic matter content and a pH of 6 – 8, Pb may form insoluble organic complexes; if the soil has less organic matter at the same pH, hydrous oxide complexes may form or Pb may precipitate as carbonate or phosphate. At lower pH of 4 – 6 (possibly as a result of acid rain) organic complexes become increasingly soluble (as reported with Zn) and may dissolve more readily and be taken up by plants (EPA, 1986b).

Chlopecka et al. (1996) also analysed the contaminated soils of southwest Poland for Pb and the results were slightly different to those for Zn (table 4.3). The consistently largest fraction for Pb was in the form of Fe/Mn oxide with nearly twice as much in this fraction than was observed with Zn. There is a correspondingly lower proportion of Pb in the highly recalcitrant residual fraction. The organic and carbonate fractions are broadly similar to those observed with Zn, but the most bioavailable exchangeable fraction of Pb is a lower proportion.

Table 4.3: Percentage contributions of Tessier extractions of Pb mean(range) in contaminated soils from southwest Poland which display low/medium/high levels of contamination (Chlopecka et al., 1996)

Extraction	Low	Medium	High
Exchangeable	1.3% (0-2%)	5.6% (0-11%)	1.4% (0.1-8%)
Carbonate	6.5% (4-10%)	14.7% (8-23%)	15.0% (2-32%)
Fe/Mn Oxide	47.8% (44-52%)	60.0% (53-66%)	56.7% (46-63%)
Organic	14.4% (11-17%)	11.2% (8-22%)	17.3% (8-37%)
Residual	30.0% (23-37%)	10.5% (4-17%)	9.6% (3-19%)

Notes:

Contamination levels were classified as: Low) equivalent to background level; Moderate) background to maximum tolerable level; High) in excess of tolerable level. Levels are expressed within the Polish threshold for agricultural soil (Dz, 2016).

4.2 Experimental Methods

4.2.1 Soil

A random grab sample of soil was taken from Bytom (Upper Silesia), Poland (50°20'43.1"N 18°57'17.9"E). The sample was taken in spring 2019. The soil was air dried and pressed through a 2 mm sieve to remove stones prior to further processing for specific techniques set out below.

4.2.2 Energy Dispersive X-Ray Fluorescence Analysis

A soil sample was oven dried at 105°C for 4 hours prior to being placed in 30 mm sample cups and sealed with Prolene film. Soil was then analysed with an Olympus X-5000 Energy Dispersive X-ray Fluorescence (EDXRF) portable analyser. The analyser was operated in 'Soil Mode' with three beams at 50, 35 and 15 kV, utilising Compton normalisation correction.

4.2.3 Tessier Extraction

The soil was first oven dried at 105°C for 4 hours, cooled in a desiccator, then finely ground in an agate mortar. A 1 g aliquot was weighed into a 50 mL centrifuge tube. Triplicate samples were used. The extraction stages were performed in series and the soil solids retained after each stage:

Stage (i) Exchangeable: 8 mL of 1 M sodium hydroxide (pH 7.75) was added to the centrifuge tubes and agitated in an orbital shaker set at 200 rpm for 1 hour. Samples were centrifuged (30 mins, RCF: 4,643 x g) and the supernatant removed by pipette and retained for analysis. A rinse solution of 8 mL of ultra-pure deionized water was added to each tube. The tubes were shaken and centrifuged again, and the supernatant liquid removed by pipette and discarded.

Stage (ii) Bound to carbonates: 8 mL of 1 M sodium acetate (adjusted to pH 5.0 acetic acid) was added to each sample and the tubes were agitated in an orbital shaker (200 rpm, 5 hours). The pH was monitored but no pH change was observed. Tubes were then centrifuged, sampled and rinsed as described in stage (i).

Stage (iii) Bound to Fe-Mn oxides: 20 mL of a solution containing 0.3 M sodium dithionite, 0.175 M sodium citrate and 0.025 M citric acid was added to each tube and agitated (200 rpm, 6 hours). Tubes were then centrifuged, sampled and rinsed as before.

Stage (iv) Bound to organic matter: samples were washed into glass digestion vessels using 3 mL of 0.02 M nitric acid and 5 mL of 30% hydrogen peroxide. The vessels were covered with a ribbed watch glass and left at room temperature for 1 hour before they were heated on a hotplate and refluxed for 2 hours (solution temperature measured as 85°C). A further 3 mL of hydrogen peroxide was added and heating was continued for another 3 hours. The vessels were allowed to cool before the contents were washed into 50 mL centrifuge tubes using 5 mL of 3.2 M ammonium acetate in 20% (v/v) nitric acid. The volume made up to 20 mL using ultra-pure deionized water and the tubes agitated in

an orbital shaker (200 rpm, 30 mins). Tubes were then centrifuged, sampled and rinsed as before.

Stage (v) Residual: Zn and Pb concentrations in the residual fraction were estimated from the difference between the sum of stage i – iv extractions and the totals obtained by XRF analysis (above).

4.2.4 Atomic Absorption Spectroscopy

The Zn and Pb concentrations within each Tessier extraction were determined using an Agilent 2000 Atomic Absorption Spectrophotometer (AAS) operated with an air/acetylene flame. The lamps/detector wavelength of 213.9 nm and 217.0 nm were adopted for Zn and Pb respectively. The extractions were made up with the addition of EDTA to 0.1 molar concentration to overcome interference of Pb by carbonate in the solution.

4.2.5 Scanning Electron Microscopy with Energy Dispersive X-Ray Analysis

A soil sample was oven dried at 105°C for 4 hours and cooled in a desiccator. An aliquot was then carbon sputter coated and analysed with a Carl Zeiss EVO MA15 Scanning Electron Microscopy with Energy Dispersive X-Ray (SEM-EDX) microscope equipped with Oxford Instruments Aztec Energy EDX system with 80mm X-Max SDD detector for secondary and back-scattered electron imaging, and fluorescence spectra acquisition.

4.2.6 XAFS Analysis

XAFS data were recorded across the Zn K-edge at beamline 10-BM-B at the Advanced Photon Source (APS), Chicago (USA). A Si(111) monochromator with an energy resolution of $1 \times 10^{-4} \Delta/E$ was used, and the spectra were

recorded in fluorescence mode using an ion chamber in Stern-Heald geometry. The ion chamber used to measure the I_0 was flooded with a mixture of 30% N_2 and 70% He gas. Samples were pressed into 3 mm thick pellets and mounted using Kapton tape in an acrylic sample holder set at 45° to the beam. Energy grid alignment was facilitated by placing a Zn reference foil between I_t and I_{ref} detectors and these ion chambers were flooded with a mixture of 50% N_2 and 50% Ar gas.

The Zn K-edge was assigned a value of 9665 eV and scans were performed using 5 energy regions: -150, -30, +60, +6k, +9k and +12k eV above/below the edge, with energy step intervals for each region being 5, 0.4, 0.05k, 0.07k and 0.1k eV respectively. Five consecutive scans were collected from each sample and the data was checked for beam damage before being merged prior to analysis.

XANES data processing, including the calibration of spectra and background removal, was performed using Athena software (Ravel and Newville, 2005). XANES spectra from the soil sample were initially compared with reference spectra for $Zn(SO)_4$, $Zn(CO)_3$, ZnO and ZnS using Linear Combination Fitting (LCF). LCF was performed in Athena (Demeter v.0.9.26) with a fit range of -20 to +50 eV below/above E_0 . Extended X-ray Absorption Fine Structures (EXAFS) analysis was performed using Artemis (also Demeter v.0.9.26) (Ravel and Newville, 2005). EXAFS were analysed with forward Fourier transform range of k between 2.5 and 10 \AA^{-1} . Fitting was conducted using crystallographic data (CIF files) for Zn compounds $Zn(CO)_3$ (Smithsonite) and $Zn(SO)_4$ (Graf, 1961; M. and R., 1978). Scattering of pathways between 1.0 and 3.0 \AA from the absorbing atom (Zn) was modelled via Ifeffit. The goodness of fit was established using Artemis' value for reduced chi-squared and the fit of an addition path adopted if the path's inclusion resulted in the value being reduced by >20%.

Table 4.4: Major elements of Bytom soil as determined by XRF

Element	mg/kg	wt%
Si	254,054	25.4
Al	31,379	3.1
Fe	15,816	1.6
K	15,235	1.5
Ca	4,856	0.5
Zn	4,006	0.4
Mg	4,000	0.4
S	3,921	0.4
Ti	3,253	0.3
Pb	1,859	0.2
P	1,000	0.1
Mn	748	0.1
Cl	377	0.0
As	38	0.0
Cu	28	0.0

4.3 Results

The bulk composition of the Bytom soil sample as determined by XRF analysis is reported in table 4.4. The data confirmed the presence of high levels of Zn (4,006 mg/kg) and Pb (1,859 mg/kg) contamination, both of the same order of magnitude reported by Krzyzak et al. (2017) for the Bytom site. The presence of As was detected but a level below the upper threshold (50 mg/kg) recommended for agricultural land (EC 86/278). Cd contamination was not detected in the sample. The results of the Tessier sequential extraction of both Zn and Pb from the Bytom soil sample are displayed in table 4.5. The majority of Pb was found to be bound to organic matter (35%) and residual (34%) fractions. Relatively little Pb was determined as bound to Fe/Mn oxides (5%). Of the two remaining fractions the great majority of Pb was in the carbonate fraction (24%) with least the amount being exchangeable (3%).

Zn fractionation was found to be highly comparable to Pb in three of the five extractions. Residual Zn (32%) was similar to that observed for Pb. However,

Table 4.5: Results of Tessier extractions for Pb and Zn in Bytom soil

Extraction	n	Pb			Zn		
		Range mg/kg	Mean mg/kg	%	Range mg/kg	Mean mg/kg	%
Exchangeable	3	64 - 40	51	3%	240 - 168	197	5%
Carbonates	3	456 - 432	443	24%	968 - 904	931	23%
Fe/Mn Oxide	3	100 - 80	87	5%	1180 - 1120	1153	29%
Organic	3	812 - 336	647	35%	506 - 366	448	11%
Residual	1	-	632	34%	-	1277	32%

the relative prevalence of Fe/Mn oxides (29%) and organic matter (11%) was the opposite pattern to that observed for Pb. The fraction of Zn in carbonate (23%) and exchangeable (5%) forms were highly comparable to Pb.

Images from the SEM-EDX showing elemental distribution across the soil are shown in figure 4.1. Images show distribution of Si, O, Fe, Al, Zn, Pb and C. Si and O are visible as a strong signal associated with all major soil particles. The Al is widely distributed, but its association with some soil particles is weaker in some cases e.g. particles at the bottom right of the image. Fe distribution is irregular, presenting a strong signal within a minority of particles but most particles showing absent/very weak Fe signal. Both Zn and Pb signals are weaker, due to their comparatively low concentration, combined with a widely dispersed occurrence of both, i.e. Zn and Pb are not associated with high concentrations within discrete particles in the way Fe is observed to be.

The EDX results of spot sampling the elemental composition of Bytom soil are displayed in table 4.6.

XAFS spectra (XANES and EXAFS) for the Bytom soil and Zn standard compounds are presented in figure 4.2. Key spectral features in the EXAFS are highlighted with vertical lines for discussion below.

Isolated EXAFS (Xk) for the Bytom soil sample and Zn standards are provided in the Appendix to this chapter (figure 4.5). The result of the EXAFS fitting (first and second shell) of the Bytom soil are illustrated in figure 4.3. Both

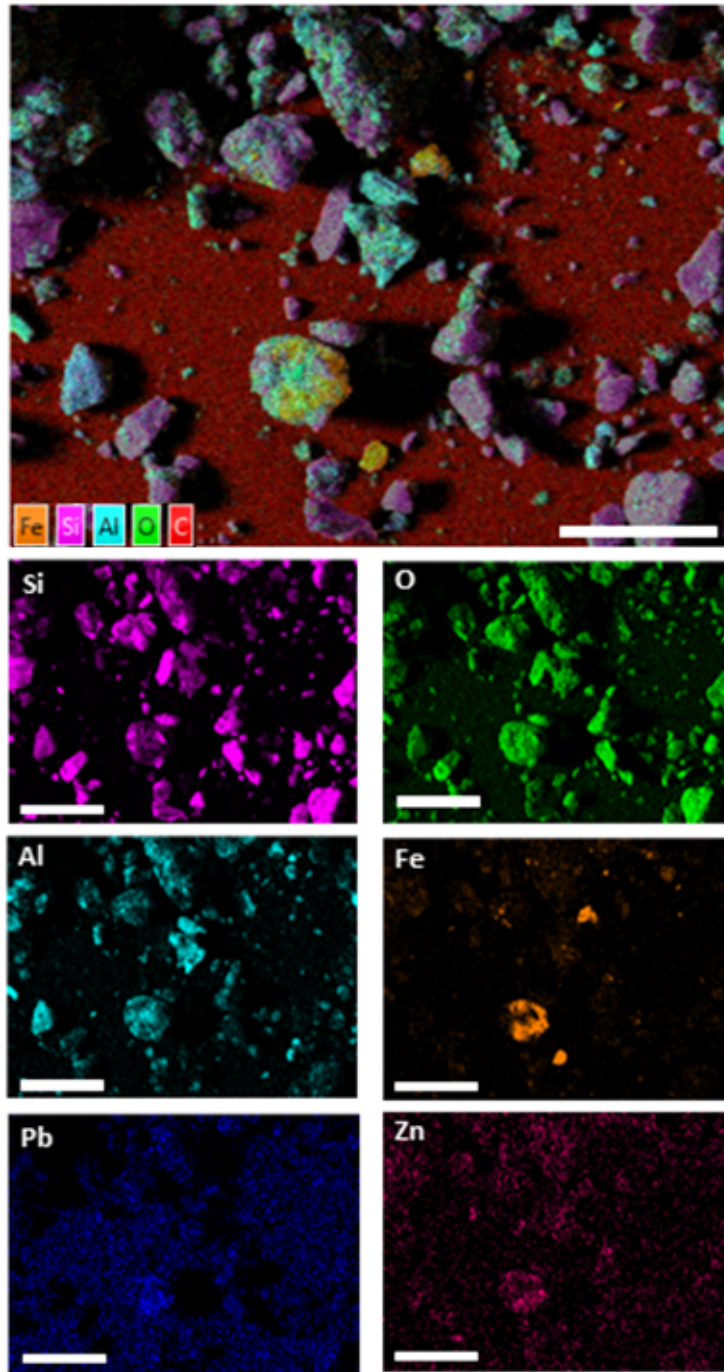


Figure 4.1: SEM-EDX images of Bytom soil showing $K\alpha_1$ transition fluorescence ($M\alpha_1$ for Pb). All scale bar = 100 μm

Table 4.6: SEM-EDX spot samples' elemental composition (n = 14, wt%)

Element	Mean	Max	Min	Std. Dev.
O	29.6%	48.7%	2.3%	11.3%
Fe	27.7%	66.3%	1.4%	21.4%
C	17.2%	40.2%	5.9%	9.8%
Si	7.1%	20.5%	1.8%	5.2%
Zn	5.8%	30.0%	0.0%	8.2%
Pb	4.9%	33.8%	0.0%	8.6%
Al	2.7%	5.4%	0.7%	1.3%
Mn	1.5%	10.1%	0.0%	3.0%
Ca	1.2%	11.7%	0.0%	2.7%
Mg	0.7%	2.9%	0.0%	0.9%
K	0.5%	2.5%	0.0%	0.6%
P	0.4%	1.4%	0.0%	0.5%
Na	0.3%	1.2%	0.0%	0.4%
Ti	0.2%	0.5%	0.0%	0.2%
As	0.2%	2.0%	0.0%	0.5%
Cl	0.2%	1.3%	0.0%	0.4%
Cu	0.1%	0.8%	0.0%	0.3%
S	0.0%	0.1%	0.0%	0.0%

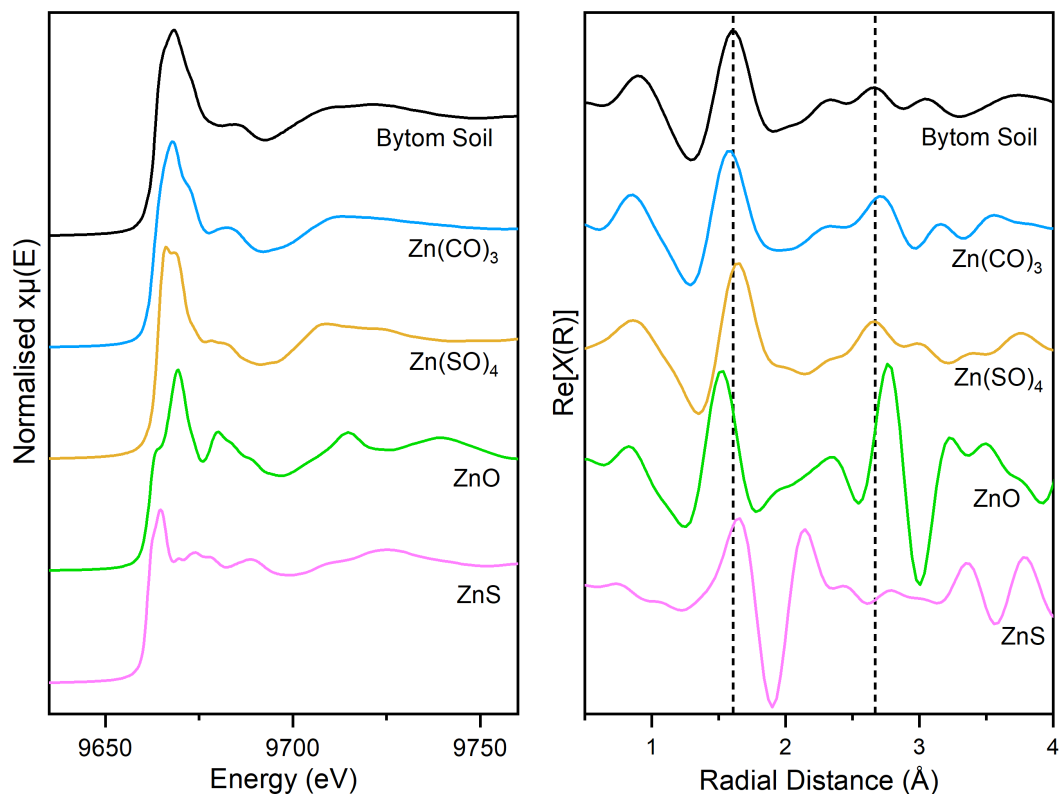


Figure 4.2: XAFS for Bytom soil and Zn standards: (Left) XANES; (Right) Real part of the Fourier Transform

weighted spectra for fitted paths (left) and the final fit compared to the original sample's spectrum (right) are illustrated. The quantified fitting parameters arising from both the EXAFS fits for Zn standard compounds and the Bytom soil are displayed in table 4.7.

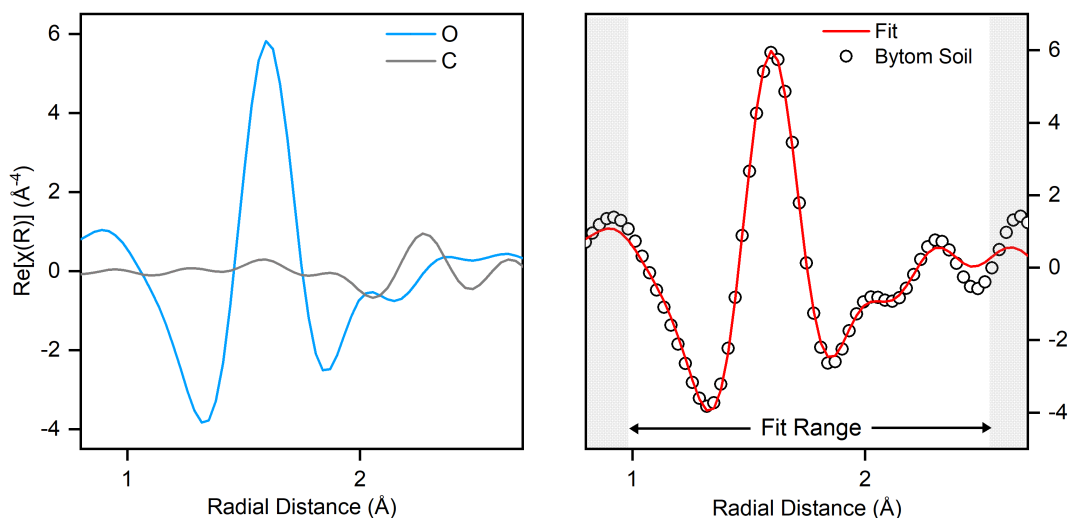


Figure 4.3: EXAFS fitting for Bytom soil. Left) weighted Real part of the Fourier Transform for first and second shell O, C and S paths; Right) Real part of the Fourier Transform for Bytom soil and final Fit result

Table 4.7: EXAFS fitting parameters for Zn standards and Bytom soil

Sample	Path	CN	R (\AA)	σ^2 (\AA^2)
Bytom Soil	O	5.2(± 0.7)	2.04(± 0.01)	0.01155(± 0.0024)
	C	0.6(± 0.6)	2.72(± 0.03)	0.00216(± 0.0084)
$\text{Zn}(\text{CO})_3$	O	5.2(± 0.6)	2.02(± 0.01)	0.00491(± 0.0047)
	C	4.9(± 2.0)	2.94(± 0.02)	0.00896(± 0.0077)
ZnO	O	3.5(± 0.5)	1.96(± 0.04)	0.01079(± 0.0027)
	Zn	12.9(± 1.9)	3.24(± 0.05)	0.00932(± 0.0152)
ZnS	S	3.5(± 0.2)	2.30(± 0.01)	0.00473(± 0.0009)
	Zn	10.7(± 1.5)	3.80(± 0.01)	0.01472(± 0.0014)

4.4 Discussion

The XRF data for the sample generally exhibited greater HM contamination than seen in the published data for the Bytom site (table 4.8). The exception to this was Cd which was not detected in the sample. As Cd uptake was not found during initial screening tests to be significant by the *Miscanthus* grown at the site (chapter 5) Cd is not considered further. The disparity between the published site data for Zn and Pb is greater when comparing the SEM-EDX spot sample data (converted to mg/kg in table 4.8). Whilst some discrepancies must be expected due to sampling errors inherent with environmental media, the differing techniques adopted must also be considered as these may impact the results. This is considered below.

Within the published data for Bytom, Rusinowski et al. (2019b) al measured HM using hot *aqua regia* digestion followed by AAS. This is a bulk technique to quantify total metals' concentration in soils (ISO-11466, 1995). The portable XRF used to determine the sample's HM concentration is also a bulk technique, providing an average figure for the sample. However, XRF must be considered a surface-sensitive technique. This is due to the penetration depth of the primary X-rays being perhaps 10-100 μm or so, depending also on the matrix of the sample, and the self absorbance of the emitted fluorescence radiation further compromises the acquisition of data beyond near-surface regions in the sample (Schmeling et al., 2005). Due to this property of XRF, the surface of the soil has to be representative of the entire sample matrix in order for XRF results to match those of bulk techniques (such as *aqua regia* digestion and AAS).

The surface sensitivity of SEM-EDX is even more acute than XRF. The precise properties (low interaction volume of $c.1 \mu\text{m}$) which provide SEM with its high resolution capability also limit the acquisition of information to near-surface regions within the samples (Liao, 2006). Therefore, heterogeneity which creates a difference between an element's prevalence on the surface of the soil particle compared with the particle's interior would result in SEM-EDX returning different values when compared with bulk techniques. For example,

Table 4.8: Comparison of XRF results for the sample soil with mean values for Bytom site data (Rusinowski et al., 2019a) and mean values for spot samples (n=14) for the sample soil using SEM-EDX

Metal	Sample XRF (mg/kg)	Site data (mg/kg)	SEM-EDX (mg/kg)
Zn	4,006	3,312	58,000
Pb	1,859	719.6	49,000
Cd	<LOD	26.5	<LOD

if the distribution of a particular element was predominantly in the form of a surface coating then SEM-EDX would provide a much higher value for that element's abundance compared to a determination using *aqua regia* digestion and AAS. The SEM-EDX data for Zn and Pb in the soil sample is an order of magnitude higher than the XRF data for the same sample. This is considered to be associated with the surface effects of the technique.

The SEM-EDX imaging provides information about spatial distribution of the elements (figure 4.1). Despite the comparatively high values for both Zn and Pb gained from the SEM-EDX spot samples, there is little indication within the images that these HM are associated with discrete particles (in the way Fe is, for example). Rather, both Zn and Pb are comparatively evenly distributed across the soil matrix.

Based upon the known surface bias of the techniques, the XRF and SEM-EDX data for the soil sample suggest that both Zn and Pb may be associated with a widespread, homogenous surface coating across the soil matrix. Further analyses would be required to confirm this with confidence. However, this would accord with general observations regarding Zn/Pb sorption onto soil particle surfaces (ATSDR, 2020; Lindsay, 1979). The data contain no suggestion that Zn and Pb are associated distinct Pb/Zn granular materials within the soil e.g. as may result from dumping solid wastes.

The results of the Tessier extractions for the soil sample can be compared with the relative distributions for Zn and Pb published by Chlopecka et al. (1996).

The distribution of Zn across the extractions from the Bytom sample is very similar to the data reported by Chlopecka. The ranked order of Zn across the different Tessier extractions is the same with the largest fraction being residual (32%), followed by Fe/Mn oxides (29%), carbonates (23%), bound to organics (11%) and finally exchangeable (5%). The individual percentage values for each fraction are also highly comparable (table 4.1). This lends confidence that the sample contains a distribution of species that is typical of Zn contamination in soils in southwest Poland.

The distribution of Pb is somewhat different. Chlopecka et al. (1996) identified the largest fraction of Pb as bound Fe/Mn oxides (mean 56.7%, range 46-63%) whereas very little Pb from the Bytom soil was detected within this fraction (mean 5%). The two most mobile fractions in the Bytom soil compare well with the ranges observed by Chlopecka et al. (1996): the Bytom exchangeable fraction was 3% compared to the reported range of 0.1 - 8%, and the Bytom carbonate fraction was 24% compared to a range of 2 - 32% (table 4.3). The Bytom organic fraction is also within range: 35% compared to a range of 8 - 37% reported by Chlopecka et al. (1996). The major difference associated with the Fe/Mn oxide fraction appears to be principally balanced by difference in the residual fraction: the Bytom residual data for Pb (34%) being above the 3 - 19% reported by Chlopecka et al. (1996).

Whereas the Tessier extractions allocate metals to operationally defined categories, the study of XAFS data can provide information about chemical speciation with more resolution. Inspection of the XANES highlights that the Bytom soil spectrum is highly comparable to that of $\text{Zn}(\text{CO})_3$, both in terms of the size of the white line and the shape of spectral features e.g. the post-edge 'shoulder' at around 9682 eV. The edge positions are slightly different, however, with E_0 for the soil being slightly higher at 9663.2 eV compared with 9662.9 eV for $\text{Zn}(\text{CO})_3$. The edge position for soil is also above the other standards of ZnO (9661.9 eV) and ZnS (9661.3 eV). This leaves the soil edge position sitting closely between that of $\text{Zn}(\text{CO})_3$ and the final standard of $\text{Zn}(\text{SO})_4$ which possesses a slightly higher E_0 of 9664.2 eV. The shape of the white line of $\text{Zn}(\text{SO})_4$ differs from that of the soil spectrum, although there

is a somewhat similar post-edge shoulder - this feature in the soil spectrum having an appearance somewhere between that of $\text{Zn}(\text{CO})_3$ (more pronounced) and $\text{Zn}(\text{SO})_4$ (less pronounced). All the edge positions are consistent with Zn being in the +2 oxidation state.

The application of Linear Combination Fitting (LCF) to the XANES confirms the above visual observations. When all four standards were fitted to the soil spectra the majority of the weighting was placed on $\text{Zn}(\text{CO})_3$ (84%) with $\text{Zn}(\text{SO})_4$ receiving 16% weighting. The fitting did not identify any contribution from either ZnO or ZnS. This strongly suggests that the majority of Zn in the soil is in some form of octahedral coordination with O, as both carbonate and sulfate exhibit this structure. Despite the principal similarity to $\text{Zn}(\text{CO})_3$, the contribution of $\text{Zn}(\text{SO})_4$ to the LCF suggests heterogeneity through mixed O-species or a disordered structure.

Isolation and analysis of the EXAFS confirms the XANES conclusions. Plotting the real part of the Fourier Transform (rFT) (figure 4.2) the first major peak (1.6 Å) associated with the soil sample is observed as sitting between similar peaks for $\text{Zn}(\text{CO})_3$ and $\text{Zn}(\text{SO})_4$. At greater radial distances the rFT for the Bytom soil exhibits similar equivalent features, e.g. at 2.7 Å where the peak structure appears similar to a slightly damped form of $\text{Zn}(\text{CO})_3$.

There is no indication in the soil's rFT that there is Zn in the second coordination shell. Zn in the second coordination shell is evidenced in the rFT for ZnO where a strong scattering signal is evident at c.2.9 Å but this is not observed with the soil's rFT. Equally, there is no clear evidence of S being present in the first coordination shell as despite the first peak (maximum) of rFT for ZnS being similar to soil, the characteristic trough (minimum) which S produces at c.1.9 Å in the first shell is not evident with the soil's rFT.

Fitting of EXAFS for Zn standards was performed to provide reference values to inform the interpretation of the soil data (table 4.7). The first shell fitting of $\text{Zn}(\text{CO})_3$ was characteristic of octahedral coordination with O: the coordination number (CN) was $5.2(\pm 0.7)$ at radial distance of $2.04(\pm 0.01)\text{Å}$. Tetrahedral coordination of O in the first shell produces different result, which

can be observed in the fit parameters for ZnO: where CN was $3.5(\pm 0.5)$ at a radial distance of $1.96(\pm 0.04)\text{\AA}$. With tetrahedral coordination the radial distance is significantly smaller than that of octahedral coordination. The ZnS standard was used to obtain fitting results for S in the first shell. ZnS is also tetrahedral in structure but the S species results in significantly larger bond length (CN $3.5(\pm 0.2)$ at a radial distance of $2.30(\pm 0.01)\text{\AA}$) which is not in evidence within the soil rFT.

Best fits of the Bytom soil EXAFS was obtained for first and second coordination shells with radial distance between 1 and 3 \AA (R-factor 0.005, reduced chi-square 143) - see figure 4.3. The fit results corroborates that Zn within the Bytom soil is predominantly as O coordinated species. The fit results for both coordination number and bond distance suggest octahedral O coordination: CN $5.2(\pm 0.7)$ at radial distance $2.04(\pm 0.01)\text{\AA}$. Satisfactory results for second shell fitting (as indicated by $>20\%$ reduction in reduced chi-square) was achieved using a C with CN $0.6(\pm 0.6)$ at $2.72(\pm 0.03)\text{\AA}$.

The fitting results indicate that Zn is predominantly in the form of octahedral O species. This is consistent with carbonate. However, the high σ^2 value returned by the fit is indicative of a highly disordered system and/or mixed coordination environment. Mishra et al. (2020) identified similar fit values for O (CN 5.98 at 2.08\AA) and C (CN 2.85 at 2.85\AA) associated with Zn complexed to organic acids such as malate within biological (plant) systems. The Tessier extractions did classify a proportion of Zn bound to organic matter within the Bytom soil, but this was a minority (11%) of the overall Zn in the sample. Karlsson and Skyllberg (2007) used EXAFS to establish the coordination chemistry of Zn in two organic soils and in addition to O/N atoms (CN 2.7 - 3.7 at $1.99 - 2.04\text{\AA}$) the presence of S in the first shell was also identified (CN 0.4 - 0.9 at $2.29 - 2.33\text{\AA}$) in all cases. Karlsson and Skyllberg (2007) assert that within soil Zn complexed with organics was identifiable as a mix of tetrahedral and octahedral O/N along with S species consistent with thiolates (RS-) within proteins. With respect to the Bytom soil results: neither the presence of tetrahedral O nor the presence of first shell S were detected to any significant extent. Therefore the EXAFS results support the Tessier extrac-

tion data in suggesting that Zn-organic complexes are a small contributor to Zn species in the Bytom soil. The XANES/EXAFS signal associated with such Zn-organic complexes was insufficient to impact either fitting process (LCF or EXAFS) to a significant extent.

The Tessier extractions indicate that the great majority of the non-carbonate species are the Fe/Mn oxide (29%) or residual (32%) fractions, representing the majority of Zn overall. Therefore, one should expect the chemistry of these fractions to have the major influence on the EXAFS signal. There is no clear signal in the Bytom EXAFS of the presence of high-Z elements, such as metals, coordinating with Zn (second shell or beyond). High-Z elements would be expected to produce a strong back-scattering signal which was not detectable in the soil EXAFS. It is therefore not proven that Fe/Mn atoms are present to any significant extent in the near coordination environment of Bytom soil Zn. However, as Tessier extractions are operationally defined categories, and do not represent positive identification of specific chemistries, a broad interpretation of the Tessier results must be used.

Lopes et al. (2021) used EXAFS analysis of Zn to study speciation in soils contaminated by mining and smelting operations. In that study low Zn mobility was linked to the predominance of Zn-phyllsilicates and Zn layered-double hydroxide (LDH) species within the Zn contaminated soils. Phyllsilicates are sheet silicas that are characterised by interconnected rings comprised of SiO_4^{-4} , typically in alternating tetrahedral/octahedral sheets around central hydroxide (OH^-) ions. Phyllsilicates can form complexes with divalent metals (often Mg^{2+} or Fe^{2+} in uncontaminated soils) which bond via the O and OH^- in octahedral coordination forming layers of metal cations (Nelson, 2015).

Manceau et al. (2000) used a suite of techniques including EXAFS to analyse Zn speciation in smelter contaminated soils. Here dust emitted from Zn smelting process was found to be high temperature minerals comprised of a mixture of franklinite (ZnFe_2O_4), willemite (Zn_2SiO_4), hemimorphite ($\text{Zn}_4\text{Si}_2\text{O}_7(\text{OH})_2 \cdot \text{H}_2\text{O}$), and Zn-containing magnetite ($[\text{Fe,Zn}]\text{Fe}_2\text{O}_4$). After weathering of these minerals the Zn was considered to be substituted into the

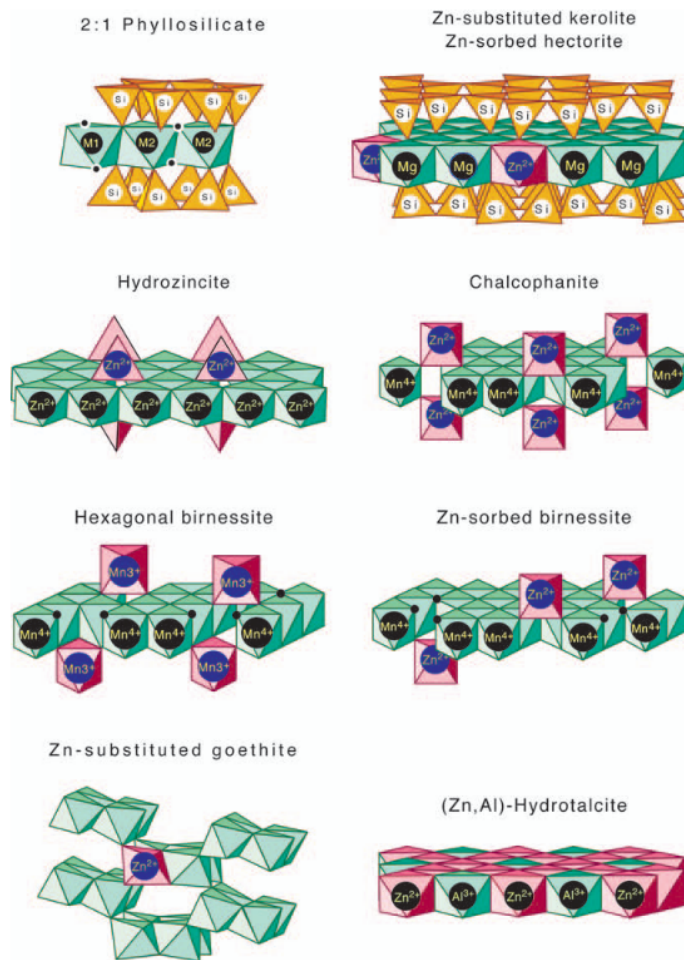


Figure 4.4: Idealised phyllosilicate structure (top left) and proposed Zn substitution into related mineral structures. After Manceau et al. (2000)

matrix of various phyllosilicates (see figure 4.4) and to a lesser degree Mn/Fe oxides.

The lack of any EXAFS signal indicating high-Z elements coordinating with Zn in the Bytom soil would preclude the significant presence of compounds such as franklinite which Manceau et al. (2000) identified within smelter dusts. Franklinite would have a strong back scattering signal associated with Fe at around 3.4 Å (Levy et al., 2000) and this is not observed in the Bytom soil. However, the presence of Zn bound with phyllosilicates in the Bytom soil would agree with both the EXAFS fitting results (which suggest octahedral O coordination) and the Tessier extractions demonstrating predominantly low mobility species (i.e. operationally classified as Fe/Mn oxide and residual fractions). Given the above combination of Tessier and EXAFS data, the industrial history around Bytom, along with the characterisation of smelter pollution by Manceau et al. (2000), it is considered likely that a large proportion of Bytom Zn is associated with sorption onto, or structural incorporation into, phyllosilicate particles.

4.5 Conclusions

A complete characterisation of HM in the Bytom soil is beyond the scope of this project. Rather, in order to support the subsequent studies of uptake by *Miscanthus*, the nature of soil Zn and Pb must be sufficiently characterised to understand how their distribution and speciation may influence bioavailability and subsequent plant uptake.

The bulk analyses confirmed the sample used for analyses contained significant Zn and Pb contamination, as is reported within literature regarding the Bytom site. The data regarding the extent of contamination are strongly influenced by the techniques employed. The more surface sensitive techniques (XRF and, particularly, SEM-EDX) produce higher values for both Zn and Pb compared to bulk chemical analysis (e.g. digestion). This suggests that the contamination is biased towards sorption onto the surface of soil particles, rather than

comprising bulk mineral particles which would have suggested the disposal of solid waste (e.g. tailings or slags). Rather, a combination of evidence points towards the contamination at Bytom as likely being the result of air deposition of smelter emissions/dusts, weathering and subsequent sorption onto silicate soil particles. There is evidence to suggest that organic complexes contribute little to soil Zn, with perhaps a higher contribution to Pb in the soil.

Despite very high levels of contamination, only a minority of total Zn and Pb is considered present as relatively mobile (and hence bioavailable) species. The Tessier data operationally classify these as exchangeable which represents 3% of Pb and 5% of Zn. The next most available is classified as carbonate which represents a much higher proportion of both Pb (24%) and Zn (23%). The EXAFS data for Zn fits well with there being a prevalence of carbonate species, although may be somewhat confounded by similar results expected from Zn sorption onto phyllosilicates. Complexation with organic matter is considered to be only a minor proportion of overall Zn species.

4.6 Appendix

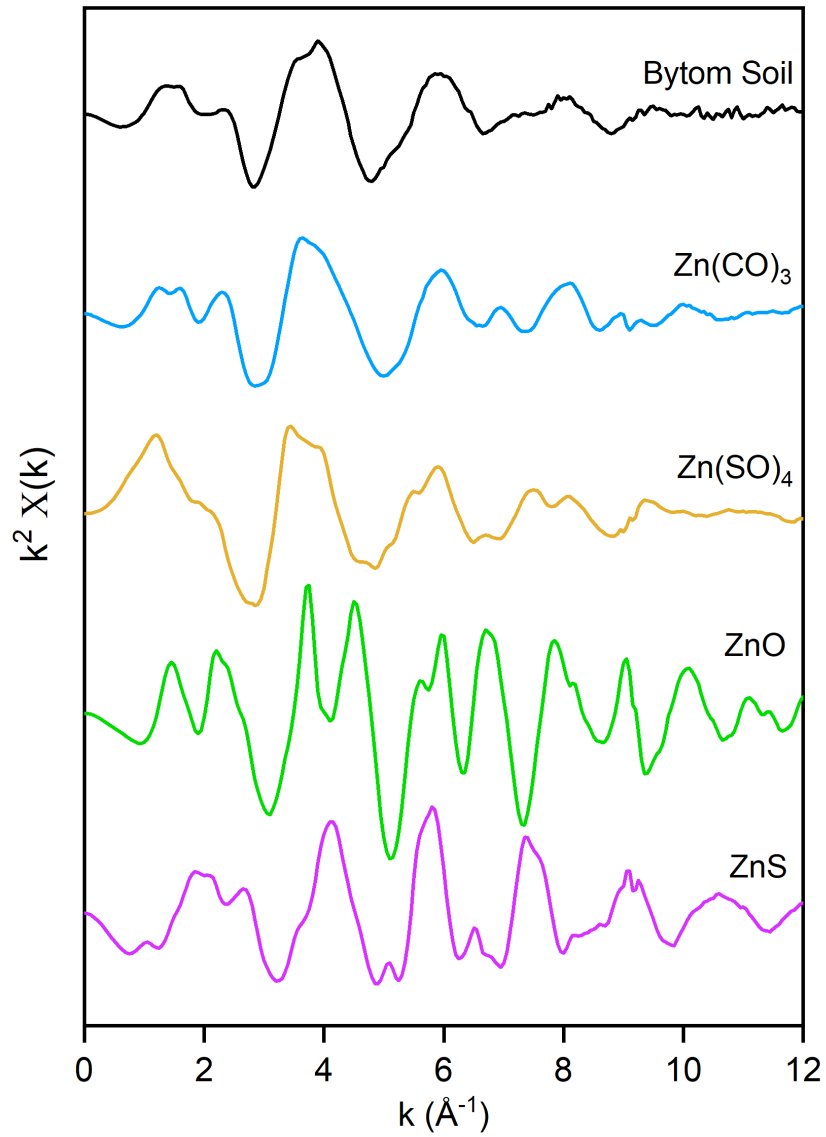


Figure 4.5: Xk for Bytom soil and Zn standard

4.7 References

- ATSDR (1992). Toxicological profile for zinc. Report, United States Agency for Toxic Substances and Disease Registry.
- ATSDR (2020). Toxicological profile for lead.
- Chlopecka, A., Bacon, J. R., Wilson, M. J., and Kay, J. (1996). Forms of cadmium, lead, and zinc in contaminated soils from southwest poland. Report 0047-2425, Wiley Online Library.
- Corrin, M. L. and Natusch, D. F. S. (1977). Physical and chemical characteristics of environmental lead. *Lead in the Environment*, pages 7–31.
- Dz, U. (2016). Decision of the polish ministry of environment on the assessment of soil contamination.
- EPA (1982). An exposure and risk assessment for lead. Report.
- EPA (1986a). *Air quality criteria for lead*, volume 4. US Environmental Protection Agency, Office of Research and Development
- EPA (1986b). Superfund record of decision (epa region 5): Forest waste disposal site, genesee county, michigan. Report.
- EPA (2013). Integrated science assessment (isa) for lead. Report.
- Graf, D. L. (1961). Smithsonite. *American Mineralogist*, 46:1283–1316.
- Harrison, R. and Laxen, D. (1981). *Lead Pollution: Causes and Control*. Springer Dordrecht, 1 edition.
- Harrison, R. M. (1986). *Analysis of particulate pollutants*, pages 155–214. Springer.
- ISO-11466 (1995). Iso 11466 - soil quality - extraction of trace elements soluble in aqua regia. Technical report, CEN.
- Karlsson, T. and Skyllberg, U. (2007). Complexation of zinc in organic soilsexafs evidence for sulfur associations. *Environ. Sci. Technol.*, 41(1):119–124.

- Krzyzak, J., Pogrzeba, M., Rusinowski, S., Clifton-Brown, J., McCalmont, J. P., Kiesel, A., Mangold, A., and Mos, M. (2017). Heavy metal uptake by novel miscanthus seed-based hybrids cultivated in heavy metal contaminated soil. *Civil and Environmental Engineering Reports*, 26(3):121–132. Fp4zu
Times Cited:2 Cited References Count:22.
- Lee Jr, R. E. and Von Lehmden, D. J. (1973). Trace metal pollution in the environment. *Journal of the Air Pollution Control Association*, 23(10):853–857.
- Levy, D., Pavese, A., and Hanfland, M. (2000). Phase transition of synthetic zinc ferrite spinel (znfe₂o₄) at high pressure, from synchrotron x-ray powder diffraction. *Physics and Chemistry of Minerals*, 27(9):638–644.
- Liao, Y. (2006). *Practical Electron Microscopy and Database*.
- Lindsay, W. L. (1979). *Chemical equilibria in soils*. John Wiley and Sons Ltd.
- Lloyd, T. B. and Showak, W. (1984). Zinc and zinc alloys. *Kirk-Othmer encyclopedia of chemical technology*, 24:835–836.
- Lopes, G., Li, W., Siebecker, M. G., Sparks, D. L., and Guilherme, L. R. G. (2021). Combining zinc desorption with exafs speciation analysis to understand zn mobility in mining and smelting affected soils in minas gerais, brazil. *Science of The Total Environment*, 754:142450.
- M., S. and R, G. (1978). H-zn s o₄, das erste sulfat mit einer kubischen h-cristobalit-struktur. *Naturwissenschaften*,.
- Ma, L. Q. and Rao, G. N. (1997). Chemical fractionation of cadmium, copper, nickel, and zinc in contaminated soils. Report 0047-2425, Wiley Online Library.
- Manceau, A. L. A. I. N., Lanson, B., Schlegel, M., Musso, M., Hazemann, J.-L., Chateigner, D., and Lambelle, G. (2000). Quantitative zn speciation in smelter contaminated soils by exafs spectroscopy. *American Journal of Science*, 300:289–343.

- Mishra, B., McDonald, L., Roy, M., Lanzirrotti, A., and Myneni, S. (2020). Uptake and speciation of zinc in edible plants grown in smelter contaminated soils. *PLoS ONE*, 15(4):.
- Nelson, S. (2015). Phyllosilicates. In *Mineralogy*.
- Nriagu, J. O. and Davidson, C. I. (1980). Zinc in the atmosphere. *Nuclear Physics, Section A*, pages 113–159.
- Nriagu, J. O. and Pacyna, J. M. (1988). Quantitative assessment of worldwide contamination of air, water and soils by trace metals. *Nature*, 333(6169):134–9. Nriagu, J O Pacyna, J M eng Review England 1988/05/12 Nature. 1988 May 12;333(6169):134-9. doi: 10.1038/333134a0.
- Pacyna, J. M., Bartonova, A., Cornille, P., and Maenhaut, W. (1989). Modelling of long-range transport of trace elements. a case study. *Atmospheric Environment (1967)*, 23(1):107–114.
- Ravel, B. and Newville, M. (2005). Athena, artemis, hephaestus: data analysis for x-ray absorption spectroscopy using ifeffit. *Journal of Synchrotron Radiation*, 12:537–541. 4 935rl Times Cited:7259 Cited References Count:23.
- Rusinowski, S., Krzyzak, J., Clifton-Brown, J., Jensen, E., Mos, M., Webster, R., Sitko, K., and Pogrzeba, M. (2019a). New miscanthus hybrids cultivated at a polish metal-contaminated site demonstrate high stomatal regulation and reduced shoot pb and cd concentrations. *Environmental Pollution*, 252:1377–1387. B Iu2jf Times Cited:1 Cited References Count:67.
- Rusinowski, S., Krzyzak, J., Sitko, K., Kalaji, H. M., Jensen, E., and Pogrzeba, M. (2019b). Cultivation of c4 perennial energy grasses on heavy metal contaminated arable land: Impact on soil, biomass, and photosynthetic traits. *Environmental Pollution*, 250:300–311.
- Saeed, M. and Fox, R. L. (1977). Relations between suspension ph and zinc solubility in acid and calcareous soils. *Soil Science*, 124(4):199–204.

- Schmeling, M., Worsfold, P., Townshend, A., and Poole, C. (2005). X-ray fluorescence and emission — total reflection x-ray fluorescence. In *Encyclopedia of Analytical Science (Second Edition)*, pages 440–448. Elsevier, Oxford.
- Tai, A. Y. C., Chen, L. W. A., Wang, X., Chow, J. C., and Watson, J. G. (2017). Atmospheric deposition of particles at a sensitive alpine lake: Size-segregated daily and annual fluxes from passive sampling techniques. *Science of The Total Environment*, 579:1736–1744.
- Vandegrift, A. E., Shannon, L. J., Sallee, E. E., Gorman, P. G., and Park, W. R. (1971). Particulate air pollution in the united states. *Journal of the Air Pollution Control Association*, 21(6):321–328.

Chapter 5

Biomass Characterisation: Uptake Response, Retention Pattern and Speciation

Abstract

The uptake by and distribution of Zn and Pb within a novel seed-based *Miscanthus* hybrid grown in contaminated soil was assessed. Results from juvenile plants in a pot-trial was compared with data for mature biomass of the same species harvested during a field-trial. Both Zn and Pb uptake by juvenile plants were observed to increase in proportion to the soil concentrations. Both Zn and Pb accumulation differed between leaf and stem structures, and both were different in the mature biomass compared with juvenile plants. Analysis of X-Ray Absorption Fine Structures (XAFS) revealed different Zn speciation in stems and leaves, and differences in Zn speciation with plant maturity. Sulfur ligands consistent with the presence of cysteine rich metallothioneins (MT) and phytochelatin (PC) complexes were the dominant Zn species in juvenile plant leaves, together with octahedral O/N species typified by Zn-malate. Sulfur ligands were also prevalent in stems from juvenile plants, but predominant O/N speciation shifted towards tetrahedral coordination. In contrast, tetrahedral Zn coordination with O/N species predominated in the mature biomass crop. The XAFS spectra for the mature biomass were consistent with Zn being retained within cell walls as pectin and/or phosphate complexes.

5.1 Introduction

In this study, a novel seed-based *Miscanthus* hybrid was grown in pot trials using a growing media with Zn and Pb contamination comparable with that observed at the Bytom field trial site. Data published for the field trial identified the uptake of Zn and Pb, and to a lesser extent Cd, by *Miscanthus* plants (Krzyzak et al., 2017; Rusinowski et al., 2019a). This study focusses on Zn and Pb due to their greater uptake.

The pot trial was conducted at the Plant Growth Suite on campus at the University of Leeds. Plants of the same hybrid that was grown at the Bytom field trial site were grown from seeds under controlled conditions. The juvenile

plants were grown in engineered growing media with varying degrees of Zn and Pb contamination. Some plants were grown in media engineered to replicate the contamination at Bytom, whilst others were grown in media with increasing contamination. In this way the plants' response to differing conditions could be observed under controlled conditions. Furthermore, the biomass of the juvenile plants could be compared to that of the mature biomass from the Bytom crop.

Bulk chemical analysis and XAFS techniques were used to determine Zn and Pb uptake and Zn speciation within the plants from the pot trial. The results from the pot trial plants were compared with uptake and speciation observed within mature biomass from the same *Miscanthus* species harvested during the field trial. In this way this study establishes patterns of uptake for these HMs, reveals significant differences in the pattern of storage within the plants, and identifies temporal and spatial changes in the biochemistry of Zn sequestration.

In Eudicot plants Zn has been found to be sequestered with several biochemical ligands, including tetrahedrally coordinated with N in Zn-histidine complexes (Kupper et al., 2004; Mishra et al., 2020; Salt et al., 1999) octahedrally coordinated with O-ligands in Zn-malate or Zn-citrate complexes (Kupper et al., 2004; Mishra et al., 2020; Sarret et al., 2002) tetrahedrally coordinated to S in Zn-cysteine complexes (Adele et al., 2018; Mishra et al., 2020) and, in roots, in Zn-phytate complexes (Adele et al., 2018; Terzano et al., 2008) where it is probably tetrahedrally coordinated to O (Neal et al., 2013; Rodrigues-Filho et al., 2005; Sarret et al., 2009). There is also evidence from eudicot plants that Zn speciation and localisation in the plants varies with the growth conditions and the amount of Zn available (Adediran et al., 2016; Adele et al., 2018; Kelly et al., 2002; Mishra et al., 2020). To date, fewer studies have investigated Zn speciation and localisation within grasses, such as *Miscanthus*, that are used as energy crops. Divergence during their evolution has led to major structural differences between both the leaves and stems of eudicot and monocot plants (Esau, 1977), so the distribution and speciation of Zn in grasses such as *Miscanthus* may differ.

The chemical composition of *Miscanthus* biomass has been shown to display seasonal variability which can be favourably manipulated to enhance combustion characteristics of the final biomass (Baxter et al., 2014; Lewandowski and Heinz, 2003). Research to date has focused on seasonal changes in the major inorganic species (N, S, Cl, K, Ca, Na, Fe, Mg). The major alkaline and earth metal concentrations are significantly lower within aerial (stem and leaf) structures when plants are senescent over winter than in other seasons and this results in changes in the fuel combustion characteristics (Baxter et al., 2012, 2014). The extent to which *Miscanthus*' uptake of HM display such temporal variations across the year is poorly understood in comparison.

5.2 Methods

5.2.1 Field Trial Biomass

A sample of *Miscanthus* was obtained from field trial at a HM contaminated site at Bytom near Katowice (Poland). The plants were a novel seed-based hybrid developed by Aberystwyth University (UK) during the GIANT LINK Program (LK0863). The hybrid's growth performance characteristics under field trial conditions has been subjected to detailed analysis (Rusinowski et al., 2019a). The biomass material used in this study was mechanically harvested and shredded in March 2018 at the end of the winter senescence period in accordance with conventional agricultural practice.

5.2.2 Pot Trial Growing Media

Soil from Spen Farm, Yorkshire, UK (53°51'39.8"N 1°20'39.7"W) was collected for formulation of growing media within the pot trials (described below). The major chemical characteristics of the Spen Farm soil compared to the Bytom soil are reported in table 5.1 and the results of Tessier extraction for Zn and Pb are reported in table 5.2.

Table 5.1: Major elemental analysis of soil from the Bytom field trial and the Spen Farm soil used for the pot trial

Determinand	Unit	Bytom¹	Spen Farm²
pH		7.3	7.6
CEC	meq/100g	13.0	18.7
Ca	mg/kg _(dm)	1370	1780
P	mg/kg _(dm)	27	20
K	mg/kg _(dm)	23	106
Mg	mg/kg _(dm)	123	499
Na	mg/kg _(dm)	6	8
Total N	%w/w	0.2	0.16
Organic matter	%w/w	6.4	2.8

References:
¹Terravesta (2018), ²NRM (2017)

Table 5.2: Results of Tessier extractions for Pb and Zn in the Spen Farm soil

Extraction	n	Zn			Pb		
		Range	Mean		Range	Mean	
		mg/kg	mg/kg	%	mg/kg	mg/kg	%
Exchangeable	3	<LOD	-	0%	<LOD	-	0%
Carbonates	3	<LOD	-	0%	<LOD	-	0%
Fe/Mn Oxide	3	<LOD	-	0%	<LOD	33	89%
Organic	3	<LOD	-	0%	<LOD	-	%
Residual	3	70 - 76	73	100%	10 - 19	4	11%

Table 5.3: Concentrations of metal added to Spen Farm soil in the pot trials ($\text{mg}_{(\text{metal})}/\text{kg}_{(\text{dm})}$)

Sample ID	n	Zn			Pb		
		as ZnCl ₂	as ZnCO ₃	total Zn	as PbCl ₂	as PbCO ₃	total Pb
Control	11	-	-	-	-	-	-
1x(Zn+Pb)	11	242	946	1188	75	469	544
High Zn							
2xZn	4	497	2162	2659	-	-	-
5xZn	4	1007	4693	5700	-	-	-
High Pb							
2xPb	4	-	-	-	172	1072	1244
5xPb	4	-	-	-	298	2249	2547
High Zn+Pb							
2x(Zn+Pb)	4	432	1877	2309	149	931	1080
5x(Zn+Pb)	4	1007	4693	5700	298	2249	2547

To create a soil contaminated with Zn and Pb present in species comparable to those measured by Tessier extractions of the Bytom soil, ZnCl₂ and PbCl₂ (exchangeable) and ZnCO₃ and PbCO₃ (carbonate) were added to Spen Farm soil. The soil which replicated the Zn and Pb concentrations in the exchangeable and carbonate fractions of Bytom soil is subsequently referred to as 1x(Zn+Pb). Other contaminated soils were created using Zn only, Pb only, and both Zn and Pb using concentrations equivalent to 2x and 5x the concentrations in Bytom soil. In each case the proportion of the metal added as a chloride or carbonate salt was the same as the exchangeable/carbonate ratio for that metal observed in Bytom soil. Spen Farm soil was used without metal addition as the ‘Control’ soil. The metal concentrations added to the Spen Farm soil in the various pot experiments are shown in table 5.3, along with the number of replicates for each growth condition.



Figure 5.1: Pot trial a) single *Miscanthus* 'plug' at the start of the trial; b) pots of *Miscanthus* growing under controlled conditions, including artificial lighting

5.2.3 Pot Trial Growth Conditions

Three month old *Miscanthus* plants were supplied by Terravesta Ltd. (UK) in small pot ('plug') trays. The plants were grown from seed at Bell Brothers Nurseries Ltd., Boston (UK). The pot trial was conducted in a 4 x 5 m controlled environment plant growth suite at University of Leeds (UK). The growth suite was equipped with lighting on a timer to maintain a consistent 18-hour photoperiod each day. Photosynthetically active radiation (PAR) at the growing trays was monitored and observed in the range of 350 – 234 $\mu\text{mol m}^{-2}\text{s}^{-1}$ with average being 281 $\mu\text{mol m}^{-2}\text{s}^{-1}$. A forced ventilation system maintained ambient O₂/CO₂ concentrations. Temperatures were controlled within the range of 30.8 – 18.7°C with the mean temperature being 21.7°C. Each plant was grown in separate 0.25 L pots and were hand-watered every second day with tap water until saturated. The pot trial was run for 66 days (figure 5.1).

5.2.4 Harvesting and Sample Preparation

Plants from the pot trial were individually harvested and divided into root, stem and leaf sections for each plant before being frozen at -20°C . Biomass from the Bytom field trial was mechanically harvested and shredded (mixed stem and leaf material) on site consistent with standard agricultural practice before further size reduction and homogenisation using a Retsch SM300 Cutting Mill to particle size ≤ 5 mm. Samples were prepared for chemical and XAFS analysis using standard drying and milling techniques (Li et al., 2019; Luo et al., 2018; Medas et al., 2019), as follows: each sample was weighed, dried at 105°C for 4 hours and weighed again to determine the moisture content and amount of dry matter. The samples for acid digestion and XAFS analysis were then ground to a fine powder using a Retch Cryo-mill using a zirconium oxide grinding jar which was cryogenically cooled using liquid nitrogen.

5.2.5 Analysis of Biomass Metal Concentration

The metal concentrations in both stem and leaf biomass was determined for approximately half of the replicates for each pot trial configuration (stem and leaf biomass from the remaining replicates were retained for XAFS analysis).

Acid digestion: Cryo-milled plant material (0.5 g) was added 10 mL of HNO_3 69% in a 250 mL flask and heated on a hot plate to achieve a strong effervescence. Once brown fumes had subsided (c.4 hours) the flasks were allowed to cool and 4 mL of 30% H_2O_2 added carefully before reheating for a further 2 hours. Digested samples were allowed to cool overnight, made-up to 25 mL with ultra-pure dH_2O , and then filtered using a $0.2\ \mu\text{m}$ Luer syringe filter.

ICP-MS analysis: The digested biomass was analysed using a Perkin Elmer Elan ICP-MS that had been previously calibrated for Zn and Pb using solution standards which had been matrix-matched for Si, Ca, Mg and K to concentrations consistent with that expected for *Miscanthus* based upon literature database values (ECN, 2018).

5.2.6 XAFS Analysis

XAFS data across the Zn K-edge were collected from the biomass samples at beamline 10-BM-B at the Advanced Photon Source (APS), Chicago (USA). A Si(111) monochromator with an energy resolution of $1 \times 10^{-4} \Delta E/E$ was used, and the spectra were recorded in fluorescence mode using an ion chamber in Stern-Heald geometry. The ion chamber used to measure the I0 was flooded with a mixture of 30% N₂ and 70% He gas. Biomass samples were pressed into 3 mm thick pellets and mounted using Kapton tape in an acrylic sample holder set at 45° to the beam. Energy grid alignment was facilitated by placing a Zn reference foil between It and Iref detectors and these ion chambers were flooded with a mixture of 50% N₂ and 50% Ar gas.

A value of 9665 eV was selected as being just after the anticipated absorption edge associated with the Zn K-edge. Scans were performed using 5 energy regions each of which start at -150, -30, +60, +6k, and +9k eV above/below this value, finishing at +12 keV, with energy step intervals for each region being 5, 0.4, 0.05k, 0.07k and 0.1k eV respectively. Thus greatest precision was achieved across the absorption edge, whilst conserving experimental time by allocating less time to data acquisition in other parts of the spectrum. Five consecutive scans were collected from each sample and the data was subsequently merged prior to analysis.

XANES data processing, including the alignment of spectra, background removal and Linear Combination Fitting (LCF) was performed using Athena software (Ravel and Newville, 2005). XANES spectra from the biomass samples were initially compared with 10 published reference spectra (ZnS, Zn-citrate, Zn-cysteine, Zn-histidine, Zn-malate, Zn_(aq), ZnPO₄, ZnO, ZnCO₃) before the LCF analysis was conducted using spectra for aqueous solutions of Zn-malate, Zn-cysteine and Zn-histidine; and ZnS in powdered form (Mishra et al., 2020). The fitting range used was from -30 to +70 eV below/above E₀ of the sample, variable weights assigned to spectra were constrained to between 0 and 1. The sum of the weights used for each fit was not constrained.

EXAFS analysis was performed using Artemis (Demeter v.0.9.26) package of software (Ravel and Newville, 2005). Initial work was conducted using crystallographic data for Zn standard compounds (CIF files) along with Demeter's Ifeffit to fit EXAFS spectra to a range of Zn reference compounds: Zn-malate; Zn-histidine; Zn-cysteine; and ZnS. Spectral fitting was conducted for O/N, S and C scattering paths between 1.2 and 2.7Å. These fitting parameters for the standards were then used as initial guess parameters for modelling EXAF of the biomass samples.

5.3 Results

5.3.1 Zinc and Lead Uptake by the Bytom Biomass

The Bytom soil contained mean concentrations for total Zn and total Pb of c.4,000 and 1,900 mg/kg_(dm), respectively, which are c.10x and c.4x the thresholds at which soil is usually considered contaminated (table 5.4). Biomass from the same seed-based hybrid grown at Bytom contained mean Zn and Pb concentrations of 93.7 and 14.4 mg/kg_(dm), respectively, which are 6x and 7x typical values for *Miscanthus* plants grown in uncontaminated soil and at levels close, or in excess, of typical biomass fuel standards (table 5.4).

5.3.2 Zinc and Lead Uptake by Pot Trial

In the pot trials with the Control soil the mean Zn concentrations in stem and leaf structures were 36 and 14 mg/kg_(dm), respectively. Compared with the Zn concentrations for *Miscanthus* plants grown in uncontaminated soil these values were marginally above (stem) and at the lower end (leaf) of the typical values reported for *Miscanthus* (see table 5.4).

Similarly, the mean Pb concentrations was below detection limit and 0.4 mg/kg_(dm) in stem and leaf structures respectively, which were at the low

Table 5.4: Comparison of HM concentration in Bytom soil and biomass compared with uncontaminated *Miscanthus* and example threshold values for defining contaminated soils. All values in $\text{mg}_{(\text{metal})}/\text{kg}_{(\text{dm})}$.

Soil			Biomass		
	Intervention Value ¹	Bytom Soil Mean	'typical' <i>Miscanthus</i> ² Mean (range)	Bytom <i>Miscanthus</i> Mean (range)	ISO 17225-7 ³ Threshold
Metal	Threshold	Mean	Mean (range)	Mean (range)	Threshold
Zn	350	4006	16 (9 – 33)	94 (60 – 116)	100
Pb	530	1859	2 (0 – 10)	14 (13 – 16)	0.1

References:

¹NOAA (2008), ²ECN (2018), ³ISO17225 (2014)

end of the typical range for Pb concentrations for *Miscanthus* plants grown in uncontaminated soil. The concentrations of both Zn and Pb in biomass from the pot trial plants increased with the amount of that metal added to the Spen Farm soil. The data show that Zn concentration in the stem exceeds that in the leaves, but in contrast the Pb concentration in the stem was lower than in the leaves (figure 5.2).

The soil of the 1x(Zn+Pb) pot trial was engineered to replicate the contamination observed at the Bytom field site. However, the Zn concentrations in the plant stems and leaves were 387 $\text{mg}/\text{kg}_{(\text{dm})}$ and 111 $\text{mg}/\text{kg}_{(\text{dm})}$ respectively ($n = 5$). This was higher than that observed in the Bytom crop, which was predominantly stem material, that contained 94 $\text{mg}/\text{kg}_{(\text{dm})}$ of Zn. In contrast, the Pb concentrations in the pot trial plants stems (1.4 $\text{mg}/\text{kg}_{(\text{dm})}$) and leaves (3.6 $\text{mg}/\text{kg}_{(\text{dm})}$) were substantially lower than in the Bytom crop (14.4 $\text{mg}/\text{kg}_{(\text{dm})}$).

5.3.3 XAFS Results

XANES spectra and plots of each LCF fit for the sample are provided in the Appendix to this chapter (figure 5.10). The XANES spectra for biomass samples possess a Zn absorption edge that varied between 9662.4 and 9662.6

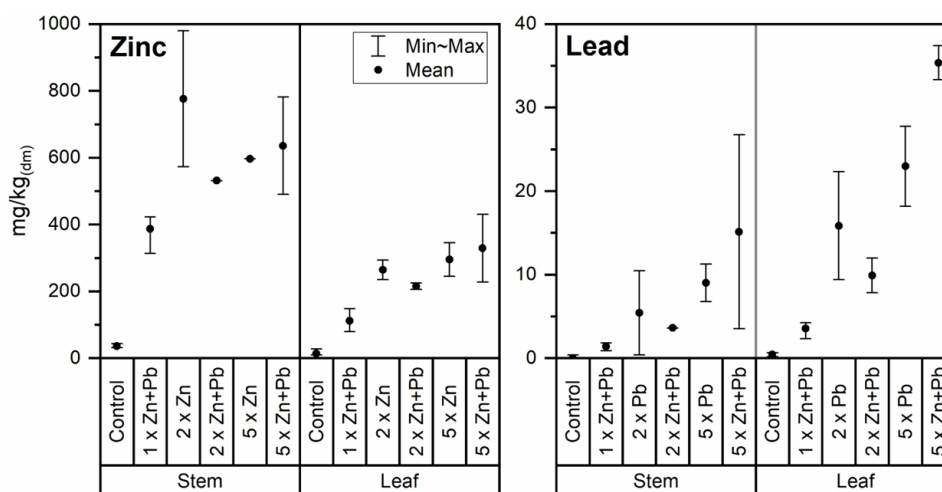


Figure 5.2: Bulk Zn and Pb concentrations in stem and leaf materials across soil conditions adopted in the pot trial

eV (figure 5.3b). These values were towards the lower end of the energy range observed for Zn standard compounds (figure 5.3a) and were consistent with the presence of S coordinated species as the absorption edges were below even tetrahedral O/N coordinated Zn species (e.g. Zn-histidine at 9663.4 eV).

Isolated EXAFS (Xk) for the biomass samples are provided in the Appendix to this chapter (figure 5.11). The magnitude of the Fourier Transform (FT) of the Zn EXAFS spectra for the Bytom field trial biomass exhibit first peaks at 1.53 Å, whereas the stem material from the 5x(Zn+Pb) pot trial has a first peak at 1.66 Å, the leaf material from the 5x(Zn+Pb) pot trial has a first peak at 1.75 Å (figure 5.4c). These values differ from the FT of the EXAFS spectra for the Zn-histidine and Zn-malate standards which have peaks at 1.51 Å and 1.58 Å, respectively (O/N coordination of Zn), while the S coordinated Zn-cysteine and Zn-sulfide standards both have peaks at 1.85 Å (figure 5.4a). The S coordinated species also display characteristic spectral features in the real part of the EXAFS FT at around 2.1 – 2.2 Å which differentiate them from O/N species (figure 5.4b). The magnitude plot of the FT from the powdered ZnS standard also displayed significant peak(s) at 3 – 4 Å, which was characteristic of strong multiple scattering pathways associated

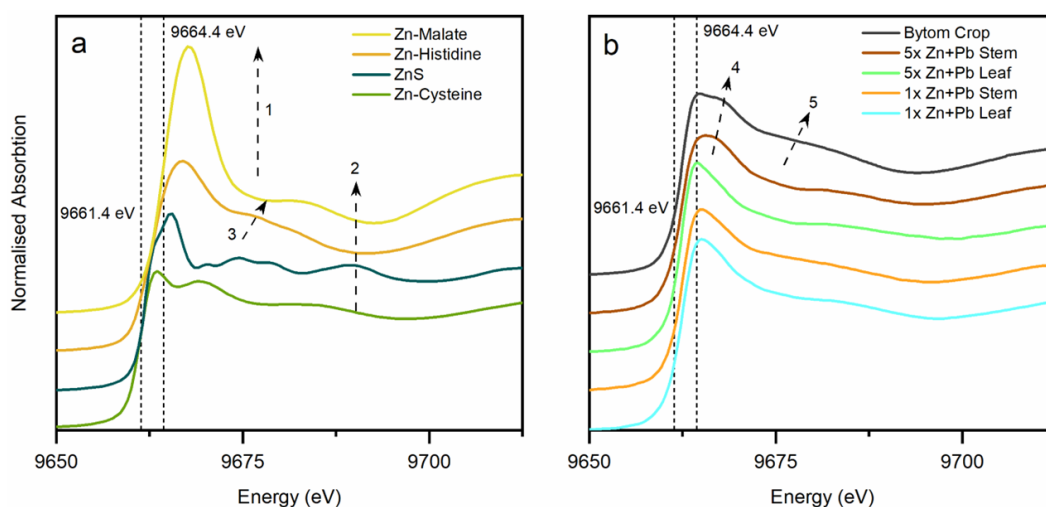


Figure 5.3: Zn XANES spectra for: (a) Zn standard compounds (Mishra et al., 2020); (b) biomass samples. Absorption edge energies are shown for Zn-cysteine (9661.4 eV) and Zn-malate (9664.4 eV).

with Zn in the second coordination shell. The other standards were aqueous solutions, so backscattering from the second coordination shell was not seen. Differences between the spectra for Zn-histidine and Zn-malate standards are less pronounced, but the most significant was observed in the first peak of the magnitude of the EXAFS FT, where the tetrahedral structure of histidine resulted in a lower peak of the magnitude of the EXAFS FT when compared with octahedral structure of malate (figure 5.4a).

Linear Combination Fitting (LCF) of XANES from the biomass samples has been undertaken using the spectra for the Zn-histidine, Zn-malate, Zn-cysteine, and ZnS standards. These four standard compounds were chosen as characteristic compounds for the range of bonding environments anticipated for Zn in biomass. In Zn-cysteine and Zn-histidine the Zn is tetrahedrally coordinated to S or N respectively within an organic compound. Whereas, in Zn-malate the Zn is octahedrally coordinated to O (Mishra et al., 2020). The Zn within ZnS is tetrahedrally coordinated with S within an inorganic compound (Kisi and Elcombe, 1989). The energy of the inflection point of the Zn K-edge associated with these standards increases in the order: Zn-cysteine (9661.4 eV), ZnS

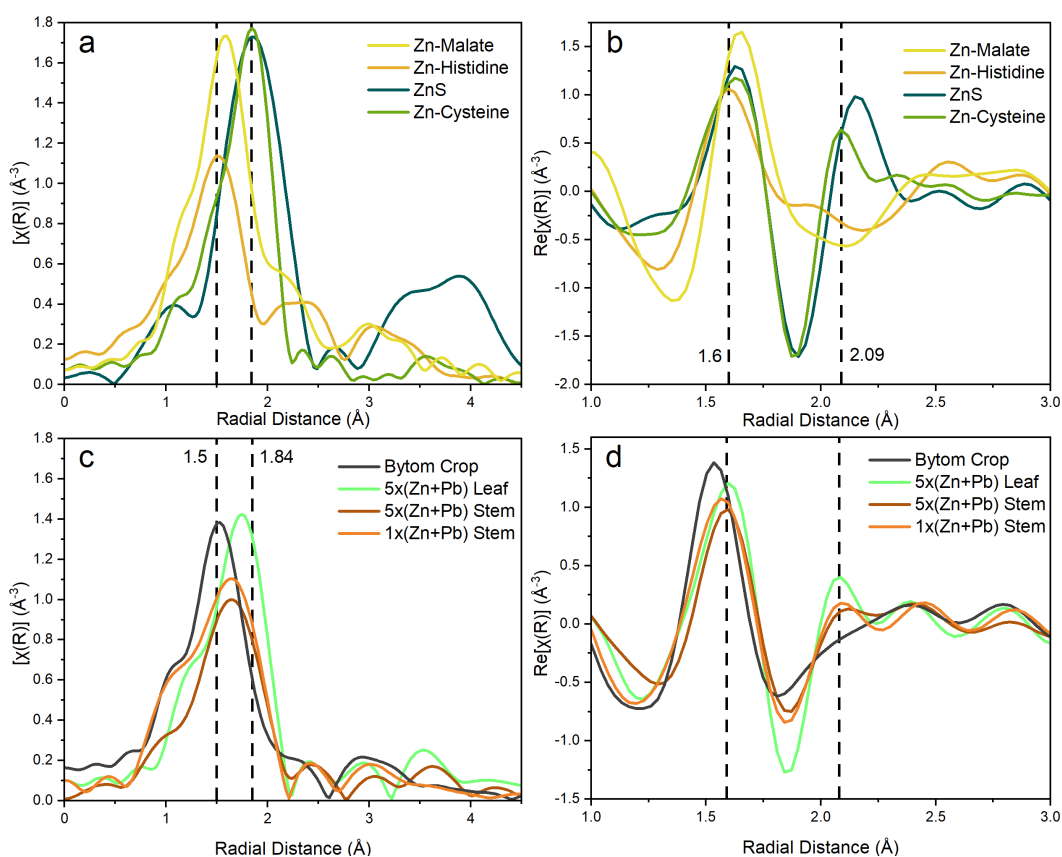


Figure 5.4: Fourier Transforms of EXAFS: (a) magnitude $|\chi(R)|$ for Zn standards; (b) magnitude $|\chi(R)|$ for *Miscanthus* samples; (c) Real part $\text{Re}|\chi(R)|$ for Zn standards; (d) Real part $\text{Re}|\chi(R)|$ for *Miscanthus* samples

(9661.9 eV), Zn-histidine (9663.4 eV), and Zn-malate (9664.4 eV) (figure 5.3a). Further spectral features differ between the standards. The octahedral O coordination of Zn-malate produces a distinctly higher and more tapered white line (arrow 1), O and N coordinated Zn-malate and Zn-histidine display spectral features around 9690 eV which are absent or opposed in S-coordinated species (arrow 2), whilst Zn-histidine can be differentiated by a shoulder (arrow 3) in the post-edge region of c.9675 eV (Mishra et al., 2020).

LCF for leaf material from the pot trials (figure 5.5 and Appendix figure 5.10) suggests Zn coordination was similar in both the 5x(Zn+Pb) and 1x(Zn+Pb) pot experiments, with best fit achieved with c.80% weighting on S species

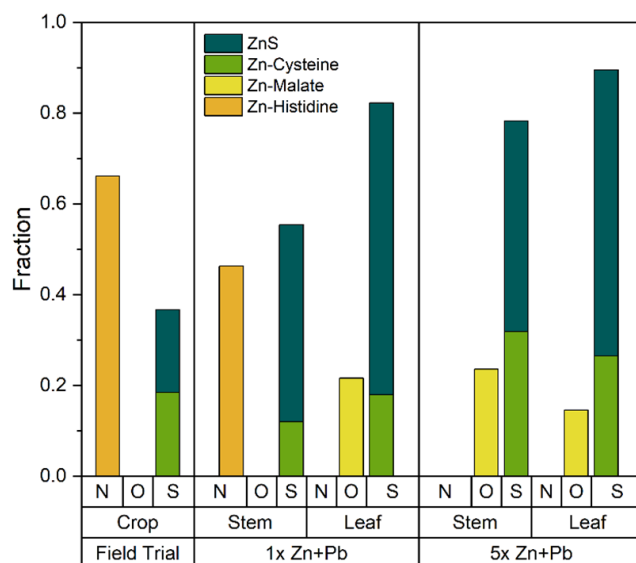


Figure 5.5: Results of LCF of the relative weight for Zn species in *Miscanthus* from the Bytom Field Trial and the Growth Trial plant sections

(ZnS and Zn-cysteine) with the remainder being O species (Zn-malate). In comparison, LCF of stem material from the pot trials suggests that the amount of Zn uptake affects the coordination environment of Zn with predominantly S-coordination in stem material from the 5x(Zn+Pb) pot experiment, but more equal amounts of S and N coordination in stem material from the 1x(Zn+Pb) experiment. The biomass from the Bytom field trial comprised mostly of stem material. In this material N species contributed about $\frac{2}{3}$ of the signal and S species contributed the remaining $\frac{1}{3}$ of the XANES signal.

5.3.4 Qualitative Analysis of EXAFS

The Bytom Crop, 1x(Zn+Pb) stem sample, and the 5x(Zn+Pb) stem and leaf samples provided sufficient signal to noise ratio to enable analysis of EXAFS spectra (noise in the data prevented EXAFS analysis for the 1x(Zn+Pb) leaf sample). Comparing plots of the Fourier Transforms (FT) for these spectra against those obtained for Zn-standard compounds enabled a qualitative anal-

ysis of the Zn ligands within the Bytom and pot trial samples (figure 5.4).

The magnitude of the FT for the samples (figure 5.4c) highlighted differences in the position of the first peaks indicating changes in Zn coordination environments. The shortest radial distance was associated with the Bytom crop (1.53 Å), followed by increasing peak position distances for the 1x(Zn+Pb) stem (1.63 Å), 5x(Zn+Pb) stem (1.66 Å) and leaf material (1.75 Å). All these phase uncorrected peak positions occur within the range of values associated with the of Zn standard compounds (figure 5.4a). Zn standards exhibit increasing radial distance as follows: Zn-histidine (1.50 Å), Zn-malate (1.60 Å), with both Zn-cysteine and ZnS having the same peak position (1.84 Å). The first peak of the 5x(Zn+Pb) leaf sample was much closer to the radial distance associated with S-coordinated species than the other samples. Stem samples from the pot trials demonstrate similar peak positions, i.e. 1.63 Å and 1.66 Å for samples 1x(Zn+Pb) and 5x(Zn+Pb) respectively. Peak position in the range of 1.63 to 1.66 Å suggest a mixed coordination environment with higher O/N contribution. In contrast, the peak position for the Bytom crop (1.53 Å) was similar to that of the Zn-histidine standard.

The real part of the FT spectra for the Zn standards (figure 5.4b) illustrate significant spectral features for the S-coordinated species (ZnS and Zn-cysteine) with characteristic peaks at radial distances 2.09 Å and 2.15 Å, respectively. These features are not observed in the FT spectra for the O/N coordinated Zn-histidine or Zn-malate standards and so it can be used to identify the presence of S-species. The real part of the FT spectra for the biomass samples demonstrates this characteristic feature to different extents (figure 5.4d). The 5x(Zn+Pb) leaf sample demonstrates a clear peak at 2.09 Å, which is consistent with the presence of Zn-cysteine. Smaller peaks at the same radial distance were observed in both 1x(Zn+Pb) and 5x(Zn+Pb) stem samples from the pot trials; however, the signal was weaker suggesting cysteine ligation was less prevalent. There was no clear indication of S species being present in the Bytom crop sample as the real part of its FT does not demonstrate the characteristic features around 2.09 – 2.15 Å.

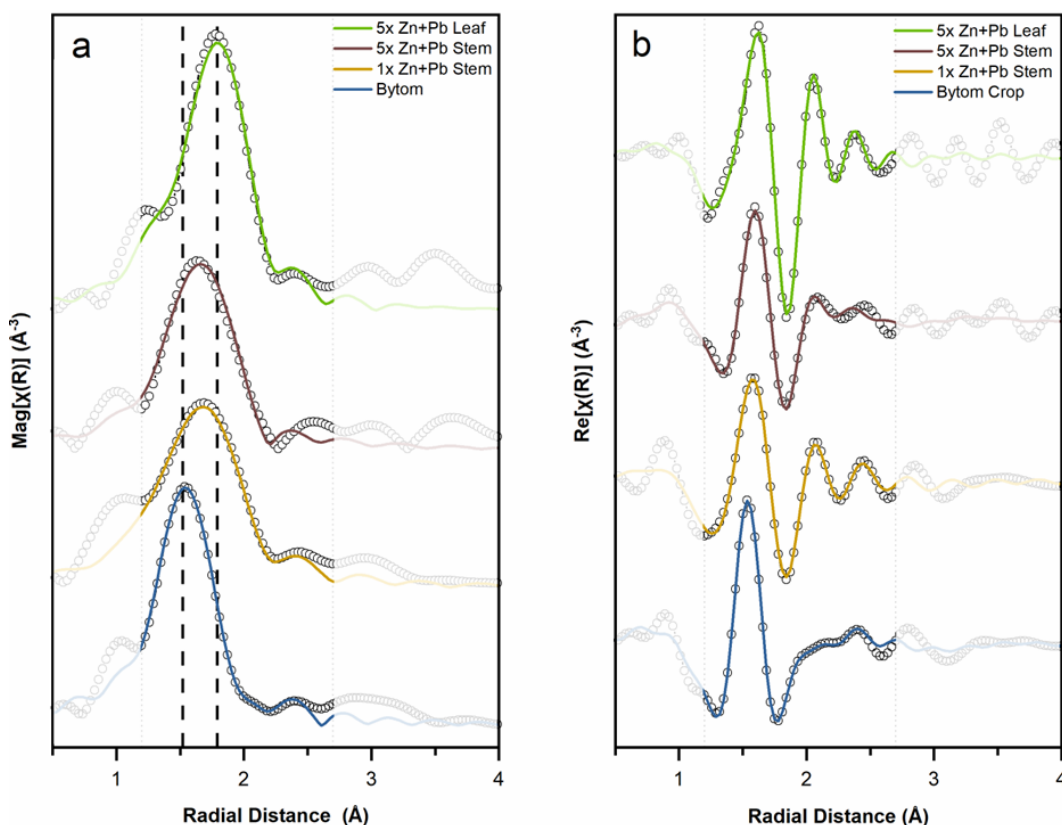


Figure 5.6: Fourier Transform (FT) analyses of biomass samples. Dashed lines are measured experimental data. Solid lines are fit simulations. Fit range (1.2 – 2.7 Å) is highlighted. (a) FT magnitude and fit results; (b) expanded real part of the FT and fit results.

5.3.5 Quantitative Modelling of EXAFS

In order to quantify Zn coordination environment in the biomass samples, a shell-by-shell fitting approach was used for quantitative modelling of the EXAFS data (figure 5.6 and table 5.5). A low signal to noise ratio for the leaf material from the 1x(Zn+Pb) pot trial sample, which has the lowest Zn concentration of all the samples, rendered that data unsuitable for quantitative modelling with satisfactory statistical parameters.

The first shell of the Bytom field trial biomass sample was best fit with coordination numbers of $0.7(\pm 0.1)$ S and $3.4(\pm 0.1)$ O/N at distances $2.27(\pm 0.01)$

Table 5.5: EXAFS fitting parameters for biomass samples

Sample	Path	CN	R (Å)	σ^2 (Å ²)
Bytom CROP	S	0.7 (± 0.1)	2.27 (± 0.01)	0.0043 (± 0.0001)
	O/N	3.4 (± 0.1)	1.99 (± 0.01)	0.0042 (± 0.0004)
1x(Zn+Pb) STEM	S	0.8 (± 0.1)	2.30 (± 0.01)	0.0000 (± 0.0013)
	O/N	3.5 (± 0.4)	1.99 (± 0.01)	0.0091 (± 0.0019)
5x(Zn+Pb) STEM	S	0.8 (± 0.6)	2.29 (± 0.01)	0.0107 (± 0.0116)
	O/N	3.4 (± 0.7)	2.06 (± 0.02)	0.0093 (± 0.0028)
5x(Zn+Pb) LEAF	S	2.1 (± 0.2)	2.29 (± 0.01)	0.0059 (± 0.0010)
	O/N	3.3 (± 0.7)	2.05 (± 0.02)	0.0168 (± 0.0041)
	C	1.1 (± 0.6)	3.01 (± 0.03)	0.0060 (± 0.0091)

and $1.99(\pm 0.01)$ Å, respectively. The stem material of the 1x(Zn+Pb) pot trial sample produced similar results within error. Best fit values for the first shell of the 1x(Zn+Pb) data were $0.8(\pm 0.1)$ S and $3.5(\pm 0.4)$ O/N at distances $2.30(\pm 0.01)$ Å and $1.99(\pm 0.01)$ Å respectively. The fit for 5x(Zn+Pb) stem sample was also comparable with the previous samples, with $0.8(\pm 0.6)$ S and $3.4(\pm 0.7)$ O/N at distances of $2.29(\pm 0.01)$ Å and $2.06(\pm 0.02)$ Å respectively. In each of these three samples the overall sum of coordination numbers for the first shell was just over 4 which suggests a predominantly tetrahedral coordination environment.

The fit for 5x(Zn+Pb) leaf material produced different results from those derived for the stem and Bytom crop samples. The first shell coordination numbers were $2.1(\pm 0.2)$ S, and $3.3(\pm 0.7)$ O/N at distances $2.29(\pm 0.01)$ Å and $2.05(\pm 0.02)$ Å, respectively. The fit was improved through the inclusion of C in the second shell with a coordination number of $1.1(\pm 0.6)$ at distance $3.01(\pm 0.03)$ Å. Inclusion of C in the second shell was statistically justified by significantly lower reduced chi-square for improving the overall fit quality. This fit was markedly different from the others, as the sum of the coordination numbers for the first shell was $5.4(\pm 0.7)$ suggesting a higher proportion of the Zn in an octahedral coordination environment.

The EXAFS fits show that the S bond distances were the same within error

Table 5.6: Published EXAFS fitting parameters for Zn compounds samples

Sample	Path	CN	R (Å)	σ^2 (Å ²)
Zn-Histidine (solution) ¹	N	3.8(±0.2)	2.03(±0.02)	0.0067(±0.0021)
	O	1.3(±0.4)	2.91(±0.02)	0.0092(±0.0034)
	C	3.9(±0.6)	3.01(±0.03)	0.0051(±0.0024)
Zn-Malate (solution) ¹	O	6.0(±0.2)	2.08(±0.02)	0.0101(±0.0032)
	C	2.9(±0.5)	2.85(±0.03)	0.0056(±0.0022)
Zn-Malate (solution) ²	O	6.0(±0.6)	2.07(±0.01)	0.007
	C	2.8(±0.6)	2.86(±0.02)	0.010
Zn-Cell Wall ²	O	4.6(±0.5)	2.00(±0.01)	0.010
	C	1.3(±0.3)	2.83 (±0.02)	0.010
Zn-Pectin ²	O	4.9(±0.5)	2.02(±0.01)	0.010
	C	2.4(±0.5)	2.86(±0.02)	0.010
Zn-Phosphate ²	O	3.8(±0.4)	1.97(±0.01)	0.008
	P	0.4(±0.8)	2.94(±0.02)	0.010
Zn-Cysteine (solution) ¹	S	4.0	2.29(±0.02)	0.0081(±0.0021)
ZnS ³	S	3.8	2.34	NR
	Zn	NR	3.90	NR

References:

¹Mishra et al. (2020), ²Sarret et al. (2009), ³Valeev et al. (2011)

(2.27-2.30 Å) for all the samples presented in Table 6, and in good agreement with tetrahedrally coordinated Zn-S ligands reported for Zn-cysteine standards (table 5.6). However, the differences in the O/N bond lengths for some of the samples were beyond the error of the fits. Both the Bytom field crop and stem material from the 1x(Zn+Pb) pot trial have O/N bond distance 1.99(±0.01) Å. Short radial distances for O/N were similar to those reported for Zn incorporation in cell wall materials, pectin or phosphates, or Zn-histidine with its tetrahedral N coordination. In contrast, both the stem and leaf materials from the 5x(Zn+Pb) pot trial returned radial distances for O/N of 2.05(±0.01) and 2.06(±0.01) Å, respectively. This longer bond distance was consistent with the presence of Zn-malate where Zn is octahedrally coordinated with O (table 5.6).

5.4 Discussion

5.4.1 Uptake by Pot Trial Plants

Miscanthus biomass from a long-term field-trial had elevated Zn and Pb concentrations relative to reported values for *Miscanthus* plants grown in uncontaminated soil, indicating that growth at a Zn and Pb contaminated site resulted in up-take of these metals. Similar uptake of Zn and Pb has been reported for other *Miscanthus* species (Barbosa et al., 2015; Kocoń and Jurga, 2017; Wanat et al., 2013; Wang et al., 2012). The uptake of Zn/Pb by the Bytom Crop was replicable in short-term pot-trials, which also showed a positive relationship between observed metal concentrations in both the stems and leaves, and the metal concentration in the soil.

The data for Zn uptake by stem and leaf sample from the pot trial were modelled using an exponential curve function (figure 5.7). The plots illustrate a non-linear relationship between Zn concentration in the soil and resultant biomass concentrations. In both the stem and leaf material, the initially rapid increase in uptake as the soil Zn concentration increases from low levels was followed by incrementally smaller increases at higher soil Zn concentrations. This plateauing was most visible in the stem material, where the highest Zn concentrations were observed, and suggests there may be a limit to the amount of Zn that can be taken-up by the biomass.

A positive correlation was also identified for the uptake of Pb from the soil in the pot trials. However, there was greater scatter in the data, particularly at lower soil Pb concentrations, which resulted in greater uncertainty in curve fitting (figure 5.8).

5.4.2 Zn and Pb Distribution

A difference between Zn and Pb uptake was also observed in the spatial distribution of these HM between stem and leaf structures. The pot-trial data

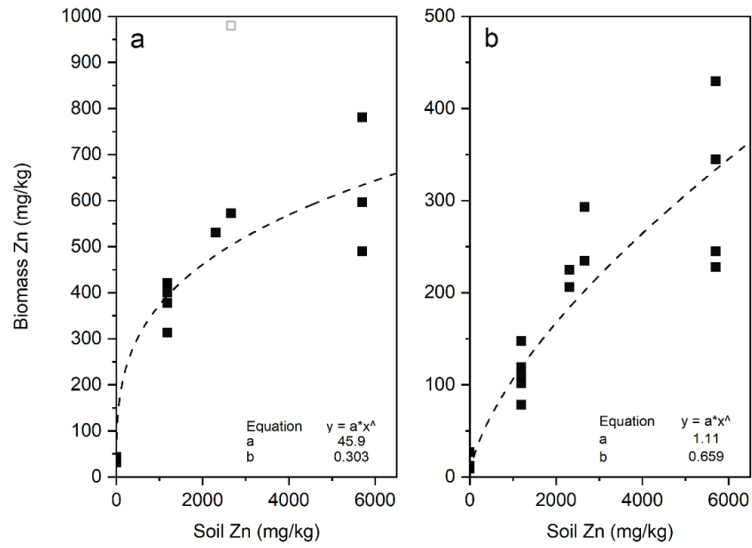


Figure 5.7: Exponential curve fits for Zn uptake in (a) stem and (b) leaf structures of growth trial plants. Soil Zn concentration are reported as sum of the bioavailable fractions (chloride and carbonate). Single outlier point (980 mg/kg) in the stem data is masked during the fitting process

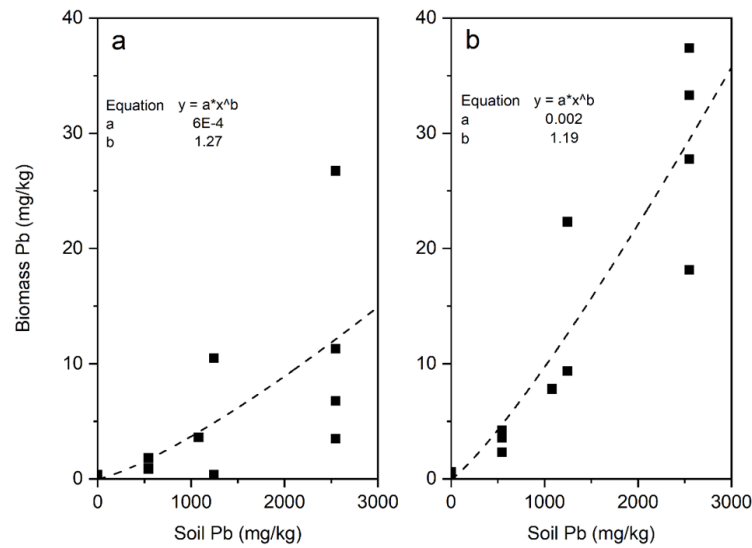


Figure 5.8: Exponential curve fits for Pb uptake in (a) stem and (b) leaf structures of growth trial plants. Soil Pb concentration are reported as sum of the bioavailable fractions (chloride and carbonate).

from this study showed that Zn accumulates to a greater extent in the stem structures than in the leaves, whereas the opposite was true for Pb. Across the 1x(Zn+Pb) replicates the median values for Zn were 400 and 109 mg/kg_{dm} for stem and leaf respectively, and 1 and 4 mg/kg_(dm) for Pb. These observed differences in distribution between stem and leaf were statistically significant for both Zn (Mann-Whitney U = 0, n₁ = n₂ = 5, p <0.05 two-tailed) and Pb (Mann-Whitney U = 24.5, n₁ = n₂ = 5, p <0.05 two-tailed). The data for seed-based hybrid used in this study conformed with the pattern observable in data from previous studies for both Zn and Pb in *Miscanthus x giganteus* hybrid (Andrejic et al., 2018; Wanat et al., 2013).

5.4.3 Pot Trial Plants vs Mature Crop

In the long-term Bytom field trial, mature *Miscanthus* biomass was harvested following the winter senescence period in March 2018. This is normal time of year for harvesting *Miscanthus* crops. This biomass consisted predominantly of stem material, and it contained an elevated Zn concentration (94 mg/kg_(dm)) relative to reported values *Miscanthus* plants grown in uncontaminated soil. However, this Zn loading was lower than that observed with actively growing juvenile plants in the pot trials containing similar levels of bioavailable Zn (where the stem biomass contained 387 mg/kg_(dm) while the leaf biomass contained 111 mg/kg_(dm)). Rusinowski et al. (2019a) analysed Zn uptake by the same hybrid grown at Bytom at the end of its second growing season in September/October 2016 and reported that the Zn concentration within the ‘shoots’ was 213.1 mg/kg_(dm). While Rusinowski’s data were not disaggregated into different plant structures, the value is midway between the values for the ‘stem’ and ‘leaf’ material for the 1x(Zn+Pb) plants in this study, and higher than that determined for the mature biomass at time when the crop was harvested.

In the juvenile plants under 1x (Zn+Pb) soil conditions, the Pb concentration was lower in all structures (stem 1.4 mg/kg_(dm) and leaf 3.6 mg/kg_(dm)) than that observed in the biomass from the Bytom field trial (14.4 mg/kg_(dm)).

Rusinowski et al. (2019a) report Pb values of 22.2 ± 2.27 mg/kg_(dm) for the same hybrid grown at the Bytom site at the end of the 2016 growing period. Hence, the data suggest that Pb uptake increases over the long-term with the lowest values being observed in the juvenile plants indicating a fundamentally different uptake mechanism. Nonetheless, Pb concentrations measured in this study after winter senescence was lower than the value measured during the 2016 growing season by Rusinowski et al. (2019a). The data suggest that the uptake and/or sequestration mechanism for Pb was different from Zn.

Senescence of *Miscanthus* has been demonstrated to produce significant changes in the biomass concentration of major cations and anions: K, P, Cl and S are known to decrease over the winter period, Si and Na increase while Ca is little affected (Baxter et al., 2012). However, the effect of senescence on HMs is so far not well documented in literature. The combination of this study and data from Rusinowski et al. (2019a) indicates that winter senescence may result in a reduction of biomass Zn concentration compared with that observed during growth phases. This would be consistent with two studies conducted by Rusinowski on *Miscanthus* grown at the Bytom site, which show a reduction in biomass Zn concentration between September 2016 and March 2017 (Rusinowski et al., 2019a,b). These data do not conform with observations made by Krzyzak et al. (2017) which reports that winter senescence resulted in no significant change or even increase in Zn within aerial structures of *Miscanthus x giganteus* and other *Miscanthus* species. Krzyzak et al do, however, concluded that Zn uptake/sequestration was species-specific with different behaviours being observed between species. The lower abundance of Zn may therefore be specific to the specific hybrid used here.

5.4.4 Zn Speciation

Zinc is an essential plant micronutrient required as a constituent of several enzymes and proteins (Broadley et al., 2007; Sharma et al., 2017). However, relatively small quantities of Zn in soil are sufficient (c.20 mg/kg_(dm); (Suganya et al., 2020)) and the normal range for Zn in plant tissue is 15-60 mg/kg_(dm)

(Singh, 1986; Venkatesh et al., 2014). Excess Zn is toxic, so plants can adopt different mechanisms to sequester surplus Zn within their cells. These mechanisms include: complexation within the cytosol with organic acids or metal-binding peptides, compartmentalisation within cell walls, and compartmentalisation within the cell vacuole (Broadley et al., 2007; Hall, 2002). Plants contain a range of organic molecules that can act as ligands to Zn, including organic acids (e.g. citrate, malate, oxalate), phytate (a hexa-phosphate that is the main storage form of phosphorus in the seeds), amino acids (e.g. histidine and cysteine), metallothioneins (MTs; cysteine rich proteins), and phytochelatins (PC, oligomers of glutathione, a tripeptide of glutamate, cysteine and glycine) (Ernst et al., 1992; Mathys, 1977; Mishra et al., 2020; Sarret et al., 2002; Verkleij et al., 1998).

The XANES LCF approach included four Zn-complexes; Zn-malate, Zn-histidine, Zn-cysteine and ZnS. Each spectrum was included in the LCF analysis through a combinatorial approach - sequentially adding one of the remaining spectra to the previous best fit and its inclusion was justified by a significant lowering of the reduced chi-square value. The LCF methodology was consistent in selecting ZnS as being present alongside Zn-cysteine. The precipitation of nanoscale sulfide crystals has been reported in plants grown under HM stress, in particular with regards to Cd contamination (Carrier et al., 2003; Dameron et al., 1989; Neumann and zur Nieden, 2001; Reese et al., 1992). The potential presence of sulfide crystals in the *Miscanthus* samples was therefore considered.

ZnS crystals can be unambiguously identified using EXAFS due to strong scattering paths arising from Zn in the second coordination shell: nano-scale ZnS exhibits tetrahedral coordination with S in the first shell of 2.34 Å and a second shell comprised of Zn at 3.90 Å (Valeev et al., 2011). The scattering paths associated with the presence Zn in the second shell are clearly distinguished via a peak at 3.90 Å in the magnitude of the FT of the ZnS standard (figure 5.4a). None of the EXAFS FTs for the samples exhibit this characteristic peak (figure 5.4c) so the presence of ZnS nanocrystals can be ruled out on this basis. Nonetheless, the LCFs strongly suggested the need for a contribution from signal at a lower energy regime (E0 c.9662 eV), around the peak position

for ZnS which is lower than Zn-cysteine peak position. The XANES spectrum for the aqueous Zn-cysteine might not serve as the best standard for higher molecular weight (cysteine rich) complexes, such as Zn-PC and Zn-MT due to differences in local S coordination environment. These differences may, at least in part, be compensated for by the features of the ZnS spectrum. The pathways for HM sequestration involving S are complex at the intracellular level, e.g. detoxification of Cd includes low molecular weight PCs in the cytosol acting as a shuttle to the vacuole, wherein Cd sequestration is achieved by the incorporation with S^{2-} in high molecular weight complexes (Clemens, 2001; Cobbett and Goldsbrough, 2002). The presence of S^{2-} within a PC complex results in higher metal binding capacity and improved effectiveness of HM sequestration (Steffens, 1990). The LCF results in this study pointed towards Zn-cysteine alone as being an imperfect representation of a more complex S ligation environment within *Miscanthus*.

A further pattern of S ligation was evident within the LCF data. The S signal (figure 5.5; combined contributions of Zn-cysteine and ZnS) was more prevalent in the leaf material than the stem materials, which in turn were greater than the Bytom crop (table 5.5). The more detailed assessment of Zn coordination environments using EXAFS fitting confirms the same general pattern for the prevalence of S ligands, i.e. pot trial leaf > pot trial stem > Bytom crop. First shell coordination numbers for S range from the highest of $2.1(\pm 0.02)$ in the leaf, to $0.8(\pm 0.6)$ in both stem samples, and $0.7(\pm 0.1)$ in the Bytom crop. The coordination number of S for stem and the Bytom sample (which was mostly stem) was similar within error. The coordination number for S in the leaf sample was substantially higher which indicates that the biochemistry for Zn within the leaf was different. The EXAFS fit result for the leaf sample suggested that S ligands comprise around half of the Zn coordination environment in the leaf, compared to only around a fifth of that in stem samples. The EXAFS data should be viewed in conjunction with the data for bulk Zn concentration within the samples (figure 5.2), which together show that higher S ligation in the leaf was associated with a comparatively low Zn concentration. The stem samples had a higher Zn concentration but

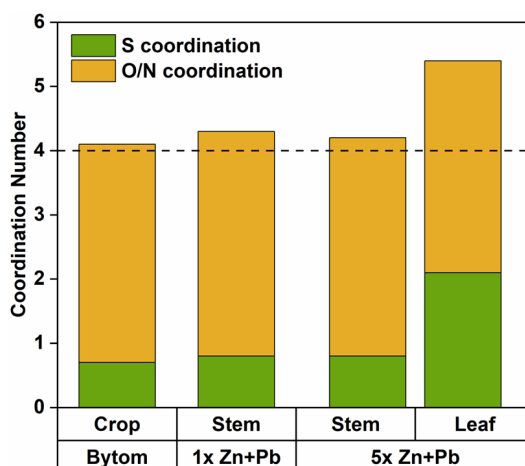


Figure 5.9: Coordination numbers derived from EXAFS fitting of samples

with the EXAFS fitting suggesting lower prevalence of S ligands (figure 5.9). It is entirely possible that -SH ligands are higher affinity yet lower abundance binding sites providing an important complexation mechanism for Zn in stem but were masked by higher abundance of O/N sites.

The EXAFS fitting data for O/N species provide further insight into the pattern of Zn complexes within *Miscanthus*. It is not possible to directly differentiate between O and N species using EXAFS due to similar atomic numbers giving a similar scattering signal. However, the coordination geometry (bond length and coordination number) of the fits can provide information about the likely Zn ligands present in the samples. In Zn-organic acid complexes, the Zn tends to be octahedrally coordinated with O-ligands, with a typical bond length 2.07 - 2.08 Å (Mishra et al., 2020; Sarret et al., 2009). In Zn-phytate complex, Zn is tetrahedrally coordinated with O-ligands, with a bond length of 1.96 Å (Sarret et al., 2002). With amino acids, Zn can coordinate with elements in sidechains, and thus the coordination environment varies with the type of amino acid. Zn-histidine has been adopted as a standard to represent amino acid complexes; here Zn is tetrahedrally coordinated with N with typical bond lengths of 2.03 Å (Mishra et al., 2020; Thomas et al., 2019).

The individual O/N coordination numbers across all samples were remarkably

similar (3.3 – 3.5) within error (table 5.5). However, O/N coordination numbers does not provide the full picture unless viewed in conjunction with the S coordination numbers for the first shell. The total coordination number for the leaf sample has a higher value of $5.4(\pm 0.7)$, followed by stem samples from the pot trials $4.3(\pm 0.3)$ - $4.2(\pm 0.7)$ with the 5x(Zn+Pb) sample having the larger uncertainty; and the Bytom crop has the lowest value of 4.1 and the smallest uncertainty. The high value (CN \rightarrow 6) for the leaf sample was consistent with octahedral O/N being present and therefore that Zn-O/N ligands being associated with organic acid complexes. A presence of organic acid complexes in the leaf was supported by the fit of bond length being $2.05(\pm 0.02)$ Å which is near the upper end of the range associated with tetrahedral O/N bond lengths and is associated with octahedral O/N geometry, as represented by Zn-malate (2.07-8 Å; table 5.6).

The data for O/N bond lengths across the stem samples display a range of values from 2.06 – 1.99 Å. The 5x(Zn+Pb) stem samples was best fit with a longer bond length of $2.06(\pm 0.02)$ Å, suggesting the predominance of Zn complexation by organic acids. The data for the Bytom crop sample was most closely aligned with O/N being in a tetrahedral form as the bond distance was best fitted at $1.99(\pm 0.01)$ Å. The 1x(Zn+Pb) stem had a similar fit to the Bytom crop with a result of $1.99(\pm 0.01)$ Å also indicating a tetrahedral coordinated O/N environment but within a more disordered system (higher σ^2) which suggests greater uncertainty/heterogeneity. The variations in the bond length data as well as Zn coordination environment suggests a continuum in the Zn speciation facilitated by the O/N ligand in stem materials – with octahedral/organic acid species most prevalent in the samples with the highest Zn concentration, whereas tetrahedral species were more prevalent at lower Zn concentration, especially in the mature crop. This suggests that Zn has a higher initial affinity for tetrahedral coordination geometry at lower Zn concentrations, with octahedral geometry becoming increasingly apparent only as Zn concentration increases.

The lowest O/N bond lengths in the samples, found in the Bytom crop, were closely comparable to those reported by Sarret et al. (2009) (table 5.6) for

incorporation of Zn within cell wall and pectin (a proxy for cell walls) material. Spatially resolved data of cellular structures would be required to confirm Zn sequestration within cell walls. Furthermore, as EXAFS data represent the averaged signal for Zn speciation throughout the entire sample, combinations of species including, for example, Zn-phosphate which has the shortest bond length ($1.97(\pm 0.01)$ Å; table 5.6) mixed with other species such as Zn-histidine cannot be ruled out by the bulk analyses presented in this work.

5.4.5 Limitations of XAFS Techniques

The bulk XAFS analyses presented in this study are constrained by the loss of spatially resolved information. Due to the homogenisation of samples, there is a complete loss of spatial information regarding potential variation in HM storage across different tissue structures (e.g. epidermis vs vascular tissues). However, some ligands have been shown in previous research to be associated with specific sub-cellular organelles. Identification of such ligands within the bulk samples could therefore provide insights into HM distribution on a cellular level - this is discussed below.

The LCF results for Zn identified tetrahedral O/N coordination in the samples. There are a range of possible tetrahedral species, including pectin and histidine ligands, which occur throughout cell structures. Therefore, the LCF data by themselves provide no information regarding spatial distribution. The data from the EXAFS fitting, however, indicate that O/N bond length in the Bytom crop and 1x(Zn+Pb) Stem samples is at the lower end of the range for tetrahedral O/N coordination. The shorter bond length is indicative of pectin/cell wall ligands, rather than the Zn-histidine standard solution. There is, therefore, evidence in the EXAFS data that these samples have significant Zn sequestration within the cell wall compartment. All other samples demonstrated longer O/N bond lengths indicating either Zn-histidine, or increasing amounts of octahedral species such as organic acids (e.g. Zn-malate), which suggests Zn as being complexed somewhere within the cytoplasm rather than the cell wall. However, no conclusions can be made regarding the location of

Zn complexation within the cytoplasm.

S ligands, such as PT and MT, have been implicated with vacuolar sequestration and may act as a shuttle mechanisms to transfer HM from the cytosol into the vacuole (Clemens, 2001; Cobbett and Goldsbrough, 2002). XANES LCF results identified a greater predominance of S species within the leaf samples. However, EXAFS FT analysis did not suggest sulfide nanocrystals in any sample, which could have been an indicator of sequestration within vacuoles (Carrier et al., 2003; Dameron et al., 1989; Neumann and zur Nieden, 2001; Reese et al., 1992). The XAFS data for S is therefore non-specific with respect to spatial distribution, other than indicating Zn is present in the cytoplasm and not suggestive of incorporation within the cell wall, where O/N bonding is expected.

The limit of spatial information within the XAFS data is suggestive of compartmentalisation within the cell wall being more prevalent in the Bytom crop, and to a lesser extent the 1x(Zn+Pb) stem, compared with other samples. Although the predominance of S species in the leaves compared to stem suggest differences in Zn sequestration mechanism within the cytoplasm, it is insufficient to identify the organelles involved in sequestration of Zn. Spatially resolved elemental mapping through application of techniques such as μ XRF microscopy would be required to provide any spatial conclusions.

As is true for any technique, XAFS studies of elemental speciation in biological samples have their own challenges. Challenges may arise through the potential for artifacts occurring in the data as a result of sample preparation or X-ray induced chemical change. For example, sample preparation through dehydration could potentially result in water-bound complexes being replaced by other ligands. Similarly, use of formaldehyde for fixing biological tissues has been shown to introduce artifacts into XAFS results (Lombi et al., 2011; Porcaro et al., 2018). The X-ray beam could result in mass loss due to heat generation and chemical changes may occur either directly as a result of photo-induced redox transformations or indirectly via the formation of highly reactive free radicals within the samples (Weik et al., 2000).

Sample preparation impacts are known to occur on elements with redox sensitive chemistry (e.g., S and Hg). Consequently, XAFS measurement of redox sensitive samples is recommended under cryogenic conditions (Hackett et al., 2012). However, in-vivo studies of more stable elements in plants, such as Fe(III), suggest drying does not significantly impact XAFS results and adopting less intensive sample preparation protocols may be preferable (Bacquart et al., 2007). Furthermore, removal of water helps minimise X-ray induced free radical formation, with both freeze-drying and air drying delivering comparable results (Hackett et al., 2012). In experiments similar to this study, Isaure et al used XANES to examine speciation of Cd speciation in plant (*Arabidopsis thaliana*) samples, comparing the results from freeze-dried samples measured at ambient temperature with hydrated samples under cryogenic conditions. No significant difference between the two samples was observed and it was concluded that Cd speciation is not noticeably altered by freeze-drying. Indeed, the hydrated cryogenic sample produced noisier spectra as a result of the lower Cd concentration and greater absorption of the fluorescence (Isaure et al., 2006). Therefore, the drying of samples appears appropriate when studying redox stable species (e.g. Zn) in plant samples.

The extent to which beam damage may impact results depends on the precise nature of the sample. Some organic acid-metal complexes such as malate are stable, whilst others such as nicotianamide have been found to be unstable, even under cryogenic conditions (Terzano et al., 2013). Similarly, many cysteine and histidine bonds are considered relatively stable for synchrotron experiments barring a few specific exceptions (Weik et al., 2000). Evidence of X-ray beam induced changes can be monitored by comparing XANES spectra of sequential scans (Bacquart et al., 2007). If multiple scans are recorded and subsequently compared with each other, beam damage reveals itself through changes in the spectra across the sequence. Changes in the white line feature of the XANES spectra suggest alteration of the coordination environment, and any shift in energy peak position suggests a change in the redox state of the element under probe. Under the environmental conditions used for this study, Zn is highly redox stable and evidence of progressive changes in spectra which

could signify beam damage were not observed (see Appendix: figure 5.12 for comparison of sequential scans).

Nonetheless, it is important to note that XAFS can only provide insights into the speciation of the element under probe (e.g. Zn). A complementary line of research may be measuring expression (either up or down regulation) of organic acids in plant tissues due to the presence of contaminants. Techniques such as chromatography may be more appropriate for such analysis, but has its own issues of interpretation and sample preparation and is out of scope of this study.

5.5 Conclusions

The uptake of Zn and Pb by a novel seed-based hybrid of *Miscanthus* has been studied in detail. Positive correlations between concentrations of bioavailable Zn and Pb in the soil and subsequent uptake by the plants has been demonstrated in juvenile plants. Uptake by juvenile plants has been shown to contain higher concentrations of Zn but lower concentrations of Pb than that reported for mature plants grown in similar soil conditions. Statistically significant differences between metals' concentrations in the stem and leaf materials have been demonstrated, with opposing patterns for Zn and Pb suggesting that different uptake mechanisms were at play. The XAFS analyses of Zn has shown that unique patterns of speciation exist in different plant structures. Leaves were associated with higher prevalence of S ligands compared with that observed in stem material and mature crop material. Leaves were also associated with a high coordination number for O/N suggesting organic acid ligands play a large role in Zn ligation within the leaf. Stem structures had a lower O/N coordination number associated with shorter bond lengths, which is consistent with tetrahedral species of histidine-like amino acids or a pectin/cell wall coordination environment. The mature (post-senescence) crop material had a distinct spectrum with the lowest prevalence of S species and a high prevalence of tetrahedral O/N species at radial distances consistent Zn complexation

within a pectin/cell wall environment.

5.6 Appendix

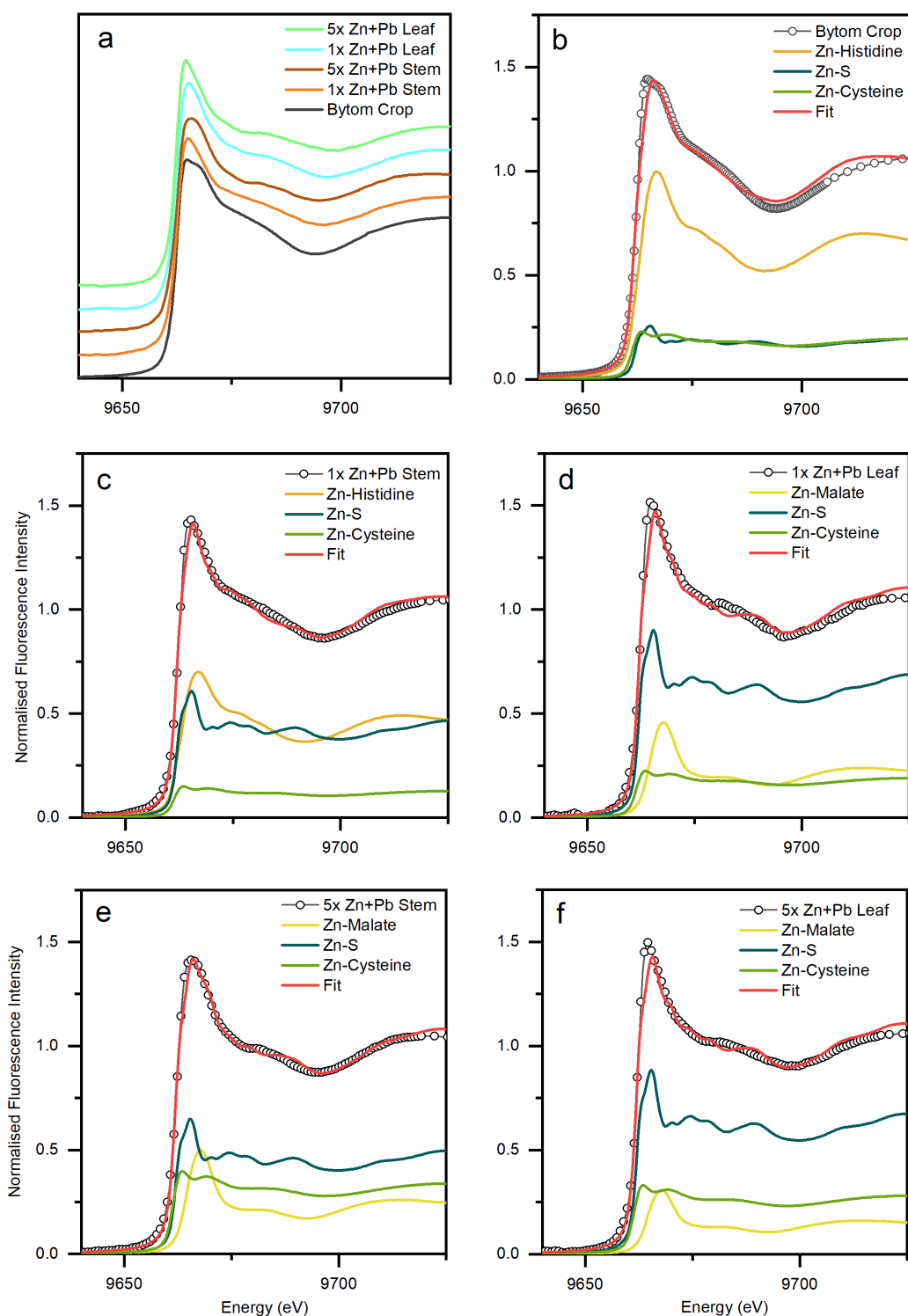


Figure 5.10: XANES spectra for biomass samples and weighted LCFs. Dashed lines are measured experimental data for the samples. Solid lines are weighted Zn standards and fit simulations: (a) measured spectra for all biomass samples; (b) Bytom Crop LCF; (c) 1x(Zn+Pb) Stem LCF; (d) 1x(Zn+Pb) Leaf LCF; (e) 5x(Zn+Pb) Stem LCF; (f) 5x(Zn+Pb) Leaf LCF.

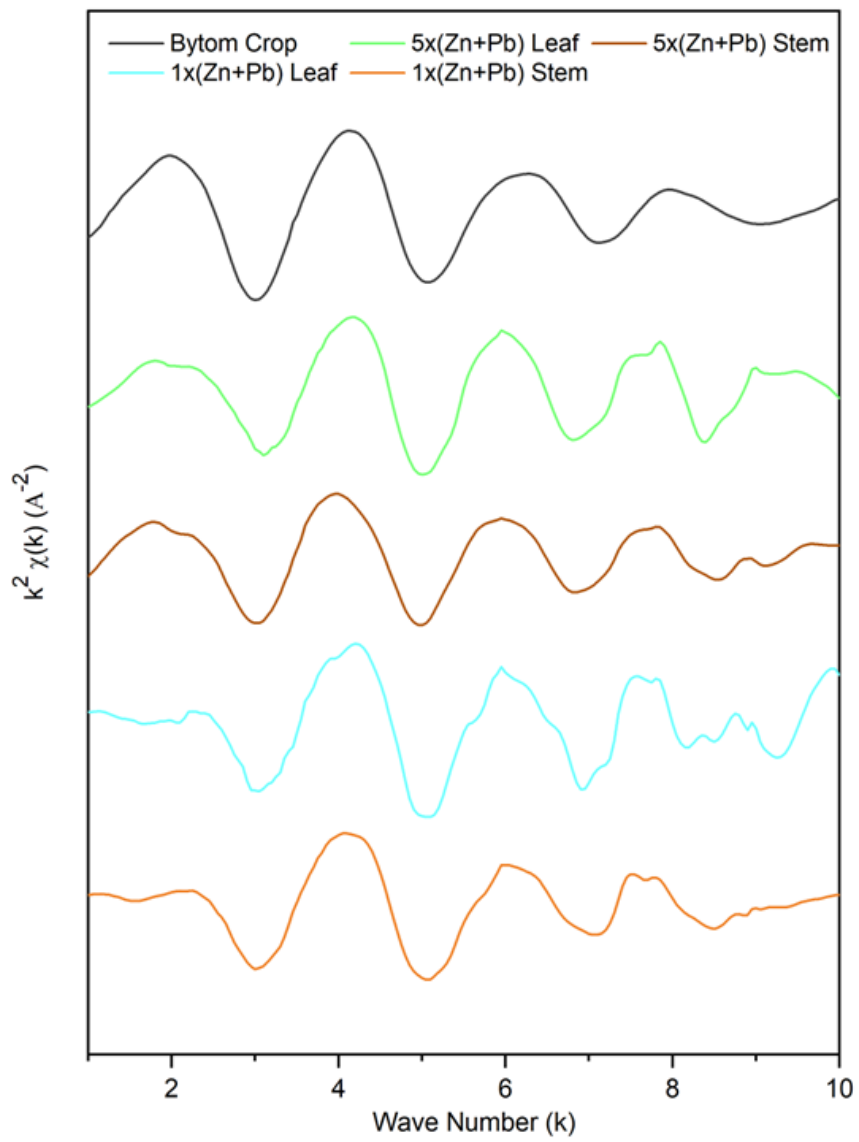


Figure 5.11: $X(k)$ for biomass EXAFS

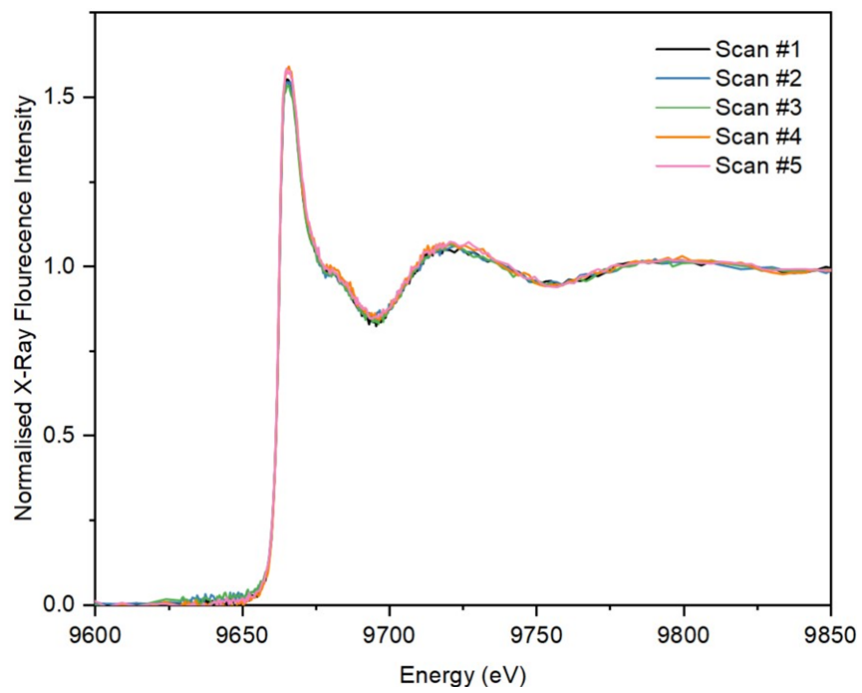


Figure 5.12: Five sequential XANES for the 1x(Zn+Pb) Stem sample demonstrating low levels of beam damage through consistency of results

5.7 References

- Adediran, G. A., Ngwenya, B. T., Mosselmans, J. F., Heal, K. V., and Harvie, B. A. (2016). Mixed planting with a leguminous plant outperforms bacteria in promoting growth of a metal remediating plant through histidine synthesis. *Int J Phytoremediation*, 18(7):720–9. Adediran, Gbotemi A Ngwenya, Bryne T Mosselmans, J Frederick W Heal, Kate V Harvie, Barbra A eng Research Support, Non-U.S. Gov't Int J Phytoremediation. 2016;18(7):720-9. doi: 10.1080/15226514.2015.1131235.
- Adele, N. C., Ngwenya, B. T., Heal, K. V., and Mosselmans, J. F. W. (2018). Soil bacteria override speciation effects on zinc phytotoxicity in zinc-contaminated soils. *Environmental Science and Technology*, 52(6):3412–3421. Ga3hu Times Cited:0 Cited References Count:74.
- Andrejic, G., Gajic, G., Prica, M., Dzeletovic, Z., and Rakic, T. (2018). Zinc accumulation, photosynthetic gas exchange, and chlorophyll a fluorescence in zn-stressed miscanthus × giganteus plants. *Photosynthetica*, 56(4):1249–1258.
- Bacquart, T., Devès, G., Carmona, A., Tucoulou, R., Bohic, S., and Ortega, R. (2007). Subcellular speciation analysis of trace element oxidation states using synchrotron radiation micro-x-ray absorption near-edge structure. *Analytical Chemistry*, 79(19):7353–7359. doi: 10.1021/ac0711135.
- Barbosa, B., Boléo, S., Sidella, S., Costa, J., Duarte, M. P., Mendes, B., Cosentino, S. L., and Fernando, A. L. (2015). Phytoremediation of heavy metal-contaminated soils using the perennial energy crops miscanthus spp. and arundo donax l. *Bioenergy Research*, 8(4):1500–1511. Cited By :28 Export Date: 1 August 2018.
- Baxter, X. C., Darvell, L. I., Jones, J. M., Barraclough, T., Yates, N. E., and Shield, I. (2012). Study of miscanthus x giganteus ash composition - variation with agronomy and assessment method. *Fuel*, 95(1):50–62. 897bm Times Cited:24 Cited References Count:38.

- Baxter, X. C., Darvell, L. I., Jones, J. M., Barraclough, T., Yates, N. E., and Shield, I. (2014). Miscanthus combustion properties and variations with miscanthus agronomy. *Fuel*, 117:851–869. A 262vv Times Cited:22 Cited References Count:25.
- Broadley, M. R., White, P. J., Hammond, J. P., Zelko, I., and Lux, A. (2007). Zinc in plants. *New Phytol*, 173(4):677–702. Broadley, Martin R White, Philip J Hammond, John P Zelko, Ivan Lux, Alexander eng Research Support, Non-U.S. Gov't Review England New Phytol. 2007;173(4):677-702. doi: 10.1111/j.1469-8137.2007.01996.x.
- Carrier, P., Baryla, A., and Havaux, M. (2003). Cadmium distribution and microlocalization in oilseed rape (brassica napus) after long-term growth on cadmium-contaminated soil. *Planta*, 216(6):939–50. Carrier, Patrick Baryla, Aurore Havaux, Michel eng Germany 2003/04/11 05:00 Planta. 2003 Apr;216(6):939-50. doi: 10.1007/s00425-002-0947-6. Epub 2002 Nov 26.
- Clemens, S. (2001). Molecular mechanisms of plant metal tolerance and homeostasis. *Planta*, 212(4):475–486.
- Cobbett, C. and Goldsbrough, P. (2002). Phytochelatins and metallothioneins: Roles in heavy metal detoxification and homeostasis. *Annual Review of Plant Biology*, 53(1):159–182.
- Dameron, C. T., Reese, R. N., Mehra, R. K., Kortan, A. R., Carroll, P. J., Steigerwald, M. L., Brus, L. E., and Winge, D. R. (1989). Biosynthesis of cadmium sulphide quantum semiconductor crystallites. *Nature*, 338(6216):596–597.
- ECN (2018). Phyllis2, database for biomass and waste.
- Ernst, W. H. O., Verkleij, J. A. C., and Schat, H. (1992). Metal tolerance in plants. *Acta botanica neerlandica*, 41(3):229–248.
- Esau, K. (1977). Anatomy of seed plants. *Anatomy of seed plants.*, (2nd edition).

- Hackett, M. J., Smith, S. E., Paterson, P. G., Nichol, H., Pickering, I. J., and George, G. N. (2012). X-ray absorption spectroscopy at the sulfur k-edge: A new tool to investigate the biochemical mechanisms of neurodegeneration. *ACS Chemical Neuroscience*, 3(3):178–185. doi: 10.1021/cn200097s.
- Hall, J. L. (2002). Cellular mechanisms for heavy metal detoxification and tolerance. *J Exp Bot*, 53(366):1–11. Hall, J L eng Review England 2001/12/13 10:00 J Exp Bot. 2002 Jan;53(366):1-11.
- Isaure, M.-P., Fayard, B., Sarret, G., Pairis, S., and Bourguignon, J. (2006). Localization and chemical forms of cadmium in plant samples by combining analytical electron microscopy and x-ray spectromicroscopy. *Spectrochimica Acta Part B: Atomic Spectroscopy*, 61(12):1242–1252.
- ISO17225 (2014). 17225-7: 2014. *Solid Biofuels. Solid biofuels. Fuel specifications and classes. Part, 7:1–14.*
- Kelly, R. A., Andrews, J. C., and DeWitt, J. G. (2002). An x-ray absorption spectroscopic investigation of the nature of the zinc complex accumulated in datura innoxia plant tissue culture. *Microchemical Journal*, 71(2-3):231–245.
- Kisi, E. H. and Elcombe, M. M. (1989). u parameters for the wurtzite structure of zns and zno using powder neutron diffraction. *Acta Crystallographica Section C: Crystal Structure Communications*, 45(12):1867–1870.
- Kocoń, A. and Jurga, B. (2017). The evaluation of growth and phytoextraction potential of miscanthus x giganteus and sida hermaphrodita on soil contaminated simultaneously with cd, cu, ni, pb, and zn. *Environmental Science and Pollution Research*, 24(5):4990–5000. Cited By :4 Export Date: 1 August 2018.
- Krzyzak, J., Pogrzeba, M., Rusinowski, S., Clifton-Brown, J., McCalmont, J. P., Kiesel, A., Mangold, A., and Mos, M. (2017). Heavy metal uptake by novel miscanthus seed-based hybrids cultivated in heavy metal contaminated soil. *Civil and Environmental Engineering Reports*, 26(3):121–132. Fp4zu Times Cited:2 Cited References Count:22.

- Kupper, H., Mijovilovich, A., Meyer-Klaucke, W., and Kroneck, P. M. H. (2004). Tissue- and age-dependent differences in the complexation of cadmium and zinc in the cadmium/zinc hyperaccumulator *thlaspi caerulescens* (ganges ecotype) revealed by x-ray absorption spectroscopy. *Plant physiology*, 134(2):748–757.
- Lewandowski, I. and Heinz, A. (2003). Delayed harvest of miscanthus—influences on biomass quantity and quality and environmental impacts of energy production. *European Journal of Agronomy*, 19(1):45–63.
- Li, Y., Wang, Y., Zhang, Q., Hu, W., Zhao, J., Chen, Y., Zhong, H., Wang, G., Zhang, Z., and Gao, Y. (2019). Elemental sulfur amendment enhance methylmercury accumulation in rice (*oryza sativa* l.) grown in hg mining polluted soil. *Journal of Hazardous Materials*, 379:120701.
- Lombi, E., Scheckel, K. G., and Kempson, I. M. (2011). In situ analysis of metal(loid)s in plants: State of the art and artefacts. *Environmental and Experimental Botany*, 72(1):3–17.
- Luo, L., Shen, Y., Wang, X., Chu, B., Xu, T., Liu, Y., Zeng, Y., and Liu, J. (2018). Phytoavailability, bioaccumulation, and human health risks of metal(loid) elements in an agroecosystem near a lead-zinc mine. *Environmental Science and Pollution Research*, 25(24):24111–24124.
- Mathys, W. (1977). The role of malate, oxalate, and mustard oil glucosides in the evolution of zinc-resistance in herbage plants. *Physiologia Plantarum*, 40(2):130–136. <https://doi.org/10.1111/j.1399-3054.1977.tb01509.x>.
- Medas, D., De Giudici, G., Pusceddu, C., Casu, M. A., Birarda, G., Vaccari, L., Gianoncelli, A., and Meneghini, C. (2019). Impact of zn excess on biomineralization processes in *juncus acutus* grown in mine polluted sites. *Journal of Hazardous Materials*, 370:98–107.
- Mishra, B., McDonald, L., Roy, M., Lanzirrotti, A., and Myneni, S. (2020). Uptake and speciation of zinc in edible plants grown in smelter contaminated soils. *PLoS ONE*, 15(4):.

- Neal, A. L., Geraki, K., Borg, S., Quinn, P., Mosselmans, J. F., Brinch-Pedersen, H., and Shewry, P. R. (2013). Iron and zinc complexation in wild-type and ferritin-expressing wheat grain: implications for mineral transport into developing grain. *JBIC Journal of Biological Inorganic Chemistry*, 18(5):557–570.
- Neumann, D. and zur Nieden, U. (2001). Silicon and heavy metal tolerance of higher plants. *Phytochemistry*, 56(7):685–92. Neumann, D zur Nieden, U eng England 2001/04/21 10:00 Phytochemistry. 2001 Apr;56(7):685-92.
- NOAA (2008). Screening quick reference tables.
- NRM (2017). Analytical report. Report EC4500900882.
- Porcaro, F., Roudeau, S., Carmona, A., and Ortega, R. (2018). Advances in element speciation analysis of biomedical samples using synchrotron-based techniques. *TrAC Trends in Analytical Chemistry*, 104:22–41.
- Ravel, B. and Newville, M. (2005). Athena, artemis, hephaestus: data analysis for x-ray absorption spectroscopy using ifeffit. *Journal of Synchrotron Radiation*, 12:537–541. 4 935rl Times Cited:7259 Cited References Count:23.
- Reese, R. N., White, C. A., and Winge, D. R. (1992). Cadmium-sulfide crystal-lites in cd-(gammaec)(n)g peptide complexes from tomato. *Plant physiology*, 98(1):225–229. 16668618[pmid] PMC1080173[pmcid].
- Rodrigues-Filho, U. P., Vaz Jr, S., Felicissimo, M. P., Scarpellini, M., Cardoso, D. R., Vinhas, R. C. J., Landers, R., Schneider, J. F., McGarvey, B. R., and Andersen, M. L. (2005). Heterometallic manganese zinc-phytate complex as a model compound for metal storage in wheat grains. *Journal of Inorganic Biochemistry*, 99(10):1973–1982.
- Rusinowski, S., Krzyzak, J., Clifton-Brown, J., Jensen, E., Mos, M., Webster, R., Sitko, K., and Pogrzeba, M. (2019a). New miscanthus hybrids cultivated at a polish metal-contaminated site demonstrate high stomatal regulation and reduced shoot pb and cd concentrations. *Environmental Pollution*, 252:1377–1387. B Iu2jf Times Cited:1 Cited References Count:67.

- Rusinowski, S., Krzyżak, J., Sitko, K., Kalaji, H. M., Jensen, E., and Pogrzeba, M. (2019b). Cultivation of c4 perennial energy grasses on heavy metal contaminated arable land: Impact on soil, biomass, and photosynthetic traits. *Environmental Pollution*, 250:300–311.
- Salt, D. E., Prince, R. C., Baker, A. J. M., Raskin, I., and Pickering, I. J. (1999). Zinc ligands in the metal hyperaccumulator *thlaspi caerulescens* as determined using x-ray absorption spectroscopy. *Environmental Science and Technology*, 33(5):713–717.
- Sarret, G., Saumitou-Laprade, P., Bert, V., Proux, O., Hazemann, J.-L., Traverse, A., Marcus, M. A., and Manceau, A. (2002). Forms of zinc accumulated in the hyperaccumulator *arabidopsis halleri*. *Plant physiology*, 130(4):1815–1826. 12481065[pmid] PMC166693[pmcid].
- Sarret, G., Willems, G., Isaure, M. P., Marcus, M. A., Fakra, S. C., Frerot, H., Pairis, S., Geoffroy, N., Manceau, A., and Saumitou-Laprade, P. (2009). Zinc distribution and speciation in *arabidopsis halleri* x *arabidopsis lyrata* progenies presenting various zinc accumulation capacities. *New Phytol*, 184(3):581–95. Sarret, Geraldine Willems, Glenda Isaure, Marie-Pierre Marcus, Matthew A Fakra, Sirine C Frerot, Helene Pairis, Sebastien Geoffroy, Nicolas Manceau, Alain Saumitou-Laprade, Pierre eng Research Support, Non-U.S. Gov't Research Support, U.S. Gov't, Non-P.H.S. England *New Phytol*. 2009 Nov;184(3):581-95. doi: 10.1111/j.1469-8137.2009.02996.x. Epub 2009 Sep 15.
- Sharma, B., Sarkar, A., Singh, P., and Singh, R. P. (2017). Agricultural utilization of biosolids: A review on potential effects on soil and plant grown. *Waste Management*, 64:117–132.
- Singh, K. (1986). The critical level of zinc in soil and plant for predicting response of cluster bean to zinc fertilization. *Plant and soil*, 94(2):285–288.
- Steffens, J. C. (1990). The heavy metal-binding peptides of plants. *Annual Review of Plant Physiology and Plant Molecular Biology*, 41(1):553–575.

- Suganya, A., Saravanan, A., and Manivannan, N. (2020). Role of zinc nutrition for increasing zinc availability, uptake, yield, and quality of maize (*zea mays* l.) grains: An overview. *Commun. Soil Sci. Plant Anal*, 51(15):2001–2021.
- Terravesta (2018). Soil analysis bytom 20.09.16.
- Terzano, R., Al Chami, Z., Vekemans, B., Janssens, K., Miano, T., and Ruggiero, P. (2008). Zinc distribution and speciation within rocket plants (*eruca vesicaria* l. *cavaleri*) grown on a polluted soil amended with compost as determined by xrf microtomography and micro-xanes. *Journal of Agricultural and Food Chemistry*, 56(9):3222–3231.
- Terzano, R., Mimmo, T., Vekemans, B., Vincze, L., Falkenberg, G., Tomasi, N., Schnell Ramos, M., Pinton, R., and Cesco, S. (2013). Iron (fe) speciation in xylem sap by xanes at a high brilliant synchrotron x-ray source: opportunities and limitations. *Analytical and Bioanalytical Chemistry*, 405(16):5411–5419.
- Thomas, S. A., Mishra, B., and Myneni, S. C. B. (2019). High energy resolution-x-ray absorption near edge structure spectroscopy reveals zn ligation in whole cell bacteria. *Journal of Physical Chemistry Letters*, 10(10):2585–2592. Hy8hz Times Cited:0 Cited References Count:55.
- Valeev, R. G., Beltukov, A. N., Gilmutdinov, F. Z., Romanov, E. A., Deev, A. N., Kriventsov, V. V., Mezentsev, N. A., and Chukavin, A. I. (2011). Exafs spectroscopy study of the atomic structure of zns nanocomposite thin films. *Journal of Structural Chemistry*, 52(1):181–185.
- Venkatesh, M. S., Hazra, K. K., and Ghosh, P. K. (2014). Critical tissue concentration of zinc in short duration mungbean (*vigna radiata*). *Indian J Agri. Sci*, 84(7):892–894.
- Verkleij, J. A. C., Koevoets, P. L. M., Blake-Kalff, M. M. A., and Chardonens, A. N. (1998). Evidence for an important role of the tonoplast in the mechanism of naturally selected zinc tolerance in *silene vulgaris*. *Journal of Plant Physiology*, 153(1):188–191.

- Wanat, N., Austruy, A., Joussein, E., Soubrand, M., Hitmi, A., Gauthier-Moussard, C., Lenain, J. F., Vernay, P., Munch, J. C., and Pichon, M. (2013). Potentials of miscanthus x giganteus grown on highly contaminated technosols. *Journal of Geochemical Exploration*, 126:78–84. 300yk Times Cited:29 Cited References Count:35.
- Wang, Y. H., Zhan, M. G., Zhu, H. X., Guo, S. J., Wang, W. S., and Xue, B. M. (2012). Distribution and accumulation of metals in soils and plant from a lead-zinc mineland in guangxi, south china. *Bulletin of Environmental Contamination and Toxicology*, 88(2):198–203. 879ko Times Cited:4 Cited References Count:13.
- Weik, M., Ravelli, R. B. G., Kryger, G., McSweeney, S., Raves, M. L., Harel, M., Gros, P., Silman, I., Kroon, J., and Sussman, J. L. (2000). Specific chemical and structural damage to proteins produced by synchrotron radiation. *Proceedings of the National Academy of Sciences*, 97(2):623–628. doi: 10.1073/pnas.97.2.623.

Chapter 6

Spatial Analysis: Tissue Distribution and the Location of Differing Species

Abstract

Data are presented which demonstrate the spatial distribution and speciation of Zn throughout the aerial biomass of *Miscanthus* grown in Zn and Pb contaminated soil. *Miscanthus* plants were grown in contaminated soil, resulting in mean biomass Zn concentration 622 mg/kg_(dm) in the stem and 312 mg/kg_(dm) in the leaves. Whole samples and microtomed cross-sections of leaf and stem tissues were analyzed using X-ray Fluorescence (XRF) imaging. A heterogeneous Zn distribution was observed within all samples with greater abundance of Zn associated with vascular bundles, in particular around phloem tissues. Micro-X-ray Absorption Spectrometry (μ XAS) of the Zn K-edge was performed at locations of varying Zn concentration. Linear Combination Fitting (LCF) revealed S-coordinated species as the most prevalent ligand across the majority of the biomass, particularly within the leaf. However, the presence of O/N ligands with tetrahedral coordination was observed to significantly increase at locations of highest Zn concentration. XRF images demonstrated that peak S and Zn signal intensity were not spatially correlated. μ XAS spectra for the S K-edge identified mixed S speciation of sulfoxide and sulphate, the proportions of which did not alter across different tissues. Therefore, whilst S ligands were most prevalent and widely involved in Zn sequestration throughout the plants, O/N ligands appeared to proportionately increase in relation to peak Zn concentration at a local level.

6.1 Introduction

The literature review identified that different objectives are possible through phyto-remediation, including the removal of the HM (phyto-extraction) or reduction in HM mobility near the ground surface (phyto-stabilization) (Ghosh and Singh, 2005; Oladoye et al., 2022; Pilon-Smits, 2005; Thomas et al., 2021). However, growing viable energy crops at contaminated sites requires balancing the desire to remediate the soil whilst producing a biomass which remains suit-

able for energy recovery. Uptake of HM and their retention within the aerial biomass (stem or leaves) of *Miscanthus* raises the concern that the presence of HM may compromise the economic value of the harvested crop. This could occur if the HM concentration exceeds recognised quality standards for solid biofuels which stipulate an upper limit of $>100 \text{ mg/kg}_{(\text{dm})}$ (ISO17225, 2014).

The literature demonstrates that *Miscanthus* can uptake some HM into its biomass and that different HM may exhibit different accumulation patterns across the root, stem, and shoot structures (Barbosa et al., 2015; Fernando et al., 2004; Korzeniowska and Stanislawska-Glubiak, 2015; Wanat et al., 2013; Wang et al., 2012). The uptake of Zn and Pb into aerial structures (i.e. harvestable biomass) has been identified in the *Miscanthus* from the Bytom site. Uptake of Zn and Pb has also been replicated in the pot trials at the University of Leeds. Under the controlled conditions of the pot trial, differential patterns of both Zn and Pb concentration were confirmed within the biomass: Zn being more concentrated in the plants' stems, but Pb being more concentrated in the leaves. Furthermore, the analysis of XAFS in this study has shown that Zn speciation is not uniform – the biochemistry of Zn sequestration differs in different plant structures.

It has been shown that Zn content of crops, such as sugarcane, rice and tomato, can be manipulated by exploiting agronomic and genetic variations that exist within a single species (Broadley et al., 2007). The ambition of many of these research projects is to *increase* the Zn content of food crop species, to the potential benefit of a local population affected by a Zn deficient diet. However, the opposite outcome (i.e. reducing Zn content) is only a matter of reversing the selection criteria. *Miscanthus* has been demonstrated to display variations of morphology and biochemical profile (Van der Weijde et al., 2017). Significant morphological differences are even seen between different cultivars of the same *Miscanthus* species resulting in measurably different tissue and cell structures, such as the area of vascular bundles (Kaack et al., 2003). It is not currently known if morphological or biochemical differences between different *Miscanthus* cultivars or hybrids influence or correlate with the its retention of HM such as Zn.

The first aim of the work presented in this chapter is to advance the understanding of the spatial distribution of Zn sequestration within *Miscanthus*. Building upon the broad observations made in chapter 5, which demonstrated Zn being more concentrated in stem than leaves, this study uses micro-focused X-ray fluorescence (XRF) imaging and X-ray Absorption Spectrometry (μ XAS) to provide insights into how Zn is sequestered within the harvested biomass (aerial structures) of *Miscanthus*. High-resolution XRF maps are used to identify specific tissue structures where Zn accumulates to the greatest extent.

The previous bulk XAFS analysis identified differing patterns of Zn speciation between stem and leaf. In this chapter micro-focussed XAFS (μ XAS) analysis is used to identify Zn speciation at a localised level within the different tissues across both stem and leaf. In this way the biochemistry of Zn sequestration at a local level can be established and compared to the ‘average’ of speciation provided by the bulk XAFS analysis.

The bulk XAFS analysis identified that S coordinated species play a variable role in Zn sequestration. The presence of S ligands appeared to be higher in the leaf structures, yet it was in the leaves that Zn concentrations was lower. The work presented in this chapter includes data specifically regarding S spatial distribution at a local level compared with Zn distribution to further explore the Zn to S relationship. In this chapter XANES data regarding S is also explored, but due to the uncertainties associated with the data the S XANES data and discussion is presented within the appendix.

6.2 Methods

6.2.1 Plant Growth

Three month old *Miscanthus* plants that had been grown in compost from seed were supplied by Terravesta Ltd. Individual plants were transferred to pots

containing topsoil collected from a working arable field at Spen Farm, Tadcaster, UK, and that had been spiked with ZnCl_2 and ZnCO_3 (1007 and 4693 $\text{mg}_{(\text{Zn})}/\text{kg}_{(\text{dm})}$, respectively) to a final concentration of 5700 $\text{mg}_{(\text{Zn})}/\text{kg}_{(\text{dm})}$, and PbCl_2 and PbCO_3 (298 and 2249 $\text{mg}_{(\text{Pb})}/\text{kg}_{(\text{dm})}$, respectively) to a final concentration of 2547 $\text{mg}_{(\text{Pb})}/\text{kg}_{(\text{dm})}$. This spike is equivalent to 5x the concentration of Zn in the exchangeable and carbonate bound phases in soil at a contaminated field site in Bytom, Poland where *Miscanthus* is being grown as an energy crop (Krzyzak et al., 2017; Rusinowski et al., 2019). The plants were grown in pots for a further 66 days under controlled environmental conditions (SI section 1). This produced *Miscanthus* biomass concentrations for Zn of 635 $\text{mg}/\text{kg}_{(\text{dm})}$ and 329 $\text{mg}/\text{kg}_{(\text{dm})}$ in stem and leaf respectively. Biomass concentrations for Pb were 35 $\text{mg}/\text{kg}_{(\text{dm})}$ in the leaf and 15 $\text{mg}/\text{kg}_{(\text{dm})}$.

6.2.2 Sample Preparation

Plants were harvested into stem and leaf parts and frozen (-20°C). Both ‘whole-mount’ samples and microtomed sections were prepared for analysis as follows:

Whole-mount: A frozen leaf sample was cut into a small (c.5x5 mm) square section across the whole leaf blade. This was mounted on a quartz slide, overlaid with Kapton film and then secured Kapton tape.

Microtome sections: Fresh samples of leaf and stem were fixed with 2.5% glutaraldehyde in 0.1 M phosphate buffer for 2.5 hours then washed twice for 30 min. with 0.1 M phosphate buffer, then soaked in 1.0% osmium tetroxide overnight. Samples were washed twice for 30 min. in 0.1 M phosphate buffer, then dehydrated using an ascending alcohol series (20%, 40%, 60%, 80%, 2x100%) for 60 min. each change.

Embedding started with two changes propylene oxide (20 min. each), then 50:50 propylene oxide-Araldite overnight. This was replaced with 75:25 Araldite-propylene oxide for several hours and finally with 100% Araldite, which was allowed polymerized overnight at 60°C . Sections were then microtomed with a diamond blade to a thickness of 10 μm and mounted on a quartz slide.

6.2.3 XRF and μ XAS

XRF and μ XAS data were collected at beamline 13-ID-E at the Advanced Photon Source (APS), Argonne National Laboratory, USA, in February 2021. XRF imaging was conducted with incident X-ray energy set to 10500 eV with a Si (111) monochromator. The nominal beam size was set to 2 μm and step sizes varied between 2 μm (large-scale maps) and 0.5 μm (small-scale maps). Dwell time was 0.025 s per pixel throughout. X-ray fluorescence spectra were collected using a Canberra SXD-7 seven-element Silicon Drift Detector (SDD) set at 45° to the beam and a distance of 60 mm. XRF image processing and data analysis (signal intensity and correlation plotting) was conducted using Larch v0.9.58 (Newville, 2013).

μ XAS spectra were collected across the K-edge of both Zn and S, for which E_0 values of 9659 and 2472 eV were ascribed respectively. A foil of pyrite was used as an initial reference sample for S calibration ($E_0=2468.8$ eV). XAS scans were performed using five energy regions between: -150, -30, +60, +6k, +9k and +12k eV above/below E_0 , with energy step intervals for each region being 5, 0.4, 0.05k, 0.07k and 0.1k eV respectively. Two consecutive scans were collected from each sample and data were subsequently merged prior to analysis.

XAS data processing, including normalisation, background removal and Linear Combination Fitting (LCF) was performed using Athena software v0.9.26 (Ravel and Newville, 2005). XAS spectra from the biomass samples were initially compared with three published Zn reference spectra for aqueous solutions of Zn-malate, Zn-cysteine and Zn-histidine (Mishra et al., 2020). LCF fitting was performed in k -space between 3 and 7 \AA^{-1} . Zn-malate fits were rejected in reported results on the basis that no combination fit resulted in its inclusion resulting in a reduced chi-squared being reduced by >20%. The S data were compared to four S standards – pyrite, cysteine, dimethyl sulfoxide and sodium sulfate. Immediately prior to gathering experimental S data, a XAS scan was performed on a pyrite standard which was used for calibration against standards.

6.2.4 Statistical Methods

Statistical analysis adopted the non-parametric Mann-Whitney U test to compare differences between groups of data. This was performed using IBM SPSS Statistics for Windows, version 27 (IBM Corp., Armonk, N.Y., USA).

6.3 Results

Large scale XRF maps showing elemental distributions for Zn and S (also K) in the whole-mount leaf sample are shown in figure 6.1 and figure 6.2. These maps are scanned in plan view (top surface of the leaf viewed from above). For interpretation: the images illustrate a striated structure which is caused by the veins running through the leaf. This parallel venation is characteristic of monocotyledons, whose veins run longitudinally along the length of the leaf.

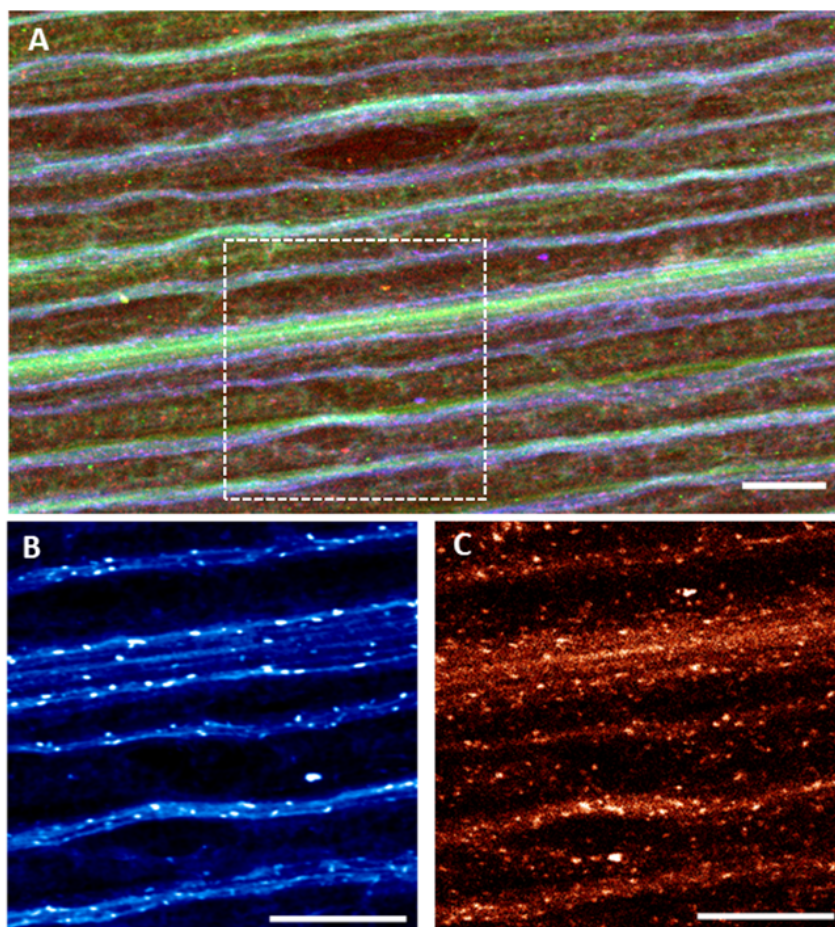


Figure 6.1: XRF maps of leaf in plan view: A) Large scale map showing K (green), Zn (blue) and S (red) with area of detailed maps highlighted; B) small scale map showing Zn; C) small scale map showing S. All scale bars = 100 μm .

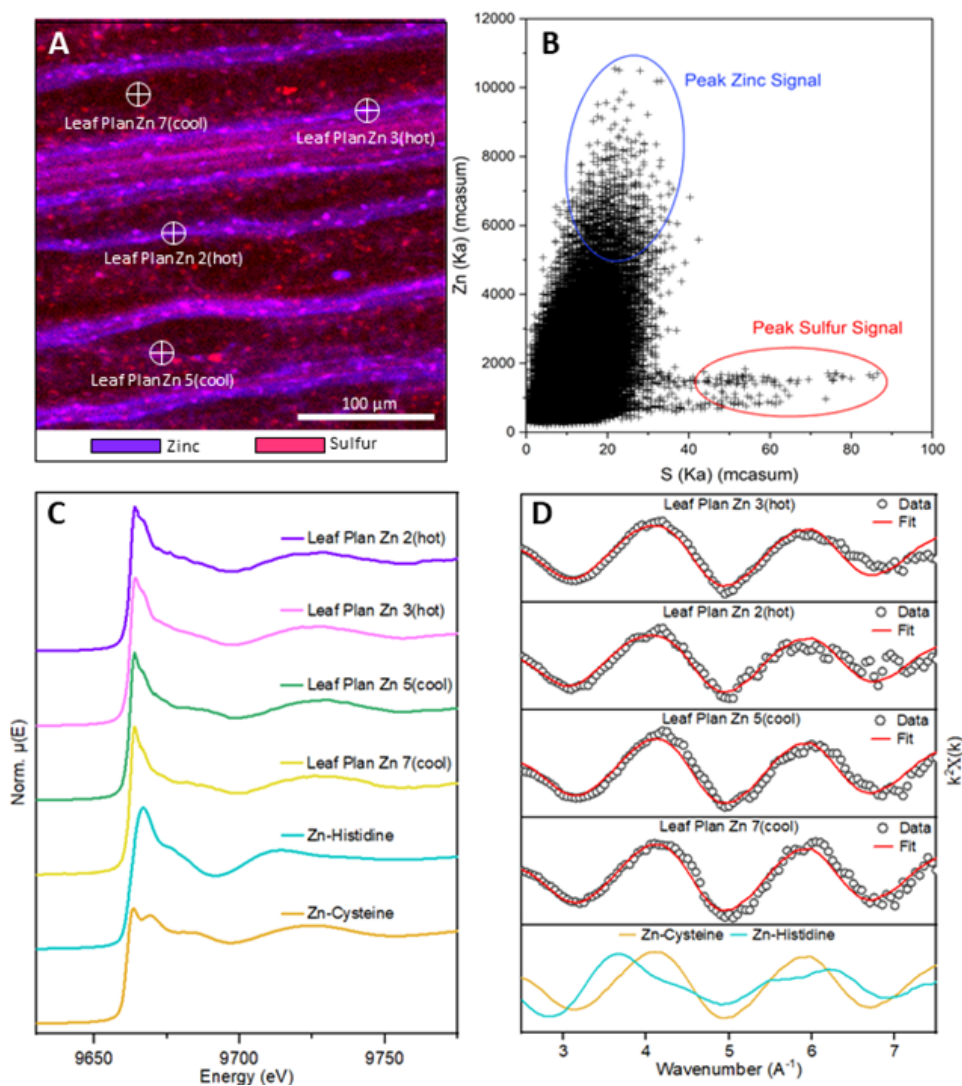


Figure 6.2: Leaf in plan view and associated data. A) small scale XRF map showing Zn (blue) and S (red) and spot locations for μ XAFS acquisition (scale bar = 100 μ m); B) correlation plot of signal intensity (sum of MCA counts) for Zn and S in each pixel of the detailed map; C) XANES spectra for spot locations and Zn standards, and; D) EXAFS data and LCF results (red line) against for highlighted spot locations and Zn standards.

figure 6.2 also displays the locations of μ XAFS sample points and their associated XAFS data (XANES and LCF fits) compared to Zn standards' spectra. The correlation plot displays the fluorescence signal intensity of Zn and S as

sociated with each pixel in figure 6.2A.

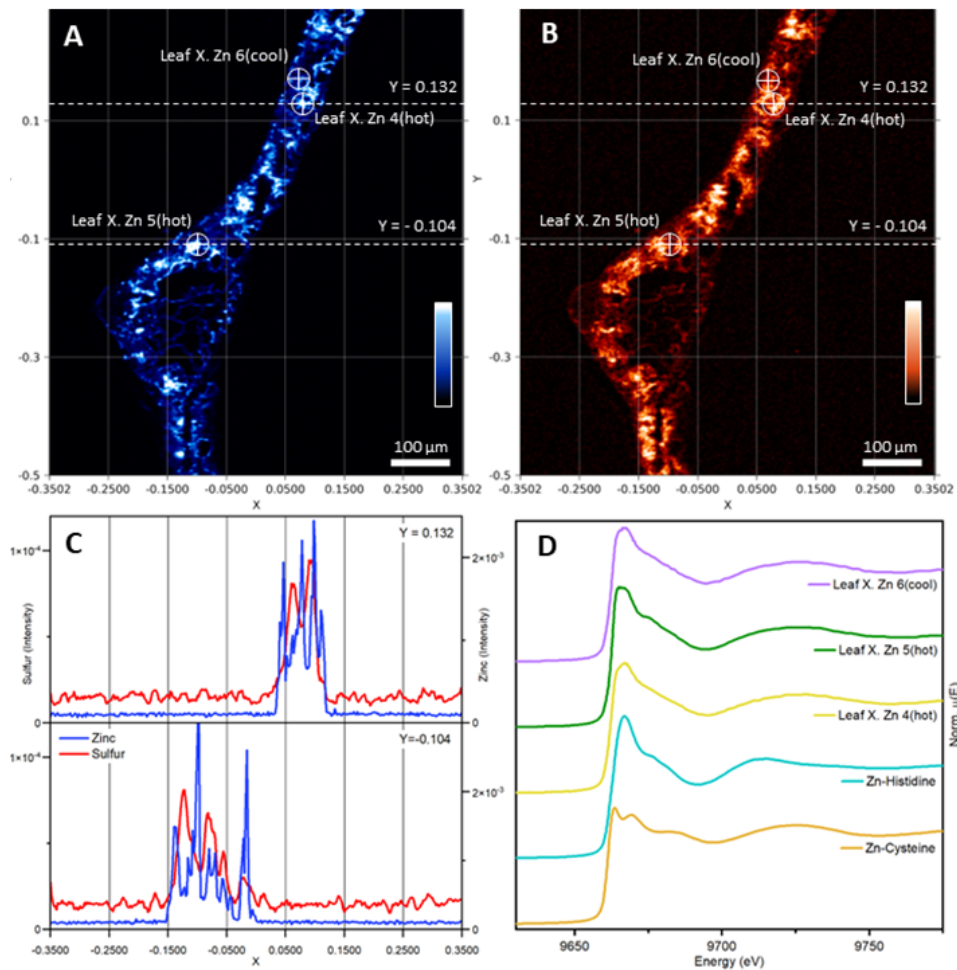


Figure 6.3: Leaf in cross section and associated data: A) XRF map for Zn showing spot locations for μ XAFS acquisition and Y-plane scans; B) XRF map for S showing spot locations for μ XAFS acquisition and Y-plane scans; C) plot of Zn and S signal intensity across Y-planes; D) XANES spectra for spot locations and Zn standards. All scale bars = 100 μ m.

XRF maps for the leaf cross section sample are shown in figure 6.3. The maps show separate Zn and S distributions. For interpretation: the cross sections cut through the (large) midrib of the leaf which is the large structure that runs the whole length of the leaf. On either side of the midrib are leaf's

lamina and within these the section cuts through multiple veins, which are clearly visible running across the plan view maps of the leaf (figure 6.1 and figure 6.2). Figure 6.3A also shows to transect lines across which the associated Zn and S fluorescence signal intensities have been plotted in figure 6.3C.

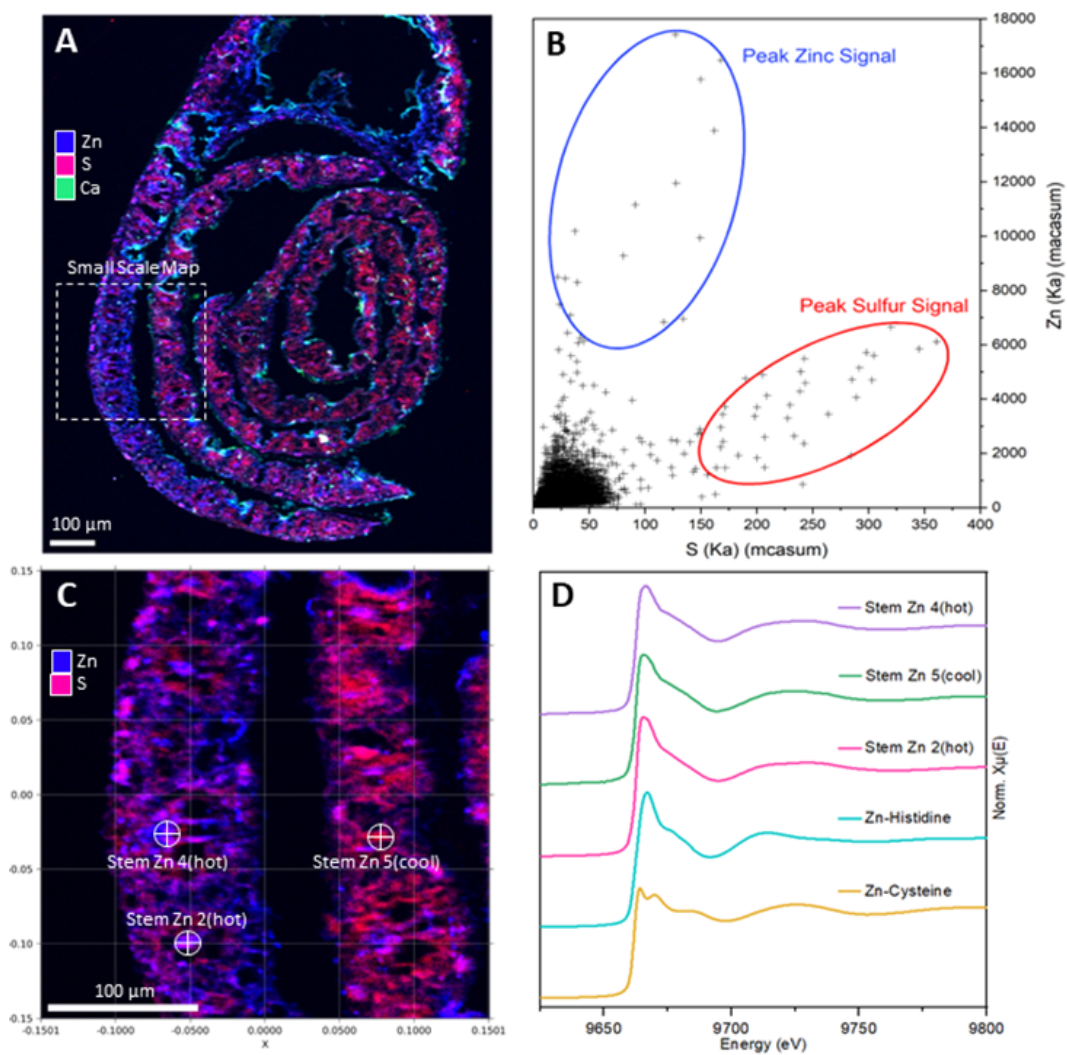


Figure 6.4: Stem cross section and associated data. A) Large scale XRF map of stem in cross section showing Zn (blue), S (red) and Ca (green) with area of the detailed XRF map highlighted; B) correlation plot of Zn and S signal intensity for the large scale XRF map; C) detailed XRF map of Zn (blue) and S (red) with locations of μ XAFS spots displayed; D) spectra for μ XANES locations in stem and Zn standards. All XRF scale bars = 100 μ m.

XRF maps of the stem cross section are shown in figure 6.4, along with the relevant μ XAFS spot locations and associated XANES spectra. The correlation plot of Zn and S fluorescence signal intensity in figure 6.4B has fewer data points compared to figure 6.2B as the stem sample's occupancy within the mapped area is only partial.

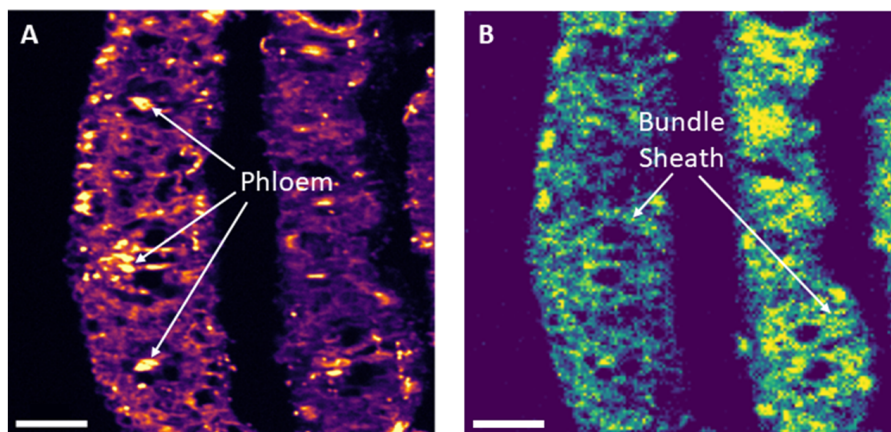


Figure 6.5: Small scale XRF maps of stem. A) Zn fluorescence; B) S fluorescence. All Scale bars = 50 μ m.

More detailed XRF maps of the stem cross section are displayed in figure 6.5. The major tissue structures associated with the vascular bundles (phloem and sheath) are indicated. These are referred to within the discussion section.

Table 6.1 shows the LCF fitting results for each of the μ XAFS spot locations in stem and leaf samples (figure 6.2A, figure 6.3A, figure 6.4C). The categorisation of each μ XAFS spot (hot/cool) based on relative Zn signal intensity is displayed, along with the relative weighting of Zn-cysteine and Zn-histidine.

Table 6.1: Results of LCF on μ XAFS sample points

Sample	Hot/Cool	r.Chi-sqd.	LCF weighting	
			Cysteine	Histidine
Leaf Plan				
Leaf P. ZnH2	Hot	0.07	0.75	0.25
Leaf P. ZnH3	Hot	0.04	0.85	0.15
Leaf P. ZnC5	Cool	0.06	1.00	0.00
Leaf P. ZnC7	Cool	0.05	1.00	0.00
Leaf X				
Leaf X ZnH4	Hot	0.12	0.57	0.43
Leaf X ZnH5	Hot	0.14	0.51	0.49
Leaf X ZnC6	Cool	0.10	0.64	0.36
Stem				
Stem ZnH2	Hot	0.08	0.43	0.57
Stem ZnH4	Hot	0.12	0.40	0.60
Stem ZnC5	Cool	0.07	0.51	0.49

Isolated EXAFS (Xk) for the biomass samples and Zn standards are provided in the Appendix to this chapter (figure 6.8).

Sulfur μ XAFS data were also collected. Due to inherent uncertainty, the S data are not considered within the main text of this chapter. However, a consideration of S data is provided within the Appendix to this chapter

6.4 Discussion

6.4.1 XRF Mapping of Leaves

The XRF mapping of the leaf in plan view shows that areas of high Zn concentration appear to be associated with the vein structures. Peak Zn fluorescence signal is observed as running along the veins and a much reduced

signal intensity is observed outside the veins (figure 6.2B). These veins contain vascular structures of both the xylem and phloem running closely adjacent to each other. Within the veins, the highest Zn signal is identified within discrete, highly localized 'hot spots' visible as points of intense fluorescence signal. Very few Zn hot spots are located outside of the leaf veins (figure 6.1B).

The distribution of the S signal displays some similar characteristics to that of Zn. There is an association of S with the leaf veins (figure 6.1C) and the S signal also shows some highly localized hot spots. However, a visual comparison of S and Zn images suggests that the respective hot spots are not necessarily collocated (compare figure 6.1B versus figure 6.1C). A quantitative analysis confirms this to be the case: the correlation plot of Zn versus S fluorescence signal intensity within each pixel of the leaf map illustrates that peak Zn signal does not correlate with the peak S signal (figure 6.2B). Whilst there is scatter in the data, the Zn signal in the correlation plot increases (vertically) between 1,000 and 10,000 counts with little or no increase in S counts (<40 at all values of Zn). Simultaneously, the S signal increases (horizontally) in a manner which appears totally independent of any increase in Zn.

The bulk XAFS analysis identified S species as having the predominant role in Zn sequestration within the leaves. However, the visual evidence suggests that Zn hotspots exist within the leaf and these do not coincide with commensurate increases in S. The clear separation of Zn and S signal intensities in the correlation plot suggests that increased Zn (by a factor 10) can occur at a local level without influencing S concentration. This suggests that either S ligands are present in excess at these locations and can accommodate higher/lower Zn without requiring up-regulation of S ligands within the cells; or that S ligands have a comparatively fixed capacity beyond which it does not increase and any additional Zn sequestration capacity at these hotspots is provided by other ligands not observed in the XRF maps (e.g. perhaps O/N ligands).

The cross-section maps of the leaf (figure 6.3) bisects the veins and larger central midrib. The Zn cross-section (figure 6.3A) displays repeated Zn hot spots where the veins are bisected which contrasts with the less bright signal aris-

ing from the surrounding mesophyll tissue. The S map also displays hotspots which are generally associated with the veins (figure 6.3B). However, a quantitative analysis reveals that peak Zn and S signals do not occur in precisely same location. This difference in location is illustrated in the plots of signal intensity in the Y-plane running across the leaf cross-section (figure 6.3C). Data across the Y-plane show that peak Zn signal occurs adjacent to (but not concurrent with) the peak S signal: the Zn and S signals appear as an alternating pattern of peaks at different locations running across the vascular structures. This is consistent with the pattern previously observed in correlation plot. These data therefore consistently suggests that localized peaks of Zn concentration are not facilitated through a corresponding increase in S within leaf tissues.

Previous research has shown that high levels of HM can accumulate within the vacuoles of plant cells (Brune et al., 1994; Frey et al., 2000). However, within *Miscanthus* samples presented here, the bands of high Zn signal running along the veins coincide with the phloem or xylem structures. These vascular structures contain sieve tube elements which do not possess vacuoles. In contrast, companion cells, which are arranged immediately alongside the phloem tissues, can contain numerous vacuoles (Kaur et al., 2018). These companion cell vacuoles could be the source of the isolated Zn hotspots which are observed to occur regularly along leaf veins; however, the relatively low resolution (2x2 μm pixel) of the XRF maps make identification of structures smaller than the major tissues/structures difficult and conclusions with respect to sub-cellular Zn distribution are therefore speculative.

6.4.2 XRF Mapping of Stem

The XRF map of the stem cross-section reveals multiple concentric layers of tissue suggesting that, despite the sample being taken below a node, a whorl of nascent leaves may form the basis of the stem in the juvenile plants used in this study (Figure 3A).

Maximum Zn and S fluorescence appear spatially differentiated between the different layers of the stem; the Zn signal is highest within the outside layers, whereas the higher S signal is associated with the enclosed layers closer to the centre of the stem. The difference in fluorescence signal between the layers is more clearly seen in the small-scale XRF map (figure 6.4C), where Zn (blue) signal is stronger in the external layer whereas S (red) signal appears stronger on the internal layer (see also figure 6.5). The correlation plot of Zn and S signal intensity across the stem cross-section (Figure 3B) displays the same separation between the locations of peak Zn signal and peak S signal as was observed within the leaf.

Within the stem the vascular bundles are much larger than those observed in the leaf, for example the highlighted spot location 'Stem Zn 4(hot)' in figure 6.4C sits on the phloem of a large vascular bundle (the large voids adjacent to this spot being the xylem). Their larger size allows the discrete xylem tubes and regions of phloem tissue to be identified. The highest Zn signal in the stem is associated with the phloem and in particular the phloem located towards the outside of the stem. In contrast, the S signal is most intense towards the interior of the stem and particularly within the circle of tissues surrounding the xylem and phloem, where bundle sheath cells would occur (see also figure 6.5A and figure 6.5B).

Overall, the XRF maps of the *Miscanthus* tissues show that Zn prevalence is highest in the vascular structures of both stem and leaf. Cross section of tissues show that highest Zn concentration is associated with the phloem, or tissues closely associated with the phloem, such as companion cells. Analyses of signal intensity show that the Zn signal increases without a commensurate increase in S signal. Peak S signal is often observed in tissue structures that are adjacent to those with maximum Zn signal, which in the stems samples are identifiable in the areas that bundle sheath cells are expected.

6.4.3 Zinc μ XAFS

Twenty six spot locations were used to acquire μ XAFS spectra across the Zn K-edge. These locations were selected from the XRF maps and categorized based upon relative Zn fluorescence intensity as either ‘hot spots’ or ‘cool spots’. Hotspots were generally associated with leaf veins and vascular bundles in the cross-sections, whereas cool spots were taken from the tissues outside these structures. The μ XAFS data are displayed in figure 6.2C, figure 6.3D and figure 6.4D alongside XAFS for standards compounds Zn-cysteine and Zn-histidine.

The μ XAFS spectra from all spot locations have an absorption edge between those associated with the standards of Zn-cysteine (9661.3 eV) and Zn-histidine (9663.5 eV). Due to close positioning of absorption edge energies Linear Combination Fitting (LCF) was performed in k -space. In k -space Zn standards possess distinct oscillatory differences which facilitate LCF, particularly around the first peak which occurs at a wavenumber of 3.7 \AA^{-1} for tetrahedral-O/N coordinated Zn-histidine, compared to 4.1 \AA^{-1} for tetrahedral-S coordination within Zn-cysteine (figure 6.2D and Appendix: figure 6.8). A spectrum from Zn-malate was considered in the LCF analysis, but its inclusion in the final fits was not justified as in no case did it result in a lowering of reduced chi-squared of $>20\%$. A summary of the LCF weightings, categorised by sample type (stem, leaf) and the hot/cool spots therein, is displayed in figure 6.6.

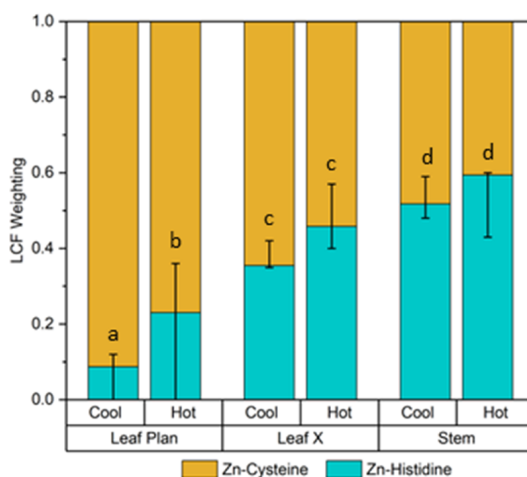


Figure 6.6: LCF results (mean and range) for Zn μ XAFS locations across the sample types grouped as high Zn fluorescence (hot) and low fluorescence (cool). Letters indicate of data with significant differences ($p < 0.05$).

The data within figure 6.6 demonstrate that within the majority of μ XAFS sample points S species (Zn-cysteine) are the most prevalent ligands for Zn. This is consistent with the bulk XAFS analysis in the previous chapter. However, the categorisation of μ XAFS sample points into hot/cool locations reveals a more nuanced picture regarding the speciation under differing Zn concentrations. The LCF data show that within all sample types (Leaf Plan, Leaf Cross-Section and Stem) the O/N species are comparatively more prevalent in Zn hot spots than in cool spots. Consequently, S species relative contribution to Zn sequestration is correspondingly lower in Zn hot spots. This difference in O/N:S weighting for hot vs cool spots within the Leaf Plan sample is statistically significant (Mann-Whitney $U = 11.5$, $n_1 = 7$, $n_2 = 9$, $p = 0.03$ two-tailed). A summary of all statistical test results is provided in the Appendix to this chapter (6.2). This suggests that *Miscanthus* utilizes increasing quantities of O/N ligands to sequester elevated levels of Zn in specific tissues where Zn is most concentrated (i.e. hot spots). No LCF fit attributed any weight to Zn-malate which possesses octahedral-O coordination. The O/N weighting within the LCFs was exclusively associated with Zn-histidine which possesses tetrahedral coordination.

This pattern of higher prevalence of O/N ligands within Zn hot spots is also observed both within Leaf Cross-Section and Stem samples. However, in these samples the differences between hot vs cool spots have lower statistical significance for both Leaf Cross Section (Mann-Whitney $U = 3.0$, $n_1 = 7$, $n_2 = 3$, $p = 0.09$ two-tailed) and Stem (Mann-Whitney $U = 9.0$, $n_1 = 9$, $n_2 = 5$, $p = 0.07$ two-tailed). This lower level of significance is influenced by comparatively few data for Zn cool spots limiting statistical power within each sample despite the consistency of the pattern being repeated (Appendix: table 6.2).

Schat (2002) studied the sequestration of increasing levels of Zn within *Silene vulgaris* plants and could not identify S ligands (phytochelatin thiols) as playing a role in sequestering Zn at elevated level as it approached toxic concentrations. Clemens (2001) identified histidine as the determinant for increased HM sequestration and, in particular, compartmentalization within cell vacuoles. These studies in combination with the Zn/S correlation plots and spatially resolved Zn/S data (Y-plane plots) presented in this study point to similar conclusions for the *Miscanthus* leaves. Zn sequestration appears to be dominated by S ligands at a general level, but at locations where Zn levels are observed to be most concentrated the increase is associated with an increase in the presence of tetrahedral O/N ligands.

The LCFs results also show that the Leaf Cross-Section sample has statistically different O/N weightings compared to the whole-mount Leaf Plan sample (Mann-Whitney $U = 0.0$, $n_1 = n_2 = 7$, $p = 0.02$ two-tailed). However, interpretation of data for the Leaf Plan sample versus the Cross-Section samples is complicated by differences in sample orientation changing the tissues which interact with the X-ray beam. For example, within the Cross-Section sample the beam is aligned with the direction of the vascular bundles and therefore the pixels' data represents individual tissues, e.g. X-rays may interact only with phloem cells. In contrast, in the Leaf Plan sample the X-ray beam will penetrate through surrounding tissues, including epidermal and mesophyll tissues, before and then after penetrating through all vascular structures, including bundle sheath cells, xylem and phloem, etc. Therefore, the different orientation of the samples provides different spatial information and could be respon-

sible for differing LCF results. Furthermore, the potential impact of different sample preparation techniques (whole-mount versus resin set and microtomed) must also be recognized. Consequently, in this comparison between the leaf samples it must be recognized that differing sample conditions may introduce bias which could affect the comparison LCF results.

Sample preparation is consistent, however, in both the Stem and Leaf Cross-Section samples. Here there is a significant difference between the LCF results for the stem and leaf hotspots (Mann-Whitney $U = 6.0$, $n_1 = 7$, $n_2 = 9$, $p < 0.01$ two-tailed) with the stem sample possessing higher prevalence of O/N ligands. The groups which demonstrate significant differences are shown in figure 6.6. The data show a trend of increasing prevalence of O/N ligands not only within hotspots, but further increasing as the sample location moves away from the leaves which is the expected direction of travel of sap within the phloem. A similar pattern was observed within the bulk XAFS where Zn-histidine was increasingly prevalent within the stem versus leaf.

6.5 Conclusions

When *Miscanthus* plants were grown in highly Zn contaminated soil, approximately twice as much Zn was accumulated in the stems (as a proportion of dry matter) as in the leaves. XRF imaging demonstrated that this Zn accumulated predominantly within the vascular system. The locations of peak Zn concentration occur within the phloem tissues; however, XRF image resolution does not facilitate attribution to sieve tube elements versus closely associated tissues around the phloem. Small, highly localized Zn ‘hotspots’ were present at regular intervals within leaf veins, which may indicate Zn was also sequestered within organelles, potentially vacuoles within companion cells.

The analysis of Zn μ XAS consistently shows that S species predominate as the most common Zn ligand throughout the biomass. However, a detailed analysis of spatial correlation shows that there is not a relationship between locations with the highest Zn and S concentrations, indicating there is not a

governing correlation between either element. While Zn in *Miscanthus* tissues is predominantly coordinated to S, the prevalence of O/N ligands significantly increases in tissues where Zn is most concentrated. The μ XAFS data suggests that O/N ligands, such as Zn-histidine, in and around the phloem represent important mechanisms for detoxification and/or transport of excess Zn within *Miscanthus* at the organism level.

Most insights into metal tolerance to date are at the level of cellular processes and comparatively little is known about such mechanisms at the organism level. This study has confirmed variable uptake of excess Zn within aerial structures, with a bias towards greater concentration within the stem. However, more specifically, elevated Zn concentrations have been demonstrated by this study to be associated with vascular tissues, particularly around the phloem. A wide range of morphology across the *Miscanthus* species has been previously documented (Kaack et al., 2003; Van der Weijde et al., 2017). These variations include wide variation in both the area and radius of vascular bundles, i.e. precisely where Zn has been shown by this study to accumulate. This raises the opportunity to explore if such morphological characteristics could be used to select *Miscanthus* cultivars for higher/lower Zn retention in the biomass, as desired for site conditions and biomass quality.

6.6 Appendix

Sulfur μ XANES

The information below is included in the appendix for information/discussion purposes.

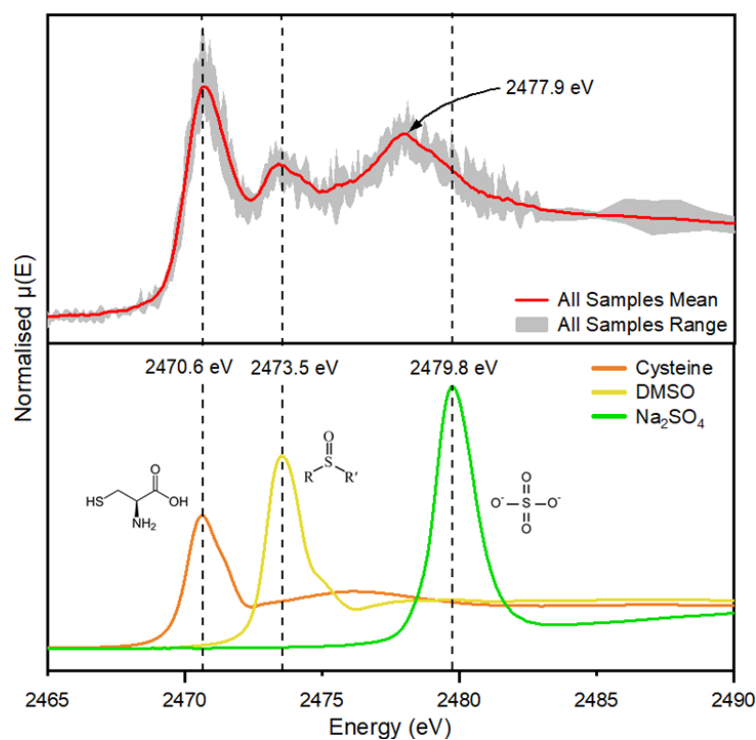


Figure 6.7: XANES for S K-edge: experimental data (top) and S standard spectra with peak energy positions marked (bottom)

Ten μ XAS scans were performed across the energy regime of S K-edges at different spot locations within the leaf and stem samples. Peaks observed within the data were compared with four standard compounds with S in different oxidation states. These compounds (with associated peak energy) were: cysteine (thiol-S, 2470.6 eV), dimethyl sulfoxide (DMSO, sulfoxide-S, 2473.5 eV) and Na_2SO_4 (inorganic sulfate-S, 2479.8 eV). These peak positions are similar to those reported in previous studies (Hackett et al., 2012).

All μ XAS across both stem and leaf samples were very similar and displayed

the same three peak positions and relative peak magnitudes (figure 6.7). The first and largest energy peak occurred at 2470.7 eV in all samples, which is consistent with the thiol-S (cysteine) peak position. There then follows a smaller peak at 2473.2 eV which correspond well with the peak position of DMSO. A third and somewhat broader peak occurs at 2477.9 eV which falls between the DMSO and inorganic sulfate standards' peak positions. The higher energy position of this third peak indicates S in a comparatively oxidized state, most similar to that reported for sulfonate-S. However, the width of the peak may be indicative of contributions from several potential S species, such as sulfone-S, sulfonic-S, organic sulfate ester, and inorganic sulfate-S, all of which are expected within the range associated with the third peak due to the wide spread of signal (Almkvist et al., 2010; Hackett et al., 2012).

The peak heights for S in the *Miscanthus* samples indicate that cysteine-S, possessing the highest peak, is the most abundant form of S in the biomass. The peaks associated with more oxidized forms of S increase significantly in size. This progression can be seen through the standards' spectra where inorganic sulphate-S demonstrates a white line almost twice the height of that associated with cysteine-S. However, within the biomass spectra the peaks corresponding with the more oxidized S species are comparatively low, which emphasizes that cysteine must be substantially more abundant within the samples in order to compensate for the comparatively small white line associated with more reduced S species.

The three S standards are proxies for the range of S compounds found in plants. S is taken up by roots plants and transported through the xylem as sulfate (Künstler et al., 2020). Cysteine is the first organic compound containing reduced sulfur synthesized by plants (Watanabe et al., 2010). Subsequent reactions incorporate cysteine into polypeptides and proteins and oxidation of the cysteine thiol to functional groups such as thioether, sulfoxide and sulfonate (Jalilehvand, 2006; Risberg et al., 2009). Excess sulfate is transported to the leaves and is stored in vacuoles that constitute a large S reservoir for plant metabolism (Iqbal et al., 2013). Major sulfur compounds in plants include amino acids cysteine and methionine, and the vitamins thiamine and biotin

(Prasad, 2014).

The relative proportions of all three S peaks remained comparable across all the μ XAS samples suggesting that S speciation is consistent throughout the samples. The general pattern observed for *Miscanthus* samples is similar to that reported for whole samples of tree leaves where mixed S speciation was observed included distinct groups of reduced S (thiol + disulfide + thioether) and oxidized S (sulfonate + sulfate) (Jalilehvand, 2005).

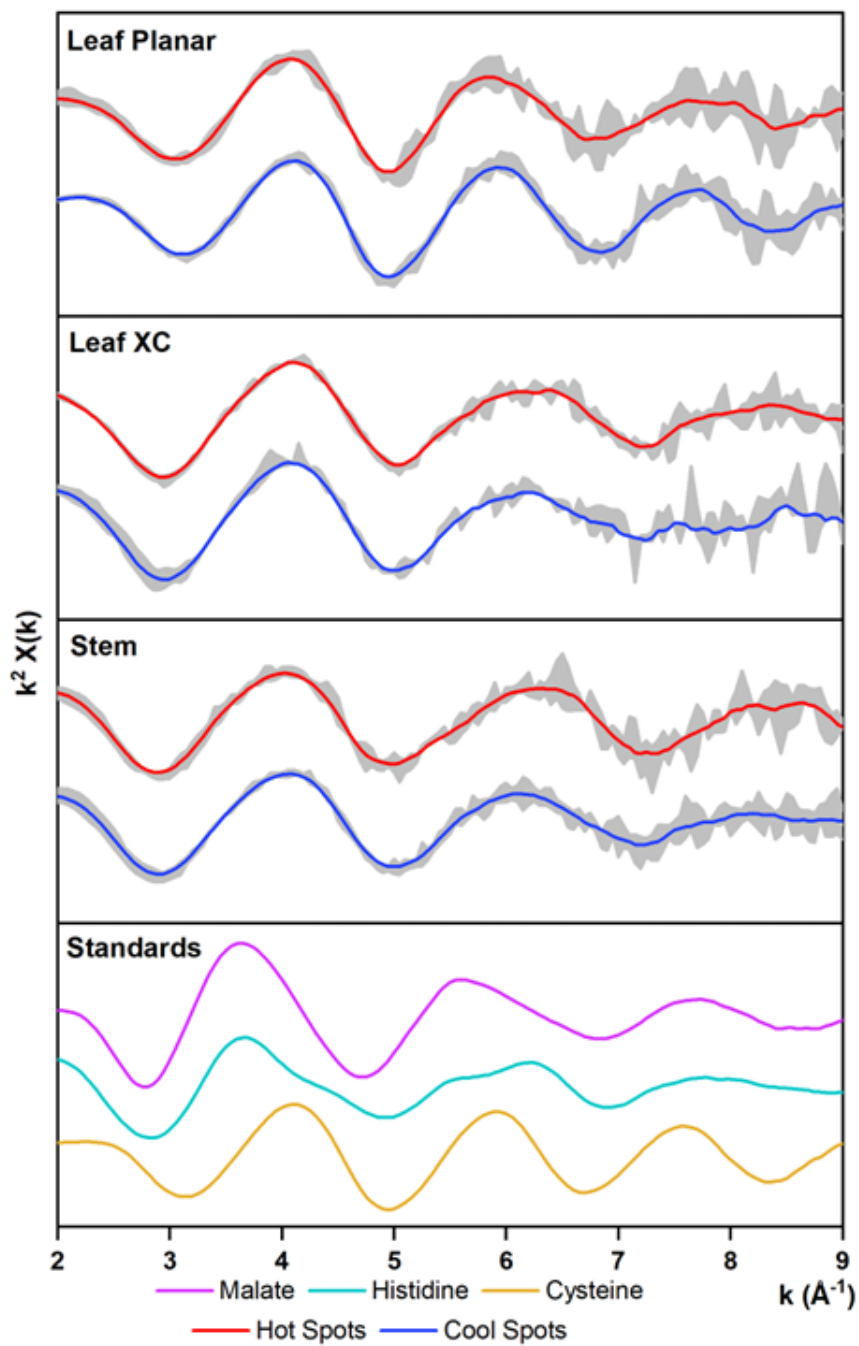


Figure 6.8: Data for the twenty six μ XAFS sample points (range and mean value) and Zn-standards.

Table 6.2: Mann-Whitney U test results comparing Zn-histidine (O/N) weighting in LCFs for hot and cool spots in each sample type

	Leaf Plan Hot	Leaf Plan Cool
Mean	0.230026902	0.086861076
Variance	0.015523941	0.00563244
Observations	7	9
Hypothesized Mean Difference	0	
df	9	
t Stat	2.684789604	
P(T _j =t) two-tail	0.025009062	
t Critical two-tail	2.262157163	

	Leaf X Hot	Leaf X Cool
Mean	0.457996726	0.354660029
Variance	0.005229908	0.004345527
Observations	7	3
Hypothesized Mean Difference	0	
df	4	
t Stat	2.20533283	
P(T _j =t) two-tail	0.092103637	
t Critical two-tail	2.776445105	

	Stem Hot	Stem Cool
Mean	0.604797639	0.517202642
Variance	0.013008006	0.001790176
Observations	9	5
Hypothesized Mean Difference	0	
df	11	
t Stat	2.062704276	
P(T _j =t) two-tail	0.063568205	
t Critical two-tail	2.20098516	

6.7 References

- Almkvist, G., Boye, K., and Persson, I. (2010). K-edge xanes analysis of sulfur compounds: an investigation of the relative intensities using internal calibration. *J Synchrotron Radiat*, 17(5):683–8. Almkvist, Gunnar Boye, Kristin Persson, Ingmar eng Research Support, Non-U.S. Gov't J Synchrotron Radiat. 2010 Sep;17(5):683-8. doi: 10.1107/S0909049510022946. Epub 2010 Jul 14.
- Barbosa, B., Boléo, S., Sidella, S., Costa, J., Duarte, M. P., Mendes, B., Cosentino, S. L., and Fernando, A. L. (2015). Phytoremediation of heavy metal-contaminated soils using the perennial energy crops miscanthus spp. and arundo donax l. *Bioenergy Research*, 8(4):1500–1511. Cited By :28 Export Date: 1 August 2018.
- Broadley, M. R., White, P. J., Hammond, J. P., Zelko, I., and Lux, A. (2007). Zinc in plants. *New Phytol*, 173(4):677–702. Broadley, Martin R White, Philip J Hammond, John P Zelko, Ivan Lux, Alexander eng Research Support, Non-U.S. Gov't Review England New Phytol. 2007;173(4):677-702. doi: 10.1111/j.1469-8137.2007.01996.x.
- Brune, A., Urbach, W., and Dietz, K. J. (1994). Compartmentation and transport of zinc in barley primary leaves as basic mechanisms involved in zinc tolerance. *Plant, Cell and Environment*, 17(2):153–162.
- Clemens, S. (2001). Molecular mechanisms of plant metal tolerance and homeostasis. *Planta*, 212(4):475–486.
- Fernando, A. L., Godovikova, V., and Oliveira, J. F. S. (2004). Miscanthus x giganteus: Contribution to a sustainable agriculture of a future/present - oriented biomaterial. *Advanced Materials Forum Ii*, 455-456:437–441. Baf50 Times Cited:7 Cited References Count:6 Materials Science Forum.
- Frey, B., Keller, C., and Zierold, K. (2000). Distribution of zn in functionally different leaf epidermal cells of the hyperaccumulator thlaspi caerulescens. *Plant, Cell and Environment*, 23(7):675–687.

- Ghosh, M. and Singh, S. (2005). A review on phytoremediation of heavy metals and utilization of its byproducts. *Applied Ecology and Environmental Research*, 3(1):1–18.
- Hackett, M. J., Smith, S. E., Paterson, P. G., Nichol, H., Pickering, I. J., and George, G. N. (2012). X-ray absorption spectroscopy at the sulfur k-edge: A new tool to investigate the biochemical mechanisms of neurodegeneration. *ACS Chemical Neuroscience*, 3(3):178–185. doi: 10.1021/cn200097s.
- Iqbal, N., Masood, A., Khan, M. I. R., Asgher, M., Fatma, M., and Khan, N. A. (2013). Cross-talk between sulfur assimilation and ethylene signaling in plants. *Plant signaling and behavior*, 8(1):e22478.
- ISO17225 (2014). 17225-7: 2014. *Solid Biofuels. Solid biofuels. Fuel specifications and classes. Part, 7:1–14.*
- Jalilehvand, F. (2005). *Sulfur Speciation in Intact Plant Leaves by XANES Spectroscopy*, pages 53–59. Backhuys Publishers, Leiden.
- Jalilehvand, F. (2006). Sulfur: not a “silent” element any more. *Chemical Society Reviews*, 35(12):1256–1268.
- Kaack, K., Schwarz, K. U., and Brander, P. E. (2003). Variation in morphology, anatomy and chemistry of stems of miscanthus genotypes differing in mechanical properties. *Industrial Crops and Products*, 17(2):131–142. 651cc Times Cited:35 Cited References Count:37.
- Kaur, P., Gonzalez, P., Dutt, M., and Etxeberria, E. (2018). Identification of sieve elements and companion cell protoplasts by a combination of brightfield and fluorescence microscopy. *Applications in Plant Sciences*, 6(9):e01179.
- Korzeniowska, J. and Stanislawska-Glubiak, E. (2015). Phytoremediation potential of miscanthus × giganteus and spartina pectinata in soil contaminated with heavy metals. *Environmental Science and Pollution Research*, 22(15):11648–11657. Cited By :14 Export Date: 1 August 2018.

- Künstler, A., Gullner, G., Ádám, A. L., Kolozsváriné Nagy, J., and Király, L. (2020). The versatile roles of sulfur-containing biomolecules in plant defense - a road to disease resistance. *Plants*, 9(12).
- Mishra, B., McDonald, L., Roy, M., Lanzirrotti, A., and Myneni, S. (2020). Uptake and speciation of zinc in edible plants grown in smelter contaminated soils. *PLoS ONE*, 15(4):.
- Newville, M. (2013). Larch: an analysis package for xafs and related spectroscopies. volume 430, page 012007. IOP Publishing.
- Oladoye, P. O., Olowe, O. M., and Asemoloye, M. D. (2022). Phytoremediation technology and food security impacts of heavy metal contaminated soils: A review of literature. *Chemosphere*, 288:132555.
- Pilon-Smits, E. (2005). Phytoremediation. *Annual Review of Plant Biology*, 56(1):15–39.
- Prasad, R. (2014). Major sulphur compounds in plants and their role in human nutrition and health - an overview. *Proceedings of the Indian National Science Academy*, 80:1045.
- Ravel, B. and Newville, M. (2005). Athena, artemis, hephaestus: data analysis for x-ray absorption spectroscopy using ifeffit. *Journal of Synchrotron Radiation*, 12:537–541. 4 935rl Times Cited:7259 Cited References Count:23.
- Risberg, E. D., Jalilehvand, F., Leung, B. O., Pettersson, L. G. M., and Sandström, M. (2009). Theoretical and experimental sulfur k-edge x-ray absorption spectroscopic study of cysteine, cystine, homocysteine, penicillamine, methionine and methionine sulfoxide. *Dalton Transactions*, (18):3542–3558.
- Schat, H. (2002). The role of phytochelatins in constitutive and adaptive heavy metal tolerances in hyperaccumulator and non-hyperaccumulator metallophytes. *Journal of Experimental Botany*, 53(379):2381–2392.
- Thomas, G., Sheridan, C., and Holm, P. E. (2021). A critical review of phytoremediation for acid mine drainage-impacted environments. *Science of The Total Environment*, page 152230.

- Van der Weijde, T., Kiesel, A., Iqbal, Y., Muylle, H., Dolstra, O., Visser, R. G. F., Lewandowski, I., and Trindade, L. M. (2017). Evaluation of miscanthus sinensis biomass quality as feedstock for conversion into different bioenergy products. *Global Change Biology Bioenergy*, 9(1):176–190. Sp. Iss. SI Ef3ia Times Cited:19 Cited References Count:52.
- Wanat, N., Austruy, A., Joussein, E., Soubrand, M., Hitmi, A., Gauthier-Moussard, C., Lenain, J. F., Vernay, P., Munch, J. C., and Pichon, M. (2013). Potentials of miscanthus x giganteus grown on highly contaminated technosols. *Journal of Geochemical Exploration*, 126:78–84. 300yk Times Cited:29 Cited References Count:35.
- Wang, Y. H., Zhan, M. G., Zhu, H. X., Guo, S. J., Wang, W. S., and Xue, B. M. (2012). Distribution and accumulation of metals in soils and plant from a lead-zinc mineland in guangxi, south china. *Bulletin of Environmental Contamination and Toxicology*, 88(2):198–203. 879ko Times Cited:4 Cited References Count:13.
- Watanabe, M., Hubberten, H.-M., Saito, K., and Hoefgen, R. (2010). General regulatory patterns of plant mineral nutrient depletion as revealed by serat quadruple mutants disturbed in cysteine synthesis. *Molecular Plant*, 3(2):438–466.

Chapter 7

Conclusions

7.1 Summary

The aim of this project has been to develop a detailed understanding of the uptake and retention of HM by *Miscanthus* when grown in contaminated soil. The underlying driver for this was a recognition within the available literature that *Miscanthus* is identified as being viable on HM contaminated sites yet some studies were observing uptake of some HM and retention within the biomass. This clearly brings with it a potential concern over fuel quality. Consequently, if *Miscanthus* is to be grown on HM contaminated sites, at the very least there is a need to understand the issues and limitations of such a strategy if it is to be successfully implemented.

The extent and sources of HM contaminated land has been reviewed in Chapter 2. Numerous techniques for managing HM contaminated sites are identified. Many of the traditional technologies (physical and chemical) are identified as having technical limitations and often come at a high cost. It is against this backdrop, even without the additional benefit of a potential income from an energy crop, that phytoremediation represents a potentially attractive option for management of HM lands. There is a body of research which already identifies *Miscanthus* as being a viable option for phytoremediation, with many site-specific data identified in Chapter 2. The speciation of HM within soil impacts its bioavailability and hence is a governing variable which impacts plant uptake. Differing levels of HM uptake are reported within the existing *Miscanthus* literature; however, the soil conditions vary widely as does the age of the plants, time of harvest (frequently not reported), and the location of HM retention is only recorded at a superficial level. Such studies represent the current state of understanding and the starting point from which this project develops. The specific materials and techniques which underpin this project were introduced in Chapter 3.

Whilst the major thrust of this project is concerned with the biomass properties of *Miscanthus*, it is critical that the results are linked to a thorough characterisation of the environmental conditions which are responsible for producing the effect within the biomass. Chapter 4 looked in detail at the soil from Bytom

and started by confirming the high levels of total Zn (4,006 mg/kg) and total Pb (1,859 mg/kg) contamination. The SEM-EDX analyses identified that these HM were evenly distributed over the surface of the soil particles rather than as discrete particles within the soil matrix. One could speculate that, given the legacy of smelter operations in the vicinity, the evidence points towards deposition of air emissions as being the cause of the soil contamination at Bytom. Notwithstanding any theory regarding source of pollution, the sequential extraction results demonstrated that both Zn and Pb in mobile forms are a comparatively small proportion of the total metals' concentration, being: Zn exchangeable 5% and carbonate 23%; and Pb exchangeable 3% and carbonate 24%. The majority of both Zn and Pb were recorded in extractions which require comparatively aggressive conditions for Zn and Pb respectively these were: Fe/Mn oxides 29% and 5%; bound to organics 35% and 11%; and residual 34% and 32%. However, HM bound within these classifications are increasingly unlikely to be relevant to plant uptake due to their high degree of recalcitrance and low bioavailability.

The soil EXAFS analysis indicated that Zn speciation is predominantly in the form of first shell octahedral-O coordinated species: coordination number $5.2(\pm 0.7)$, radial distance $2.04(\pm 0.01)\text{\AA}$, which is consistent with carbonate species. Second shell EXAFS data indicate the presence of C (coordination number $0.6(\pm 0.6)$ at $2.72(\pm 0.03)\text{\AA}$). EXAFS did not identify high Z elements (Fe/Mn/Zn) in coordination with Zn and its substitution into phyllosilicate matrices is considered a plausible form for the more recalcitrant species.

The key findings of the soil study were related to the proportion and speciation of the most mobile Zn and Pb species, namely exchangeable and carbonates. The use of matched quantities of Zn/Pb chlorides and carbonates was adopted to engineer a soil for the *Miscanthus* pot trial with comparable levels of bioavailable metals as were observed at the Bytom field trial location. The same hybrid species of *Miscanthus* was used in the pot trial as had been successfully grown at the Bytom site. A matrix of different soil conditions with increasing (x2 and x5) contamination were also engineered to enable observation of the plants' responses to changing conditions.

The analysis of bulk biomass composition of the *Miscanthus* from the pot trials shows a clear increase in biomass composition of both Zn and Pb with increasing concentration in the soil (FIGURE 5.7 and 5.8). Statistically significant differences in the patterns of both Zn and Pb concentrations within the stem versus leaf samples were identified. Notably these patterns are the opposite of each other, with Zn being higher in stem material but Pb being higher in the leaves, which suggests a fundamental difference in how these HM are sequestered by *Miscanthus*.

There were also significant differences observed between Zn and Pb within the Bytom biomass compared to the pot trial plants grown in comparable soil. Zn in the juvenile plants' stems was much higher (387 mg/kg_(dm)) than that observed in the Bytom biomass crop (94 mg/kg_(dm)). The opposite pattern was observed with Pb which was lower in the pot trial plants (1.4 mg/kg_(dm)) than in the Bytom biomass (14.4 mg/kg_(dm)). Whilst unavoidable differences in trial conditions cannot be ruled out as a factor explaining the difference, the scale of the difference is large (factor of x4 to x10). Others have identified significant variations in *Miscanthus* biomass properties over time (Baxter et al., 2014; Krzyzak et al., 2017; Rusinowski et al., 2019a,b) and a full explanation of the observed differences between Zn/Pb in the juvenile plants versus the mature biomass requires further research.

The XAFS analysis of the bulked samples revealed a changing pattern of Zn speciation on top of the changing pattern of Zn biomass concentration. The XANES analysis demonstrated a greater prevalence of S coordinated species (Zn-cysteine and ZnS) in the leaf compared to the stem biomass. With respect to the juvenile pot trial plants, this means the tissue with highest Zn concentration (i.e. the stem) was associated with an increased prevalence of O/N ligands (although S species are still the higher proportion of ligands overall). The LCF indicates that the O/N species are generally octahedral (Zn-malate). The mature biomass from the Bytom site provided different results compared to the pot trial plants: here the balance of ligands is reversed, with O/N species being more prevalent than S species. Furthermore, the LCF identifies the O/N species as being tetrahedral (Zn-histidine).

The EXAFS analysis corroborated the XANES/LCF observations with the Bytom sample returning a fit with coordination number of $0.7(\pm 0.1)$ for S and $3.4(\pm 0.1)$ for O/N at distances $2.27(\pm 0.01)\text{\AA}$ and $1.99(\pm 0.01)\text{\AA}$, respectively. Both the coordination number and the comparatively short bond distance for O/N are consistent with tetrahedral coordination. This can be compared with the result from the juvenile plant's leaves where the coordination numbers were $2.1(\pm 0.2)$ for S, and $3.3(\pm 0.7)$ for O/N at distances $2.29(\pm 0.01)\text{\AA}$ and $2.05(\pm 0.02)\text{\AA}$, respectively. In the leaves the higher aggregate coordination number and longer O/N bond distance suggest octahedral coordination, more consistent with organic acid ligands (e.g. malate).

Overall, the XAFS results provided a strong indication that the Zn retained in the final crop biomass is bound by a significantly different mechanism than that present within the juvenile plants. The Bytom biomass was harvested in the early spring period following winter senescence. The low O/N bond is closely comparable to those reported by Sarret et al. (2009) for cell wall and pectin ligands. Whereas the pot trial plants, still in their growing phase, have a profusion of S ligands which are considered indicative of sequestration somewhere within the cytoplasm. The precise location of the Zn in the cytoplasm cannot be identified from the bulked data as the S ligand distribution lacks a unique marker which would associate the result with a specific organelle.

The application of XRF imaging provides the ability to resolve the spatial distribution of Zn and S (the Pb concentration was too low to provide a useful signal from the L edge fluorescence). Samples from stem and leaf (in two planes) were mapped and established both Zn and S distribution in *Miscanthus* tissues. Both elements possessed a broad association with the vascular structures of both leaf and stem. However, more detailed quantitative analyses of the images (signal intensity sections and correlation plots) demonstrate that peak Zn and S, whilst closely arranged around vascular bundles, are not co-located. Peak Zn signal was identified as occurring within the phloem cells, whereas peak S signal was immediately adjacent and considered to be within the companion cells which surround them.

The μ XAFS of Zn at spot locations within the tissues confirmed the observations from the bulk XAFS of the pot trial plants. The Zn is predominantly coordinated with S ligands across leaf samples where the LCF weighting on S is up to c.90%. The observations were significantly different for the stem samples where O/N ligands received equal or greater weighting (50-60%). This shift to greater prevalence of O/N ligands within the stem μ XAFS mirrored the pattern observed within the bulk XAFS. However, a more granular analysis is possible as a result of μ XAFS technique. The LCF analysis of spot locations consistently shows that locations with highest Zn concentration have a greater prevalence of O/N ligands than observed at locations with lower Zn concentration. Where sufficient data were available (leaf plan sample) this difference was statistically significant within the sample. The μ XAFS also illustrated that the sample points more closely aligned with the phloem (leaf cross section and stem cross section samples) produced significantly higher weighting for O/N ligands.

The results presented in this thesis provide calibrated models of the uptake response of *Miscanthus* to well characterised Zn and Pb levels within the soil. Through comparison using engineered growing conditions it has been established that juvenile plants retain these HM to a different pattern compared to mature biomass. These differences are apparent within the concentration and distribution within the biomass, and the biochemistry employed in Zn sequestration. The specific tissues associated with Zn retention have also been identified.

7.2 Future Directions

The scope of this project has involved assembling data from many different techniques, including highly specialised synchrotron techniques. The logical progression for research is to seek to exploit the variable patterns of HM retention identified above and, in particular, the HM association with specific tissues. Furthermore, given the demonstrated ability of *Miscanthus* to uptake

and retain HM to an extent whereby it threatens biomass quality, understanding how the data and experience of short term pot trials can be used to make informed decisions about the viability of crops in the longer term. Examples of projects which would contribute to these research directions are given below:

There remains considerable scope to extend the contribution of synchrotron techniques within the field of plant sciences. The variable distribution of HM within different tissues has been established in this project but only in a qualitative, or at best semi-quantitative manner. A fully quantitative approach regarding HM distribution is possible through synchrotron XRF imaging if the matrix of the experimental sample (i.e. resin composition) is well characterised, data from appropriate standards are incorporated into the beamtime and data processing is achieved using PyMca software. This would provide improved understanding of the role of ‘hot spot’ tissues in the overall retention of HM within plant biomass.

Coherent X-ray beamline techniques such as ptychography and tomography have had comparatively limited application to date, and no significant research application into HM within biological samples. They hold the potential to provide much greater image resolution than the micro-probe beamlines adopted in this study. A significant challenge to successfully securing greater image resolution with such techniques will be achieving very high quality sample preparation.

The variable distribution of HM between leaf and stem was identified as a major and statistically significant characteristic of the *Miscanthus* studied. Some hybrids of *Miscanthus* are known to retain leaves over the winter senescence period, whilst others exhibit ‘leaf drop’ where the leaves are not retained in the final standing biomass. The impact of these differing leaf retention/leaf drop characteristics could provide insight into how such hybrids differ in HM retention within the final crop and therefore biomass quality.

Through XRF imaging this project has established for the first time an association between *Miscanthus*’ retention of HM and their concentration within specific tissues (e.g. vascular bundles). The work of Kaack et al. (2003) identi-

fied the broad spectrum morphological characteristics of *Miscanthus*, including the number and cross sectional area of vascular bundles. A valid research question is therefore: can HM retention in the biomass be positively manipulated (increased or decreased depending on desired strategy outcome) by screening for and selecting hybrids which display specific morphologies? Such a question could be addressed through medium to long term growth studies.

7.3 References

- Baxter, X. C., Darvell, L. I., Jones, J. M., Barraclough, T., Yates, N. E., and Shield, I. (2014). Miscanthus combustion properties and variations with miscanthus agronomy. *Fuel*, 117:851–869. A 262vv Times Cited:22 Cited References Count:25.
- Kaack, K., Schwarz, K. U., and Brander, P. E. (2003). Variation in morphology, anatomy and chemistry of stems of miscanthus genotypes differing in mechanical properties. *Industrial Crops and Products*, 17(2):131–142. 651cc Times Cited:35 Cited References Count:37.
- Krzyzak, J., Pogrzeba, M., Rusinowski, S., Clifton-Brown, J., McCalmont, J. P., Kiesel, A., Mangold, A., and Mos, M. (2017). Heavy metal uptake by novel miscanthus seed-based hybrids cultivated in heavy metal contaminated soil. *Civil and Environmental Engineering Reports*, 26(3):121–132. Fp4zu Times Cited:2 Cited References Count:22.
- Rusinowski, S., Krzyzak, J., Clifton-Brown, J., Jensen, E., Mos, M., Webster, R., Sitko, K., and Pogrzeba, M. (2019a). New miscanthus hybrids cultivated at a polish metal-contaminated site demonstrate high stomatal regulation and reduced shoot pb and cd concentrations. *Environmental Pollution*, 252:1377–1387. B Iu2jf Times Cited:1 Cited References Count:67.
- Rusinowski, S., Krzyzak, J., Sitko, K., Kalaji, H. M., Jensen, E., and Pogrzeba, M. (2019b). Cultivation of c4 perennial energy grasses on heavy metal contaminated arable land: Impact on soil, biomass, and photosynthetic traits. *Environmental Pollution*, 250:300–311.
- Sarret, G., Willems, G., Isaure, M. P., Marcus, M. A., Fakra, S. C., Frerot, H., Pairis, S., Geoffroy, N., Manceau, A., and Saumitou-Laprade, P. (2009). Zinc distribution and speciation in arabidopsis halleri x arabidopsis lyrata progenies presenting various zinc accumulation capacities. *New Phytol*, 184(3):581–95. Sarret, Geraldine Willems, Glenda Isaure, Marie-Pierre Marcus, Matthew A Fakra, Sirine C Frerot, Helene Pairis, Sebastien Geoffroy, Nicolas Manceau, Alain Saumitou-Laprade, Pierre eng

Research Support, Non-U.S. Gov't Research Support, U.S. Gov't, Non-P.H.S. England *New Phytol.* 2009 Nov;184(3):581-95. doi: 10.1111/j.1469-8137.2009.02996.x. Epub 2009 Sep 15.